EXPERIMENTAL INVESTIGATION OF SODIUM *SURFACTIN* AS POTENTIAL METHANE-WATER HYDRATE FORMATION INHIBITOR

SALIHU MAIWALIMA SULEIMAN

(B.Eng., MSc)

Experimental Investigation of Sodium *Surfactin* As Potential Methane-Water Hydrate Formation Inhibitor

Salihu Maiwalima Suleiman

Petroleum and Gas Engineering division
School of Science, Engineering and Environment
University of Salford, United Kingdom

Submitted in Partial Fulfilment of the Requirements for the Degree of Doctor of Philosophy,

October 2020

List of Contents

List of Tables

List of Figures

ix

x

List of Appendices

List of Publications

1. Suleiman, S. M., Abbas, A. J, Babaie, M., Akpan, E. U., Yahaya, A. A. and Hassan, K. Y. 2019, Effect of temperature and salt concentration on rheological behaviour of *surfactin*, in: SPE NAICE Conference Lagos 2019. (doi: 10.2118/198731-MS)

2. Suleiman, S. M., Abbas, A. J., Babaie, M. and Nasr, G. G. 2018, 'Physicochemical characterization of sodium surfactin for oil and gas industry application', Journal of Engineering Technology, **7** (2), pp. 342-353.

3. Abba, M. K., Abbas, A. J., Nasr, G. G., Athari, A., Burby, M. L., Saidu, B. and Suleiman, S. M., 2019, 'Solubility trapping as a potential secondary mechanism for CO_2 sequestration during enhanced gas recovery by CO_2 injection in conventional natural gas reservoirs : an experimental approach' , Journal of Natural Gas Science and Engineering, **71**(103002) pp1-13 (doi: 10.1016/j.jngse.2019.103002)

4. Nuhu Mohammed, Abbas J. Abubakar, Enyi C. Godspower, Suleiman M. Salihu, Donatus E. Edem, (2020). 'Alternating N_2 gas injection as a potential technique for enhanced gas recovery and CO_2 storage in consolidated rocks: an experimental study', Journal of Petroleum Exploration and Production Technology 83 pp 1-14 (doi: 10.1007/s13202-020-00935-z)

5. Nuhu Mohammed, Abbas J. Abubakar, Enyi C. Godspower, Donatus E. Edem, Suleiman M. Salihu, (2020). 'Enhanced Gas Recovery by Nitrogen Injection: The effects of injection velocity during natural gas displacement in consolidated rocks', Journal of Natural Gas Science & Engineering 83(2020) pp 1-14 (doi: 10.1016/j.jngse.2020.103513)

6. Bashir Hayatu, Suleiman M. Salihu, Abbas J. Abubakar, Kabir Y. Hassan, Ahmadu A. Abdullahi, and Umar M. Hadiza. 2020, Experimental Analysis of Methane Adsorption Potential in Cored Clay-Rich Sandstones. Adsorption Science and Technology (under review)

Acknowledgement

All profound and unreserved 'Hamd and Shukr' (unreserved praise and gratitude) are due to Allah (Subhanahu wa ta'ala). He bestows His mercy and bounties on whoever He wishes. I cannot praise and thank Him enough for His bounties upon my life, and among many things for this PhD accomplishment. May His blessings and praise be showered upon the best of mankind and seal of prophethood, His messenger Prophet Muhammad (SAW).

My deep gratitude goes to my parents, Alhaji Suleiman Maiwalima and Hajiya Hauwa'u Tanimu. I fervently pray that Allah grant you the best of His mercy in this world and crown it with Jannat Firdaus in the hereafter. To my amazing family members; uncles, aunties and siblings whose names this page cannot contain, I am eternally grateful for your moral, spiritual and financial support.

My profound gratitude is extended to my admirable team of supervisors, Dr Abubakar J. Abbas and Dr Meisam Babaie for their untiring support and constructive review of the PhD journey. I humbly remain appreciative of your being pillar to the PhD process. I acknowledge the efforts and contributions of other departmental staff. Forever, I will remain grateful of your gesture and may you all be rewarded accordingly. To Petroleum Technology Development Fund (PTDF), my gratitude for the sponsorship.

To my other half, your encouragements, understanding and prayers I will forever cherish. You patiently stood by my side and comforted my stressful late-night comings. My thankfulness to Allah for giving me a wonderful, loving and caring wife such as you will be eternal. To my 'cry cry' Minal, thank you for always taking the stressful face away from daddy. I am sorry for those times you had to go to bed while daddy is away struggling to sort his PhD data. But the journey has come to an end and daddy will take you to Nigeria to see grandma as promised.

To friends (even foes alike), and my colleagues too numerous to mention, my gratitude to you will remain eternal. You all have been contributory to the success of this Ph.D. Thank you all.

Declaration

I, Salihu Maiwalima Suleiman, declare that this thesis is entirely my original work, and has not been submitted elsewhere for any award. Any section, part or phrasing that has been used or copied from other literature or documents has been clearly referenced at the point of use as well as in the reference section of the thesis in accordance to standard practice.

…………………….......   ………………………….
    Signature   Date

…………………….......   ………….……………….
Dr Abubakar J. Abbas   Dr Meisam Babaie
   (Supervisor)   (Supervisor)

Dedication

This PhD thesis is dedicated to my loving parents. May the Almighty grant them the best in health, wealth and highest rank in Jannah.

Nomenclature

π	Constant variable
ρ	Density
β	Shape factor
η	Viscosity
Υ	Shear rate
γ	Surface tension
Γ	Surface concentration
μS	Microsiemens
η_o	Viscosity at zero shear rate
E_{24}	Emulsification index after 24 hours
δA	New surface
δx	Incremental surface area
$\Delta \rho$	Phase density differential
$\rho_{gas\ phase}$	Density of gas phase
$\rho_{liquid\ phase}$	Density of liquid phase
ANOVA	Analysis of variance
API	American Petroleum Institute index
^{o}C	Degree Celsius
$CaCl_2$	Calcium chloride
CH_4	Methane
cm	Centimetre
CMC	Critical Micelle Concentration
cm^3	Cubic centimetre
CO_2	Carbon (iv) oxide
C_s	Surfactant concentration
dm^3	Cubic decimetre
D_s	Surfactant diffusion coefficient
DSC	Diffraction scanning calorimetry
E_i	Emulsification index
E_μ	Flow activation energy
EGR	Enhanced gas recovery

EOR	Enhanced oil recovery
F	Force
FTIR	Fourier transform infrared
g	gram
H^+	hydrogen ion
H_2O	Water
HP	High pressure
IFT	Interfacial tension
IR	Infrared
K	Kelvin
K	Material constant
Kg	kilogram
l	Length
m	Mass
m	Metre
M	Molarity
ml	Milli litre
mM	Milli molar
mN	Milli Newton
mPas	Milli pascal
mS	Milli siemens
m^2	Square meter
N	Newton
Na^+	Sodium ion
NaCl	Sodium chloride
OH^-	Hydroxyl ion
$P_{gas\ phase}$	Pressure of gas phase
$P_{liquid\ phase}$	Pressure of liquid phase
ppt	Part per thousand
R	Gas constant
R1, R2	Bubble surface curvature
RPM	Revolution per minute
SDS	Sodium dodecyl sulphate

sec	Second	
ST	Surface tension	
t	Time	
T	Temperature	
TGA	Thermal Gravimetry Analysis	
v	Volume	
wt%	Weight percent	
X, Y, S	Dimensionless parameters	

Abstract

The leading technologies employed in gas processing operations, including gas pipeline transport, are generally chemical based technologies. Chemical based substances are widely used as surfactants in these operations, including hydrate formation prevention and control. Surfactants usage in oil and gas processes stem from their tensioactive capabilities. However, dosage and environmental compatibility continue to be an issue arising from the use of these chemical surfactants. More so, chemical surfactants are being used as hydrate formation inhibitors. This is because, the effect of pipe plugging (due to hydrate formation) could be devastating as it may lead to the eventual shut down of operation. Besides, economics of unplugging and maintenance is a huge burden to the industry. Biosurfactants, on the other hand, are low-dosage and environmentally friendly surfactants. Their application was tested and therefore has been established to serve as alternative to conventional chemical surfactants in enhanced oil recovery (EOR). However, the application of biosurfactants in multiphase methane/water system under field operating conditions has not been duly investigated and reported. Thus, this provided the primary motivation for this study.

In view of the above, this novel research study experimentally investigated the potential of sodium *surfactin* as methane-water hydrate formation inhibitor. The investigation was conducted in three (3) phases using sodium *surfactin*. Evaluation was made considering surfactant's macro size (dosage) and its interaction in the solution, temperature stability and salinity tolerance. Parameters that were employed for the experimental investigation were: temperature in the range of 1 to 50 $^{\circ}$C, surfactant dosages of 0.025 to 1 % and 0.1 to 1.5 M saline (NaCl) concentration.

Phase I of the study investigated the physicochemical (density, pH, electrical conductivity, functional group) and thermal characteristics of *surfactin*. The results revealed that *surfactin* was effectively soluble and foams in aqueous medium. This confirmed the surfactant's adsorptivity, a critical property that enhance performance at reducing surface tension. However, the characteristics were significantly affected by salinity at 1.0 Molarity (M) and above. Dispersion and adsorptivity potential were further confirmed by the lowest density value of 996.641 kgm^{-3} at 0.075 and 0.5 % *surfactin* dosages. More so, temperature increase resulted in density decrease to a minimum value of 988.262 kgm^{-3} at 50 $^{\circ}$C. Nonetheless, density was significantly affected by changes in salinity. Aqueous *surfactin* will pose no threat of corrosion in pipeline, with pH value of 6.68 and 7.31 respectively at 0.025 and 1.0 % *surfactin* dosage. Functional group analysis indicated that *surfactin* is cyclic and contains aliphatic chains ($-CH_3$; $-CH_2-$), carbonyl group (C=O), CO–N bond and aromatic C—H group. The cyclic nature of the molecule confirms its ability for surface adhering properties. Also, thermal stability test showed that *surfactin* is thermally stable within the temperature range of -20 to 170 $^{\circ}$C.

Flow behaviour of *surfactin* was investigated in the phase II of the study. This was performed using rheology as the basis for the investigation, at variable temperature and salinity. Findings revealed that *surfactin* exhibited pseudoplastic flow behaviour characteristic based on viscosity-shear rate interactions. More so, solution of *surfactin* satisfied the shear rates for situations involving mixing

and stirring and pipe flow which are respectively in the range of 10^1 to 10^3 s^{-1} and 10^0 to 10^3 s^{-1}. This finding is an indication of ease of flow of *surfactin* solution during fluid transport in pipes.

Phase III investigated the effect of *surfactin* on methane-water surface tension (ST) using rising bubble technique at different operating conditions. The finding showed that *surfactin* effectively reduced methane-water surface tension from 72 to 34.13 mN/m at 32.5 °C and pressure of 7.58 MPa. As a key indicator of surfactant's ability to alter fluids interfacial interaction, the ST result further demonstrated that *surfactin* can potentially confer on multiphase gas/water system. Hence the potential of sodium *surfactin* as hydrate formation inhibitor.

Hydrate formation is a surface activity and therefore surfactants must effectively adhere at fluids surface to efficiently be able to reduce surface tension. Dispersion and adsorptivity characteristics are key indicators of surface activities which were confirmed by density and surface tension measurements. Furthermore, s*urfactin* will flow to delivery point in pipeline without failure (considering both laminar and turbulent flow regime). More so, utilization of *surfactin* is expected to be safe without risk of corrosion based on the pH and electrical conductivity results. Therefore, sodium *surfactin* can be said to be a potential hydrate-formation inhibitor. These new experimental data will provide a basis for further investigation into mechanism of biosurfactant's effect on methane-water hydrate formation inhibition.

CHAPTER ONE

1   INTRODUCTION

1.1   Chapter Overview

Chapter one of this report introduces the concept and motivation for this study. Background and stimulus prompting the evaluation and potentials of sodium *surfactin* has been outlined in Section 1.2. Moreover, the need and justification for conducting the research study is presented in Section 1.3. Furthermore, Section 1.4 presents the significance and impact of the study to body of knowledge. Research aim and objectives were further presented in Section 1.5 and Section 1.6 present to the reader an outline of how the research report was structured.

1.2   Research Background

The technologies mostly employed in the oil and gas operations, such as enhanced oil recovery (EOR), enhanced gas recovery (EGR), hydrate-formation inhibition during gas transport in pipelines are chemically based technologies. They are widely used due to ease of application and availability of wide range of chemicals, most of which are a derivative of petroleum. Principles behind the application of these chemicals, known as surfactants, rely on their tensioactive capabilities. Studies have indicated that chemically based (synthetic) surfactants can effectively reduce surface tension of oil/water, oil/gas and gas/water systems. Despite the significant features of synthetic surfactants, industry operators are becoming critical of their continuous usage. Besides, environmental legislation regarding disposal and exposure of chemical substances to the environment continue to increase. Furthermore, toxicity and difficulty of chemically derived surfactants to be broken down through the action of microorganisms becomes a great concern. Additionally, it is important that materials disposed into the environment are biodegradable mainly to; assess their damage-causing potential to the ecosystem, and prevent the possibility of future harm due to accumulation in the environment. Consequently, environmental compatibility becomes increasingly important in industrial processes with respect to selection of chemicals. Moreover, economics (in terms of dosage use), sustainability and use of renewable resources is a stimulant for a shift towards green resources. Hence the need for environmentally friendly surfactants, that will serve as alternative to chemically derived surfactants. This class of surfactants are known as biosurfactants.

Biosurfactants or microbial surfactants, like chemical surfactants, are surface active molecules. However, unlike their chemical counterparts which are derived from chemical processes,

1

biosurfactants are derived from biological or biochemical processes. They have been proven to be non-toxic, biodegradable, and can be produced from various sources. Additionally, studies have indicated the effectiveness of biosurfactants at lowering surface and interfacial tension (IFT) between water-oil system, Carbon (IV) oxide (CO_2)-water-oil system. This is in addition to their effective utilization as emulsifiers/demulsifiers, foaming agents, and solubilizers. Details of these features are discussed in Section 2.2.3.

Applications of biosurfactants in different fields results from their tensioactive characteristics, and therefore suitability in oil and gas operations. Moreover, oil and gas processes are operations involving multiphase components which are fundamentally surface-process dependent. Surface processes govern material transfer or transport at either macro or micro level. Therefore, knowledge of surface properties will significantly, if not completely, influence control and management of mass transport phenomenon during oil and gas operations (including methane (CH_4) hydrate – formation inhibition). Principal among these surface properties is surface and interfacial tension.

Interface and surface tension are critical surface activities. Interface refers to a boundary between any two immiscible phases; whereas surface, in this context, may represents an interface involving a gas phase, usually air (Rosen & Kunjappu, 2012). At molecular level, interfacial and surface tension are phenomena that occurs due to energy differential between molecules at a fluid interface when compared to their bulk counterparts (Berry et al., 2015). Therefore, interface is a thin layer (film) that separates two or more (solid-liquid, gas-liquid or solid-liquid-gas) phases, thereby creating a boundary between them. The thin layer region exists due to intermolecular force imbalance resulting from physical attraction between the molecules at interface and bulk fluid. Force field exists at fluid interface than in the bulk phase. Consequently, the molecules at the interface possess different chemical potential, intermolecular spacing and internal pressure. It therefore creates a tension at the interface which can only be overcome by excess surface free energy or increasing surface area along the interface. For example, during gas (e.g. methane) hydrate formation, hydrogen bonded water molecules envelopes and trapped the hydrocarbon molecule thereby forming a cage-patterned crystal around it (Palodkar & Jana, 2017). Typically, hydrate structure is formed at favourable equilibrium temperature and pressure conditions. Formation and stability of the ice-like crystal largely depends on the intermolecular imbalance between hydrocarbon 'guest' and adjacent water molecules. Moreover, the imbalance shortens the surface area available for hydrocarbon molecules, hence making it an easy 'guest' to be trapped by the water molecule. This phenomenon, therefore, becomes one of the most dominant factors affecting

interface mass transfer during hydrate formation process. In addition to other physicochemical characteristics relating to surface activities (adsorption), This research study, therefore, focus on the measurement of surface tension (ST), along with other parameters, as an indicative measure of hydrate–formation inhibition potential of biosurfactant.

As previously noted, inhibiting the caging of hydrocarbon molecule is made possible by increasing surface area available for the hydrocarbon molecule. Before this study, this has been achieved by the use chemical surfactants, such as sodium dodecyl sulphate (SDS). However, studies also indicated that the use of such surfactants contribute to environmental degradation, prompting the need for environmentally friendly alternatives. Furthermore, continuous studies in the area of hydrate inhibition are still required due to the cost of managing hydrate deposits on pipe walls (plugs).

1.3   Research Justification

Several studies have been conducted to understand the dynamics and mechanism of gas hydrate-formation inhibition in pipelines. Efficiency, efficacy and sustainability of numerous synthetic surfactants, as inhibitors, were studied by many authors (Kim et al., 2018; Nguyen et al., 2017; Sohn et al., 2015). Thermodynamic hydrate inhibitors (THIs), such as methanol and glycols were used to shift hydrate formation equilibrium conditions. Aside being environmentally unfriendly, THIs requires high dosage which could be 50-60 % in deep seabed zones. Similarly, kinetic inhibitors such as polyvinylcaprolactom (PVCap), ensures that the nucleation proceed at a very slow rate. Despite this, however, surface behaviours involved in gas hydrate formation is dynamic. Facility installation environment, type and composition of hydrocarbon gas, type and amount of impurities, and the operational conditions (Koh et al., 2002) plays vital role in hydrate formation. Moreover, the goal of all studies is to ensure that an effective and sustainable means of hydrate prevention is achieved.

Studies have indicated successful and effective use of biosurfactants in oil and gas operations involving surface behaviours. Many authors (de Araujo et al., 2019; Geetha et al., 2018b; Hadia et al., 2019; Haq et al., 2019; Purwasena et al., 2019; Veshareh & Ayatollahi, 2019) noted use of *surfactin* for EOR. The authors employed the use of either surfactant physicochemical characterization, core flooding experiments or measurement of physical removal of oil from packed sand samples. Characteristics analysed include emulsification index, functional group analysis and reduction of water surface tension at variable temperature, pH and salinity and contact angle measurement. It is therefore safe to note that results of physicochemical characterizations can be

employed to infer potential applications of biosurfactants. However, it must be clearly established that correct and acceptable experimental analysis procedure was followed. In line with this, Madihalli, Sudhakar and Doble, (2016) noted use of *Mannosylerythritol* Lipid-A as pour point depressant to enhance fluidity of biodiesel at low temperature. The authors findings indicated effective reduction in cloud point to as low as 1.5 $^{\circ}$C. This therefore demonstrates that biosurfactants are capable of effective performance at low temperature similar to hydrate-forming condition. Additionally, success of these studies relies on the wettability alteration and surface tension reduction, details of which are discussed in Section 2.2.3.5.

Further to surface characteristics applications in gas systems, Park *et al.*, (2017) studied (through contact angle and IFT and measurement) capability of lipopeptide biosurfactant—*surfactin* (isolated from *Bacillus subtilis* strain ATCC6633), in enhancing geological carbon storage. The authors noted that secretion of *surfactin* decreased CO_2 and brine ST from: 49.5 to 30 mN/m (~39 % for $CO_{2(g)}$); 28.5 to 13 mN/m (54 % for $CO_{2(l)}$); and 32.5 to 18.5 mN/m (~43 % for supercritical CO_2). The study was conducted at conditions of 3 MPa, 30 °C for gaseous CO_2; 10 MPa, 28 °C for liquid CO_2; and 10 MPa, 37 °C for supercritical CO_2. This indeed indicates the potential of using biosurfactant for gaseous systems. Furthermore, formation of hydrates at ocean sediments (seabed) may be influenced by the presence of biosurfactant-producing microorganisms. As a result, studies on how biosurfactant influenced the mechanism (as promoters) of hydrate formation were also conducted. Zhang *et al.*, (2007) investigated influence of *surfactin* on gas hydrate formation at seabed and their findings revealed that *surfactin* remarkably catalyzed induction time and consequently gas hydrate formation rate. Similarly, Arora *et al.*, (2016) noted that rate of methane hydrate formation increased by 42.97 % when 1000 ppm of *rhamnolipids* solution is used in silica gel (C type) bed system. Consequently, the induction time reduced by 22.63 %.

Conversely, Altamash *et al.*, (2017) investigated the capability of amino acid-biomolecules ((L-*Alanine*, *Glycine*, L-*Histidine*, L-*Phenylalanine* and L-*Asparagine*) and their synergy effect when combined with synthetic surfactant in CH_4 hydrate formation inhibition. The authors revealed the suitability of the biomolecules, combined with synergists (PVCap and PEO), for increased kinetic inhibition. At process pressure condition (up to 55 bars), the synergy increased (shift) hydrate formation time up to 35 h. Hydrophobic effect is an essential characteristics behaviour of biosurfactant particularly when in aqueous or saline medium. Besides, amphipathic surfactants efficiently reduce surface tension compared to linearly structured surfactants. Similarly, Altamash *et al.*, (2017); Hou, Liang and Li, (2018); Lee *et al.*, (2019) indicates anti-agglomeration of methane

hydrate using biosurfactants. These are indicators of potential uses of biosurfactant in multiphase CH_4-H_2O system.

Though there were studies on use of biosurfactant for gas-water systems, only Park *et al.*, (2017) and Zhang *et al.*, (2007) reported case of use of *surfactin*. Moreover, Park et al., reported use of *surfactin* on CO_2/water system while Zhang et al., reported use of *surfactin* as hydrate promoter adopting hydrate induction time in a sand packed column. Additionally, biosurfactants promote or reduces formation of gas hydrate when water is associated to the hydrophilic head of the surfactant molecule and the hydrophobic tail attracts hydrocarbon gas. One of the effective and promising way of associating structured water/hydrocarbon gas is by means of micelle formation (Rogers et al., 2003). It is shown in Section 2.2.3.3 that biosurfactants form micelles at concentration beyond the critical micelle concentration (CMC). This is a threshold beyond which increasing biosurfactants will result to no further surface tension decrease. This is because as surfactant saturation increase, hydrophilic heads form an assembly around the border edge of the sphere while at the same time forming a core composing of hydrophobic tail. The arrangement pave way for the core to readily solubilize adjacent hydrocarbon gas and may resultantly become a nucleation centre for hydrate crystals to form. Conversely, below the CMC, saturation of biosurfactant molecule is low and therefore core formation condition becomes unattainable. Consequently, solubilisation of hydrocarbon gas becomes impossible hindering hydrate crystallization. This principle is what will be adopted as the basis for potential of sodium *surfactin* in preventing CH_4 hydrate formation.

1.4 Research Contribution

Undoubtedly, fossil fuels will continue to dominate as major global fuel source to the ever-increasing world population. To improve availability, sufficiency and ensure fuel demands are met, gas hydrates has been highlighted as potential energy source. Consequently, means to improve its formation is being enhanced including use of biosurfactants. However, efficient and sustainable field operations involving gas transport for processing, storage or utilization is also hindered by gas hydrate formation leading to pipeline blockage. Cost of maintaining, controlling and cleaning of pipelines has also been a burden to the operating companies. Moreover, the need to abide by the increasing stringent environmental regulation necessitate that an environmentally friendly alternatives are utilized in process operations. In view of these, therefore, this study will;

  a. Highlight the role surfactin, an environmentally friendly surfactant, in increasing surface area thereby preventing methane-water hydrate formation.

b. Establish *surfactin* optimal performance condition as potential methane-water hydrate formation inhibitor.

1.5 Research Aim and Objectives

1.5.1 Research aim

The overall goal of the study is to evaluate the potential of sodium *surfactin* as a CH_4 hydrate-formation inhibitor.

1.5.2 Research objectives

The following research objectives are geared towards achieving the set aim of this study:

a. To experimentally characterize the physicochemical and thermal properties of sodium *surfactin* as a potential hydrate inhibitor. This will be accomplished taking into consideration solute (macro) size (dosage) and its interaction in the solution, in addition to evaluating temperature and salinity effect.

b. To investigate, experimentally, the flow behaviour of sodium *surfactin* by evaluating viscosity response to changes in shear rate, temperature and salt concentration at different surfactant dosage.

c. To investigate effect of sodium *surfactin* on ST of methane-distilled water system at variable conditions of temperature, pressure and *surfactin* dosage.

d. To optimize effect of sodium *surfactin* on ST of methane-distilled water system.

1.5.3 Research questions

The study will seek to answer the following questions pertaining to application of *surfactin* in surface activity.

a. What is the dispersive nature of *surfactin* in aqueous and saline media?

b. How safe is *surfactin,* relating to corrosion in pipes and personnel safety, when utilized in gas pipeline?

c. How will *surfactin* behaves when subjected to pipeline flow under laminar and turbulent regime?

d. To what degree will *surfactin* reduce tension between multiphase methane-water system?

1.6   Structure of the Report

This PhD thesis report is organized in chapter formats, with each chapter providing the set of information and actions performed as contained in the body of the research report as follows:

Chapter One: Introduction

Chapter one of this report introduces the concept of hydrate formation, use of surfactants for hydrate formation prevention and motivation for this study. Background, stimulus prompting the study, justification, impact of the study to body of knowledge, research aim, and research objectives were discussed in the chapter.

Chapter Two: Review on biosurfactants (production, characteristics and applications) and gas hydrates and surface tension

Review of previous related investigations regarding biosurfactant, their production, characteristics, classes and applications are presented in this chapter. Arrangements of biosurfactants when introduced in an aqueous medium and at water/oil/gas boundaries, due to their amphipathic characteristics is reviewed and presented in this chapter. More so, biosurfactant producing microorganisms and production processes were identified and critically discussed in chapter two.

Gas hydrate formation is a physical surface (interphase) phenomenon involving interaction between gas molecule, as 'guest', and water molecule as ('host'). Chapter two further present a review of previous related investigations on CH_4 hydrate; formation mechanism and condition, classes, role of surface and interfacial tension in hydrate formation and various methods for surface tension measurement.

Chapter Three: Materials, experimental design and method

Chapter four outlined the techniques adopted to successfully achieve the set aim and objectives. Details of experimental procedures that were carefully followed to investigate each feature of *surfactin* and standards adopted, where necessary, are highlighted in this chapter. Additionally, sources of errors associated with each procedure/technique were also indicated. Experimental design for surface tension measurement, including software used, was further detailed in the chapter.

Chapter Four: Results and discussion

After careful implementation of experimental procedure in chapter three, data (observations) obtained for each of the characteristics investigated are presented in this chapter. These were

carefully evaluated using applicable plots and discussed accordingly. Tables of average repeatable values generated from the experiments were arranged and presented in the Appendix section of the report.

Chapter Five: Conclusion and recommendations

Evaluation of the characteristics investigated and presented in chapter five were eventually noted down in the body of the text. Consequently, these were summarily presented in chapter six as conclusions. Further research to enhance the current study were as well presented as future work.

CHAPTER TWO

2   REVIEW ON BIOSURFACTANTS, METHANE HYDRATE AND SURFACE TENSION

2.1   Chapter Overview

Surfactants are a class of either organic or inorganic molecules used as surface active agents. These molecules are classified into two categories; synthetic or chemical surfactants, which are derived from chemical processes, and biosurfactants which are derived from biological/biochemical processes. Numerous types of surfactants, and their mixtures, have been employed in the oil and gas operations, including enhanced gas recovery, drilling mud preparation, emulsion preparations, site and equipment cleaning. Traditionally, petrochemical-derived surfactants have been in use, until recently. Although these chemically derived surfactants had, for example, proven to be a promising method to recover trapped oil through IFT reduction (Jia et al., 2019) and wettability alteration (Hosseini et al., 2019). Concerns are, however, increasing on the dosage involved and the continuing damage of these chemicals on the environment. Alternatively, surfactant from biological and renewable sources (biosurfactants) are now being employed in these applications in recent time (Paraszkiewicz et al., 2018). Use of biosurfactant, including surfactin, stem from their having better characteristics, compared to chemical surfactants, in terms of toxicity, selectivity, and higher efficiency in terms of surface and interface properties (Torres et al., 2011; Zhang et al., 2015). These sterling properties of biosurfactants, and many more, are discussed in this chapter.

Therefore, chapter two (2) present an aspect of the research study report which critically reviews articles, studies and analyses relating to the authors' subject area of research. In particular, aspect relating to general overview of biosurfactants, their origins, classification, and characteristic behaviours were critically analysed. Therefore, a discussion on specific family of biosurfactant, *surfactin*, was made and presented in Section 2.4.4.

Additionally, critical review of studies conducted on gas hydrate; formation, characteristics, class/types and prevention methods were also reported. Discussion on various hydrate formation inhibition technologies will include classes of surfactants used, elaborating on both their strength and limitations. More so, review of surface tension and its relation to hydrate formation and inhibition is discussed in this chapter.

2.2 Biosurfactants

Surfactants simply refers to surface-active materials that are amphiphilic. Biosurfactants are therefore surfactants originating from different biological sources. The sources include, but not limited to, bacteria, fungi and yeasts (Santos et al., 2016). Structurally, they are diverse group of surfactant molecules which are mainly synthesized by microorganisms. As such, they exhibit broad spectrum multi-variant function. For this reason different sectors of industries employ the use of biosurfactant for different purposes including agricultural, oil and gas, food, cosmetic, biotechnological and pharmaceutical industries (Fracchia et al., 2019; Kubicki et al., 2019; Naughton et al., 2019; Varjani & Upasani, 2017). Increasing interest in the applications of biosurfactants by many industrial sectors stem from their higher competing qualities compared to chemical surfactants. These have been indicated in the reports of Silva *et al.*, (2014); Vijayakuma and Saravanan, (2015); McClements and Gumus, (2016); Santos *et al.*, (2018) to include higher biodegradability, low toxicity, better environmental compatibility and effective performance characteristics at extreme pH, temperature and salinity.

Additionally, application of biosurfactants for any purpose mediated from their amphipathic characteristics (Marchant & Banat, 2012a). Amphipathic characteristics is a situation where both hydrophobic and hydrophilic moieties (shown in Figure 2.1) are attached to one entity of biosurfactant (Liu et al., 2015). The hydrophobic moiety, often referred to as tail, is either a long-chain or hydroxy fatty acid of varying length, and the hydrophilic moiety (head) could be an amino acid, carbohydrate, phosphate, carboxylic acid, alcohol or peptide.

Hydrophobic tail
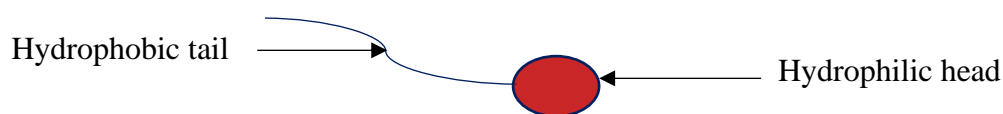
Hydrophilic head

Figure 2.1 Amphipathic assembly of biosurfactant showing hydrophilic head and hydrophobic tail (Santos et al., 2016)

Amphiphilic nature of biosurfactants offers them an affinity to adhere to gas-liquid and liquid-liquid interfaces. Once exposed to such interfaces, the surfactant molecules orient themselves so that their hydrophilic head groups are in the aqueous phase and their hydrophobic tails are in the gas phase, satisfying both ends of the molecule (Salaguer, 2002). Surfactant's molecules adsorption/orientation at gas–water interface is shown in Figure 2.2.
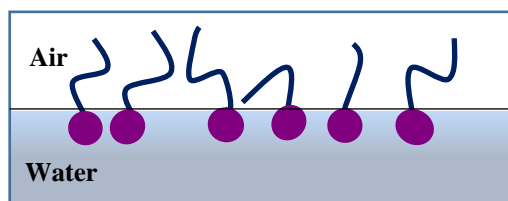
Figure 2.2 Orientation of surfactants when adhered at gas – liquid interphase

Characteristic ability of biosurfactant to orientate themselves at fluid interface enhances their potential and ability in many oil and gas operations. These include tertiary oil recovery, known as microbial enhanced oil recovery (MEOR), crude oil emulsification, wettability alteration and enhanced sweep efficiency for geological carbon (iv) oxide (CO_2) injection and storage. Details of these applications are presented in Section 2.2.5 of this report.

Despite the abilities mentioned in the last preceding paragraph, variability in the chain length and organic building molecules making up the amphiphiles results in the surfactants having variable molecular structures. Therefore, when considering the likely and potential applications of biosurfactants, emphasis on diversity of their microorganisms becomes critical. Consequently, their chemical assemblies and surface and interfacial characteristics differ. That is to say, different group of microorganism produces surfactants of different chemical structure, hence potential applications. However, surfactants belonging to same class of producing microbe exhibit same or very near characteristics.

It therefore becomes significant for the author of this report to review various sources from which biosurfactants are produced. Doing so will not only identify potential sources, but as well make analysis of biosurfactants' characteristics behaviour and identification easier.

2.2.1 Biosurfactant producing microorganisms

Biosurfactants exhibits varying characteristics, and specific superior applications. In their study, Ron and Rosenberg (Ron & Rosenberg, 2001) indicated that biosurfactants can accomplish many roles of physiological nature which include;

- emulsification of water-insoluble substrates, through increasing of surface area,
- increasing bioavailability of hydrophobic substrates,
- binding of heavy metals,
- pathogenic activity involvement,
- possession of antimicrobial activity,

This physiological performance is critical to the success of bioprocesses. However, superiority of these roles and robustness of biosurfactants is predominantly dictated by the characteristic nature of the microbes and substrate. Substrate concentration and chemical features have been reported to affect physiological properties of biosurfactants. Details of these effects are presented in Section 2.2.2.

Biosurfactants are produced from various sources, largely bacteria, yeast and fungi. Specific microorganisms, belonging to class of bacteria, fungi or yeast, have been isolated from various sources for biosurfactant production. Adopted from the work of Chen, Juang and Wei, (2015), Table 2.1 gives an overview of some biosurfactant producing microbes.

Table 2.1 Some biosurfactants and their respective producing microorganism

Biosurfactants	Origins	Reference
Rhamnolipids	*Pseudomonas* (P.) *aeruginosa, P. desmolyticum* NCIM-2112, *Achromobacter* sp, KT2440 *Marinobacter* sp. and *P. mendocina,*	(Hrůzová et al., 2019; M. Jadhav et al., 2011; Joy et al., 2019; Twigg et al., 2019)
Sophorolipids	*Starmerella bombicola, Candida bombicola, Torulopsis* species, *Trichosporon ashii*	(J. V. Jadhav et al., 2019) (Chandran, 2010; Daverey & Pakshirajan, 2010; Desai & Banat, 1997; Finnerty, 1991)
Cellobiolipids	*Ustilago cynodontis, ustilago maydis*	(Morita et al., 2008; Sandra et al., 2005)
Mannosylerythritol lipids	*Pseudozyma* species, *Candida* species, *Ustilago scitaminea*	(Fan et al., 2016; Morita et al., 2012; Niu et al., 2019; Yu et al., 2015)
Trehalose lipids	*Rhodococcus* species, *Fusarium fujikuroi,*	(Bages-Estopa et al., 2018; Reis et al., 2018; White et al., 2013)
Serrawettin	*Serratia* species	(Matsuyama et al., 2011; Su et al., 2016)
Surfactin	*Bacillus* species	(Q. Wu et al., 2019; Zhi et al., 2017a; D. Zhou et al., 2019)
Subtilisin	*Bacillus* species	(Mechri et al., 2019; Sung et al., 2010)
Viscosin, amphisin and putisolvin	*Pseudomonas* species, *Leuconostoc mesenteriods*	(Kruijt, Tran and Raaijmakers, 2009; Banat et al., 2010; Rokni-Zadeh *et al.*, 2012; Oni *et al.*, 2019)
Syringafactin	*Pseudomonas* species	(Geissler et al., 2019; Zouari et al., 2019)
Liposan	*Candida lipolytica*	(Cirigliano & Carman, 1985)
Emulsan, Biodispersan	*Acinetobacter calcoaceticus*	(P. Das et al., 2008; Finnerty, 1991; Shabtai & Gutnick, 1985)

Although protozoa and algae form important members of microbial community, reports of their utilization as biosurfactant producing microbes for oil and gas applications are scanty. This is because of difficulty, in terms of economics, in synthesizing active ingredients from them. Additionally, few of the biosurfactant-producing microorganisms are however used on an industrial scale for mass biosurfactant production. This is because maximizing yield and production comes at a great expense, in addition to downstream processing of tailoring biomolecules to specific applications (Marchant & Banat, 2012b). Nonetheless, emerging biosurfactant production technology is bridging the challenging gap, through engineered functionality production procedure (Singh et al., 2019; Wu et al., 2019; Zhang et al., 2009), enhanced production through use of gene cloning (Sekhon et al., 2011), production process optimization including kinetic study (Heryani & Putra, 2017; Sallada et al., 2019), and use of cheap agro industrial waste as substrate. Moreover, addition of solid carriers, such as activated carbon or clay was reported to increase surfactin production 36-fold higher that that without carrier (Yeh et al., 2005). Combination of these innovations have enhanced sustainable cost-effective biosurfactant production.

Section 2.2.2 presents to an aspect of the report which reviews various procedures for biosurfactant production from various sources. Specific emphasis was made of production of surfactin from various species of *Bacillus*.

2.2.2 Biosurfactant production

Legislation regarding use and disposal of chemical substances is on the rise. Additionally, dynamic nature of process industries in meeting up with market demands as well as legislation compliance is compelling. Consequently, demand for biosurfactant as a sustainable alternative is steadily increasing due to rise in environmental consciousness (Gudiña et al., 2015). Sustainable and profitable field operations require that materials withstand variable operational conditions and can be obtained at low cost. Satisfactorily, biosurfactants are competitive with synthetic surfactants in this regard. Both laboratory and field reports indicates production of biosurfactants from renewable resources and their stability at extreme environmental conditions (Gudiña et al., 2015). These sterling characteristics of biosurfactants are as result of their molecular and functional makeup. Biosurfactant fingerprint are developed during production, part of which could be deliberate to suite application. As a result, many components and unit operations are involved in biosurfactant production. In addition to producing microbes, biosurfactant can be produced from many substrates (Santos et al., 2016), which include soap stocks, whey, molasses, frying oils, oil mill effluent, starchy substrates, and corn steep liquor.

Thus far, biosurfactants have been produced employing various technology and materials. Isolates are prepared from interaction of microorganisms with nutrients sources (for growth). This include carbon source and insoluble substrate sources, such as hydrocarbons, carbohydrates, and vegetable oils (Gautam & Tyagi, 2006). Molecular interaction of producing organism with nutrients in the culture medium ensure the amphipathic characteristics of biosurfactants. However, large scale biosurfactant production remain a challenge economically, because the acquisition of substrates required for their production is at high expense. Accordingly, low-cost substrates especially from agro industrial waste are now been used for biosurfactant production (Batista et al., 2018; Cruz et al., 2018; Das & Kumar, 2018; Radzuan et al., 2017; Rane et al., 2017; Tazdait et al., 2018; Vecino et al., 2017). Furthermore, isolates from animal-based microbes is being employed biosurfactant production. However, exploring the use of plant-based sources of biosurfactant production by researchers is increasing. For instance, Adnan, et al., (Adnan et al., 2018) characterized and evaluated potential application of *Xylaria regalis,* an Endphytic fungi, as strong promoter of plant growth. In vivo testing of the biosurfactant basically resulted in significant increase in root and shoot root length of chilli seedlings. Additionally, Hussien *et al.*, (2019) indicated use of BIO-TERGE® AS-40 (coconut-based surfactant) as fracking fluid for improving shale gas production. The study further indicates that the biosurfactant reduced methane-water surface tension from about 69 mN/m to 32.49 mN/m. BIO-TERGE® AS-40 was however used as cosurfactant in the study.

In order to produce plant growth promoting traits, and as well degrade crude petroleum, Baoune *et al.*, (2018) isolated endophytic *Streptomyces* species from plants grown in contaminated sandy soil of Ouargla, southern Algeria. There is need to enhance these studies to improve not only the clean-up of crude oil–polluted environments but also soil viability for agricultural activities. Nonetheless, these studies were targeted at specific biosurfactant utilization— sustainable soil utilization after bioremediation.

Generally, biosurfactants production from various strains of microorganism is accomplished following basically the steps below;

a. identification and preparation of culture media,
b. isolation of strain of microbial strain for inoculation,
c. inoculation of strain in nutrient rich media for biosurfactant production,
d. test for yield, and identification of produced biosurfactant,
e. biosurfactant characterization and performance test.

In addition to these general stages of biosurfactant production, and depending on requirement, an additional downstream purification, and sometimes drying stages may be employed. Cost of which is the principle factor in economics of biosurfactant production. The purification, and the technique, is usually employed when shelf life, storage and ease of transport of isolated strain becomes a factor to be considered. Section 2.2.2.2 briefly describes some of the industrial scale biosurfactant purification methods used.

Likewise, different routes/methods of detecting biosurfactant production can be adopted. For example, Youssef *et al.*, (2004) compared oil spreading, drop collapse and blood agar lysis methods to detect biosurfactant production from 205 environmental strains. The authors' findings indicated that the three methods gave conflicting results. While sixteen percent of the strains tested positive using blood agar test, the same strains tested negative with the other two methods for biosurfactant production. No significant surface tension reduction was noticed with the oil spread and drop collapse methods, having values above 60 mN/m. Nevertheless, thirty eight percent of the tested strains was confirmed positive with oil spread and drop collapse methods as against blood agar lysis technique. Confirmation of biosurfactant production was validated by surface tension measurement which yielded value of about 35 mN/m. Similarly, Burch *et al.*, (2010), (2011) indicated that atomized oil assay is used to detect biosurfactant at much lower concentration compared to drop collapse assay.

Please note that the steps mentioned above are generic for all class of biosurfactants, applicable to different types of microorganism, details of which can be found in studies by Youssef *et al.*, (2004); Sekhon, Khanna and Cameotra, (2011); Gomes *et al.*, (2018); Innemanová *et al.*, (2018); Jahanbani Veshareh *et al.*, (2018); Mouafo, Mbawala and Ndjouenkeu, (2018); Teixeira Souza *et al.*, (2018).

Having the right culture media for isolation of potential biosurfactant-producing strain may be very important, but not enough to guarantee sustainable yield. That is because both nutritional and environmental factors (Guerra-Santos et al., 1986) affect the production process. These factors have been reported by Ilori, Amobi and Odocha, (2005); Franzetti *et al.*, (2009), on a broad perspective, to include incubation period, temperature, pH, salinity, type and concentrations of nutrients such as carbon, nitrogen, iron, and phosphorus. For instance, Atlas (Atlas, 1985) stated that when a major oil spill occurs in marine and freshwater environments, supply of carbon becomes increased significantly and hence availability of phosphorus and nitrogen become the limiting factor for oil degradation.

Therefore, to ensure sustainable and cost-effective biosurfactant production, the bioprocess parameters may be optimized. Different design methods and approach have been reported in bioprocess optimization for biosurfactant production. Response surface methodology and statistical methods have been used to optimize production parameters (Hema et al., 2019; Sharma et al., 2019; Vera et al., 2018). The studies suggest favourable nutrient source that increase production. Additionally, promising emerging technology/approach such as use of Artificial Neural Intelligence coupled with Genetic Algorithm and recombinant DNA technology is been tested (Jovic et al., 2019; Kandasamy et al., 2019). Various producing microbes in different nutrient sources were analysed for the bioprocess. Sustainability, efficiency and efficacy of each the process strongly relies on ability of microbe to metabolize nutrient for growth. More so, optimization studies however indicated that effect of these factors varies. Section 2.2.2.1 reviews the various factors affecting biosurfactant production process.

2.2.2.1   Factors affecting biosurfactant production process

Sensitivity of microorganisms to their growing environment as well as the surrounding environment is high. For example, *Rhamnolipids* production was reported to be influenced by two categories of factors, environmental and nutritional factors (Varjani, 2018). As a result, changes occurring in either growing or surrounding environment could potentially affect yield of biosurfactant.

2.2.2.1.1   Effect of nutrients: carbon, nitrogen and trace elements

Biosurfactant production requires appropriate condition (media) for the growth of producing-microbe. Generally biosurfactant production media contains, majorly, sources of carbon and nitrogen components, along with buffering agent such as phosphorous, phosphates, and trace of metal salts such as Mn^{3+}, Mg^{2+}, Fe^{3+}, etc. (Geetha et al., 2018a). Carbon sources may consist of carbohydrates, lipids, hydrocarbons in stand-alone or as combinations, and nitrogen sources in the form of yeast extract, nitrate salts, ammonium salts. Ali Khan *et al.*, (2017) indicated that maintaining appropriate level of nutrients is vital in improving biosurfactant production.

In their study, Antoniou *et al.*, (2015), extracted two biosurfactant-lipid mixtures; *Rhamnolipids* and *Sophorolipids,* from bacterial strains and marine hydrocarbon-degrading groups. The authors indicated that biosurfactant yield, using crude oil and molasses as carbon source, is low and remains constant. It further that the yield is independent of the carbon source, temperature and total biomass culture. However, Ramírez *et al.*, (2015) reported 191.46 mg/l and 8.78 mg/l *Rhamnolipid* optimal production respectively at 10 %(w/v) and 2 %(w/v) oil mill waste as carbon source compared to glycerol and waste frying oil. In the same study, *surfactin* production was 3.12 mg/l and 0.057 mg/l

at 2 %(w/v) and 10 %(w/v) respectively. The studies indicated that the nutrient effect is also dependent on the class of producing microbes. This is similar to those reported by Sharma, Sangwan and Kaur, (2019). Paraszkiewicz *et al.*, (2018) further confirmed the combined effect of nutrient and producing microbes when they noted, regardless of the used growth medium, KP7 strain of *Bacillus subtilis* produced more surfactin than *iturin*, while I′-1a strain overproduced *iturin* with only traces of surfactin.

While studying effect of carbon sources on biosurfactant production using strains of *Lactobacillus spp*. Mouafo, Mbawala and Ndjouenkeu, (2018) indicated that using molasses as carbon source yielded maximum of 3.03±0.09 g/l compared to glycerol which yielded 2.82±0.05 g/l. Similarly, Meena *et al.*, (2018) found that use of sorbitol (among sucrose, fructose, glucose, starch and maltose) as carbon source had highest yield of 1900 mg/l of lipopeptide biosurfactant produced from *B. velezensis*. On the other hand, in the same study, beef-extract (among ammonium sulphate, peptone, sodium nitrate, ammonium nitrate, ammonium chloride and yeast extract) had optimal lipopeptide yield of 1852 mg/l. Additionally, Anjum *et al.*, (2015) noted higher production from *Bacillus spp*. using glycerol in combination with soybean oil at 1:1 ratio as carbon source. Result was similar to that of De Franc¸a *et al.*, (2015), which indicated 1290 mg/l yield of biosurfactant using *Bacillus subtilis* ICA56.

Other constituents in the culture medium, other than source of carbon, were reported to affect yield of biosurfactant (Varjani & Upasani, 2016). For *Rhamnolipid* production by *Pseudomonas* 44T1 and *Rhodocuccus* ST-5 nitrates remains the choice for source of nitrogen when they are respectively grown on olive oil and paraffins. Similarly, production of surfactin by *Bacillus subtilis* in dissolved oxygen-depleted nitrate limited media results in very high yield (Davis et al., 1999). Addition of manganese and iron to the culture medium was reported to increase the production of biosurfactant by *Bacillus subtilis* (Wei et al., 2003). Likewise, Cruz *et al.*, (2018) noted that 5 %(v/v) of glycerol and 0.05mM of manganese was the best combination to produce biosurfactant using *Bacillus subtilis*.

2.2.2.1.2 Effect of growth conditions

Conditions of culture medium may favour or mare the growth of producing microbes. Reactor temperature, speed of agitation, amount of dissolved oxygen and pH were reported to affect yield of biosurfactant (Desai & Banat, 1997). *Candida glabrata* UCP 1002, and *Candida. batistae*, both species of the genus *Candida* had maximum biosurfactant yields respectively at pH 5.7 and pH 6.0 (Konishi et al., 2008; Sarubbo et al., 2006). Equally, Kiran *et al.*, (2009) showed that *Aspergillus ustus* produce maximum biosurfactant yield at pH 7.0. Therefore, while some producing microbes

are stable and yield better at slightly acidic pH, it becomes unfavourable for other species and yield better at neutral or alkaline pH.

Temperature is known to affect diverse bioprocesses in different ways, sometimes by the slightest change. 30 °C temperature was observed to favour optimal biosurfactant production from species of *Candida*, viz. *Candida* spp. SY16, and C. *batistae* (Kim et al., 1999; Konishi et al., 2008). However, maximum yield of biosurfactant from C. *lipolytica* occurs at 27 °C. Additionally, Meena *et al.*, (2018) noted that 30 °C temperature and pH 7 are the optimum condition for lipopeptide production from *Bacillus velezensis*. Although both conditions of temperature and pH separately affect yield of biosurfactants, optimal yield thus take into consideration combine effect of all factors.

Accordingly, growth time (incubation period) could play a significant role on biosurfactant yield. Besides, different organisms are made up of diverse molecules. As such, yield of biosurfactants from producing-microbe is likely to occur at different time intervals. Optimal biosurfactant yield by C. *bombicola* occurs between seven and eleven days (Felse et al., 2007), and 68 hours when grown in animal fat (Santa Anna et al., 2001). Besides, increasing agitation speed was shown to have increased biosurfactant accumulation by *Pseudomonas aeruginosa* UCP 0992 when grown in glycerol (Silva et al., 2010). Similarly, cultivation of P. *alcaligenes* on palm oil was found to be affected when agitation is increased from 50 – 200 rpm (Oliveira et al., 2009). This finding suggests that surface tension reduction was favoured by rotation velocity increase. The cell-free broth surface tension reduced to 27.6 mN/m. Contrary to this however, Cunha *et al.*, (2004) findings using *Serratia* spp. SVGG16 grown in a hydrocarbon culture indicates negative effect of agitation speed increase on surface tension reduction. This therefore indicates that effect of growth conditions does not only depend on the type of producing microbe but also on the growing culture medium.

2.2.2.2   Biosurfactant purification processes
Many methods are employed by different producing companies for biosurfactant purification and recovery as revealed in Table 2.2.

Table 2.2 Property-based biosurfactant recovery methods and their relative advantages, adopted from (Mukherjee et al., 2006)

Downstream recovery procedure	Biosurfactant property responsible for separation	Instrument/set-up required	Advantages
Acid precipitation	Biosurfactants become insoluble at low pH values	No set-up required	Low cost, efficient in crude biosurfactants recovery
Organic solvent extraction	Biosurfactants are soluble in organic solvents due to the presence of hydrophobic end	No set-up required	Efficient in crude biosurfactant recovery and partial purification, reusable nature
Ammonium sulphate precipitation	Salting-out of the polymeric or protein rich biosurfactant	No set-up required	Effective in isolation of certain type of polymeric biosurfactants
Centrifugation	Insoluble biosurfactants get precipitated because of centrifugal force	Centrifuge required	Reusable, effective in crude biosurfactants recovery
Foam fractionation	Biosurfactants, due to surface activity, form and partition into foam	Specially designed bioreactors that facilitate foam recovery during fermentation	Useful in continuous recovery procedures, high purity of product
Membrane ultrafiltration	Biosurfactants form micelles above their CMC which are trapped by polymeric membranes	Ultrafiltration units with porous polymer membrane	Fast, one-step recovery, high level of purity
Adsorption on polystyrene resin	Biosurfactants are adsorbed on polymer resins and subsequently desorbed with organic solvents	Polystyrene resin packed in glass columns	Fast, one-step recovery, high level of purity, reusability
Adsorption on wood-activated carbon	Biosurfactants are adsorbed on activated carbon and can be desorbed using organic solvent	No setup required, can be added to culture broth, can also be packed in glass columns	biosurfactants, cheaper, reusability, recovery from continuous culture
Ion-exchange chromatography	Charged biosurfactants are attached to ion-exchange resins and can be eluted with proper buffer	Ion-exchange resins packed in columns	High purity, reusability, fast recovery
Solvent extraction (using Methyl tertiary-butyl ether)	Biosurfactants dissolve in organic solvents owing to the hydrophobic ends in the molecule	No set-up required	Less toxic than conventional solvents, reusable and cheap

2.2.3 Physicochemical characteristics of biosurfactant

The uniqueness and superiority of biosurfactants, for various commercial applications, over synthetic surfactants are because of their distinct characteristics. These distinguishing characteristics of biosurfactants are linked to their low toxicity, biodegradability, tensioactive capability, stability at different pH, ionic strength and temperature (Chakrabarti, 2012) among others. Moreover, Belhaj *et al.*, (2019) in their review indicated that surfactant adsorption during EOR is dependent on many factors. These include surfactant type, surfactant dosage, ionic strength, pH, salinity, and temperature. The key characteristic features of biosurfactants are discussed in Section 2.2.3.

2.2.3.1 Biodegradability

The ease of interaction of biosurfactant with degrading microorganism makes them biodegradable (Gregorich et al., 2015). Moreover, studies showed that, compared to synthetic surfactants, range of toxicity effects of biosurfactant are less (Shah et al., 2016). Likewise, biosurfactants degrades at faster rate when disposed in comparison to synthetic surfactants such as sodium dodecyl sulphate (SDS). In support of this, Lima *et al.*, (2011), noted that much lesser CO_2 was released when bacterial culture in soil microcosms is mixed with SDS compared to those containing biosurfactants. Intensity of the SDS degradation was about 10 times lower than that of biosurfactant degradation by *Pseudomonas* sp. LBBMA $_{101}$B.

Similarly, test on ease of *sophorolipids* (produced by yeast *Candida bombicola*) biodegradability showed that the biosurfactants starts degrading immediately after cultivation. Additionally, the biodegradability, after 8 days of cultivation was able to reach 61 % (Klosowska-Chomiczewsca et al., 2009). Likewise, (Hirata et al., 2009) noted that s*urfactin* and *arthrofactin* exhibited related biodegradability behaviour as *sophorolipids*.

Environmental and aerating conditions may affect rate of biodegradability behaviour. On this note Mohan, Nakhla and Yanful, (2006) showed that *rhamnolipid* biosurfactants are capable degrading under both anaerobic and aerobic environments. Efficiency of soluble chemical oxygen demand removal COD) was 74 % after 10 days and decreased to 47.2 % after 6 days. On the other hand, same study indicated that under anaerobic conditions Triton X-100 (a chemical surfactant) is non-biodegradable. However, it partially biodegrades under aerated experimental conditions (soluble COD removal efficiency of 47.1 % after 10 days at concentrations below 900 mg/L).

2.2.3.2 Temperature, pH and ionic strength stability

Considering the various operational fields of biosurfactants applications; pharmaceutical, cosmetics, food and agro industries and oil and gas, one may infer of their stability in different conditions. Besides, it was indicated that biosurfactants are mostly stable at varying conditions of pH, temperature, and salinity (Ben Ayed et al., 2014). In addition, continued interest in utilising biosurfactants is an affirmation of their characteristic functions are rarely altered by changes in operating parameters.

Studies by Mouafi, Abo Elsoud and Moharam, (2016) indicated that biosurfactant produced by *Bacillus brevis* is thermally stable in the range of 30 – 80 °C and at pH 4 to 9. Moreover, Ben Ayed *et al.*, (2014) noted diesel solubilisation and emulsification index of biosurfactant produced by *Bacillus mojavensis* was optimal at 60 °C (pH 6 —10) and 20 – 80 °C (pH 6). These suggest that the biosurfactant can be used in environment of extreme condition similar to that of oil and gas industry. By measure of surface tension and emulsification index (after 24 hours), (Zhang et al., 2016) indicated that biosurfactant produced by *Bacillus atrophaeus* 5-2a is stable at conditions of pH 6-13, 20-120 °C and salinity up to 15 %. Similar stability was exhibited by non-*Bacillus* sp. producing microbes. Stability of biosurfactants produced by *Cryptococcus strain YLF* and *Wickerhamomyces anomalus* CCMA 0358 were respectively studied by Derguine-Mecheri *et al.*, (2017); Teixeira Souza *et al.*, (2018). The authors both noted stability of the biosurfactants produced at conditions of 100 °C, pH 12 and 10 % NaCl salinity. Chen *et al.*, (2018) further indicated that biosurfactant produced by *Pseudomonas aeruginosa* is stable at 20 – 100 °C temperature, 6 – 12 pH, and salinity of 2 – 20 w/v%. These data are indications that biosurfactants are stable at near-neutral to basic pH, an average of 20 – 80 °C and average salinity up to 15 %. This is unlike synthetic surfactants which was indicated by Santos *et al.*, (2016) to become inactive above 2 % NaCl concentration.

It is worth noting that produced biosurfactants mentioned are harvested isolates of the microbes. Dissolution of the biosurfactants, after purification and drying, may be affected by NaCl concentration above 0.5 Molarity (M), as indicated in study by Salihu *et al.*, (2018). Fouling of, and scale formation on operational equipments are possible consequence of partial dissolution of surfactants generally.

2.2.3.3 Critical micelle concentration (CMC)

Behaviour of surfactants at an interface is determined by their concentration in the bulk solution. As the bulk surfactant concentration is increased the number of surfactant molecules adsorbed to the interface rises, causing the surface activity to fall in a concentration dependent manner. However,

there is a limit to the number of surfactant molecules that can adsorb to a surface before saturation level is reached, leaving no 'room' for further rearrangement of surfactant molecules. The surfactant concentration at which this saturation level is reached is termed critical micelle concentration (CMC) (Drew, 2006; Krister et al., 2003). At this point the surface activity is at minimum. Further addition of surfactant molecules does not significantly alter the surface activity because no more adsorption to the surface can occur. Instead increasing the concentration of surfactant in the bulk leads to self-assembly of the surfactant molecules, which aggregate into various types of structure (micelles) depending on concentration and the specific properties of the surfactant. Campos *et al.*, (2013) noted this point to be the point at which lowest stable surface tension is achieved. Figure 2.3 shows the general relationship between surfactant surface coverage and surface activity (surface/interfacial tension). When the CMC is reached the surface becomes fully covered with a monolayer of surfactant molecules and further increasing the surfactant concentration leads to aggregation and the formation of micelles in the bulk solution.
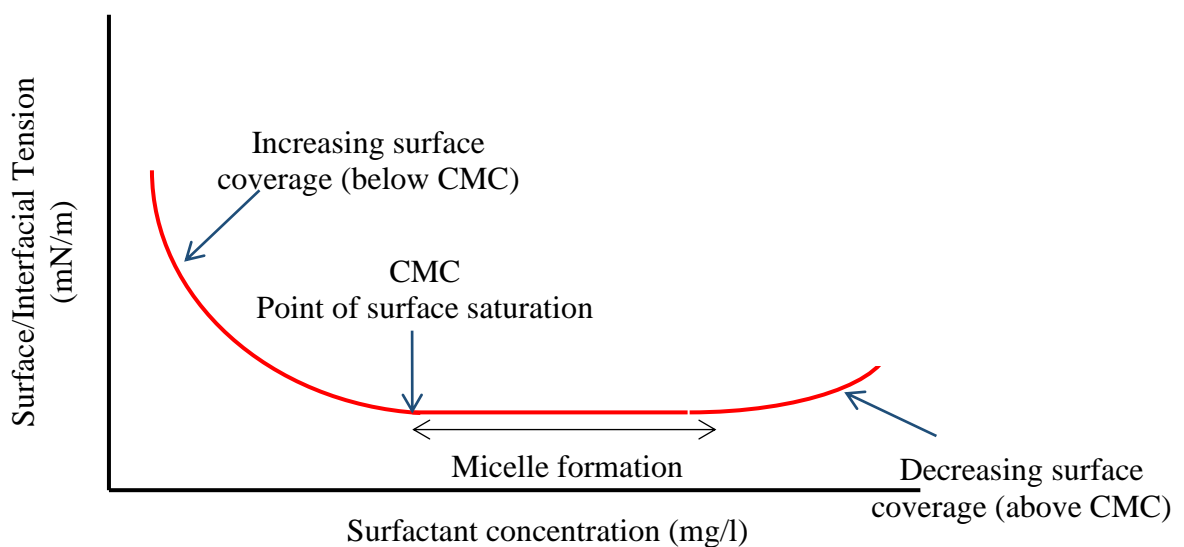
Figure 2.3 Effect of surfactant concentration at below, and above CMC, modified from (Santos et al., 2016)

The aggregation of surfactants in solution leading to formation of micelles is known as micellization. Figure 2.4 shows sequence of activities on introduction of surfactant in aqueous surfactant into air – water system, leading to formation of micelles above CMC.
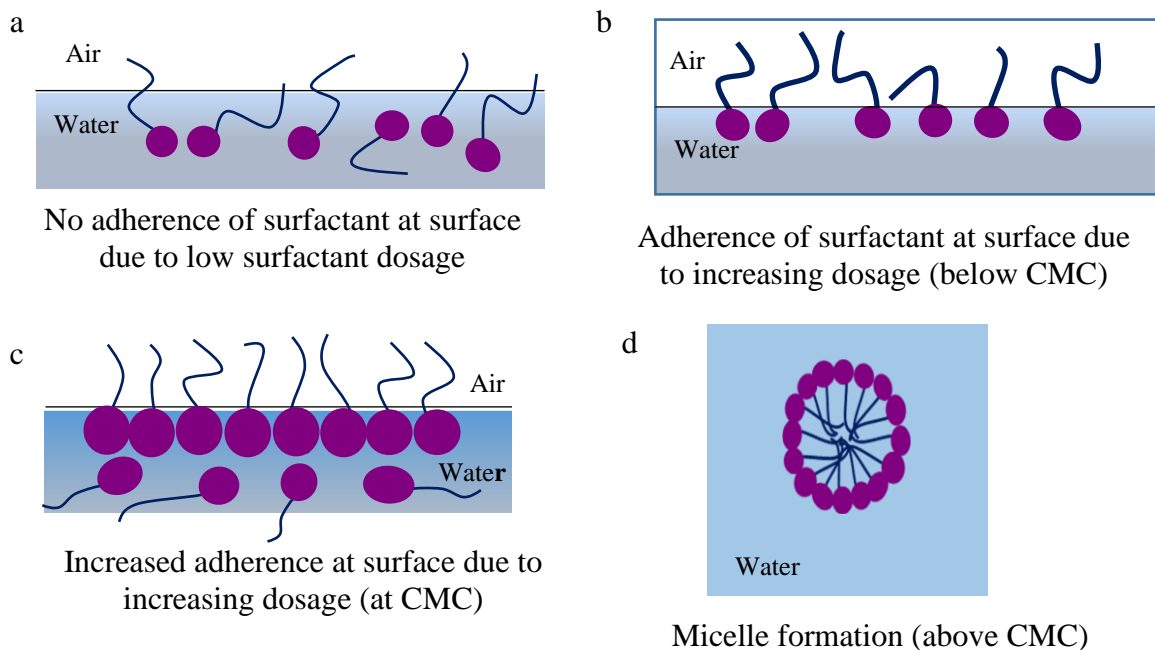
Figure 2.4 Sequence of surfactant activities in aqueous solution leading to micellization

Surfactants generally display varying CMC, depending on their molecular architecture. However, as a characteristic that significantly influenced their tensioactive property. Biosurfactants have very low CMC compared to surfactants from chemical processes. Gargouri *et al.*, (2017) reported biosurfactants' CMC to be 10 to 40 times lower than synthetic surfactants. Having a low CMC ensures that maximum efficiency is achieved using low surfactant dosage. That is why researchers (Yanagisawa et al., 2018) are devising means of reducing surfactants' CMC.

2.2.3.4   Rheological characteristics

Fluids rheology deals with the science of how fluids behave when they become exposed to any form of applied force. These could be in the form of applied stress or stress resulting from changes in pressure. For example, in oil and gas industry operations where mass transport are principally through pipelines, the form of stress process fluids becomes exposed to are in the form of pressure (Kumaran, 2010). Combined with impact of other process variables such as temperature and salt concentration, effect of pressure on fluids flow could be critical. Flow failure and/or aggregation may be one of the consequences.

Biosurfactants are materials that composed of highly complex structures. They formed molecular interactions of various complex organic molecules at a molecular level. Hence, they exhibit specific properties and functionalities, either in aqueous or saline medium. These structures could be bound

24

by weak forces, causing them to be easily deformed by an applied force. However, biosurfactant molecules can form highly organized structures through spontaneous self-assembly. Biosurfactant plays a critical role in many processes that impact on human lives. In upstream oil and gas operations, biosurfactants are critical in secondary/and or tertiary recovery of oil and gas. Similarly, downstream operations rely on surfactants during production post-production activities such as equipment clean up. Flow behaviour of biosurfactants during these operations are critical to their performance in achieving efficiency.

Characterization of fluids behaviour could be done in terms of shear stress – shear rate behaviour or viscosity – shear rate responses. While stress – rate characterization defines the flow behaviour (see Figure 2.5), viscosity – rate characterization defines the fluids viscosity response to rate of shear.
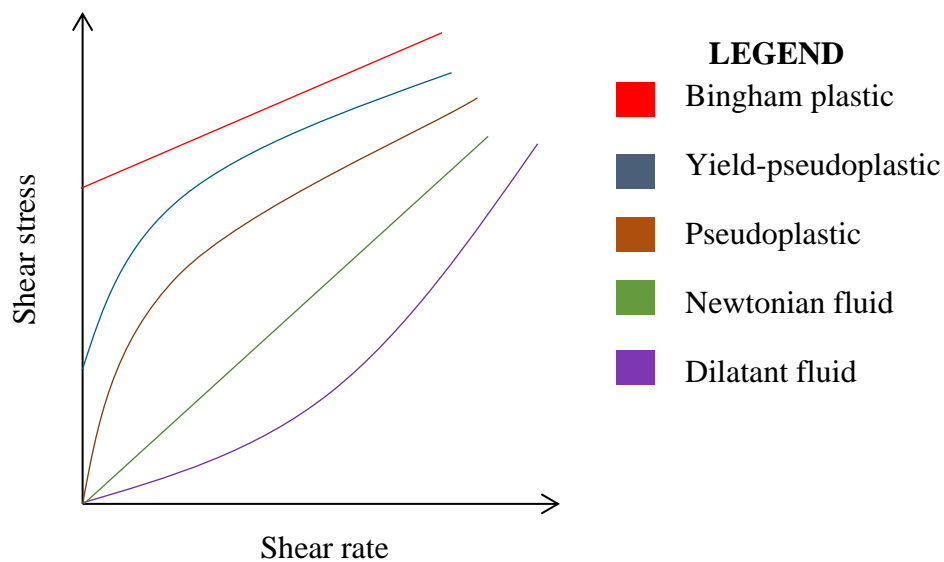
Figure 2.5 Shear stress – shear rate behaviour of fluid flow (Chhabra, 2010)

Viscosity – shear rate response of fluid behaviour, for non-Newtonian fluids, is shown in Figure 2.6.

25
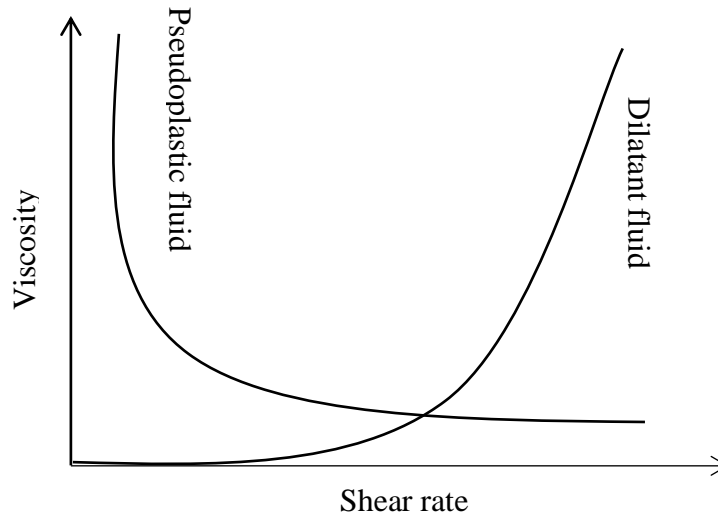
Figure 2.6 Viscosity – shear rate behaviour of non-Newtonian fluids (Kumaran, 2010)

Detail studies on rheological characteristic behaviour of biosurfactant are still scarcely reported, particularly that of surfactin. Available studies have however noted biosurfactant behaviour to be pseudoplastic. For instance, de Oliveira, Amaral and Burkert, (2018) noted that *exopolysaccharide* EPS-M816 produced by *Mesorhizobium loti,* exhibited pseudoplastic non-Newtonian fluid behaviour at 1.0 w/v%. Similarly, studies by Maalej *et al.*, (2016); Castellane *et al.*, (2017) showed that viscosity of biosurfactants produced from *Rhizobium tropici* and *Pseudomonas stutzeri* AS22 respectively decreases concomitantly with increase in shear rate. This led to the biomolecules exhibiting shear-thinning fluid behaviour.

Various approach is adopted for characterizing biomolecules depending on the intended application. For oil and gas application, for instance, interaction of working fluids with formation water (which is saline) is very common. More so, fluctuations in operating parameters, either deliberate or otherwise, is associated with oil and gas process such hydrate-formation control. As such, to sustain efficient performance of working fluid, their interactions with saline environment and fluctuations in operational variables should not affect their physical or chemical makeup. Consequently, flow behaviour study of biosurfactant under variable temperature and salt concentration will be helpful in evaluating their resilience in these conditions. While temperature may influence hydrophobic effect in terms of molecular average kinetic energy, salt effect influences electrostatic coalescence or repulsion. Study on effect of temperature and salt concentration on rheology of *surfactin* was presented by Salihu *et al.*, (2019). Similarly, Machale *et al.*, (2019) indicated that addition of 1 wt% biosurfactant synthesized from water *hyacinth* was able to improve rheology 0.5 wt% Xanthan gum polymer for EOR. In the same study, addition of the biosurfactant was shown to be thermally stable

26

by stabilizing xanthan gum polymer at different temperatures. This study affirms thermal stability of biosurfactants and their suitability in different conditions.

2.2.3.5   Surface and interface activity

Sustainable proficiency and effectiveness are generally indispensable characteristics of a good surfactant. CMC is a measure of surfactant proficiency, while its efficiency is associated to surface activity, particularly interfacial and surface tensions (Barros et al., 2007). Biosurfactant's CMC is in the range of 1 to 2000 mg/L, whereas oil/water interfacial and surface tensions are approximately 1 and 30 mN/m respectively (Santos et al., 2016). Sub-sections 2.2.3.5.1 and 2.2.3.5.2 discuss the surface activity of biosurfactants.

2.2.3.5.1   Emulsification characteristics

Biosurfactants are identified for their outstanding surface performance activity involving formation and stabilization of emulsions. When in solution, biosurfactant confer on fluids surface/interface by adhering unto the surface (Uzoigwe et al., 2015), consequently enhancing dispersion of droplets of one liquid into an immiscible liquid. Mixing of the two immiscible liquids, through dispersion, is referred to emulsification (Maurya & Mandal, 2018). However, the droplets in some mixtures coalesce to create an unstable emulsion. As a result, emulsifiers, such as surfactants are required to provide resistance to the droplets coalescing, and consequently ensure emulsion stability. Biosurfactants have been reported to have both emulsifying and demulsifying features. Emulsification capability of biosurfactants are measured in terms of their emulsifying index (E_{24}), usually assessed after twenty four hours, as noted by Kanmani *et al.*, 2017; Akshatha *et al.*, (2018). Equation (2.1) defines how emulsification index is calculated.

$$E_{24}(\%) = \frac{Height\ of\ emulsion\ layer}{Total\ height\ of\ liquid} \times 100 \qquad (2.1)$$

Different strains of biosurfactant producing-microbes exhibits variable index of emulsification. Kanmani *et al.*, (2017) indicated 54.79 % emulsification activity of biosurfactant produced from *Bacillus* sp. using crude oil. Similarly, (Ndlovu et al., 2016) showed that bacteria isolates from waste water were able emulsify diesel, kerosene and mineral oil at 90, 77 and 29.7 % respectively. This finding suggests that the emulsifying activity depends on the complexity of the hydrocarbon molecule. Study by (Shavandi et al., 2011) validate this assertion. In their findings, *Rhodococcus* sp. strain TA6 emulsifies n-pentane, kerosene, n-Heptane, Toluene, n-hexadecane, gas oil, motor

oil and light crude oil at variable index. Motor oil was emulsified at index of about 80% and light crude oil at about only 10%.

External factors were reported to have considerable effect on emulsification index of biosurfactants. Long *et al.*, (2017) indicated that surfactin biosurfactant was able to emulsify crude oil up to 98 % at pH 11. However, the index was completely lost when pH was reduced to strongly acidic level (3.0). Biosurfactants were shown in section 2.2.3.2 to be stable in the pH range of 6—12. The sensitivity is, although, dependent on the type of producing-microbe. Contrary to Long *et al.*, (2017) reports, Gargouri *et al.*, (2017) noted that emulsification activity of *Stenotrophomonas* biosurfactant B-2 was stable at pH range of 2—6.

2.2.3.5.2   Surface/interfacial tension reduction

Inclusive of the measure of effectiveness of biosurfactants is their extent to which they reduce surface and interfacial tensions to lowest minimum value. On this note, Mulligan, (2005) noted that good surfactants reduces oil-water interfacial tension from 72 to 35 mN/m, and n-hexadecane IFT from 40 to 1 mN/m. However, (Shaligram & Singhal, 2010) indicated that *surfactin* isolated from strain of *Bacillus subtilis* is able to reduce water surface tension from 72 to 27 mN/m. Study by Jahanbani Veshareh *et al.*, (2018) showed isolates of *Bacillus subtilis* MJ01 reduced surface tension of distil water to 29 mN/m. Similar results were presented by Pereira *et al.*, (2013); Wang *et al.*, (2018) for both *surfactin* product and its isoform (C_{13}, C_{14}, and C_{15} isoforms).

Unlike biosurfactants, synthetic surfactants were reported to have less tensioactive effect on some systems. For example, Urum and Pekdemir, (2004) reported decrease in interfacial tension of Ekofisk crude oil-water system by SDS (7.0 mN/m), *lecithin* (5.0 mN/m), *rhamnolipid* (4.5mN/m), *saponin* (6.0 mN/m) and *tannin* (4.5 mN/m). Similarly, Pereira *et al.*, (2013) compared surface activity of three isolate strains of *Bacillus subtilis*, in terms of crude oil recovery, with synthetic surfactants (Enordet and Petrostep). The authors found that use of biosurfactant strains recovered more oil compared to the synthetic surfactants.

The variations in the physicochemical characteristics exhibited by biosurfactants, as discussed in Section 2.2.3, indicates differences in their complexes. As such, biosurfactants of same or similar complexes exhibits analogous features hence their classification. Therefore, Section 2.2.4 will present to the reader of this report different classes of biosurfactants.

2.2.4 Classification of biosurfactants

Biosurfactants are primarily classified based on their chemical complexes and microbial origin. This is unlike their chemically synthesized counterpart whose classification are based on their functional group polarity (Muthusamy et al., 2008; Vijayakuma & Saravanan, 2015). Additionally, Karlapudi *et al.*, (2018) indicated that biosurfactants are classified, based on molecular weight, into two; low, and high molecular weight compounds. The low molecular weight class of surfactants are efficient in lowering interfacial and surface tension, while high molecular weight, such as biopolymer, are efficiently used as stabilizing and emulsifying agents. *Surfactin*, *rhamnolipids*, *iturin* and *sophorolipids* are examples of low molecular weight biomolecules while *emulsan*, *mannoproteins* are examples of high molecular weight biomolecules

Depending on the chemical composition, Karanth, Deo and Veenanadig, (1999) classified biosurfactants into glycolipids, phospholipids (fatty acids), polymeric, particulate and lipopeptide (lipoproteins). These classes are summarily discussed in the subsections below.

2.2.4.1 Glycolipids

Glycolipids class of lipids biomolecule which are important in the bioprocess industries. They are the most known biosurfactants (Muthusamy et al., 2008). Glycolipids belongs to a class of carbohydrates attached to fatty acids chain. The attachment is by means of an ester group or ether. *Sophorolipids, rhamnolipids, cellobiolipid, Mannosylerythritol lipids, Trehalose lipids* are examples of glycolipid biosurfactants. However, the most commonly known of this class are *rhamnolipids*, *trehalolipids* and *sophorolipids* (Rikalović et al., 2015). Characteristics of each of these class are summarized as follows.

2.2.4.1.1 Rhamnolipids

These are class of glycolipids that consist of either one or two (l)-rhamnose molecules linked to glycosidic β-hydroxy fatty acids (Chong & Li, 2017; Nickzad & Deziel, 2016). The rhamnose molecule make up the hydrophilic head while β-hydroxy fatty acids make up the hydrophobic tail of the surfactant. Rhamnolipids biosurfactants can be produced from various species *Pseudomonas*, details of which is presented in Table 2.1. Many industrial applications of *rhamnolipids* have been reported. These include EOR, bioremediation of soil, dispersant in pesticides, foaming and wetting agent, and anticancer agent. Figure 2.7 indicates *rhamnolipid* chemical structure.
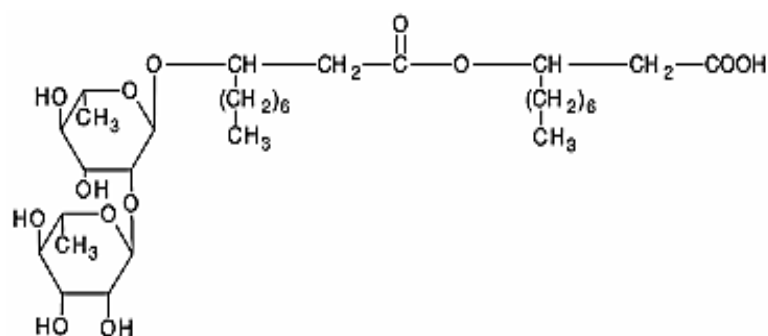
Figure 2.7 Structure of rhamnolipid (Abdel-Mawgoud & Stephanopoulos, 2018)

2.2.4.1.2 Trehalose lipids

Trehalose, shown in Figure 2.8, is a form of glycolipid consisting of disaccharide sugar attached to long chain fatty acids of mycolic acid at the 6th position of trehalose carbon backbone (Karlapudi et al., 2018). Size and structure of the mycolic acid vary from one organism to another. *Arthrobacter sp.* and *Rhodococcus erythropolis* produce trehalose lipids that effectively reduces interfacial and surface tension in the growth medium (Sharma et al., 2016). Like Rhamnolipids, Trehalose lipids have wide applications including medical and bioremediation.
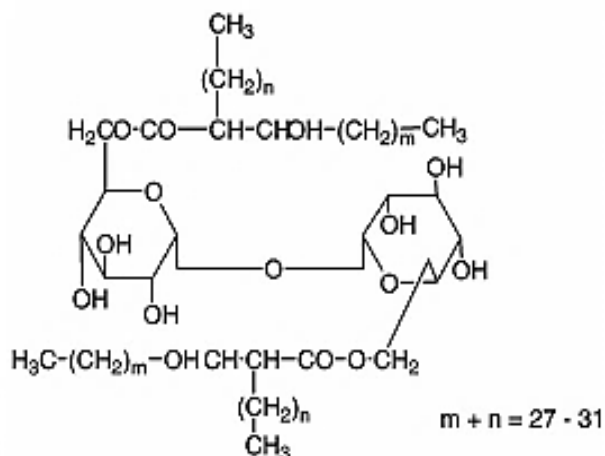
Figure 2.8 Structure of trehalose lipids (Muthusamy et al., 2008)

2.2.4.1.3 Sophorolipids

Primarily, sophorolipids are produced by yeast including *Torulopsis bombicola* (Cooper & Paddock, 1984)*, T. petrophilum* and *T. apicola.* They consist of a dimeric carbohydrate (disaccharide) *sophorose* linked to a long chain hydroxyl fatty acid. These biosurfactants are a combination of 6 to 9 different hydrophobic sophorolipids (Muthusamy et al., 2008). Sophorolipids generally occur as a mixture of free acid form and macrolactones (see Figure 2.9).
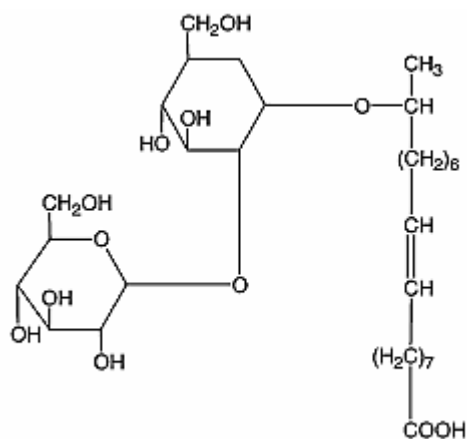
Figure 2.9 Structure of free-acid form of sophorolipids (Muthusamy et al., 2008)

2.2.4.2 Phospholipids and fatty acids

Phospholipids and fatty acid biosurfactants are synthesized by numerous forms of bacteria and yeast particularly when grown on a medium rich in n-alkane. *Acinetobacter* sp. produces rich vesicles of phosphatidylethanolamine which form microemulsions that are clear in water. *Rhodococcus erythropolis* produce phosphatidylethanolamine when grown on n-alkane (Helfrich et al., 2015). Phosphatidylcholine is commonly occurring phospholipids, whose structure is given in Figure 2.10.
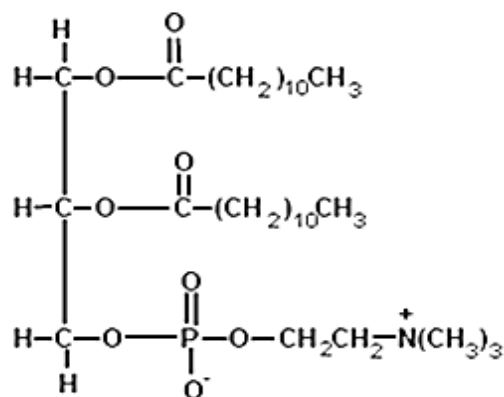
Figure 2.10 Structure of *Phosphatidylcholine*, a *phospholipid* (Korathar, 2018)

2.2.4.3 Polymeric biosurfactants

These are high molecular weight biomolecule used as surface active agents. The unsurpassed polymeric biosurfactants studied include *liposan*, *emulsan*, *liposan*, *lipomannan, alasan,* and other polysaccharide–protein complexes (Muthusamy et al., 2008; Santos et al., 2016). Additionally, at very low surfactant dosage of 0.001 to 0.01 %, e*mulsan* can effectively emulsify hydrocarbons molecules in water (Zosim et al., 1982). Polymeric biomolecules can be synthesized from different organisms including *acinetobacter calcoaceticus* RAG-1 and *Candida lypolytica*.

2.2.4.4   Lipopeptide and lipoproteins

These classes of biosurfactants generally consists of many cyclic lipopeptides linked to a fatty acid. Biosurfactants in this class include *serrawettin*, surfactin/iturin/fengycin, and Lychenysin. Numerous bacteria have been used for the isolation and production lipopeptide molecules. Predominantly the cyclic lipopeptide, *surfactin*, produced by *Bacillus subtilis*, stand to be among the most active and effective biosurfactants (Ron & Rosenberg, 2001). More so, *surfactin* is made of seven ring structure of amino acids, joined to fatty acid chain by a lactone linkage. It was reported by (Nguyen & Götz, 2016) that surfactin can reduce surface tension below 28 mN/m.

Surfactin (shown in Figure 2.11) is synthesized from different *Bacillus* strains, apart from *Bacillus subtilis*. These include *Bacillus pumilus* (Nieminen et al., 2007), *Bacillus mojavensis* (From et al., 2007), *Bacillus licheniformis* (Liu et al., 2016b; Pecci et al., 2010), *Bacillus atrophaeus* (J. Zhang et al., 2016) and *Bacillus amyloliquefaciens* (Nam et al., 2016; Zhi et al., 2017b). However, strains of *Bacillus subtilis* remains the most widely utilized isolates for *surfactin* production.

Moreover, Perfumo, Banat and Marchant, (2018) indicated in their review that biosurfactant of *Bacillus* sp. origin can be produced from very low-temperature (4─32 °C) environment. This indicates that *surfactin* may be utilized in low-temperature operations. Gas hydrate phenomenon occurs and is favoured by low temperature region. Therefore, surfactants for the prevention of hydrate must maintain its effectiveness (withstand) in low temperature conditions.
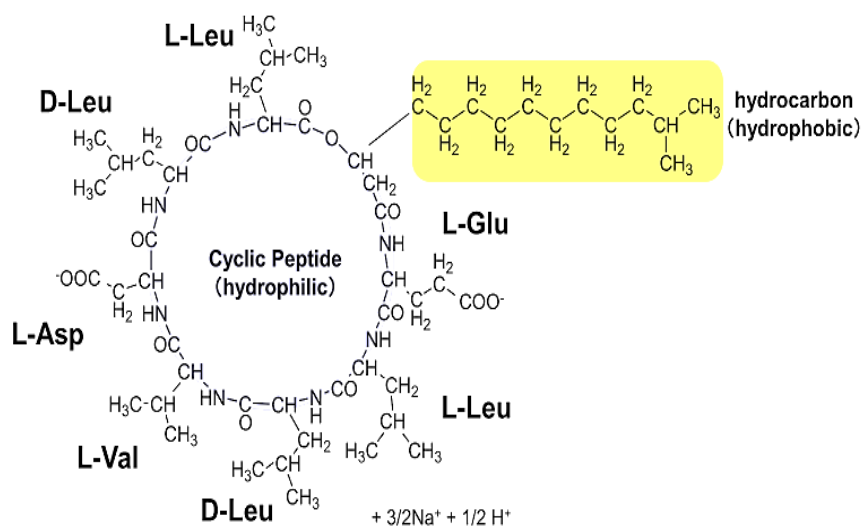
Figure 2.11 Structure of surfactin adopted from (Kaneka, 2017)

Reader may recall that surfactin is the biosurfactant of interest in this study, whose characteristics performance feature has been improved through increased alkalinity with sodium. Consequently, the biosurfactant bears the name 'sodium *surfactin'*.

Section 2.2.4.5 summarily describe the properties and potentials of sodium *surfactin* as biosurfactant and its choice for this study.

2.2.4.5 Sodium surfactin

Sodium *surfactin* (branded as Kaneka surfactin) as define in the preceding section belongs to the lipopeptide class of biosurfactants. It is a cyclic biosurfactant produced by a non-pathogenic bacterium, *Bacillus subtilis*, through fermentation process. The biosurfactant displays distinctive characteristics resulting from its cyclic structure consisting of seven (7) amino acids. Due to the cyclic structure, Kaneka *surfactin* is able to function effectively at low surfactant dosage of 3 ppm (Kaneka, 2017). Besides, performance of some chemical surfactants such as linear alkylbenzene sulfonate (LAS) and SDS shows multiplying effect improvement when in synergy with *surfactin*.

Accompanying brochure indicates that sodium *surfactin* is distributed as white powder, soluble in aqueous solvents. However, forms precipitate at acidic pH or with alkaline earth metal ions such as Mg^{2+}, Ca^{2+}. The surfactant was initially produced in 2001 as cosmetic ingredient. However, its potential application and effective performance in other areas, particularly in enhanced oil recovery (EOR), has been tested (Saito et al., 2016), details of which is discussed in Section 2.2.5. Similarly,

Park *et al.*, (2017) investigated effectiveness of *surfactin* on CO_2/water system and indicated that *surfactin* effectively reduces CO_2/water surface tension. These examples show that; surfactin has been tested in oil and gas field, and that it is effective for gas/water system. However, characteristics of CO_2 differs from that of CH_4, particularly its density, hence the need for further evaluation of the surfactant.

2.2.5 Biosurfactant applications

Industry operators, in recent years, are becoming critical of the most widely used chemically synthesized surfactant. Instead, biosurfactants are increasing being tested in every aspect of industrial process. This is due to their broad range of functionality and various abilities. Most important of these features is being environmentally friendly, for their ease of biodegradation and low toxicity than synthetic surfactants. Additionally, owing to their natural origin and environmental compatibility, biosurfactants use has been applied in many industries. These include food, agriculture, pharmaceutical and biomedical, cosmetic, environmental and oil and gas.

Review study conducted by Bezerra *et al.*, (2018) indicated use of *saponins* as formulating agents in cosmetic products, such as shampoos. Adopting metal-biosurfactant complexes formation, Singh, Glick and Rathore, (2018) noted that biosurfactant can be employed to make nutrients available to plants via soil solubilization and mobilization. Biosurfactant has also been utilized in environmental bioremediation of hydrocarbon spill and disposal. Biodegradation of diesel-contaminated water was enhanced through the use *rhamnolipid* and *surfactin* (Whang et al., 2008). Addition of 40mg/l of *surfactin* increased diesel biodegradation by 94%, whereas addition of *rhamnolipid* up to 80mg/l increased diesel degradation up to 100%. Soil fertility and environmental clean-up has also been reported through bioremediation of soil contaminated due to oil spill or disposal. Dadrasnia and Ismail (Dadrasnia & Ismail, 2015) indicated 71.5% lubricating oil degradation in 20 days using biosurfactant from *Bacillus salmalaya*. Similarly, (Liu et al., 2016a; Marti et al., 2014; Sharma et al., 2018; de Silva et al., 2014) have also reported significant biodegradation and bioremediation of soil contaminated due to oil spill. These applications are in addition to the use biosurfactants in enhanced oil recovery (EOR), known as microbial (MEOR). MEOR is effective through many techniques including surface and IFT reduction, reducing the viscosity of heavy oil by biodegradation, selective plugging of highly porous rocks, wettability alterations, and oil/water or water/oil emulsion formation (Joshi et al., 2016). Two isolates of *Bacillus amyloliquefaciens* SAS-1 and *Bacillus subtilis* BR-15 accounted, respectively, for 56.91 ± 1.52 and 66.31 ± 2.32% EOR in sand packed column (Sharma et al., 2018). Similarly, (Al-Bahry et al., 2013; Fernandes et al., 2016;

Liu et al., 2014; Pereira et al., 2013; Saito et al., 2016; Zhao & Wen, 2017) noted potential application of biosurfactant produced from *Bacillus* sp. for EOR.

Efficiency of biosurfactant from *Bacullus subtilis* strain for residual oil recovery was enhanced from 30 % (100 % biosurfactant) to about 48% when mixed with 25 % chemical surfactant in the ratio 75:25 (Al-Sulaimani et al., 2012). Finding in this study indicates the possibility of synergy between biosurfactants and synthetic surfactants. Similar findings were also reported by (Al-Wahaibi et al., 2016), where efficiency increased to 34 % at 50:50 surfactant ratio. The synergy could reduce the potential environmental effect synthetic surfactants. Experimental studies to ascertain this effect will be an addition to the field of biosurfactant utilization.

As one of the promising methodologies for geological carbon storage, injection and storage of CO_2 has been recently enhanced through understanding of mechanism of wettability alteration by biosurfactant, *surfactin*. In their study, Park *et al.*, (2017) investigates effect of *surfactin* on CO_2/water/quartz systems IFT reduction and contact angle alteration, under a laboratory setup simulating *in situ* reservoir conditions. Their findings revealed that surfactin was able reduce CO_2-brine ST by; 39 % for gaseous CO_2, 54 % for liquid CO_2, and 43 % for supercritical CO_2. The finding in the study further suggest that technique of geological CO_2 storage can be enhanced through biostimulation with biosurfactant, either by *in situ* production or *ex situ* (through injection).

2.3   Gas (Methane) Hydrate Formation and Structures

Blockage of gas pipelines were revealed, by field operators, to be due to presence of ice-like solid structures deposited in the pipeline, particularly at permafrost regions. Consequently, seamless flow assurance of gas became difficult. Studies were then conducted to identify and determine the cause of the ice-like structure. Therefore, in 1934, Hammerschmidt discovered that the solid structure is indeed not of ice but hydrate of transported gas (Hammerschmidt, 1934; Makogon et al., 2007). Decades after this discovery, the subject and occurrence of gas pipeline plugging as a result of gas hydrates remains a critical concern particularly in the gas industry. This is due to potential threats to production equipment, personnel and the significant economics associated with gas hydrate control and cleaning.

Gas hydrates, depending on the intended application, could have both beneficial and hazardous consequences. For instance, *in situ* natural gas hydrates commonly originating in permafrost regions and underneath ocean bed could be emerging potential energy resources (Qin et al., 2016). Contrary

to this, however, existence of gas hydrates in oil and gas pipelines, production and/or transport equipment leaves an undesirable consequence, such as plugging (Sloan, 2003). Field experience indicates that unplugging and eventual cleaning of pipelines is done at great economic expense.

2.3.1 Formation of gas hydrates

Gas hydrates are ice-like, non-stoichiometric crystalline substances comprising of suitable gas molecule, such as CH_4, enveloped by water (H_2O) molecule under equilibrium temperature and pressure condition (Palodkar & Jana, 2017; Sloan & Koh, 2008). The water molecule (being *host*) forms a cage-like hydrogen-bonded structure which physically envelopes the *guest* gas molecules (see Figure 2.12). To prevent the cage-like structure from collapsing, the enveloped gas molecules exert a multi-directional force (Sloan, 2003). This sort of interaction by host-guest causes gas hydrates to become thermodynamically stable. Therefore, hydrates are formed when suitable amounts of water and gas molecules exist, typically at low temperatures and high pressures (Zerpa et al., 2011). Moreover, the interface allying *host* and *guest* phases in hydrocarbon production systems constitute a perfect site for gas hydrate formation.
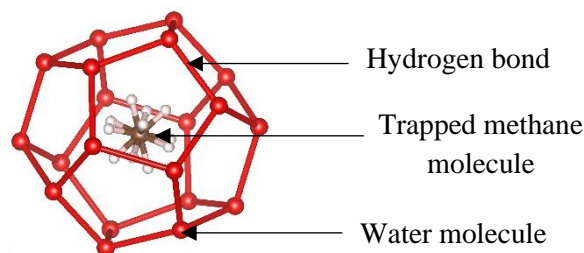
Figure 2.12 Illustration of trapped methane molecule surrounded by water molecules, modified from (Crystallography365, 2014)

However, notwithstanding the favourable thermodynamic equilibrium conditions at the gas-water interface, many other complimentary factors significantly affect formation and stability of gas hydrate. These factors include hydrocarbon gas composition, amount of impurities and composition of the aqueous phase (Makogon et al., 2007). Furthermore, Mondal *et al.*, (2018) noted that early formation of encapsulated CH_4 hydrate depends on the geometry and relative stability of small *host* clusters, weak *van* der Waals type of force, integrity and cavity radius of water molecules and presence of CH_4 guest.

These conditions can be explored to the advantage of researchers in order to enhance or inhibit hydrates formation. For example, Daraboina, Pachitsas and Von Solms (Daraboina et al., 2015)

indicated that complexity in behaviour of natural gas-aqueous-crude oil system can affect natural gas hydrate formation and stability. Moreover, hydrate can as well easily form, under specific temperature and pressure conditions, in the presence of nonhydrocarbon components (nitrogen, CO_2 and hydrogen sulphides) and light hydrocarbons (methane, ethane, propane, isobutene). Furthermore, in order to investigate proficiency of carbon capture from flue gas, Linga, Kumar and Englezos, (2007) noted that under same condition of vessel pressure and 273.7 K temperature, hydrate growth in CO_2/H_2 mixture was faster than those of CO_2/N_2 system. Obviously, at favourable equilibrium condition, presence of H_2 in the system enhances 'caging' of the gas mixture by water molecule through hydrogen bonding. Hydrogen easily form dipole-dipole attraction with oxygen compared to N_2 which forms covalent bonding. To investigate and promote storage of natural gas using clathrates, Veluswamy et al., (Veluswamy et al., 2016) noted that use of tetrahydrofuran rapidly promotes formation of methane hydrates. The use of tetrahydrofuran altered both the equilibrium and kinetic condition, hence acted as thermodynamic and kinetic hydrate-formation promoter.

The preceding case studies outlined in the above paragraphs of section 2.3.1 indicated cases where the needs for promoting gas hydrate formation exist. Moreover, instances requiring natural gas storage or transport do exist. Consequently, optimal and fastest hydrate-forming processing route need to be assessed, case of which is reported in the work of (Rajnauth et al., 2012). While some hydrate forming processes are desirable, some are problems to the entire oil and gas operations leading to economic loss.

During oil and gas processing operations, associated water molecules are found along with crude oil or natural gas. This associated water is undesirable and problematic, and therefore needs to be removed from the products flow line or streams. Presence of produced water in process streams, beyond certain threshold could be problematic, including risk of scale formation, corrosion, and enhancing hydrate formation. Therefore, hydrate formation is one of the most concerns phenomena oil and gas industry operators are being critical of, particularly at deep-water offshore exploration and production. Figure 2.13 shows a typical gas hydrate deposited in pipeline.

Figure 2.13 Gas hydrate plug in a pipeline (Boschee, 2012)

2.3.2 Structures/types of methane hydrates

Like other crystalline solids, gas hydrates are constructed from unit cells. Depending on composition and size of the guest, the resulting gas hydrate can have one of three types of unit cells shown in Figure 2.14 (Sloan, 2003) . The corresponding hydrate structures are termed as structures I (sI), II (sII) and H (sH) (Aman et al., 2011). Therefore, it may be safe to conclude that hydrates are classified generally based on the type of *guest* molecules involved.

2.3.2.1 Structure I (sI)

In structure I, the unit cell is a body-centred cubic lattice constituted by two small cages and six large cages. The small cage is a pentagonal dodecahedron and has a notation of 5^{12} which indicates that the cage has twelve pentagonal faces. The large cage is a tetra-decahedron (14-faced) and has a notation of $5^{12}6^{2}$. This notation means that each large cage consists of twelve pentagonal faces and two hexagonal faces. In an ideal combination, each cage (small and large) contains one gas molecule (i.e. CH_4 or CO_2). This means there are eight gas molecules being encaged in one-unit cell of sI. Since the cages share their vertices and faces with others, only 46 water molecules are needed to form eight cages in the unit cell of sI.
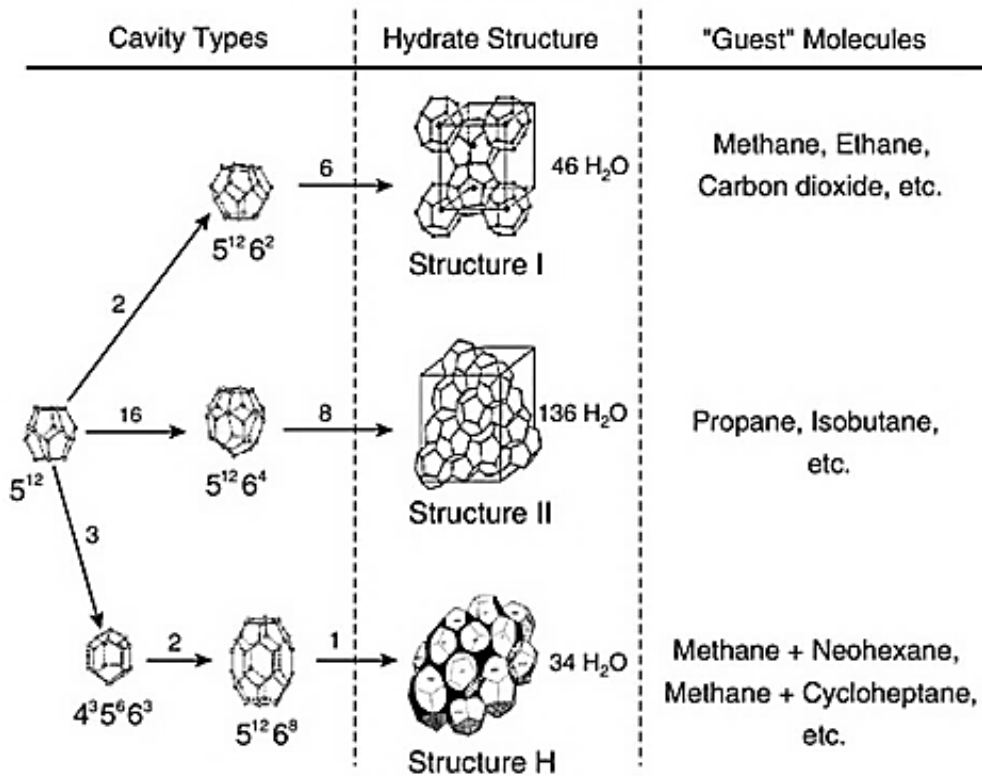
Figure 2.14 Structures and cavities for sI, sII and sH hydrates, adopted from (Aman et al., 2011)

Figure 2.15 illustrate how water and gas molecule combine to form each of the different structures of gas hydrates. Example is given in the figure for formation sI structure using methane.
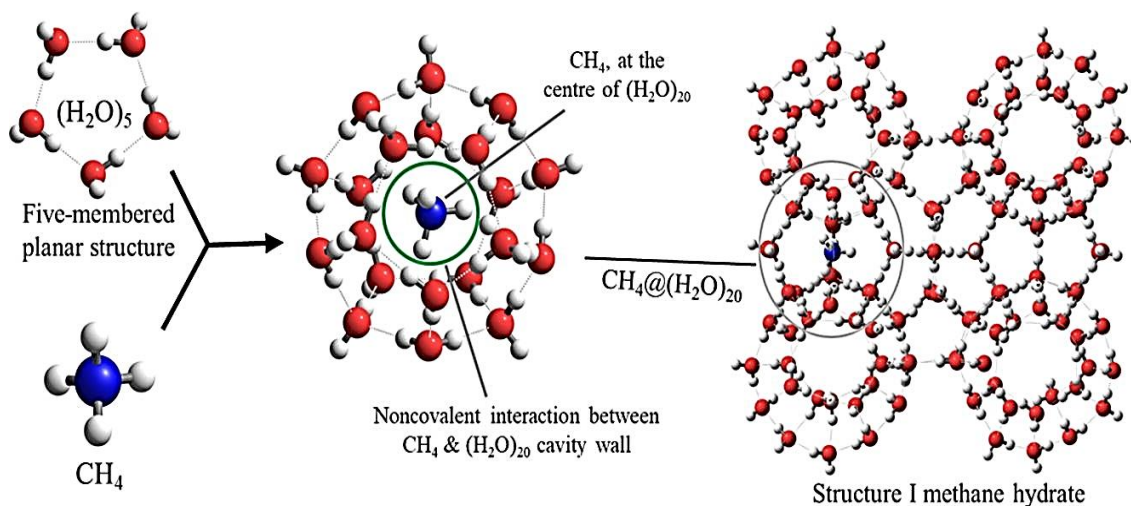
Figure 2.15 Sequence of formation of sI methane hydrate (Mondal et al., 2018)

2.3.2.2 Structure II (sII)

The unit cell of structure II is a face-centred cubic lattice which comprises 16 small cages (5^{12}) and eight large cages ($5^{12}6^4$) (Giavarini & Hester, 2011). The notation $5^{12}6^4$ indicates that the large cage is a hexakaidecahedron with twelve pentagonal (5-sided) faces and four hexagonal (6-sided) faces. The sII large cage is larger than the sI large cage so sII structure can fit bigger guests such as propane, iso-butane and so on. Each sII unit cell is composed of 136 water molecules and 24 guest molecules in the full occupancy configuration.

2.3.2.3 Structure H (sH)

Structure H is less common, and its unit cell is more complex than those of sI and sII. The unit cell of sH is composed of three types of cages; three small cages (5^{12}), two medium cages ($4^3 5^6 6^3$) and a large cage ($5^{12}6^8$) (Giavarini & Hester, 2011). The notations of the cages are as explained in the case of sI and sII above. To form sH clathrate hydrates, it needs a big guest such as cyclo-heptane to fill the large cage and a small "help guest" such as methane to fit the small and medium cages (Carolyn et al., 2011). While the big guest cannot occupy the small and medium cages, these cages still need to be filled by a small guest to make the whole structure stable. Because of this reason, the small guest is called "help guest".

Gas hydrates have continued to be topic of interest, despite their amazing simplicity in terms of chemical composition. This interest increasingly sparked an attracted attention of researchers. Indeed, findings of Hammerschmidt ignited a thriving development in research on gas hydrate. Primarily with more vigorous focus on preventing hydrate formation in gas transmission pipelines.

2.3.3 Gas hydrate phase equilibrium

Different materials, depending on their molecular makeup, exhibit different characteristics. One of the fundamental features of gas hydrates that distinguish it from that of ice is the phase equilibrium (Sloan & Koh, 2008). With the presence of appropriate amount of water molecule and *guest* molecule at low temperature and elevated pressure, hydrate will form (Meindinyo et al., 2015). In addition, fluid velocity, nucleation site, agitation and free water enhanced hydrate formation. Though these may not be requirement for onset of gas hydrate nucleation, however, they accelerate the formation process. Moreover, hydrates may form at any point in a process stream, particularly at pipe bend or dip where flow pattern changes. Additionally, presence of sand, weld slag or rust could also serve as good nucleation site for hydrate to form.

Seasonal climatic condition can influence pressure and temperature stability. Consequently, winter season could favour hydrate formation in onshore and shallow water offshore fields, as well deep-water fields offshore. Figure 2.16 illustrate the dependence of methane hydrate formation on pressure and temperature.
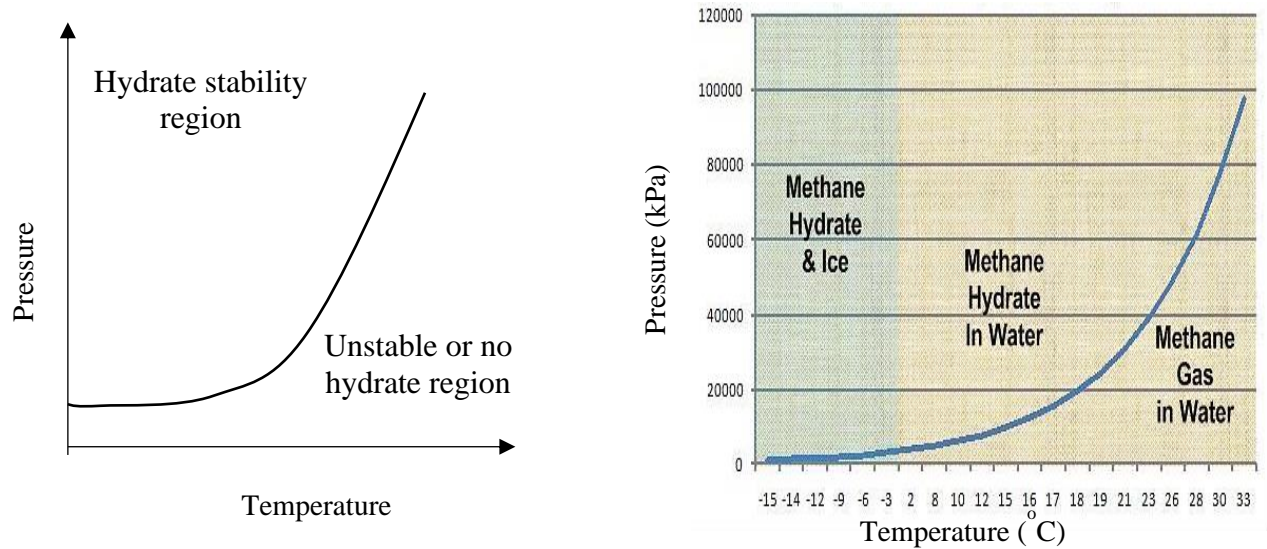
Figure 2.16 Hydrate stability curve, redrawn from (Gupta et al., 2015)

The region below the curve indicates the safest conditions at which the system will operate without risk of hydrate formation.

2.3.4 Gas hydrate formation prevention

Principally, there are two techniques of hydrate prevention used in industrial systems, which are based on the basic physics of hydrate formation. These techniques rely on deliberate adjustment of process parameters, with the intent of avoiding the conditions for hydrate formation:

i. Flow dehydration, which reduces the water content in the transport system. This to rid the system, or at least reduce it to minimal, of host molecule. Flow stream(s) can be channelled through dehydrator to achieve this.

ii. Based on understanding of phase diagram in Figure 2.16, deliberate alteration of system pressure-temperature conditions outside region of hydrate stability can be employed. To achieve this in field operation, pipeline heating is employed via mounted electrical cables, or employ pipeline thermal insulation.

However, the above-mentioned techniques may be economically impractical or at the least economically unsustainable due to high cost associated with it. Besides, formation of gas hydrate is a surface phenomenon, involving multiphase materials, which is time dependent. Therefore, other methods that can limit the interfacial activity from occurring can be adopted. As such, use of additives, known surfactants, is widely adopted as alternative and sustainable technique. The technique is employed to either completely prevent hydrate from forming, delay the formation kinetics or prevent the hydrate from agglomerating. Section 2.3.5 summarily discusses the forms in which surfactants (additives) are used in hydrate-formation prevention.

2.3.5 Effects of additives on gas hydrate formation

Among the many factors influencing formation of gas hydrate, amount and nature of impurities in the flow system is critical. Therefore, gas hydrates formation becomes sensitive to the purity of the medium. Existence of any foreign entities other than water and the *guest* can cause significant effects on either thermodynamic or kinetic property of the gas hydrate system. However, presence of 'impurities' in the flow system may be deliberate or otherwise. Presence of weld slag or sand particles in flow lines are capable of initiating rust, a good site for hydrate nucleation. On the other hand, additives may be intentionally added to upset the hydrate thermodynamic activity or formation kinetics. Additionally, additives may as well be present in hydrate systems naturally in the form of salts. This section reviews the effects of common additives on gas hydrate formation. These additives are known as inhibitors.

Mechanism of gas hydrate inhibitors are greatly dependent on their molecular structures. Some inhibitors alter the phase equilibrium of hydrate system such that it prevents its formation. On the other hand, certain class of inhibitors ensures that formation of hydrate is prevented based on time scale. Dynamics and mechanism of this class of inhibitor is such that it affects the kinetics of hydrate formation. This mechanism forms the basis for classification of hydrate inhibitors.

2.3.5.1 Effects of thermodynamic hydrate inhibitors

Thermodynamic hydrate inhibitors (THIs) function by altering the hydrate system phase equilibrium to higher temperature at a fixed gas phase pressure. This result in hindering the gas hydrates formation under the prevailing condition. As noted in Section 2.3, researches into hydrate formation and its prevention were systematically started in 1934 when Hammerschmidt (Hammerschmidt, 1934) established that subsea pipeline plugging were caused by ice-like structures. Top on the known THIs include the alcoholic compounds (such as methanol), glycols (e.g., mono and

polyethylene glycol) and aqueous solutions of inorganic salts (Sloan et al., 1998). Performance effect of THIs is in the bulk phase of the hydrate system. Consequently, high inhibitor dosage in the range of 30 to 50 % (by mass) is required to yield a significant and efficient inhibition effect (Kelland, 2006). The high dosages involved therefore becomes a concern regarding environmental and operational costs.

Basically, THIs prevent hydrate formation through water activity decrease. Additionally, these forms of inhibitors are strongly polar therefore sturdily bind with water by hydrogen bonds. Consequently, competition for water molecule between the hydrate former the inhibitor becomes amplified. Hence, less water molecule becomes available for hydrate formation. Therefore, performance efficiency of THIs can be said to be largely dependent on its binding ability with water (Lee et al., 2018). For instance, the molar volumes of ethylene glycol and ethanol are similar. However, ethanol has mono hydroxyl group available for bonding with hydrogen while ethylene glycol has two. Ethylene glycol will consequently provide a better hydrate inhibition performance compared to ethanol. Nevertheless, several THIs also exhibited hydrate promoting effect when low inhibitor dosage is used. Use of dilute alcohol solution was experimentally reported to have enhanced formation of methane hydrate (Abay & Svartaas, 2010). Despite being in low concentration, the promoting effect could be attribute do surfactant micellization as earlier discussed in Sections 1.3 and 0.

2.3.5.2 Effect of low-dosage hydrate inhibitors

Low-dosage inhibitors (LDHIs) impact on the interfacial properties of gas hydrates, dissimilar to THIs. Their effective mechanism is based on the increase of the induction time up to time scales comparable to the residence time of the system, i.e., so long that a significant amount of the hydrate is not formed in the line.

The low working dosage of LDHIs is the motivating factor in their increasing acceptance and use as hydrate inhibitors. Typically, this dosage is reported to be less than 1 mass % (Al-Eisa et al., 2015; Kelland, 2006). However, despite the low dosage, as compared to THIs, some of these surfactants do not meet the ecological and toxicity requirements and thus cannot be widely used due to environmental considerations.

Conventionally, LDHIs are categorised as either anti-agglomerates (AAs) or kinetic inhibitors (KHIs). Primarily, KHIs prevents hydrate nucleation, whereas AAs prevents agglomeration of hydrate nuclei into forming large hydrate mass that will plug pipelines. Therefore, AAs does allow

hydrate nucleation which however flows along the pipe. The most popular of the conventional vinylic polymers KHIs include polyvinylcaprolactam (PVCap), polyvinylpyrrolidone (PVP), and antifreeze proteins (AFPs) (Fleming et al., 2004). Thus, it is anticipated that LDHIs prevent formation of gas hydrate by binding to the surface of an ensuing hydrate nuclei (Anderson et al., 2005). Consequently, its adsorbing unto the surfaces of hydrate nuclei upsets hydrate crystals growth.

Various reports indicating application of biosurfactants in oil and gas processes suggest that they belong to the low-dosage class of additives.

2.4 Surface Tension and its Effect on CH$_4$-H$_2$O Multiphase Boundary System

Transport processes in fluids systems are affected by physical and chemical properties. Therefore, surface tension, like density, viscosity, etc., is critical property which affects mass and heat transfer processes in fluids (Khattab et al., 2017). Surface tension arises from the imbalance that exist between intermolecular cohesive forces of multiphase (two immiscible) fluids. As such, it is a boundary that exist between a phase (liquid or vapour) and has an ever-present effect on the dynamics of such interfaces. Additionally, the intermolecular imbalance existing at the interface creates a tension (excess free energy) which can only be overcome by work. Therefore, addition of appropriate amount of surfactant ensures that the surface is relaxed, through creation of new surface. Consequently, a work is done to create the new surface. Adamson and Gast, (1977) indicates that the work done required to create the new surface is given by Equation (2.2).

$$Work = \gamma \delta A \qquad (2.2)$$

Where γ is the surface tension (N/m), an energy per unit area and the proportionality constant for the work required to create an amount of new surface δA (m^2).

Considering the increase in area of some surface with a perimeter of length l (m) by a small amount δx gives rise to the consideration of surface tension as a force per unit length Equation (2.3).

$$Work = \gamma l \delta x \qquad (2.3)$$

Interpreting Equation (2.3) as the work done by a force F (N) on the perimeter of the same surface leads to Equation (2.4), which shows surface tension can be thought of as a force, F, per unit length, l.

$$\gamma = \frac{F}{l} \tag{2.4}$$

Prelude to hydrate formation is the formation of hydrate nuclei. More so, formation of CH_4 hydrate typically inducts at the CH_4-H_2O interface rather than in the bulk liquid (Warrier et al., 2016). This phenomenon is critical and therefore becomes important in understanding mechanism of hydrate inhibition. Thus, it then suggests that hydrate formation may effectively be controlled using interface-active agents more than bulk-active agents. Additionally, to explain the phenomena of gas hydrate, interfacial water may need to be reported. Formation of gas hydrates at interface, in quiescent state, is proved by the appearance of interfacial hydrate thin film at the CH_4-H_2O interface (Daniel-David et al., 2015). Thickness of hydrate film continue to will grow provided interfacial diffusion of gas molecule occurs. However, the thickness stops growing when it becomes diffusion resistant. Thus, it hampers interface mass transfer across the boundary. For example, the final thickness of methane hydrate film was reported to be between 20-100 μm depending on experimental condition (Taylor et al., 2007). Formation of hydrate film was more evident in a system comprising small water droplet placed in a *guest* phase or a small *guest* bubble placed in an aqueous phase.

As previously discussed in Section 2.2.3.5, behaviour of surfactants at an interface is determined by their concentration in the bulk solution. As the bulk surfactant concentration is increased, number of surfactant molecules adsorbed to the interface rises causing the surface tension to fall in a concentration dependent manner. There is a limit to the number of surfactant molecules that can adsorb to a surface before that surface becomes fully covered or saturated. The saturation leaves no 'room' for further alignment of surfactant across the surface. This saturation point is known as CMC, as defined earlier. At this point the surface tension is at minimum. Further addition of surfactant molecules may not alter the surface tension as no more adsorption to the surface can occur. Instead increasing the surfactant dosage in the bulk leads to self-assembly of the surfactant molecules. Consequently, the surfactant molecules aggregate into various types of structure (micelles) depending on concentration and the specific properties of the surfactant.

2.5 Methane–Water Surface Tension and its Control

Gas liquefaction has been the most common medium for storage and transport of particularly natural gas. However, low-temperature liquefaction conditions are critical for pipeline operations (Hayama et al., 2017). At this low temperature and appropriate equilibrium pressure, achieving flow assurance in pipelines during liquefied gas transport becomes difficult. This is due to ease of formation gas hydrates. To solve this problem, technologies were developed to understand the mechanism of the hydrate formation at these conditions. One of these technologies is the understanding of the ST existing at the point of contact between gas (CH_4) and water. It was earlier noted in Section 2.3.1that formation of gas hydrate occurs preferentially at water and *guest* interface (Saito et al., 2011). Therefore, alteration of the interfacial area (ST) becomes the underlying phenomena to efficient control of methane-water interaction at interface. Various methods have been employed either to promote or inhibit hydrate formation, and in some cases inhibit agglomeration where hydrate nucleation cannot be prevented in the first instance. Regarding hydrate-formation inhibition, alteration of thermodynamic equilibrium conditions has been employed through process controls. This ensures that conditions favouring hydrate formation do not set in. Similarly, hydrate-formation inhibitors have also been used to either alter the thermodynamic conditions or slows down crystal growth arising from nucleation. This targets the CH_4-H_2O interface and ensuring that increased surface area (unfavourable ST) for the formation of hydrate exist.

Recalled that in Section 2.3.2, it was mentioned that hydrates are classified into different structures depending on the guest molecule. As such, control of hydrocarbon-water hydrate through ST alteration could be dependent on type, and to some extent the phase, of hydrocarbon guest molecule(s) involved. For example, Erfani and Varaminian, (2017), suggest that for sH hydrate, lower ST increases hydrate formation rates and consequently reduces induction times. This is for system involving methane in combination with methylcyclohexane, methylcyclopentane and tertbutylmethylether as guest molecules. ST measurement were however made for the system in a liquid/liquid state. Conversely, Qin *et al.*, (2016) indicated that lower ST corresponds to longer hydrate nucleation onset time for methane/water system. Methane/water hydrate system is typical example of sI type of hydrate structure. Additionally, control of hydrocarbon/water hydrates is made possible by use of additives such as surfactants or even salts. Prasad and Kiran, (2019) indicated that increasing NaCl concentration to 5.0 wt%, gas uptake decreased by about 10 %. The study further conclude that the hydrate formation kinetics is relatively slower at higher NaCl concentration. Fundamentally, however, the interfacial characteristics remain one of the most important tools in

controlling dynamics of multiphase flow in pipelines. To this end, accurate measurements of methane-water ST become a critical factor in control of methane hydrate.

Measurements of methane-water ST were carried out by many authors, at various conditions in combination with different chemical surfactants to ascertain their hydrate formation inhibition capabilities. Experimental investigation of CH_4-H_2O system were conducted by (Hayama et al., 2017; Yahaya et al., 2018; Yasuda et al., 2016). Both authors' findings agreed that temperature plays less significant factor in reducing ST, compared to pressure. However, at elevated pressure, the temperature effect in ST reduction becomes evident.

2.6 Surface Tension Measurement Using Pendant Drop (bubble) Method

Many techniques (shown in Figure 2.17) have been suggested for interfacial tension measurement, details of which is described by Drelich, Fang and White, (2006). However, in terms of instrumentation, the pendant drop method is the simplest of the methods. This is because of its robustness and versatility, where the measurement consists simply of a fluid droplet suspended from a needle.
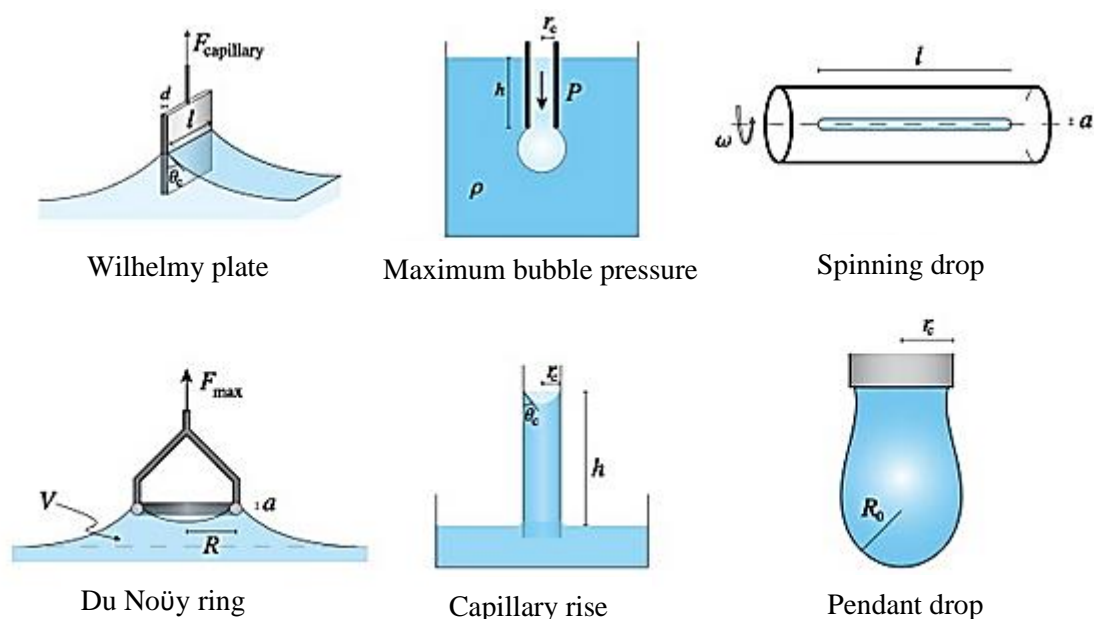
Figure 2.17 Schematic presentation different experimental methods of ST measurement, adopted from (Berry et al., 2015)

Surface and interfacial tension measurement using drop shape analysis is a suitable technique for surface tension measurement. Its theory is based on Young-Laplace equation, where the change in

pressure across the surface is directly proportional to the surface tension, γ, and to the mean curvature of the surface, $R_1 R_2$. Mathematical representation of this theory is given in Equation (2.5).

$$P_{gas\ phase} - P_{liquid\ phase} = \gamma(\frac{1}{R_1} - \frac{1}{R_2}) \qquad (2.5)$$

Additionally, the ST of methane bubble is determined from the profile of the bubble created using a radius of the curvature (R_0) and the shape factor (β) by the Equations (2.6) and (2.7).

$$\gamma = \Delta\rho g(\frac{R_o^2}{\beta}) \qquad (2.6)$$

$$\Delta\rho = \rho_{gas\ phase} - \rho_{liquid\ phase} \qquad (2.7)$$

$\Delta\rho$ is the density difference between the continuous and risen bubble phase; R_0 is the radius of curvature at the hanging bubble apex; g is the gravitational constant; and β is the shape factor.

An inverted pendant drop with same coordinates as the Young-Laplace equation is shown in Figure 2.18. The drop has a neck at the bottom, which indicates that the two principal radii have opposite signs. At the top of the drop, the two radii have the same signs which give a larger mean curvature.
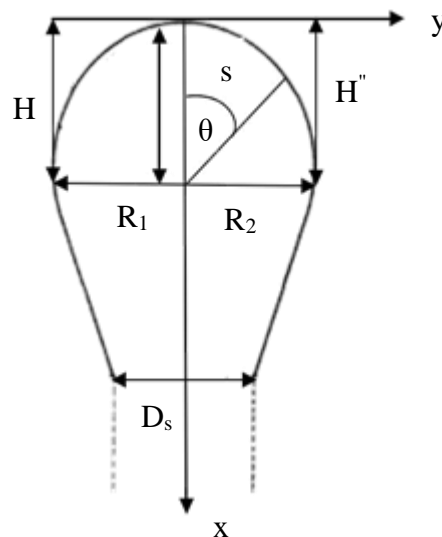
Figure 2.18 An inverted pendant drop with characteristics dimension

The bubble profile has been described using Young-Laplace equation, which is presented in a dimensionless form as shown in Equation (2.8), (2.9) and (2.10).

48

$$\frac{dX}{ds} = cos\theta \qquad\qquad (2.8)$$

$$\frac{dY}{ds} = sin\theta \qquad\qquad (2.9)$$

$$\frac{d\theta}{ds} = 2 - \beta Y - \frac{sin\theta}{x} \qquad\qquad (2.10)$$

The distance along the drop profile from the drop apex is represented by s. X, Y and S represent dimensionless parameters calculated by dividing x, y, and s, respectively by R_0. H" and H' are the distances from the centre of the curvature to the drop apex.

The bond number β, also known as the shape factor, is a parameter that describes the shape of the drop. It can be calculated from Equation (2.6).

2.7 Chapter Summary

The idea of biosurfactants as molecules from biological process was defined and their characteristics features critically analysed in this chapter. Mechanism of biosurfactant performance relies on their amphipathic property where they align themselves along the hydrophilic and hydrophobic phases. Furthermore, biosurfactant are increasingly accepted for diverse application. To satisfy this increasing demand, there is need for sustainable techniques to make biosurfactant availability more cost effective. These methods were identified to include robust optimization of procedure and production operating conditions, genetic algorithm and recombinant DNA technology. This is in addition to utilizing cheap nutrients sources such use of waste agro resources. Additionally, application of biosurfactants were examined. It was established that biosurfactants have been tested for both oil/water (in the form MEOR) and gas/water systems. However, applications for multiphase gas/system is just emerging and therefore requires further investigations. Particularly, mechanism of biosurfactant application, such as *surfactin*, in multiphase methane/water is not established. Though utilization involving CO_2/water system was reported, application of biosurfactants must take into consideration a critical property known as CMC. This property may result to desirable or undesirable consequence depending on the intended use of the biosurfactant.

Highlight on the mechanism of methane hydrate formation, characteristics and underlaying principles were presented. It understood that methane hydrate is formed when water in a multiphase

methane/water system envelopes methane making it its 'guest'. This, under equilibrium condition of temperature and pressure, forms an ice-like structure consequence of which is pipe plugging. Gas hydrates may serve as useful alternative for gas storage and/or transport. However, it is upheaval to process operation in gas processing facilities, particularly during gas transport through pipelines. More so, unplugging and control of hydrates in pipelines comes at a huge cost. It becomes obvious that preventing hydrate formation might be cost effective. Moreover, hydrate formation is a surface phenomenon. Therefore, effective control of surface interaction and cohesive and adhesive force between methane and water will result to effective management of hydrate formation. Use of surfactant has been identified as one of the effective methods of surface interaction control. Surface and interfacial tension measurement is a technique that is employed to evaluate and predict effectiveness of surfactants. Different methods of surface tension measurement have been highlighted in this chapter, as well as theory behind measurement using pendant drop.

CHAPTER THREE

3 MATERIALS, EXPERIMENTAL DESIGN AND METHOD

3.1 Chapter Overview

Experimental studies do follow standard procedures in order to achieve desirable outcome. These procedures describe fully the steps taken and conditions applied at every stage of the experiment. This study is no exception to these norms. On this note, Chapter four (4) introduces to the reader details of materials and equipment used, and the experimental set up, procedures and description of stages involved in ensuring acquisition of accurate results. The sequence of the research method, shown in Figure 3.1, and how their various objectives were achieved, are detailed in this chapter. These have been categorized into three phases:

Phase I: This phase involved characterization of Sodium *surfactin* in terms of its physical, chemical and thermal behaviour. Characteristics behaviours, such as density, electrical conductivity, foaming ability and solubility, and pH were determined as described in Section 3.3. The experimental characterization was conducted for 0.025 – 1.0 w/v% dosages of sodium *surfactin* in aqueous state, and in NaCl salt (saline) solution. Application of sodium *surfactin* is intended for hydrate-inhibition during gas (methane) transport in pipelines. Since hydrate formation process is equilibrium temperature dependent, surfactin characterization were as well conducted at variable temperatures of 1 to 50 °C. Similarly, concentration of the saline solution was varied in the range of 0.05 to 1.5 M. Additionally, availability of active site for adherence of sodium surfactin at fluid interface was characterized through functional group analysis. Fourier Transform Infrared spectroscopy was employed for this analysis, details of which were also described in section 3.3.5.

Phase II: Second phase of the experimental study involves characterization of sodium surfactin in terms of rheological behaviour. The investigation involves subjecting various dosages (0.025 – 1.0 w/v%) of sodium surfactin to variable rate of shear, details of which is described in Section 3.4. Temperature in the range of 23 – 50 °C, and ionic (salt) concentration range of 0.05 – 1.5 M were considered. The experiment was conducted using ORCADA® software-controlled OFITE viscometer (Model 1100).

Phase III: Effect of sodium *surfactin* on methane – water system surface tension was investigated using rising bubble method. Experimental study on effects of change in surfactant dosage, temperature and pressure condition was conducted as described in Section 3.6. To do this, the

experimental set up was designed using Statease© Design expert software v.12. Following the design, surfactant performance in reducing CH_3-H_2O ST was optimized.

Outline of these phases are generally described as activity flow chart shown in Figure 3.1. Furthermore, details of precautionary measures and sources of error associated with each step, as elaborated in each respective section, are also presented in this chapter.
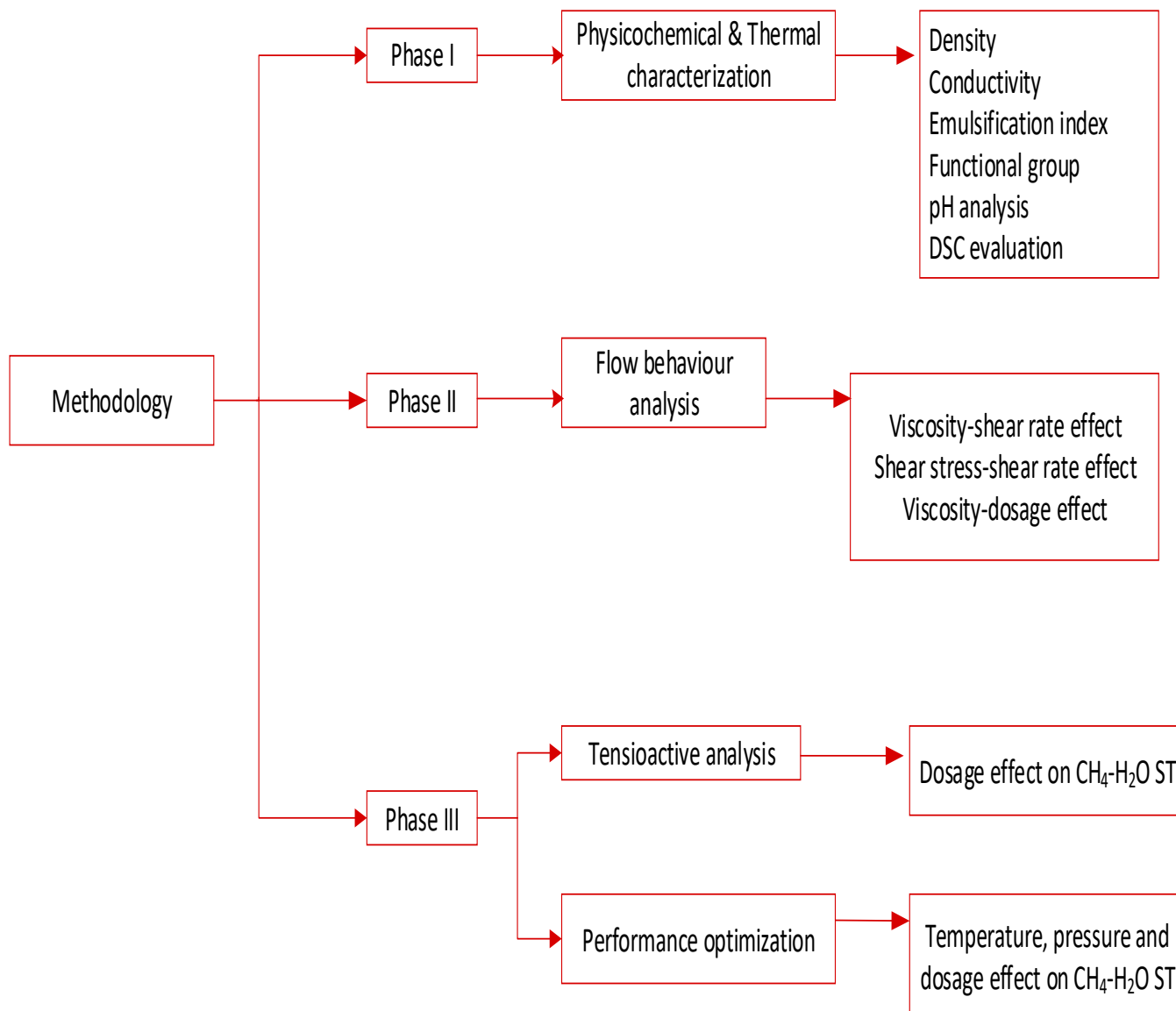
Figure 3.1 Activity flow chart/methodology

3.2 Samples Preparation

3.2.1 Materials

Sodium *surfactin* (also branded as Kaneka *surfactin*) bought from Kaneka Europe Holding Company, Belgium was used as received. Distilled water was used to prepare aqueous solution of

the *surfactin*. The surfactant has a molecular formula of $C_{55-n}H_{95.5-2n}N_7O_{13}Na1.5$, and unique Chemical Abstracts Service (CAS) numerical identifier number 302933-83-1. It is a biosurfactant containing a cyclic lipopeptide that is attached to hydrocarbon (hydrophobic) chain.

In addition to the surfactant, Acros Organics[TM] brand (207790010) of analytical grade monovalent salt, Sodium chloride (NaCl) with 99.5 % purity, and CAS number 7647-14-5, was purchased from Fisher Scientific, UK. The NaCl salt assay is shown in Table 3.1.

Table 3.1 Sodium chloride (NaCl) salt assay (fisherscientific, 2018)

Property	Characteristic range
Purity grade	For analysis
Assay	99.50 %
Formula weight	58.44 g/mole
Solubility information	Solubility in water: 360 g/L (20 °C). Other solubility: soluble in glycerol (1g/10 mL), ammonia, slightly soluble in alcohol, nearly insoluble in hydrochloric acid
Total Nitrogen	0.001 % maximum
Colour	White
pH	5 to 8 (5 % solution at 20 °C)
Assay percent range	99.50 %
Barium (Ba)	10 ppm maximum
Calcium (Ca)	20 ppm maximum
Iodine (I)	10 ppm maximum
Potassium (K)	100 ppm maximum
Sulphate	20 ppm maximum
Bromine (Br)	50 ppm maximum
Heavy metals (as Pb)	5 ppm maximum
Iron (Fe)	3 ppm maximum
Phosphate	5 ppm maximum
Boiling Point	1461.00 °C
Melting Point	801.00 °C

3.2.2 Samples preparation procedure

The first and most important stage of the experimental work is to prepare and make ready the samples to be used for all experimental runs required.

Aqueous solution of surfactant was prepared by measuring (using weighing balance) and directly adding 0.025, 0.05, 0.075, 0.1 0.5 and 1.0 w/v% dosages of sodium *surfactin* into sample container. Subsequently, required amount of distilled water measured and added to the container. The mixture was vigorously agitated and stirred and allowed at least for 5 hours to completely dissolve. Surfactant dosages were adopted based on the works of Saito *et al.*, (2016), Al-Wahaibi *et al.*, (2014), and Whang *et al.*, (2008).

Saline solutions of 0.05–1.5 M concentration were as well prepared by measuring and dissolving appropriate amount of salt (corresponding to each concentration) into 2 litres of distilled water. The solution was well stirred using hotplate magnetic stirrer. Each concentration of the saline solution was then used to prepare solution of the surfactant, using the various dosages stated above. Figure 3.2 showed the saline solutions prepared.
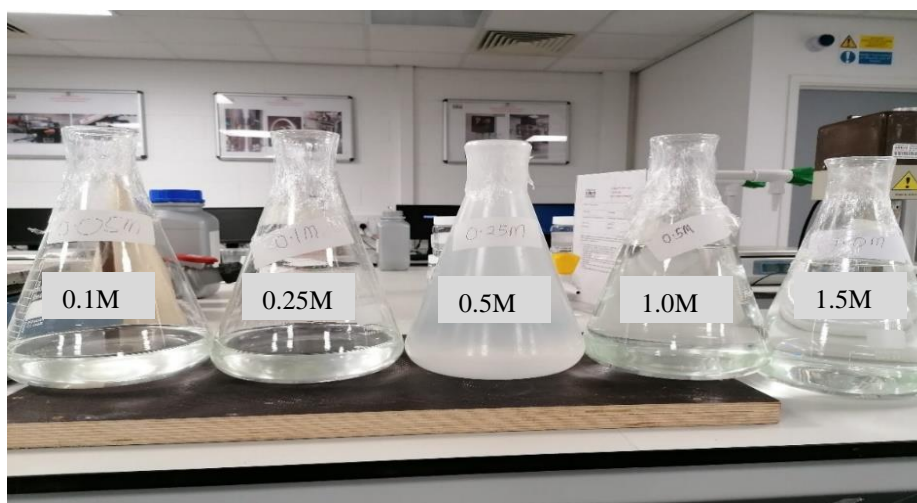
Figure 3.2 NaCl salt solution prepared

3.3 Physicochemical Characterization of Samples

3.3.1 Emulsification index (E_i) measurement

Surfactant emulsification index is a measure of their ability to effectively and sustainably enhance miscibility of two or more immiscible phases. On this note, the emulsifying potential of sodium

surfactin was analysed against hydrocarbon using light crude oil of 34.97º API gravity (0.85 specific gravity).

However, before the actual measurement of the emulsification index, properties of the crude oil need to be validated. This was done by evaluating the specific gravity of the oil, using OFITE mud balance. The procedures are as elaborated in section 3.3.1.1.

3.3.1.1 Crude oil specific gravity measurement procedure

As mentioned in the preceding section, OFITE mud balance, shown in Figure 3.3 was used.

Mud balance is a device used for measurement of liquid density. It consists of a fixed-volume sample cup with a lid on one end of a graduated beam and a counterbalance on the other end. A rider attached to the beam is used to equilibrate the device, by moving it along the graduated arm. State of equilibrium is ascertained when a bubble vial indicator stabilizes at the centre. At this point, density of the liquid is read at the point where the rider sits on the beam at level. The mud balance has an accuracy of +/- 0.01 g/cm^3.

As a starting point, the balance was calibrated to validate accuracy of measurement. Calibration was made using water. The mud balance was first cleaned with unsoiled moist tissue, then a clean dry tissue. This is to ensure that no trace of contaminant is found in the equipment. Thereafter, the water was then poured into the sample cup until filled to the brim. Sample cup lid was then gently placed to cover the cup, ensuring that excess water spilled through the pin hole of the lid. The balance was then placed on its fulcrum, and rider adjusted until a balance was obtained. Confirmation of state of equilibrium was made when bubble vial indicator stabilizes at the mid-position, and density of water was taken at this point. Accuracy of the device was confirmed when density reading was approximately equals to unity.
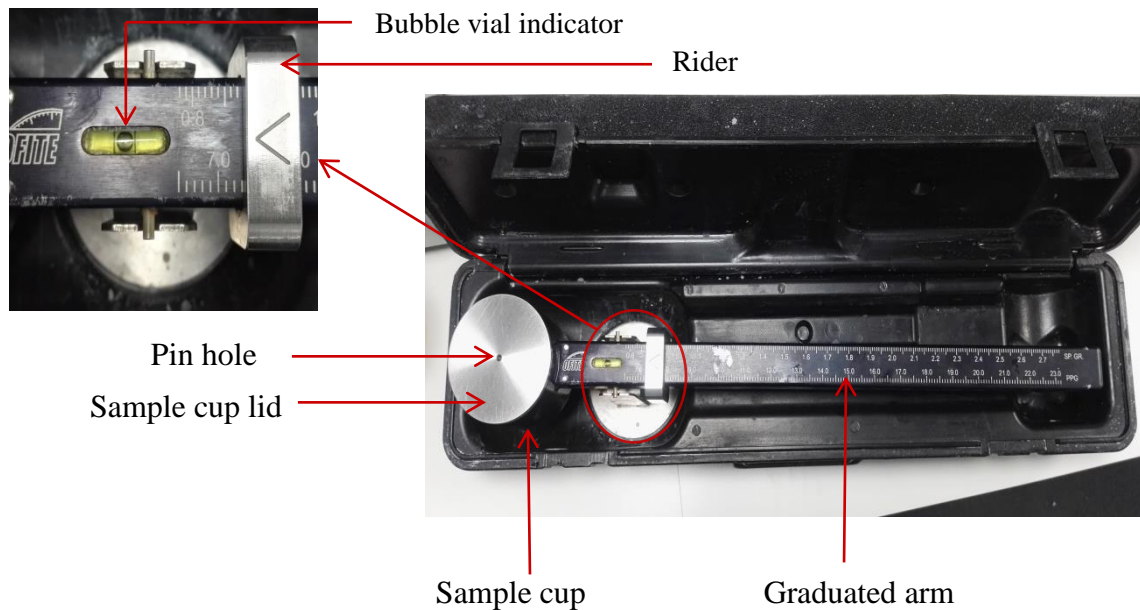
Figure 3.3 Mud balance arrangement during specific gravity measurement of crude oil sample

The calibration procedure outlined earlier was repeated, but in this case using crude oil sample. Certainly, this was after the device was again cleaned and dried, ensuring all trace of water and other materials are visibly wiped. For this sample, specific gravity value of the sample crude was noted, and API gravity calculated using the procedure outlined in section 10, step 4c of ASTM (standard) D1298–12b (ASTM, 2017). The formula is indicated in Equation (3.1).

$$API = \frac{141.5}{Relative\ density} - 131.5 \tag{3.1}$$

Thereafter, sodium surfactin samples and measuring cylinders were prepared and made ready for the emulsification index measurement.

3.3.1.2 E_i measurement procedure

It is critical of every measurement to ensure that errors from any source are minimized. On this note, test tubes to be used for the experiment were again cleaned, after been washed and dried a day before. The following steps were followed as described in the studies conducted by Kanmani *et al.*, (2017; Akshatha *et al.*, (2018), using 10ml graduated test tubes.

5ml of each of the surfactant samples (0.025 – 1.0 w/v%) were poured into different test tubes marked accordingly.

5ml of the hydrocarbon sample (crude oil) was then poured into each of the test tubes containing the surfactin samples.

The mixture was then vortexed for 2 minutes and allowed for 24 hours (h).

Height of emulsion formed after 24h was taken, and E_i calculated using Equation (2.1).

3.3.2 Measurement of pH

Oil and gas operation are mostly associated with presence of dissolved minerals and elements, such as chlorides, sulphates and to a less extent bicarbonates, from the formation. In addition, it is critical to analyse surfactants in various dissolving media to ensure a stable and favourable condition is met for its safe and efficient utilization. More importantly, integrity of equipment, personnel and environmental safety must be sustainably ensured. This is because, some of the dissolved substances/minerals might alter the amount of free hydrogen ion (H^+) or hydroxyl ion (OH^-) dissolved in the solution. As a result, the acidic or basic condition (pH) of the phase mixture becomes changed due to alteration in number of free H^+ or OH^- in the solution. Consequence of which is the increased tendency of precipitation and corrosion in pipelines. Additional negative effect includes alteration of surfactant solubility and distortion of active site available for surfactant adsorption at fluid surface leading to increased surfactant inefficiency.

In chemistry, the pH may be calculated numerically, using Equation (3.2), when the molar concentration of solution is known. Use of the equation, however, requires that one must take into consideration the self-ionization equilibrium of some solutions at higher concentrations.

$$pH = -\log(H^+ or\ OH^-) \tag{3.2}$$

In this study, however, the following steps/procedure was adopted using JENWAY Model 570 pH meter shown in Figure 3.4. The meter has a pH measurement capacity in the range of -2 – 16, resolution of 0.01 pH and accuracy of ±0.02 pH. Measurement using this meter can be performed either in terms of pH or mV. Furthermore, the model meter is equipped with both manual and automatic temperature compensation. It therefore measures pH at every given temperature, in the range of -39.9 to 149.9 °C. Construction of Model 570 pH meter comes with in-built USA automatic buffer recognition standard. This standard is based on the established buffer pH values of 4, 7 and 10. However, the meter has only two (2) point calibration windows. Moreover, it has the capability of withstanding temperatures (operational) in the range of 0 – 100 °C.
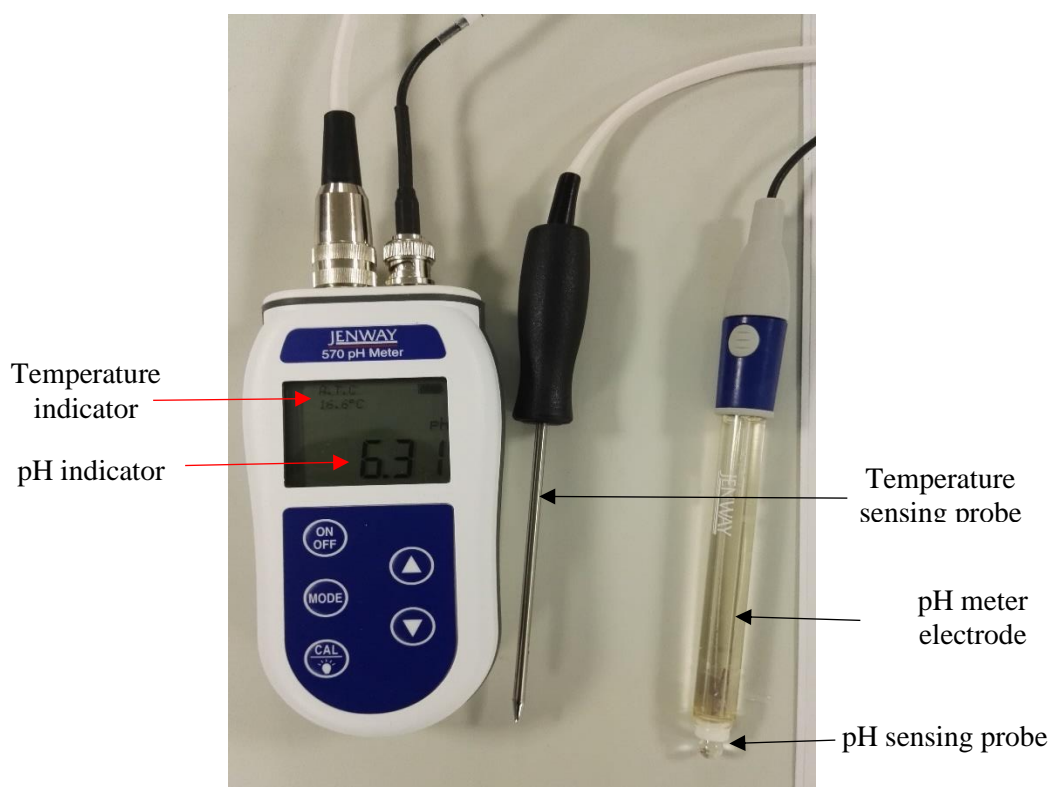
Figure 3.4 JENWAY Model 570 pH meter

Readers should note that the pH meter electrode is housed in a sensitive glass in contact with the solution, which develops a potential (voltage) relative to the pH of the solution. The potential signal, in millivolt, is read and recorded as the solution pH.

3.3.2.1   Buffer preparation

JENWAY Model 570 pH meter package was delivered in such a way that the pH sensing probe was already immersed in storage fluid. Therefore, the probe is said to be already conditioned, and wet. However, where this is not the case, or in the event of loss of storage fluid, it is advised that the probe is conditioned in de-ionized water for at least 30 minutes before first operation.

Buffer preparation involves dissolution of pH buffer in 100 ml of de-ionized water following the equipment manufacturer's guidelines. The solution was allowed to stale for 24 hours, as a way ensuring complete dissolution of the buffer. This set the stage for the pH meter calibration, details of which is outlined in section 3.3.2.2.

Please note the buffers are capsulated and color-coded as pH 4.01 buffer (orange), pH 7 buffer (green) and pH 10.01 buffer (white). An example of the coded capsule is shown in Figure 3.5 using pH 4 buffer.
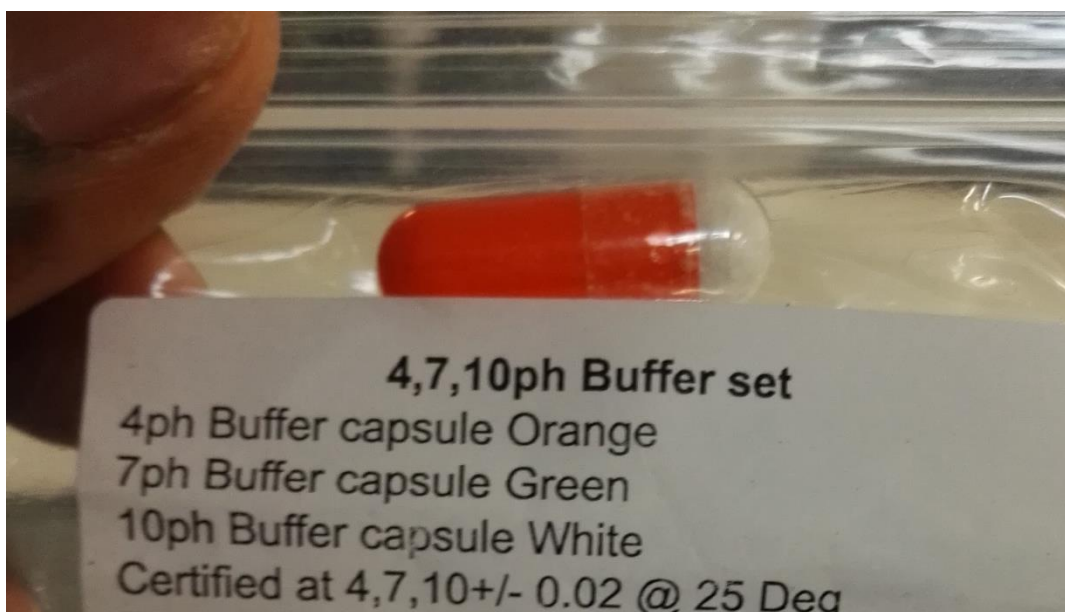
Figure 3.5 pH 4 buffer capsule

Succeeding section presents the calibration procedure that was followed in ensuring that pH measurement conducted was accurate and precise.

3.3.2.2 pH meter calibration

Accuracy and precision are critical components of any successful experiment. One of the key elements of achieving a precise and accurate measurement is equipment calibration. The pH measuring device is no exception to this norm.

JENWAY Model 570 pH meter has only two (2) calibration points, despite having three (3) buffer solutions. More so, the calibration is carried out depending on the expected pH value. Consequently, a constant buffer (pH 7 buffer) in combination with either pH 4 buffer (if the expected pH is in the range of value 5 and below) or pH 10 buffer (if the expected pH is in the range of value 6 and above). Calibration of the meter was conducted following the equipment manufacturer's instruction, which can be found on http://www.jenway.com/adminimages/570_pH_meter_rev_B.pdf.

pH meter was rinsed in deionized water, blotted with clean soft tissue and then switched on. The electrode was then dipped about 2 to 3cm into the pH 7 standard buffer solution and CAL button was pressed to enter calibration mode. The 'CAL' indicator was displayed on the meter screen which indicates the equipment readiness for calibration. Buffer pH reading displayed was allowed to stabilise and the HOLD/ENT button was then pressed to confirm the calibration point. The sensing probe was again rinsed in deionized water, and dried. It was then placed in pH 10.01 buffer solution. Once the reading stabilises, HOLD/ENT button was then pressed, and the calibration readings were

recorded in the system. The calibration mode was then aborted by pressing the CAL button, indicating that the meter is now ready for pH measurement. It was turned off to allow for sample readiness, and to conserve battery power.

3.3.2.3 Measurement procedure

The pH tester was switched on by pressing the ON/OFF button. Electrode was then dipped into the prepared samples by about 2 to 3 cm and stirred to ensure that any form air bubble within the solution is displaced. The value indicated on the display was simply taken and recorded as the pH. Of course, the value must be allowed to stabilise before any reading was taken. Consequently, this step of procedure was followed for all other samples prepared.

Hydrate formation condition involves exposure of multiphase fluids to condition of low temperature. Therefore, any potential surfactant that is to be used as hydrate inhibitor should be able to withstand such temperature conditions. Surfactant's stability and efficiency should not significantly alter at such temperature condition, and perhaps it's alteration. On this note, effect of temperature on pH of sodium surfactin was evaluated.

Surfactin sample container (with a magnet immersed in it) was placed in a bath that was filled with ice. The bath was then placed on a magnetic stirrer. Temperature and pH sensing probes (see Figure 3.4) were dipped into the sample. Stirrer was then started to ensure that temperature equilibrium is attained between the bath and the sample. This contact ensures that the sample temperature was cooled down to 1 $^{\circ}$C. On obtaining a stable temperature reading, a stabilized pH value displayed on the meter screen was recorded as the sample pH at that temperature. Heating mantle was then on to heat the bath and in turn heat the sample at an average rate of 2.5 $^{\circ}$C/sec. The sample was heated within the temperature range of $1 - 50$ $^{\circ}$C. pH readings were taken at given equilibrium temperature intervals. The procedure was followed for all other dosage of samples used in this study. Values obtained were tabulated (see Appendix D 2) and discussed in section 4.2.5.

3.3.3 Density measurement

Density is a measure of how much mass is contained in a given volume of liquid/fluid. The density of a solution is a measure of the degree of total solid that is dissolved in a given amount of solvent to from the solution. This is often referred as mass concentration. It is a physical property that relates the volume occupied by molecules of a given mass. Conventionally, the higher the amount of total dissolved solids in the solution, the greater its density. This property is critical with all fluids, in which is one of determinant factor in measuring kinematic viscosity, surfactant dispersion ability,

and surfactant stability during adsorption at fluids surface. Fluid density is in fact one of its fundamental characteristics.

Many instruments can be employed in the measurement of density. In this study, however, pycnometer was used.

3.3.3.1 Equipment calibration

Pycnometer (Figure 3.6) used in measuring the density of surfactin solution was purchased from fisher scientific industry. The device consists of flask/bottle (where the sample is been poured into) and stopper which has an in-built capillary tube. Built-in capillary tube in this device allow the expulsion of entrained air in the sample. Additionally, the stopper is used to guarantee that the flask is only filled to its full capacity.
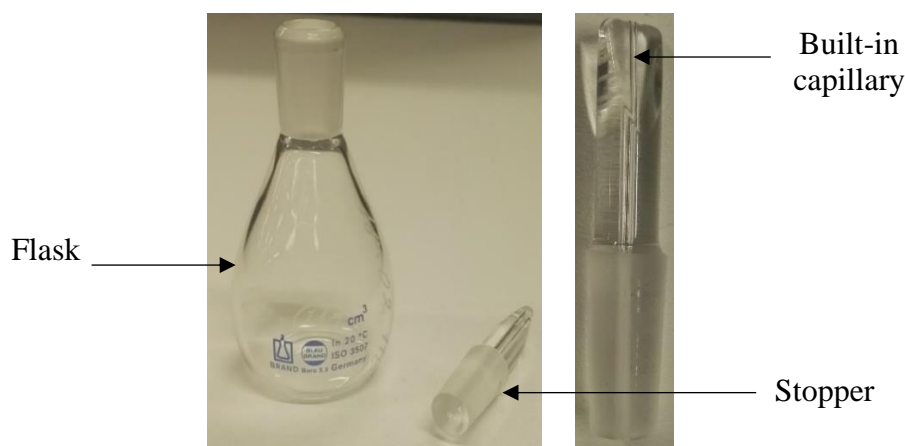
Figure 3.6 Pycnometer used in surfactin sample density measurement

Validation of the device become critical to ensure accurate density measurement. As a result, distil water was used as the validation fluid via the following procedure. Choice of distil water guarantees that the water is devoid of dissolved minerals which could impact on the accuracy of the density measurement.

The weight of empty pycnometer was measured using weighing balance, and the value recorded. The device (flask) was then filled with distil water to it 'neck'. The stopper was then inserted ensuring that excess water spilled through the neck. As a precaution, care was taken to ensure that no bubble was visible in the bottle. The flask was then wiped clean and made free of any spilled water. This whole content was then weighed to calculate the weight of distil water used. The procedure was repeated at different average temperatures of $20 - 60\ ^{\circ}C$. Standard values of density

of water was obtained at these temperatures. The density values were then used to calculate the volume of the flask using Equation (3.3). These values are shown in Table 3.2.

Table 3.2 Summary of pycnometer calibration data

Quantities	Values				
Temperature (^oC)	20	30	40	50	60
Weight of empty pycnometer (g)	23.34	23.34	23.34	23.34	23.34
Weight of meter + distil water (g)	48.33	48.27	48.20	48.11	48.04
Weight of distil water (g)	24.99	24.93	24.86	24.77	24.70
Standard density of water (g/cm^3) [*]	0.998207	0.995648	0.992215	0.98804	0.98320
Volume of pycnometer (cm^3)	25.0349	25.0390	25.0551	25.0698	25.1221

[*] (Patricia, 2011b)

Average value of 25.0642 cm^3 was evaluated from Table 3.2 as the volume of the pycnometer. This value almost equates to 25.011 cm^3 indicated by the equipment manufacturer. Using the new average value, density of water was again evaluated, following the steps previously described at room temperature of 20 ^oC. The value obtained was able to validate the standard value available in the text. Therefore, not only that the meter was calibrated but also that the measurement method was as well validated.

3.3.3.2 Measurement procedure

Following the calibration procedure, the average density of sodium surfactin, in both aqueous and saline media, were measured by weighing each of equal volume of the sample. The density value was then calculated numerically using Equation (3.3).

$$\rho = {m}/{v} \tag{3.3}$$

Additionally, the effect of temperature (in the range of 1 – 50 ^oC) on density of sodium surfactin was evaluated and presented in Appendix D1.

3.3.4 Conductivity measurement

Conductivity measurement is a means by which flow of electric current through a solution is investigated. It is a measure of the ionic concentration (cations and anions) in a solution. Therefore, it may be safe to remark that conductivity is also a measure of the concentration of dissolved solids

which have been ionized in a polar solution such as water. The conductivity of ionic solutions is dependent on several factors, prominent of which are; ionic concentration, mobility of ions, valence of ions, and temperature.

Electrical conductivity in solutions, unlike in metals (which depends on electrons), is dependent on ionic transfer. Therefore, changes in temperature could increase or decrease drift velocity and consequently ionic mobility.

3.3.4.1 Equipment description

In this study conductivity of sodium surfactin was measured, in aqueous and saline media, using ORION STAR A222 conductivity meter (Figure 3.7). The meter is a robust device which is portable and can be used both indoor and outdoor. It has measurement capability of 4 quantities; conductivity, salinity, total dissolved solids (TDS) and resistivity.

Figure 3.7 ORION STAR A222 conductivity meter

Below is a summary of some of the Orion Star A222 conductivity meter features.

i. Conductivity range of 0.00 to 300 mS/cm with up to four figure significant resolution and up to five calibration points, and relative accuracy of 0.5% ± 1 digit.

ii. TDS range of 0 to 200 ppt with up to four figure significant resolution.

iii. Salinity range of 0.01 to 42 ppt practical salinity or 0.01 to 80 ppt NaCl equivalent with 0.01 resolution. Relative accuracy and resolution of ±0.1 and 0.01 respectively.

iv. Resistivity range of 2 ohms to 100 mega-ohms with 2 ohms-cm resolution.

v. AUTO-READ and continuous (with 'hold' option) measurement m modes.

vi. 1000 points data log

vii. Manual and automatic with AUTO-READ data logging functions.

Using this meter, the conductivity of sodium surfactin, in aqueous and saline media, was directly measured at variable temperatures of $1 - 50$ $^{\circ}$C, using 2.1 $^{\circ}$C temperature adjustment factor. Alternatively, Light *et al.*, (2005) suggest that conductivity can as well be measured in terms of the solution's electrical resistivity, and values numerically evaluated using Equation (3.4).

$$Conductivity = \frac{1}{Resisitivity, R}$$
(3.4)

As is the case with every other experimental device, conductivity meter was first calibrated to ensure precision and result accuracy.

3.3.4.2 Conductivity meter calibration

ORION STAR A222 conductivity meter was calibrated automatically using 1413 µS/cm and 12.9 mS/cm (Figure 3.8) conductivity standard solutions, following the equipment manufacturer guidelines.
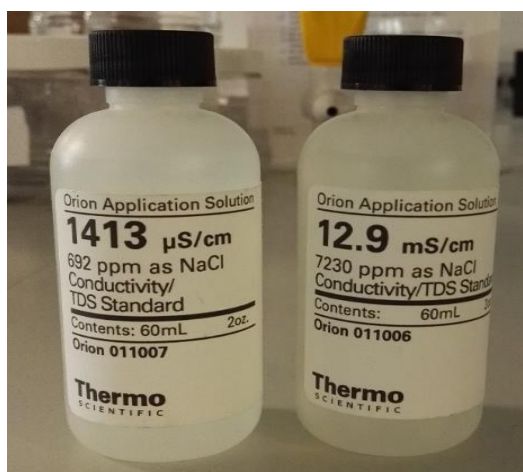
Figure 3.8 1413 μS/cm and 12.9 mS/cm conductivity standard solutions

The following steps were taken to ensure precision and accuracy during the calibration process.

    i.   Conductivity cell was connected to the meter.

   ii.   The cell was then rinsed in distil water and blot dry using a lint-free tissue.

  iii.   Once the displayed conductivity value was confirmed, 'f3' (cal done) button was pressed to end the calibration process.

  iv.   Meter was then powered on, and the cell placed into 1413 μS/cm calibration standard.

   v.   'f1' (cal) button was then pressed to initiate the calibration process, bearing in mind that the conductivity cell constant, k, inputted into the meter equals to 0.475.

  vi.   Once the cell and the calibration standard were ensured to be ready, 'f3' (start) button was pressed to start the calibration process.

 vii.   The meter will then read and display the conductivity of the standard. Displayed reading must be allowed to stabilize before it is accepted or recorded.

viii.   Once the reading stabilises, 'f2' (accept) button was pressed to accept the displayed conductivity value.

  ix.   'f2' (next) was thereafter pressed to proceed to the next standard, and steps ii – vii were repeated using 12.9 mS/cm conductivity standard.

Sodium surfactin samples were then made ready for conductivity measurement. Readiness of the meter for conductivity, after calibration, ensured by pressing the 'f1' (meas) button on meter.

3.3.4.3   Conductivity measurement procedure

Procedures for measurement of conductivity, as outlined in the equipment operating manual, were as follows:

After conductivity meter was powered on by pushing the 'power' button and the display screen allowed to stabilize. This was confirmed by display of 'ready' on the meter screen.

Conductivity meter probe was then immersed into the solution samples and stirred. This is to ensure release of any trapped air bubble in the probe and sample. The sensitivity of the meter is configured in such a way that it immediately begins to read the solution conductivity.

These values are displayed on the screen. Final conductivity value is taken when a stabilized conductivity reading is obtained. These procedures were followed for all samples prepared.

Moreover, an increase in the solution's temperature could potentially cause a decrease in its viscosity. Consequently, the mobility of the ions in the solution increases. Additionally, temperature increase perhaps results in molecular dissociation, and consequently increase in number of ions. Therefore, changes in temperature could affect the ionic conductivity of the solution samples.

On this note, effect of temperature on conductivity of surfactin samples was experimentally evaluated as follows:

A bath was half-filled with crushed ice.
Container containing surfactin sample was the immersed in the ice (bath), ensuring that that ice level is slightly above sample level.
The bath was then placed on magnetic stirrer.
With conductivity meter probe immersed in the sample, the stirrer was started to ensure temperature equilibrium within the sample.
Sample temperature was continuously monitored on the meter display screen, until lowest value of 1 $^{\circ}$C was reached. Conductivity reading at this temperature was obtained and recorded.
Heating mantle was then on to gradually heat the sample at average temperature increase of 2.5 $^{\circ}$C/sec. Conductivities at every 0.5 $^{\circ}$C temperature increase were recorded as indicated in Appendix D 3, and analysis conducted. These analyses are presented in section 4.2.6 of this report.

3.3.5   Fourier-transform infrared spectroscopy (FTIR) analysis

FTIR analysis has been a useful device for qualitative analysis of polymeric, organic and perhaps inorganic materials. It functions by scanning samples, using an infrared light, and consequently observe their chemical characteristics. Functional group and cyclic or planar nature of materials can be deduced using FTIR analysis. Analysis using FTIR is based on theory of absorptivity, where the instrument sends an infrared radiation (typically in the range of 10,000 to 100 cm^{-1}) through a

sample. While some of the radiations passed (transmitted) through the sample, some becomes absorbed, as illustrated in Figure 3.9a. The absorbed radiation is then transformed to rotational and/or vibrational energy in the form of signal (see Figure 3.9b) by the sample molecules. Resultant signal is detected and presented as a spectrum, typically from 4000 cm^{-1} to 400cm^{-1} wavenumber (Coates, 2006), which signify a molecular fingerprint of the sample. Each chemical structure or molecule will produce a distinctive spectral fingerprint, making FTIR analysis a great tool for chemical identification.
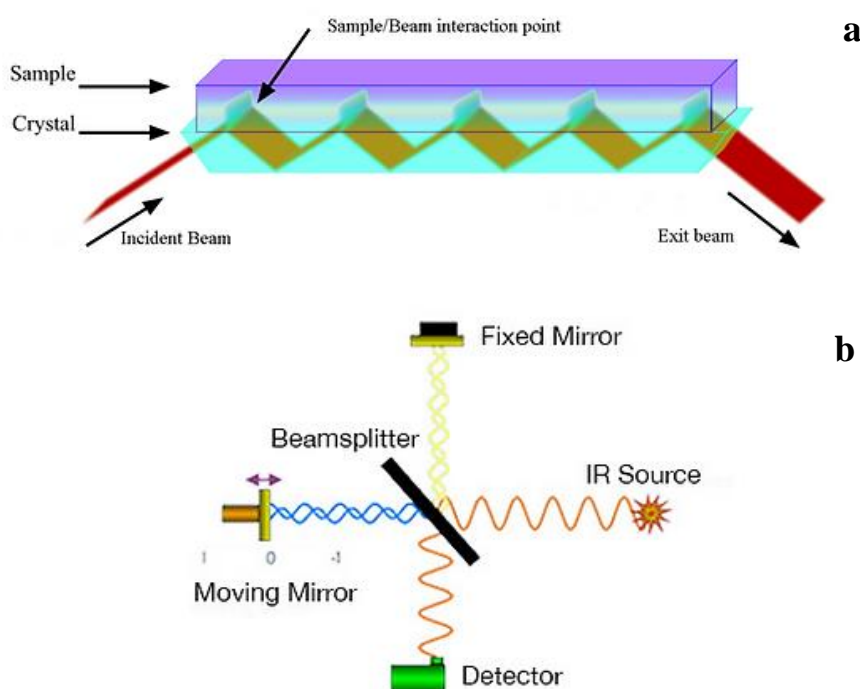
Figure 3.9 Transmission and absorbance of radiation (a) and conversion of absorbed radiation into signal (b) during FTIR analysis

The procedures of FTIR analysis followed in this study are stated in the sub-section 3.3.5.1.

3.3.5.1   Experimental procedure

Fourier-transform infrared spectroscopy (FTIR) analysis of dry, powdered surfactin was conducted using Nicolet™ iS10 FTIR Spectrometer, set up is shown in Figure 3.10. The equipment is situated at the Analytical Laboratory of the School of Environment and Life Science, Cockcroft Building, University of Salford, UK. It is operated using OMNIC–controlled software. Having a dedicated computer for the equipment and initiating the analysis by opening the OMNIC software window, the following steps were thereafter followed.
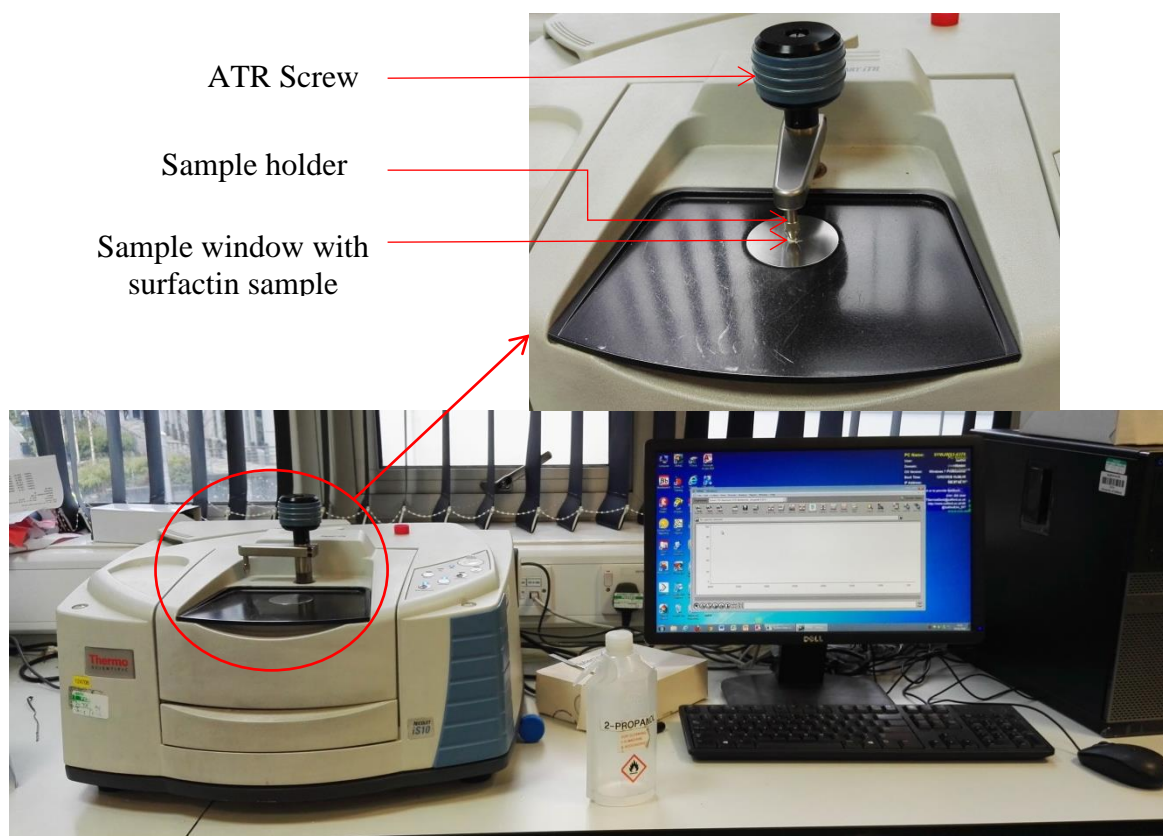
Figure 3.10 Set up of Nicolet™ iS10 FTIR Spectrometer

   i.   Smart iTR Diamond ATR accessory was selected.

   ii.   Sample drop window was cleaned using 2-Propanol, and soft tissue.

   iii.   ATR screw and sample holder were placed as shown in Figure 3.10 and screwed until a click sound was heard. Background of the sample window was 'run' by clicking on 'Col Bkg' on the software window/menu. 36 scans were made at completion of the collection, and a background spectrum was generated as shown in Figure 3.11. Status of the scan was monitored using the status bar.

   iv.   Sodium surfactin sample the put onto sample window, ATR was screwed until a click sound was heard.

Readers should note that absorption spectra were plotted using a built-in plotter, and the IR spectra were collected from 4000─500 cm⁻¹ wavenumbers.

Collect background button

Collect sample button

Scan status bar
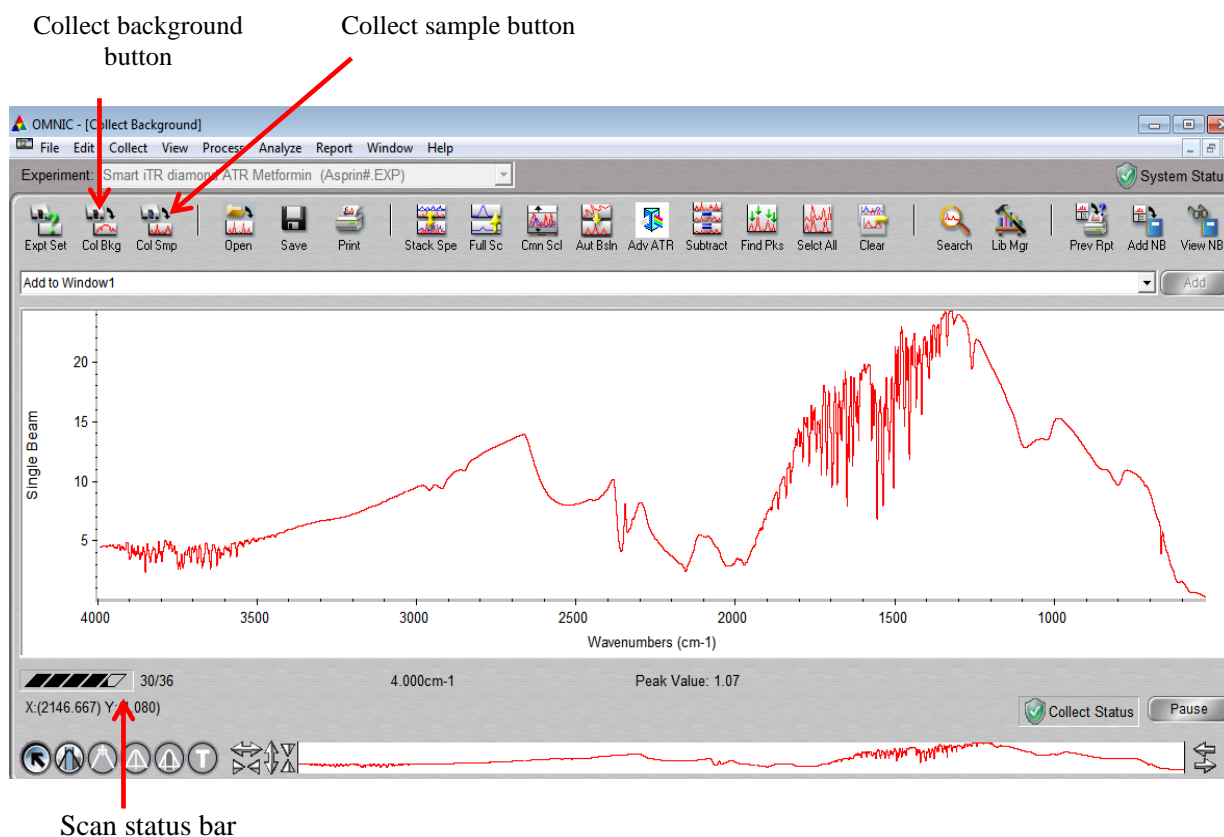
Figure 3.11 Spectrum of FTIR background before surfactant was analysed

v. Sample spectra were obtained by clicking on 'Col Smp' button. As the case with background collection, 36 scans were as well performed.

vi. On the 'Analyze' menu, peaks of interest were selected, and axis was changed from absorbance to transmittance, and new specified spectra were then used to replace the generated spectra.

Results generated were both saved and printed as desired by the researcher and is presented in Section 4.2.7.

The IR sample window was then cleaned using 2—propanol for next round of analysis.

These procedures were repeated for all prepared samples.

3.4   Flow Behaviour Characterization

Rheology is a measure of fluids deformations when exposed to any form of stress. Study of rheology assesses how fluids respond to varying rate of shear. Relating to this study, measurement of rheological properties is important in assessing level/condition of failure of sodium surfactin, and its stability during adsorption at fluid surfaces. Characterization is presented in terms of effect of

variable rate of shear, temperature and salt concentration on extent of samples resistance to flow (viscosity). Thereafter, the flow behaviour is then defined using standard behaviour of fluids available in literature (see Figure 2.5 and Figure 2.5). Besides, flow behaviour can be a tool for indirectly measuring fluids consistency and quality. Since during operations, materials physical characteristics should be consistent from one process unit to the other. Some of the direct effect of viscosity, and the need for this phase of the experimental study has been highlighted in Section 4.3.

The steps taken to characterize rheological behaviour of sodium surfactin are presented in the Subsection 3.4.1 and 3.4.2.

3.4.1 Equipment calibration

The rheological experiments were carried out using ORCADA® software–controlled OFITE viscometer (Model 1100), set up of which is shown in Figure 3.12. The viscometer has a shear rate range of 0.01–1000 s^{-1} and 0.001 RPM speed accuracy. The device is configured with a rotor bob, whose notation is R1B1. It is basically fitted with a thermocouple that senses any variation in temperature and consequently sends the signal to the system; a bob that senses and transmit the shear stress response during experimental runs; sample cup where samples are poured into to be attached to the rotor, which is fitted with a nut which aid in attaching the cup to the rotor; and heat bath for raising temperature of samples.
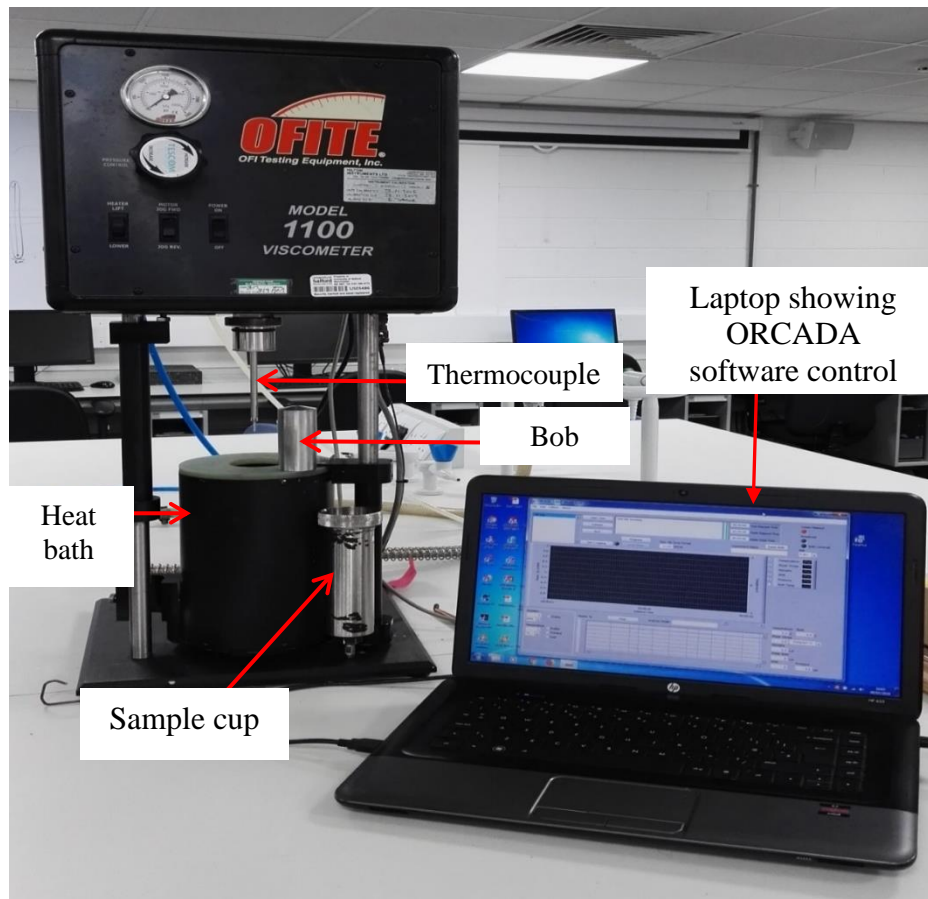
Figure 3.12 Rheology measurement equipment set-up

As is the case with most devices, the viscometer was first calibrated before any run of experiment was conducted.

Calibration procedure

Based on its configuration of B1, 42 ml of calibration fluid was used to first calibrate the viscometer, following equipment manufacturer operating procedure. The sample cup was unscrewed, and both sample cup and rotor bob were gently but thoroughly washed with detergent to remove any trace of previous samples that were worked on using the equipment. After complete drying of the washed components, the bob was gently screwed to the thermocouple, followed by screwing of the sample cup (via sample cup nut) containing 42 ml of the calibration fluid unto the rotor. The equipment was turned on via the ON/OFF switch, and ORACADA software was opened to start the calibration process. On the 'Utilities' tab of the ORCADA window, 'Calibrate Shear Stress' was selected which pop-up another window (Figure 3.13) for keying the calibration variables. To begin, fluid manager button (indicated by red arrow in Figure 3.13) was selected. Doing that popped-up another mini sub–window (Figure 3.14) for keying the calibration variable.
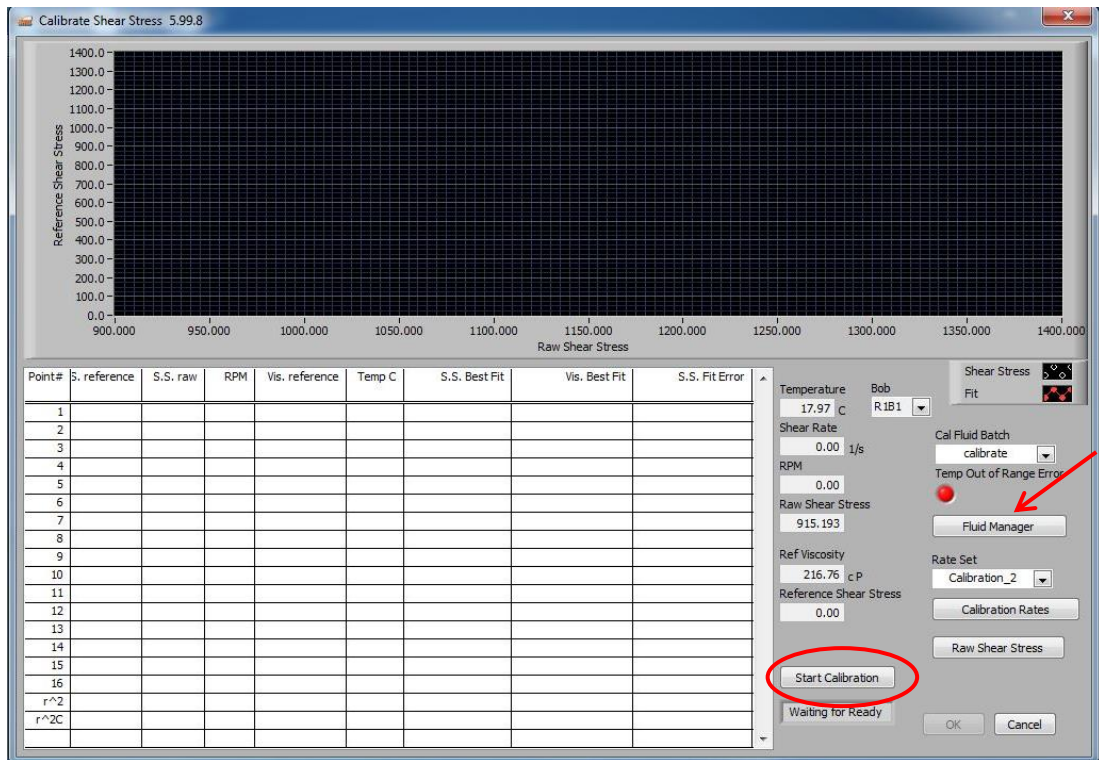
Figure 3.13 Viscometer calibration window

Based on equipment manufacturer's specification, temperatures and corresponding viscosity values shown in Appendix A 1 (red circled in Figure 3.14) were keyed in, as well the calibration batch. This is to differentiate the current calibration from previous calibrations. It is important to note, while calibrating the device, that: (1) 'Table Linearity Error' indicator (green circled) must remain red, (2) the viscosity-temperature plot must as well be linear, and (3) the sample temperature is within the range of calibration temperatures specified, using indicator circled in purple. These are indicators and sources of calibration errors. Once these are Okayed, 'raw shear stress values' in the range of 1≤raw shear value≤300 were inputted via 'Calibration Rates' button.
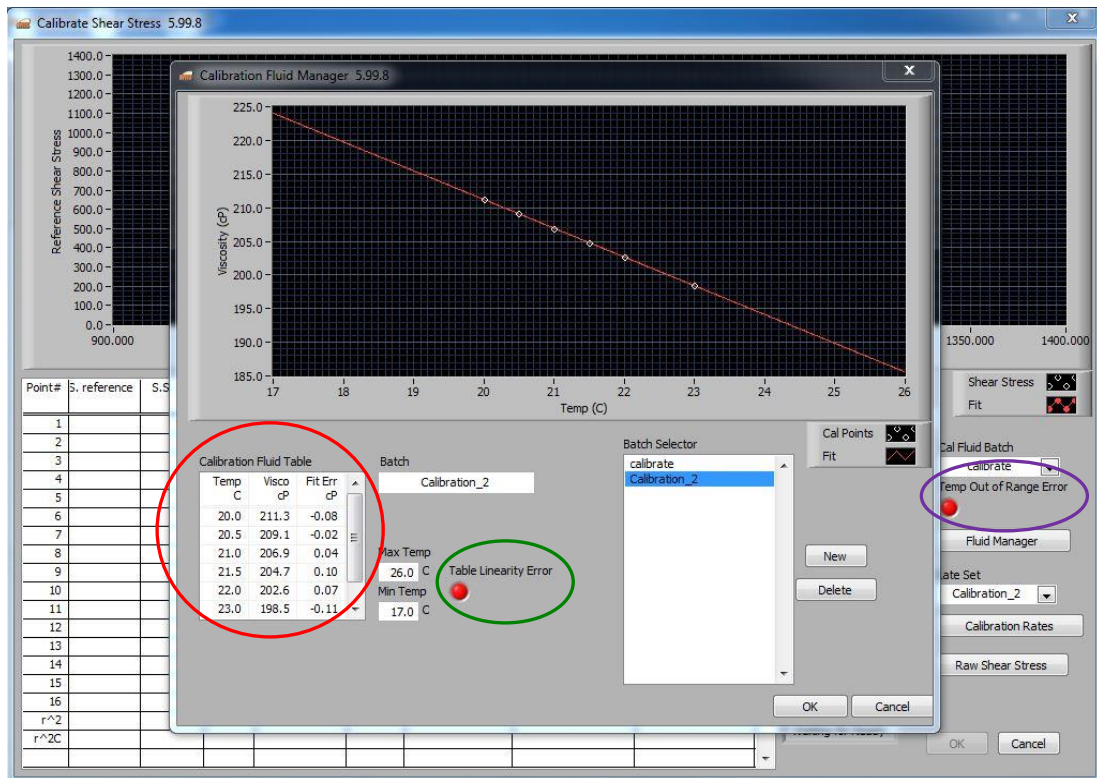
Figure 3.14 Calibration data input window (Fluid manager)

On completion of the input process, the 'Start Calibration' button (red circle in Figure 3.13) was pressed and the equipment calibration began. On completion, calibration result window, shown in Figure 3.15, pop-up which indicates the status and accuracy of the calibration. The accuracy was ascertained when "r^2C" value is greater than 0.9990. A value of 0.9998 was obtained for this study, as shown using red circle in Figure 3.15. Completion of this step marked the end of the calibration, and consequently indicates the readiness of the viscometer for rheology measurement.
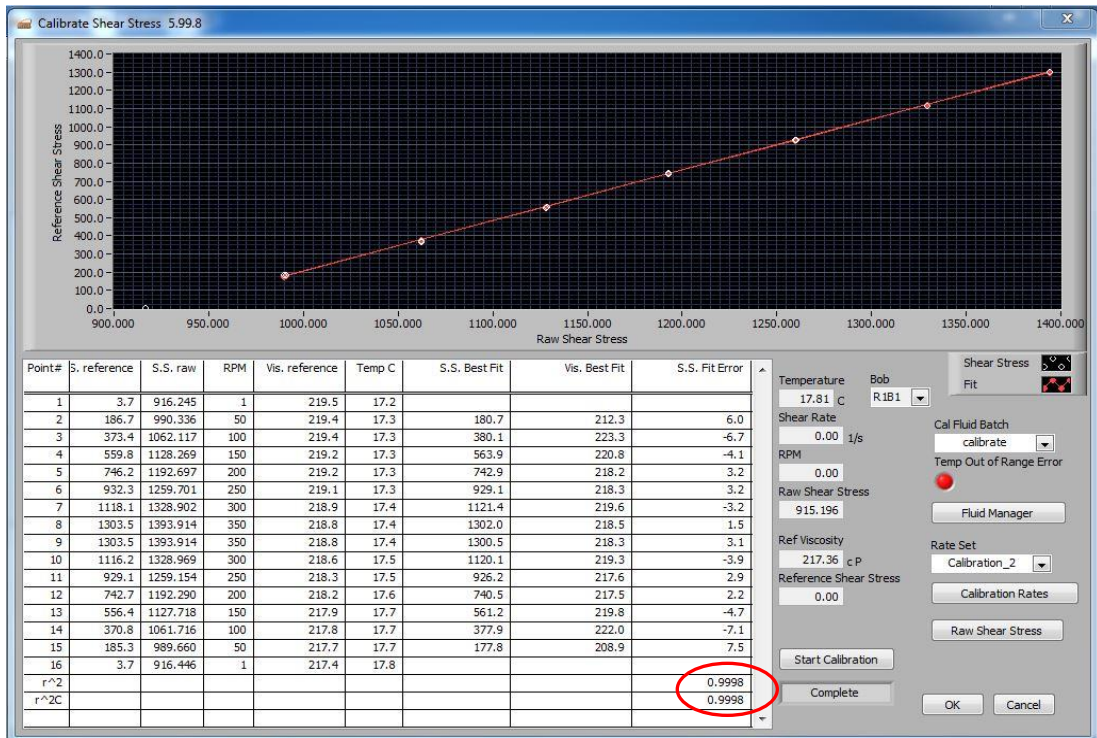
Figure 3.15 Calibration output ("r^2C" value)

3.4.2 Rheology measurement procedure

To properly and accurately measure the rheology of the samples, sample cup, bob and thermocouple were washed and cleaned to remove any trace of calibration oil. Presence of calibration oil will greatly impact on the results of the samples under study.

On the 'Edit' menu of the ORCADA interface, Test Builder (Figure 3.16) was selected to in order to specify the input data (RPM, temperature, etc.) and Test analysis model/template. RP 10B analysis model/template (combination of Power Law and Bingham Plastic Models) was selected for this study (see red circle in Figure 3.16). Temperature in the range of 23 (ambience) 30, 40 and 50 ^{o}C were inputted with an allowance of ± 1 ^{o}C, and shear rate of 50 – 600 RPM were specified for the test. An example is shown within purple circle in Figure 3.16. Thereafter, units of shear stress and viscosity were then specified accordingly in the process variable section of Figure 3.17. Having keyed in the input data and the test analysis mode selected, 42ml of each of dosage samples prepared was measured and poured into the sample cup and tightly screwed. "Start Test" button was entered to begin analysis, until all RPM specified were completed.
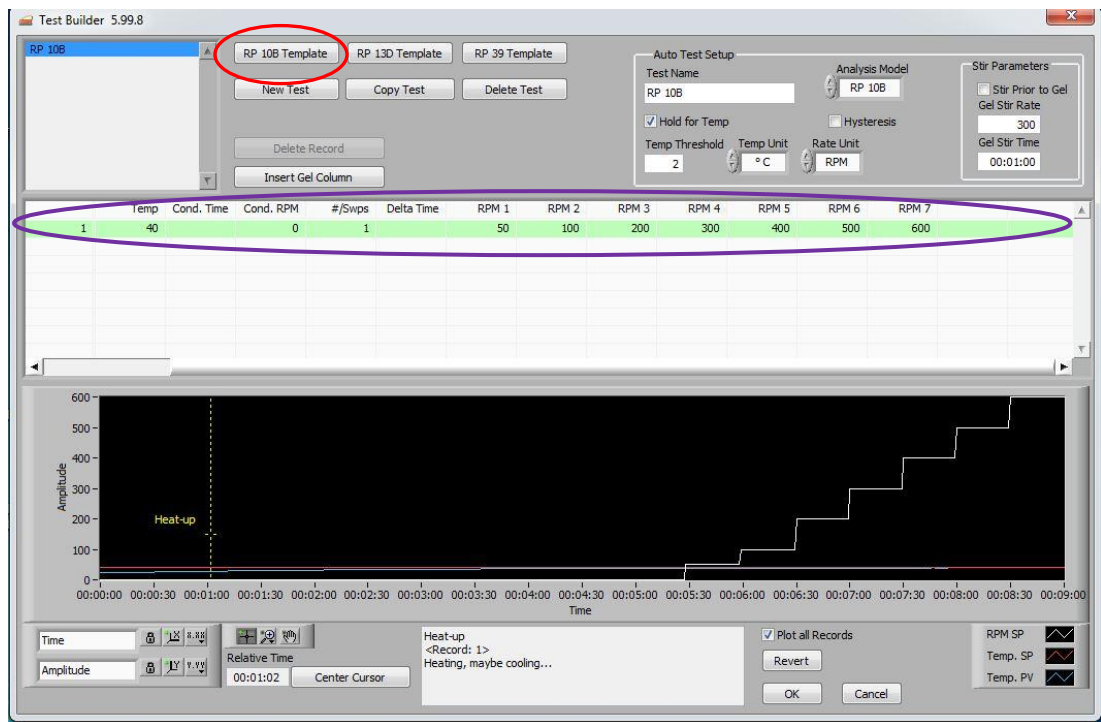
Figure 3.16 Rheology analysis 'test builder'

Progress of all running test was monitored using the identified (process) variable as labelled in Figure 3.17. Additionally, readers should note that to increase temperature, heat bath control was used to raise and lower the heat bath. Each desirable temperature was manually inputted via the manual temperature control. Rise, decline and equilibrating of temperature were as well monitored on the process variable section/panel (indicated by green circle).

This same procedure was repeated for the samples prepared with saline solution, except that the temperature was not varied. The test was conducted at ambient temperature of 23 $^{\circ}$C with an allowance of ± 1 $^{\circ}$C.
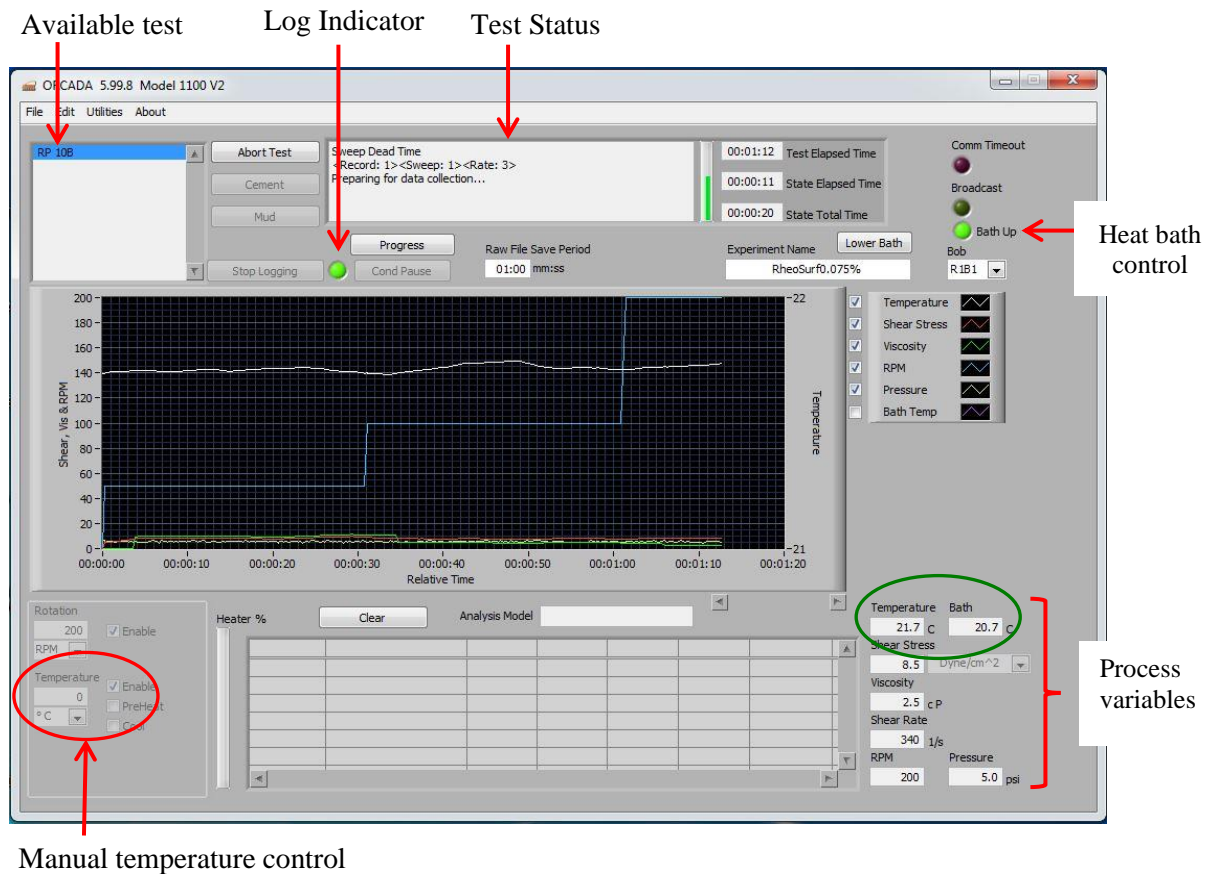
Figure 3.17 Rheology test and variable control window

The ORCADA software is robust such that results of rheology test conducted can be extracted in the form of output data. Extracted output values were then used to make appropriate plots that were subsequently employed to characterize the surfactant rheological behaviour. These are presented in Section 4.3.

3.5 Thermal Analysis – Diffraction Scanning Calorimetry (DSC)

During oil and gas operations, materials (oil, gas, water, or mixture of both) flow from one process unit to the other. These units may operate at different conditions of temperature or pressure required for desired product outcome. Additionally, the conditions may be altered intentionally to achieve specific objective. For example, during oil and gas transport, operating conditions are deliberately altered to prevent certain incidences from happening. Conditions of temperature or pressure may be altered to prevent wax or hydrate deposits. However, fluctuations in variables such as temperature, pressure, concentrations, etc, could change thermodynamic properties of the system. Consequently, components of the system may in turn experience this effect which could increase or decrease their performance.

Performance of other components within the system, such as surfactants, may however be influenced by the change in thermodynamic properties. Moreover, many chemical molecules are susceptible to temperature and pressure fluctuations during operations. Mahmood and Al-koofee, (2013) indicates that critical micelle concentration of Tween series chemical surfactant was affected by changes in temperature. They further reported that the critical micelle concentration of Tween series (20, 21, 40, 60 and 80) decreased with temperature increase. Recall that CMC is the concentration above which surfactant performance remains constant or begins to decline. Therefore, increasing temperature perhaps will increase the performance of the Tween series surfactants—a chemical surfactant. However, to a critical surfactant concentration or dosage. Much lower CMC may as well hinder surfactant activity effectively at fluid interphase.

Biosurfactants on the other are biomolecules and are perhaps no different from the chemical molecules. To satisfy this curiosity, it is important to conduct a thermal analysis on surfactant system. Though studies have indicated that biosurfactant have good thermal stability, it is important to validate findings and method to understand general applicability of a published result. Furthermore, findings of studies may be intended for specific application. For instance, Saxena *et al.*, (2018) conducted thermal characterization of biosurfactant isolated from *Sapindus laurifolius*. The thermal gravimetry analysis (TGA) result showed an initial thermal weight loss of 6 % between 370 K and 540 K. Further to these findings, the authors also indicated that with increasing temperature, the system entropy and negativity of the Gibbs free energy increases. Entropy of a system denotes the degree of randomness of the system. Therefore, increased entropy is an indication that micellar structures (micelles) are been destroyed by the temperature increase.

Similarly, Chandankere *et al.*, (2014) conducted TGA analysis on *Bacillus methylotrophicus* and reported two phase thermal degradation. First phase degradation showed a weight loss of 8.87 % at 30–150 °C while second phase degradation occurred at 300 °C (with a weight loss of 54 %). The weight loss at 30–150 °C could be loss due presence of moisture in the sample. Such temperature regime is perhaps low for the decomposition of the biosurfactant to occur. Besides, previous studies reported biosurfactants to be thermally stable within the 30–150 °C temperature regime. Additionally, (Karlapudi et al., 2018) indicated that lipopeptides biosurfactants produced from *Bacillus subtilis* isolates were thermally stable at temperatures below -15 °C and above 121 °C when stored for 180 days.

3.5.1 Equipment description

Differential scanning calorimetry (DSC) machine is used to characterise, among other things, thermal analysis of materials. The TA DSC2500 machine comprises of 3 components; cooling section, DSC machine control section including an automatic sampling area, and a computer in which TRIOS software is installed and via which the DSC machine is controlled. The TRIOS software provides a convenient is a combined package for that allows for instrument control, data analysis and reporting. Figure 3.18 shows the TA DSC2500 model machine.

DSC Control panel/touch screen interface
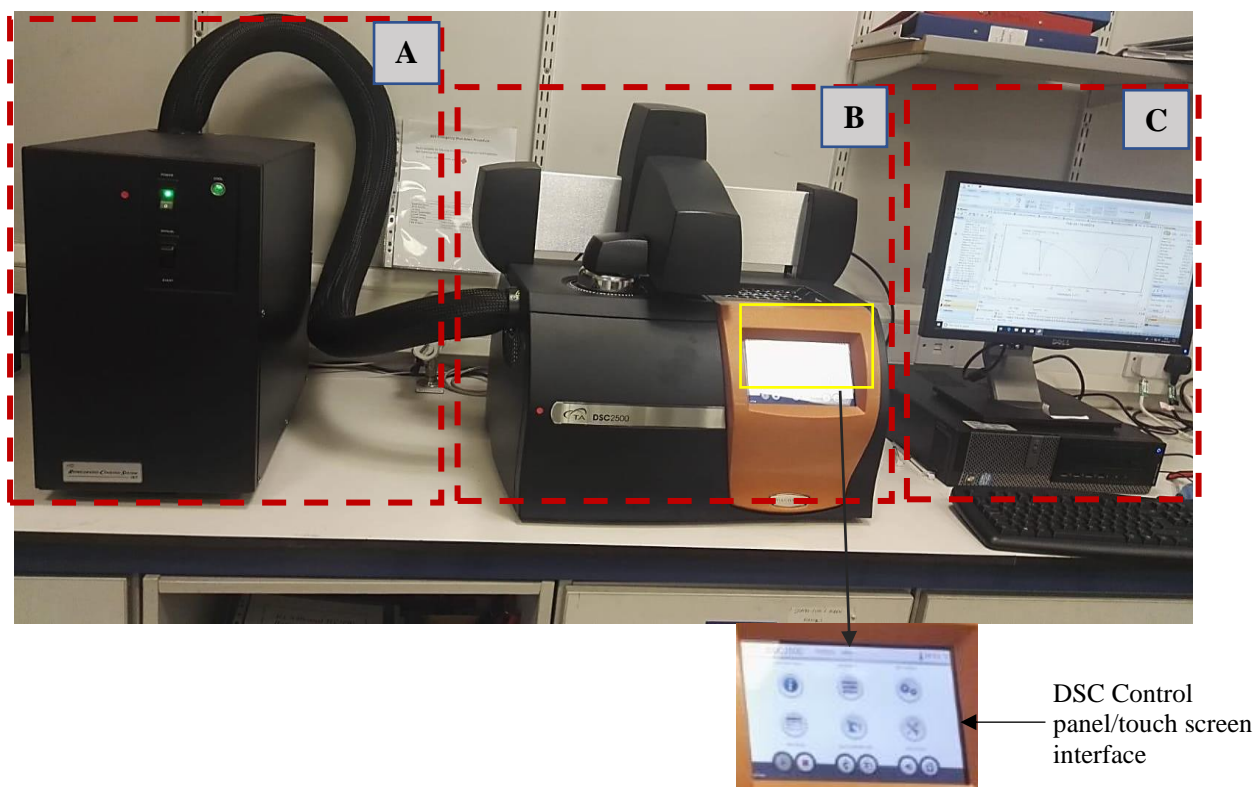
Figure 3.18 TA DSC2500 set up along with (a) cooling section/accessory (b) DSC instrument, and (c) Controller (computer)

TA DSC2500 is a high-sensitivity equipment that is fortified with a 54-position autosampler and dual-stage mechanical cooling, allowing a -180 to 725 °C temperature range that enable evaluation of various thermal transitions. It has an accuracy of ±0.025 °C; Temperature and enthalpy precision of ±0.005 °C and ±0.04 % respectively (TA instruments, 2019).

3.5.2 Experimental procedure

Generally, outline of thermal analysis experiment using TA DSC2500 machine is as follows:

i.   Instrument calibration.

ii.   Sample pan selection.

iii.   Sample preparation.

iv.   Configuration of autosampler or manually loading the DSC cell.

v.   Designing and running experimental runs using the TRIOS software.

3.6   Methane-Water Surface Tension (ST) Measurement

Nearly all field operations in oil and gas processes involves multiphase interaction of process fluids. Critical to interaction of multiphase fluids at both upstream and downstream operations is the surface interaction. Surface or interfacial tension is one physical process that is fundamental to the characterization and understanding of multiphase fluids interactions at interface. One may therefore deduce that results of accurate interfacial tension measurement will be a significant tool in prediction multiphase fluid interaction, including hydrate formation and inhibition. As Kodera *et al.*, (2020) will put it, interfacial tension is one of the most vital thermodynamic properties that controls the dynamic behaviour of multiphase flows. Therefore, promotion and inhibition of methane hydrate can be predicted by accurate interpretation of interfacial tension data. On this background, interfacial tension of multiphase CH_4-H_2O system was measured at different temperatures, pressure and surfactant dosages. Various methods, described in Figure 2.17, are employed to measure multiphase gas-water ST. However, in this study, the bubble rise method is been employed, using Corelab high pressure high temperature IFT10 equipment.

To capture in real time the simultaneous effect of temperature, pressure and surfactant dosage, the experimental procedure was designed using Design-Expert software v.12. The experimental design result is described in Section 4.5.2.

3.6.1   Experimental design

Experimental measurement of methane-water interfacial tension was design using Design-Expert software v.12. Design-expert is a statistical software package by Stat-Ease Inc, which is purposely created for experimental designs. It is a robust software that has the capability of comparative screening, characterization, parameter design and optimization. These robust features and performances were leveraged on to design the ST measurement experiment. Typical interface for creating new experimental design using Design-Expert is shown in Figure 3.19. Two-level factorial was selected for factors interaction, and Response Surface Methodology (RSM) for model creation.
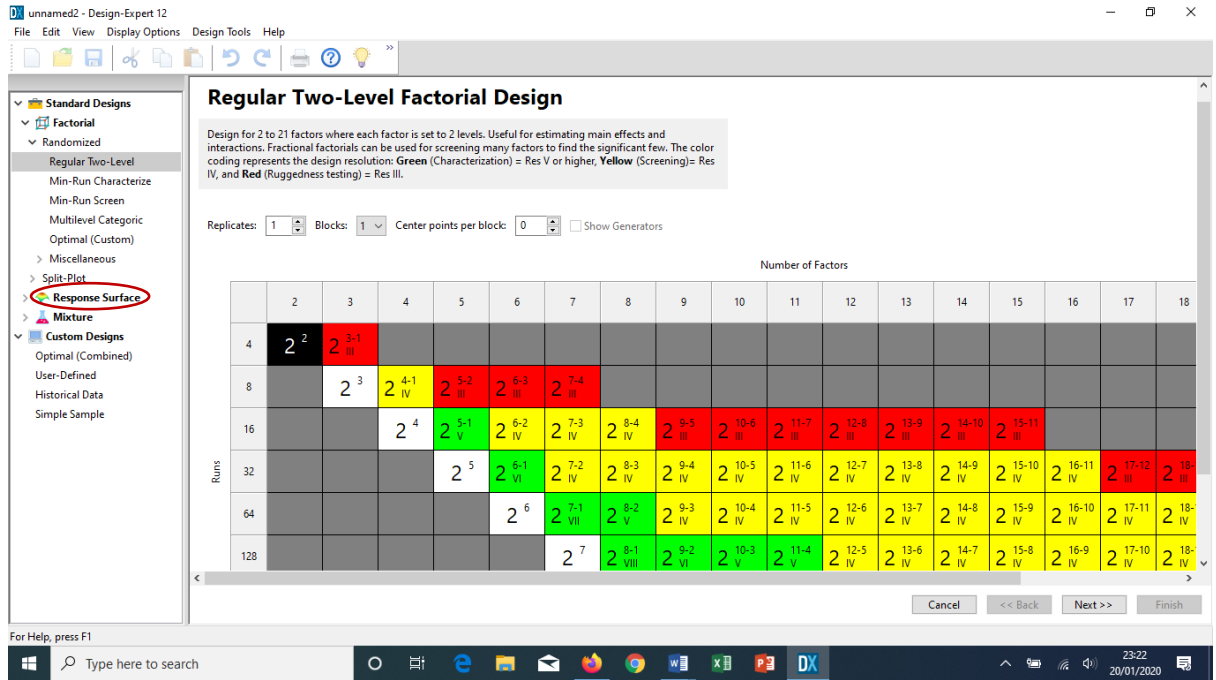
Figure 3.19 Design-Expert interface for choosing factorial level during experimental design

For purpose of flexibility in inputting all available factors under study, custom (user defined) design option was selected in the next window shown in Figure 3.20. Thereafter, output response is then specified in next window shown in Appendix B 1. Table of permutations generated by the software is shown Appendix B 3.
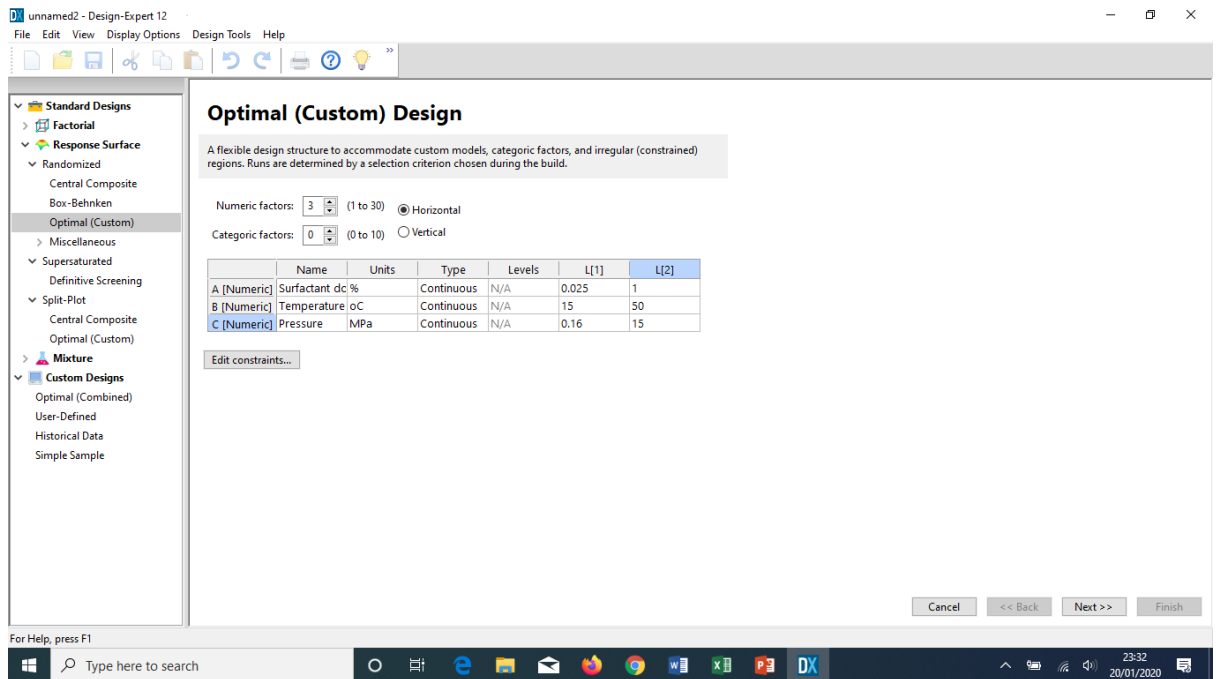
Figure 3.20 Custom design window where interacting parameters are defined

The experimental runs generated were then cautiously executed in the lab using appropriate equipment described in Section 3.6.2 and procedure described in Section 3.6.3.

3.6.2 Equipment description

Experimental setup for the surface tension measurement, using Corelab IFT10, is shown in Figure 3.21.

Figure 3.21 Experimental setup for ST measurement (1 Computer, 2 Temperature and pressure controller, 3 Vibration control bench, 4 ST cell, 5 Rame-hart camera, 6 &7 Accumulators, 8 manual pump, 9 Automatic pump)

The setup comprises of high-pressure (HP) measurement cell with a pressure rating of up to 10,000 psig, through which the rising bubble is generated. The bubble is captured by an attached Rame-Hart optical camera system which transmit live image display on to a data acquisition system (computer). Cable connection ensures that the camera is interfaced with the data acquisition system which has digital image processing software (DropImage software) preinstalled. Captured image (gas bubble) from the optical camera is processed by utilizing an inbuilt mathematical algorithm to evaluate the bubble profile generated. Bubble width, height, area and volume are simultaneously evaluated by the system and consequently the interface ST measured. Pressure and temperature are critical parameters in hydrate formation, including this experimental setup. Therefore, the setup is also fitted with temperature controller which ensures that elevated temperature within the system is

achieved. More so, high pressure HiP 62-6-10 manual pump is incorporated to: ensure delivery of liquid dispersion phase into the cell; and create a pressure built-up within the cell to mimic hydrate-forming equilibrium condition.

Bubble cell (Figure 3.22) is a critical component in this experiment. It is a stainless-steel component designed to accommodate both high pressure/temperature and low pressure/temperature. The cell is equipped with a sealed port for insertion injection needle. The needle is used for gas delivery into the cell and consequently used to generate bubble. The cell has the capacity of 39 cm^3 of sample volume.

Figure 3.22 Surface tension cell

3.6.3   Surface tension measurement procedure

In this study, "rising bubble" method was used to measure CH$_4$-H$_2$O ST. The pendant drop configuration was changed to rising bubble in order to minimize/eliminate error due to needle wettability. In pendant drop position, the needle appears to get wet and therefore did not allow the droplet to form good profile. To do so, the injecting needle was mounted upward from the bottom of the window cell. In this case the gas bubble (lighter phase) forms at the tip of the needle which is surrounded by aqueous surfactant (heavier phase) in the equilibrium condition.

Before start of any experiment, it essential to ensure that the experimental setup is rid of any remnant or trace of alien material that could potentially impede acquisition of accurate results. As such, the equipment setup was first cleaned by passing acetone through, and the blown with dry compressed

air. Warm distilled water was then charged through the setup to wash/flush the system. Thereafter, dry compressed air was again passed through system. Methane source was coupled to the system via the needle. Distil water was then charged into the ST cell, with the aid of manual pump, to create the liquid phase within the cell. Injection control was then gradually controlled to generate a desirable bubble. Bubble profile was then evaluated using the Drop image software and consequently methane-water ST measured. The system was then evacuated and dried using dry compressed air. 0.025 % aqueous surfactant (distil water-surfactant mixture) was then charged into the cell, bubble generated, and ST measured. Of course, this was at laboratory ambient temperature of 20.5 $^\circ$C and ambient pressure. Temperature and pressure were then specified accordingly based on the experimental design. Methane gas was then gradually released into the liquid dispersion phase until desirable bubble is generated (see Figure 3.23). Bubble was allowed to stabilise, and ST then measured. The steps outlined above were followed for 0.05, 0.075, 0.1, 0.5 and 1.0 % dosages of aqueous surfactant, and ST measured in each case.

For repeatability and data accuracy, at least 3 bubbles were generated in each experiment conducted and ST repeatedly measured in each case.

Figure 3.23 Methane gas bubble generated for ST measurement

3.7 Chapter Summary

Every research study has proscribed design procedure, particularly experimental research. These procedures have been highlighted in this chapter. Physicochemical characteristics such as density, emulsification index, pH, surface tension (ST) and functional group were investigated. Pycnometer was used for density; Orion Star A222 conductivity meter was used for conductivity measurement; Nicolet iS10 was for functional group analysis; and OFITE IFT10 was used for ST measurement. Repeatability was ensured by taking average of at least three readings for each measurement made.

CHAPTER FOUR

4 RESULTS AND DISCUSSION

4.1 Chapter Overview

This section presents the outcome of the experimental investigations carried out on the course of the PhD study. According to the outlined target, objectives and the activity scheme of the study presented in Figure 3.1, results and analysis are presented in this chapter. Phase I which involved physicochemical characterization and identification of various properties of sodium *surfactin* including availability of active site for adsorption inferred by functional group and density identification are presented in Section 4.2. Other characteristics identified and discussed in the chapter include pH, electrical conductivity, foaming and solubility in various solutions containing different ionic (salt) concentrations. It is important to consider different dosages of sodium surfactin while conducting investigations of this nature. The upcoming sections will as well highlight to the reader the numerous reasons for considering variable surfactin dosages.

Section 4.3 of the chapter presents the results of Phase II investigations on level of response of sodium surfactin to various rate of shear (rheological study). Consideration was made of effect of variations in temperature, and definition of the characteristics features of such responses discussed.

Section 4.4 presents result of thermal stability test conducted on sodium surfactin using DSC machine. Lastly, in Phase III, performance of sodium surfactin in reducing surface tension between methane-distil water system at different conditions of temperature and pressure is presented in section 4.5.

4.2 Phase I: Physicochemical Characterization of Samples

One of the most important phases to investigating and analysing the effectiveness of sodium *surfactin* application in the oil and gas operations is the physicochemical characterization. It is a critical tradition in the engineering practice that material specifications are set at the design early stage. Material characterization therefore becomes an integral part of this stage. Therefore, it is important to evaluate physical, chemical, electrical, and biological and thermal properties of every material before use.

Characterization of *surfactin* solution guarantees accurate identification of the surfactant. Furthermore, it makes it easier and possible to classify the nature of interaction and relationship of the surfactant with the utilization phase/system. Physical, chemical, and electrical characterization of surfactants are done by analysing and determining its properties. These properties include density, viscosity, conductivity/resistivity, pH, chemical/elemental composition, and functional group. Additionally, enhancing the nature of the surfactant interaction with its utilizing phase/system is greatly dependent on its solubility capabilities. Investigating surfactant's extent of solubility in different media is very significant in ensuring accuracy of the characterization.

More so, most oil and gas operations involve medium containing certain range of salt content as part of reservoir fluid. The content of the salt differs from one reservoir to another. This is because composition of saline medium depends on the history, source and thermodynamic conditions of a reservoir. Thermodynamic and chemical changes are perhaps very common in oil and gas field operations. Therefore, it is very critical if the surfactant characterizations are also investigated in saline (salt-containing) medium. Response of *surfactin* to changes in salinity and temperature will, to a large extent, effectively and significantly describe its chemical and thermodynamic behaviour. As a way of prediction, these properties will serve as tools in the design and estimation of best performance point/condition of the *surfactin*, including its tensioactive capabilities. Furthermore, the physicochemical characteristic assessment will enhance thermodynamic analysis of *surfactin* phase behaviour.

4.2.1   Characteristics of NaCl salt (saline) solution

Dissolution of NaCl salt in distil water was endothermic, with heat being absorbed by the system. Figure 4.1 indicates that complete physical dissolution of NaCl in distil water led to formation of clear, homogenous solution. Increased mass (amount of salt) dissolved in the solution has led to progressive increase in density and conductivity. NaCl do not expand when dissolved in water.

Figure 4.1 Aqueous NaCl salt (saline) solution prepared

Therefore, after dissolution no volume increase could compensate for the mass increase, hence the progressive increase in density with increase in salt concentration (Figure 4.2a). Salt solution prepared had minimum and maximum density of 998.433 kgm^{-3} and 1054.891 kgm^{-3} respectively at 0.05 and 1.5 M concentrations. Strong interaction occurs between sodium cations and chloride anions with water. Consequently, oxygen atom of water molecules acts as a Lewis base and coordinates to the Lewis acidic sodium cation in donor-acceptor bonds (Patricia, 2011a). Moreover, aqueous NaCl has a density which is close to that of water. Conductivity characteristics exhibited is similar to that of density (Figure 4.2b). Increasing ionic concentration in the aqueous media increased electrostatic repulsion between the ionized NaCl molecules.

Conversely, pH exhibited a somewhat monotonic behaviour (Figure 4.2c). At initial concentration of 0.05 – 0.1 M, the solution pH increased from 5.61 at 0.05 M to 6.22, at 0.1 M concentration. The pH, however, began to decrease to lowest value of 5.47 at 0.5 M concentration. The decrease could be attributed to a potential related to the Na^+ concentration being produced in the same way as with H^+ ions. Therefore, the electrode detects a combined activity of H^+ and Na^+ ions that resulted in pH decrease. Beyond 0.5 M concentration, the pH began to increase again to 5.5 and 5.94 respectively at 1.0 and 1.5 M.
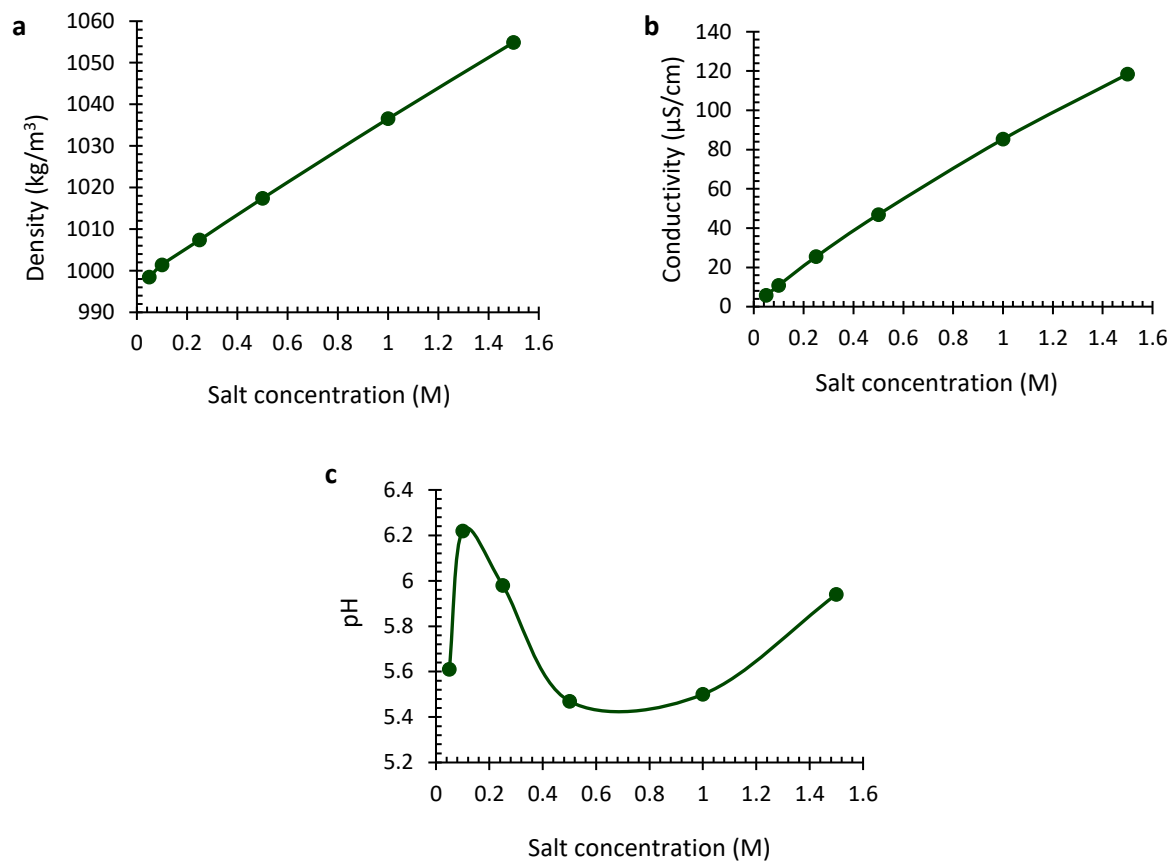
Figure 4.2 Characteristic (a) density, (b) conductivity and, (c) pH behaviour of aqueous NaCl solution prepared

Additionally, it is important to note that the pH behaviour in saline solution indicates that pH is a dependent factor on the ionic activity, rather than the superficial concentration alone.

4.2.2 Surfactant foaming and solubility characteristics

Different chemical substances exhibit different form of physical or chemical behaviour when dissolved in a solvent. Surfactants on the other hand exhibits its unique properties when dissolved in distil water. Foaming is a one of the characteristics exhibited by surfactant.

Generally, during field operations, aqueous foams are produced simply by introduction of gas or air beneath the surface of surfactant-laden liquid, which expands and enclose the gas with a film of liquid (Apaydin & Kovscek, 2001; Rosen & Kunjappu, 2012). However, most surfactant are themselves foam-forming in nature. This characteristic is one reason that endears surfactant as good foaming agents for many oil and gas field applications. Irawan, Permatasari and Bayuaji, (2017) reported that foam injection is a useful and promising practice for enhanced oil and gas recovery,

87

through fluids mobility control in porous media (formation). More so, foam-forming additives are a good way to reduce water use during hydraulic fracking production.

Similarly, surfactant concentrations (dosages) and its solubility in appropriate solvent affect its foam texture and stability. In addition, solubility efficiency of surfactants will enhance their desirability for use in field operation equipments, such as tanks, drums, pipelines. Partially soluble surfactant will not only influence its performance on IFT/ST reduction but may as well cause deposition on walls of equipment. This will eventually lead to deposit and scale formation on equipment and clogging of formation pores (in case of injection for enhanced recovery). On these notes, section 5.2.2 discuss the foaming and solubility behaviour of sodium surfactin in distil water and NaCl (salt) solution of varying concentrations.

4.2.2.1   Foaming and solubility in distil water

Foam formation is an essential characteristic of surfactants. Previous studies revealed that biosurfactants have high foaming ability, hence their usage as foaming agents. Studies by (Ferhat et al., 2017; Razafindralambo et al., 1996; Wu et al., 2019) indicates that biosurfactant and indeed surfactin produced from *Bacillus subtilis* foams. The foams could be transient though. Moreover, the authors findings agree with those in this study. Figure 4.3 indicates that formation of aqueous solution of sodium surfactin in distil water led to foam formation, at zero (0) hour (h). Foam height and consequently foam volume significantly increase with increasing surfactin dosage, at 0 M NaCl concentration (Figure 4.3a). Perhaps, increasing the surfactant dosage consequently increases the concentration of the surfactant molecules at the air-water interface. This indicates linear dependence and relationship of surfactin foaming ability and surfactin dosages. The rate of mass transport of surfactant molecules to the interface perhaps depend on the amount of surfactant in the bulk solution. Therefore, increase in the surfactant dosage will increase the rate of surfactant diffusion towards the interface. Moreover, a reduction in ST/IFT is proportional to the adsorption of surfactant molecules at interface. This adsorptive phenomenon is predicted by the Ward-Tordai equation (Chang & Franses, 1995), in the form Gibbs adsorption, indicated in Equation (4.1).

$$\Gamma(t) = 2c_s^0 \left(\frac{D_s t}{\pi}\right)^{1/2} - \left(\frac{D_s}{\pi}\right)^{1/2} \int_0^t \frac{c_s(0, \tau)}{(t - \tau)^{1/2}} d\tau \tag{4.1}$$
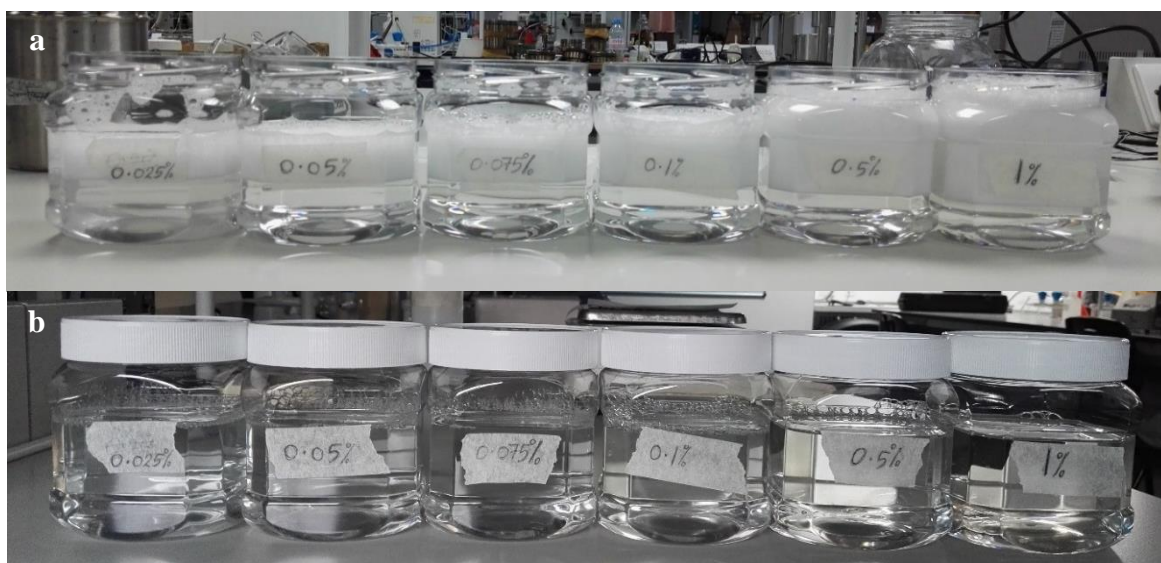
Figure 4.3 Foaming and solubility capability of aqueous sodium surfactin at variable dosages; (a) immediately after agitation at 0 hour and (b) after samples were left for 24 hours

Moreover, the solution formed a two (2) distinct layer; the top foam layer, and bottom clear solution (signifying a good solubility). However, after some time, top foam on the solution transient (collapsed) by being absorbed into the bulk solution. That resulted in a completely homogenous clear solution (Figure 4.3b). Reason for this being that the liquid membrane that envelops the air bubbles does not possess sufficient elastic counter (opposing) force that will prevent the foam from thinning out into the bulk of the solution (Rosen & Kunjappu, 2012). Sodium *surfactin* is unable to sustain the cohesive force between water molecules surrounding a foam bubble. And therefore, the surface area between the water molecules increases. Consequently, adhesive force between air and water increases and therefore the foam collapses. Fundamentally, actions of surfactants at decreasing surface tension relies on this principle of surface area increase. Failure of sodium surfactin to provide an elastic opposing force at liquid membrane surface is an indicative of its adsorption tendencies. Hence its ability to reduce surface/interfacial tension. In that state, agitating the mixture is the only way to make it foam again, yet with same height and volume as previously indicated in Figure 4.3.

Molecules of solvents, as are those of solutes, are held together by intermolecular forces which must be broken to form a solution (dissolution). The cohesive forces of both solvent and solute must be effectively broken to create and form a new adhesive force between solute and solvent. The effectiveness and efficiency of this simultaneous breakage and formation of forces defines the efficacy of dissolution process. Dissolution and consequently solubility of sodium surfactin in distil

water follows this trend. This is because, sodium surfactin being an ionic surfactant, has the same type of strong intermolecular forces as distil water (polar substance). Referring to Figure 4.3, solubility of sodium surfactin has therefore been proven to be excellent in distil water at ambient condition. At this condition and in distil water; sodium surfactin will pose no difficulty of scale formation in pipes, due to deposition of undissolved solid surfactant, during operation. Additionally, the surfactant will pose no threat to clogging of formation pore during surfactant injection. The foaming ability of the surfactant will furthermore enhance its utilization as foaming constituents for enhanced oil and gas recovery at sub-surface using foam flooding (Gbadamosi et al., 2019; Irawan et al., 2017). Furthermore, it will also play an important role as component in preparation of drilling fluid.

4.2.2.2 Foaming and solubility in saline solution

To test and, perhaps, validate effect of salt on foaming and solubility of sodium surfactin, equal amount of the surfactin (previously described in Section 3.2.2) was dissolved in 0.05, 0.1, 0.25, 0.5, 1.0 and 1.5 M NaCl salt solution. Various dosage of surfactin was then dissolved in the saline solution prepared.

Result indicates that foam formation was affected by the change in NaCl salt concentrations. The foaming ability decreases with increasing concentration of NaCl salt. Figure 4.4 indicates that effect of salt is less significant on foam formation particularly at 0.05 and 0.1 M. However, the salt effect became significant above 0.25 M concentration. Presence of salt in the solution mixture increased ionic activity of the mixture. Consequently, electrostatic repulsion between foam bubble increased leading to less coalescence and eventually collapse of the charged (surfactant-salt solution) bubble (Katsir et al., 2015). Similarly, the result indicates that this effect is more evident at 0.5 M salt concentration where only a thin layer of foam occurs. It is worth noting, however, that in real engineering processes dealing with liquid bubbles, salt effects are not entirely reliant on the coalescence factor. Bubble approach speed, salt type or valency of the ions involved (mono or di-valent), type and nature of the surfactant and hydrodynamic conditions are critical factors (Firouzi & Nguyen, 2014; Nguyen et al., 2012). Therefore, ascertaining effect of salt concentration on foam formation and stability depends not only on the salt type or concentration alone but many factors.

Nonetheless, salt effect on foam height and texture is also dependent on surfactant dosages. Behera *et al.*, (2014) studied effects of surfactant and salt on micellar solution and found that effect of NaCl salt on foam volume is dependent on micellar dosage and salt concentration. In the study, foam volume produced by 0.5 g/dm^{-3} and 1.5 g/dm^{-3} surfactant dosages were about 510 cm^{-3} and 880 cm^{-}

[3] respectively at zero NaCl concentration. However, introduction of 50 mol m^{-3} NaCl reduced the foam volume to about 450 and 580 cm^{-3} respectively for 0.5 g/dm^{-3} and 1.5 g/dm^{-3} surfactant dosages. Additionally, physical observation of Figure 4.4 further indicates that bubble size (foam texture) decrease with increasing salt concentration. This indicates that addition of NaCl – monovalent ion, enhances surfactant adsorption capability at water-air interface. Adherence of surfactants at fluid interface is a critical characteristic that enhances its performance application in oil and gas fields

Similar to the foam behaviour in aqueous medium, the foam collapsed into the bulk of solution when checked after 24 hours. Generally, Figure 4.4 indicates the ability of sodium surfactin to foam in saline solution, and that foam formation increases with surfactant dosage but decreases with salt concentration.

Solubility of sodium surfactin follow similar trend as the foaming ability. It is, however, dependent on the salt concentration. Salt concentration up to 0.5 M gives a clear homogenous solution.
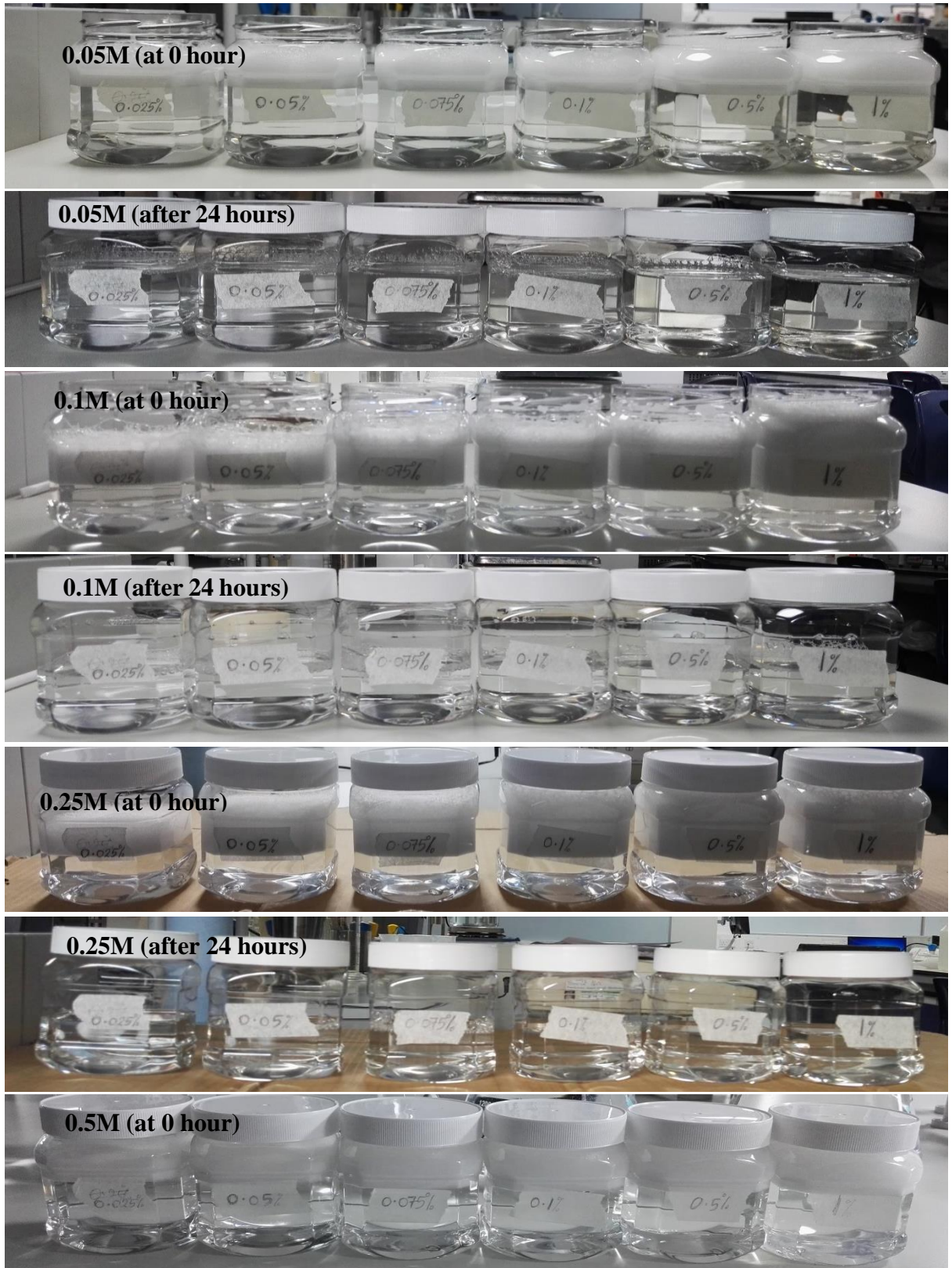
Figure 4.4 Foaming and solubility of dosages of sodium surfactin in saline solution

However, at 1.0M concentration, the effect becomes more evident on both solubility and foaming. Only a thin layer of foam was formed at 0.025 % surfactin dosage (indicated by red arrow), which

only slightly increases with increasing surfactin dosages (Figure 4.5a). This is because the presence of increasing ionized components in the solution impeded the complete solubility of the surfactin in the saline solution. As a way of extension of consequence, the partial solubility of the surfactin then affected foam formation. That led to formation of relatively clear solution at 0.025 % surfactant to a very cloudy, heterogeneous solution at 1.0 % (Figure 4.5a). The solubility of the system could not improve by allowing the solution stale for 24 and 48 hours as shown in Figure 4.5b and c (aerial view) respectively. Rather, it led to formation of more physically compacted sediment at the bottom of the container.   On agitation and stirring, the solution became more whitish and cloudier (precipitate).
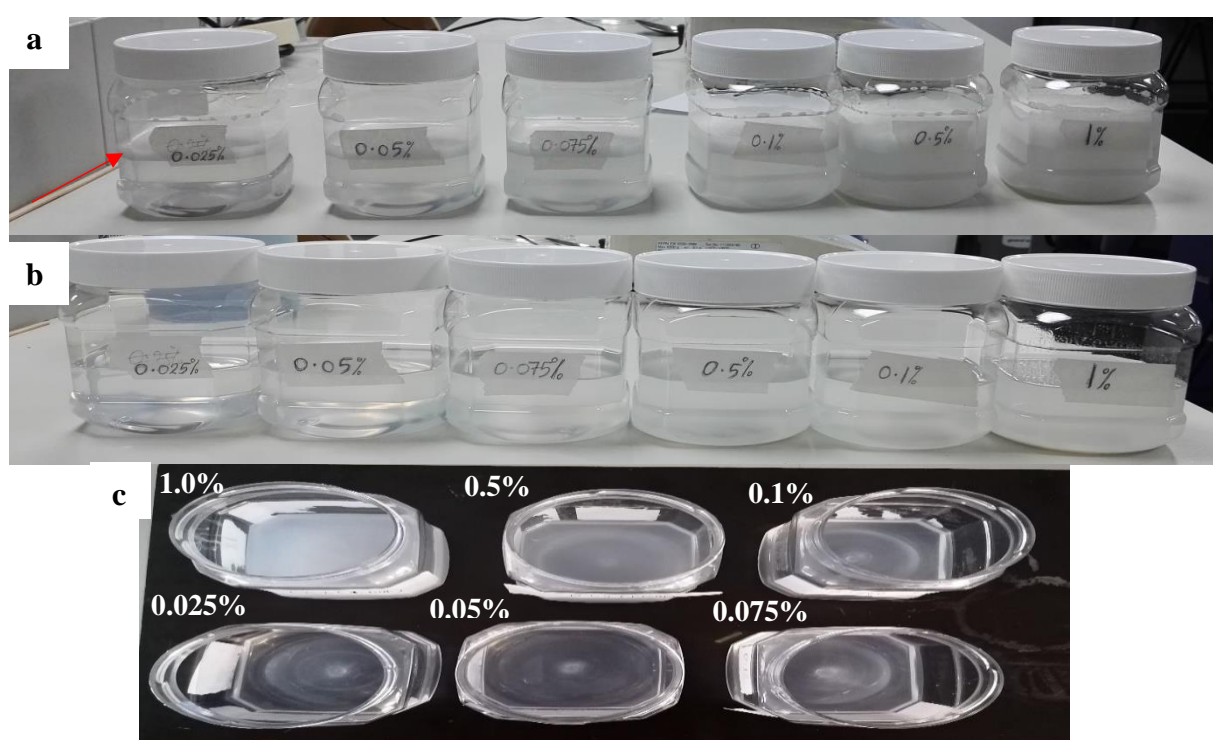
Figure 4.5 Foaming and solubility of dosages of sodium surfactin in 1.0 M saline solution (a) at 0 hour, (b) after 24 hours and (c) after 48 hours

Evolution of heat (exothermic) or absorption of heat (endothermic) during bond breakage or reformation accompanied dissolution processes. More so, temperature elevation influences solutes solubility and dispersion (diffusivity). On these bases, increase or decrease in temperature could perhaps effect a change in the solubility behaviour. To put this effect to test, the solution mixtures was heated, and stirred, to 30 and 40 °C using magnetic stirrer heater. The solubility of the surfactant in saline solution at 1.0 M concentration did not show any significant improvement.

The change in NaCl salt concentration therefore has an induced effect on solubility and foaming ability of sodium surfactin, as portrayed further by increasing concentration to 1.5 M (Figure 4.6). Not only that the solution is cloudy but also a clear precipitate was formed. Extent of precipitation however increased with increasing surfactant dosage. That is to say, an inverse relationship exists between the salt concentration and solubility and foaming ability of the surfactant. Filtering the solution may be one way to safely use the precipitated solution with minimal risk of scale deposit.
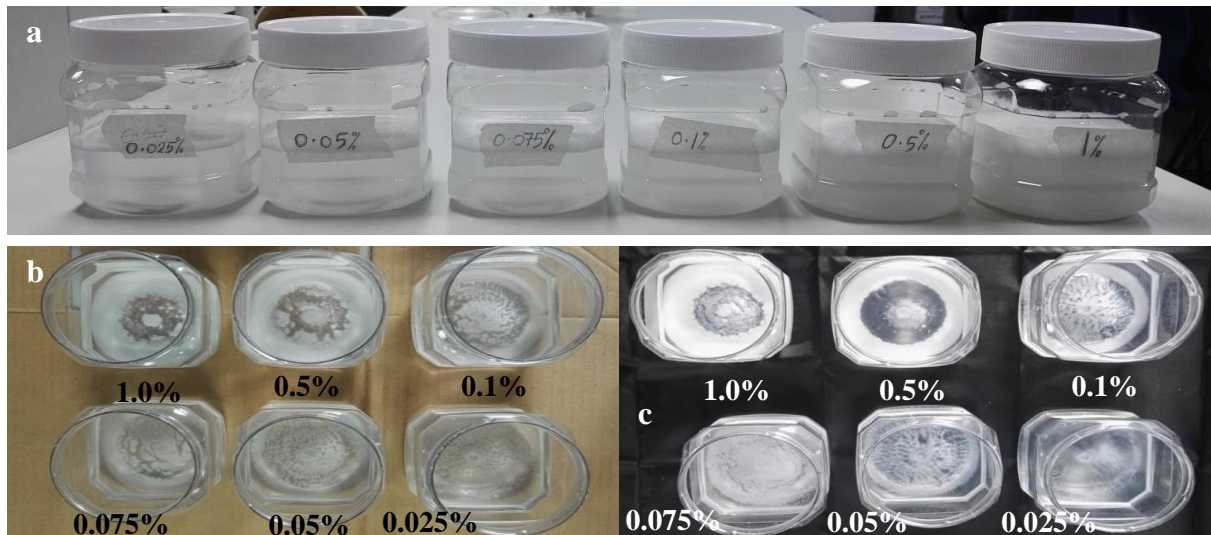
Figure 4.6 Foaming and solubility of dosages of sodium surfactin in 1.5M saline solution (a) at 0 hour, (b) after 24 hours and (c) after 48 hours

4.2.3   Emulsification index

Emulsification/demulsification is a functional characteristic of surfactant in which the dispersion of one liquid phase in another becomes possible. As consequence, it causes the mixing of two liquids that are immiscible (Inès & Dhouha, 2015). This property is important in enhancing the separation of oil in methane–water–oil system. Thereby ensuring that not only methane–water interface surface area increase, but also oil separation from the pipeline system.

Figure 4.7 shows the emulsification index (E_i) of sodium *surfactin* (calculated using Equation (2.1)) when mixed with light crude of 34.97° API gravity. The curve indicated that emulsion ability of the surfactant increases with increase in surfactant dosage. There was initially little emulsion layer formed by the surfactant and oil mixture which suggest low interfacial effect by the surfactant. As a result, 0.025 % surfactant dosage yielded only 27 % E_i. However, the E_i increased as the dosage increases up to 82 % at 1.0 % surfactant dosage (Figure 4.7a). Emulsification effect seem to increase

with surfactant dosage increase. More surfactant molecules accumulate at the fluids interface (Peele, 2017) thereby enhancing hydrophobic interaction with the crude. Consequently, mixing of the aqueous surfactant with the crude becomes enhanced. Generally, the result indicates both demulsification and emulsification ability (that is surfactant dosage-dependent). This, according to (Satpute et al., 2010), is an indicative of surface tension reduction capability.
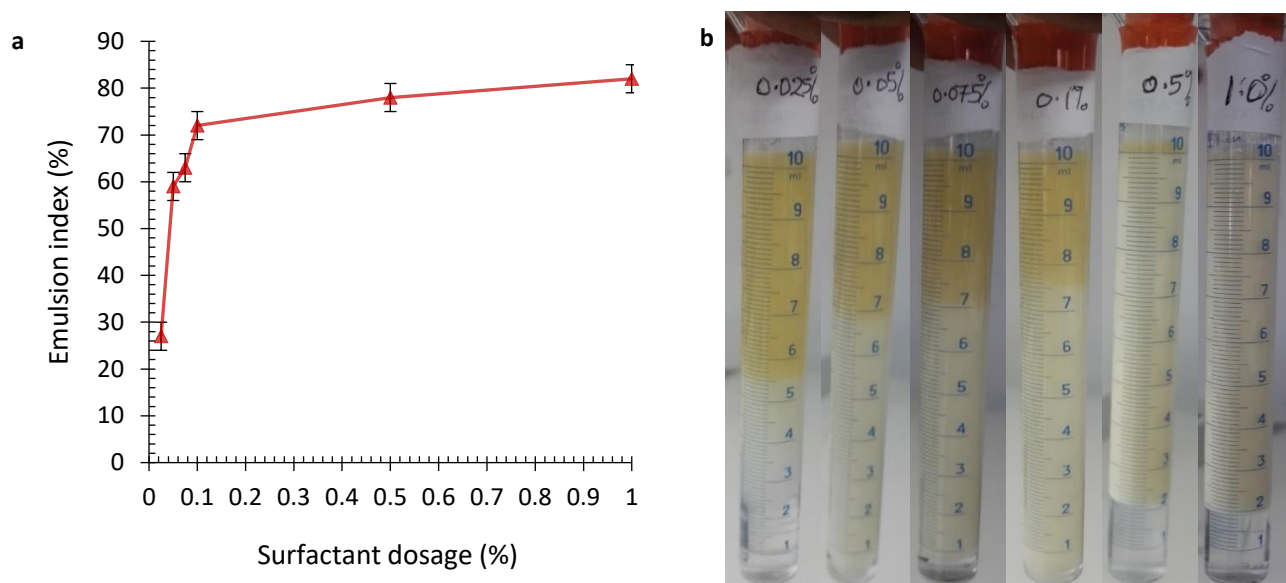
Figure 4.7 E_i of 0.025 – 1.0 % aqueous surfactin after 24hours

Figure 4.7b shows the transition between demulsification and emulsification ability of sodium surfactin. Surfactant dosages 0.075 % and below may be suited for application as demulsifier, whereas 0.1 % dosage and above may be applied for emulsification purposes. These behaviour further indicates the usefulness of sodium surfactin in bioremediation of environments contaminated with hydrocarbon (Moldes et al., 2013; Moldes et al., 2011; Thavasi et al., 2011). Additionally, (Diab & Din, 2013; Matsui et al., 2012; Rocha e Silva et al., 2014) shows it is an indication of good agent for cleaning of oil and gas equipment such as drums and storage tanks.

4.2.4 Density characteristics

Density is a degree of how much mass is contained in a given volume of liquid/fluid. The density of an aqueous surfactin or saline solution, therefore, is a measure of the degree of total solid (surfactin or salt as the case may be) that is dissolved in water to form the solution. Hence, it is referred as mass concentration. Conventionally, the higher the amount of total dissolved solids in

the solution, the greater its density/specific gravity. This however may not be case with all fluids owing to their different solute components/compositions. Density characterization is very important in that it tells the extent to which a fluid migrate and get distributed within a system. Additionally, performance efficiency and efficacy of any surface-active molecule on interfacial tension strongly relies on its adsorption ability. Aqueous surfactant molecules adsorb unto surface in monomeric form. As the surfactant concentration increases, the monomeric molecules begin to form aggregates known as micelles. Increasing concentration of micelles could potentially results in surfactant coagulating within the disperse/aqueous phase. Consequently, the surfactant dispersion in the phase becomes affected which may result in poor adsorption. Similarly, Naullage, Bertolazzo and Molinero, (2019) suggested that interfacial film density, among other factors, prevent coalescence and agglomeration of clathrate particles with water droplets in oil. Therefore, density of dispersion phase is critical to the surface interaction between phases. Young-Laplace equation (Sayed et al., 2019) shows this relationship as indicated in Equation (4.2), where $\Delta\rho$ is the fluids density difference. R_o is the radius of curvature, g is the gravitational acceleration and β is the shape factor.

$$\gamma = \frac{\Delta\rho g R_o^2}{\beta}$$

(4.2)

Therefore, density as a measure of level of mass transport of surfactant in the dispersion phase is critical to evaluating surfactant surface activity. And thus, its performance in reducing CH_4-H_2O ST. Hence, density characteristics behaviour of sodium *surfactin* is discussed under this section.

4.2.4.1 Surfactant density behaviour in aqueous solution

At room temperature (20.5 °C) and atmospheric pressure, density behaviour of aqueous *surfactin* is somehow monotonic. Figure 4.8 shows the density characteristics of sodium *surfactin* in aqueous medium. When more solutes are added to a solution, the composition of particles in a given volume of the solution changes. Consequently, the mass per unit volume of the solution changes as well. Sodium *surfactin* behaves in this manner when dissolved in aqueous medium. The density of the biosurfactant decreases with increasing surfactant dosage. However, this behaviour only last up to surfactant critical dosage 0.075 % with lowest density value of 996.641 kg/m^3 then it began to increase. Basically, all dosages, except 1.0 %, shows density less than that of water at about the same temperature. These values are in agreement with the studies of Zdziennicka, Krawczyk and Jańczuk, (2018). The density of distil water used in the experimental (as solvent) is 997.0 kg/m^3 while that of normal water is 998.2 kg/m^3 at approximately the same temperature. Therefore, the density decrease behaviour could mean that the surfactant expands when added to distil water. The

96

expansion consequently led to increase in volume without corresponding increase in mass. Having a larger denominator number, which could not be compensated by the available mass of surfactant added, resulted in lower density value.
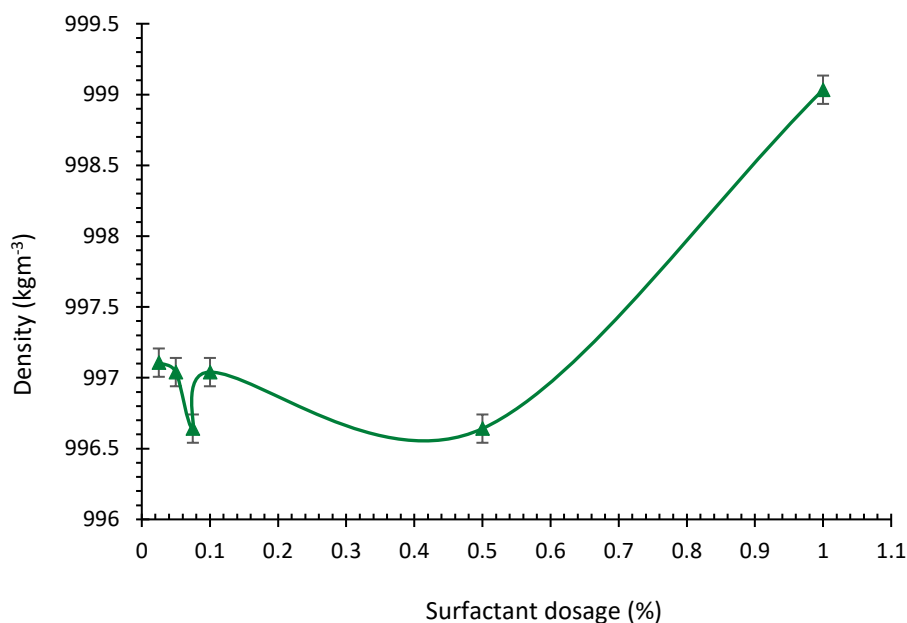
Figure 4.8 Density of sodium surfactin in aqueous solution

Another remarkable behaviour was observed at dosages 0.075 and 0.5 %. The density remained constant at 996.641 kg/m^3, which indicate the establishment of saturation points (micellization).

Micelles are assembly of surfactant molecules in which individual components are in thermodynamic equilibrium with unimers in the surrounding medium. Two possibilities could be attributed to the density decrease; (1) increase in size of *surfactin* molecules in solution which, despite been physically soluble, are not able to completely occupy the intermolecular empty spaces, (2) the solution expands which caused an increase in volume that neutralizes the mass addition.

Furthermore, the density behaviour at 0.075 % perhaps signify that the aqueous *surfactin* has likely attained its CMC. This behaviour therefore indicates that density measurement can be employed as a tool in determining surfactant CMC, in addition to conventional surface tension measurement. It was mentioned in section 2.2.3.3 that below CMC, surfactants remained adhered at fluid surfaces. At CMC, surfactant may remain adhered but will have no further effect on ST/IFT reduction. However, surfactants may become immersed into the solution above the CMC, due to increased self-molecular assembly. The immersion consequently reduces the surface area at the fluid interface,

hence failing in effecting ST/IFT reduction. *Surfactin* dosage 1.0 % could exhibited immersion tendency where the density increased to 999.034 kgm^{-3}.

Therefore, the density behaviour suggests sodium *surfactin* ability to confer on methane– water ST. Furthermore, performance of sodium *surfactin* at 0.075 % dosage in ST reduction could be inferred to be optimal. Again, the density characteristics will be of significance in enhancing performance of *surfactin*: (a) as dispersant for asphalt, wax, and hydrate deposition control thereby enhancing oil and gas transportation; (b) for rheology reduction during drilling mud preparation, as well as enhancing heavy crude transport (Dardir et al., 2017; Yunita et al., 2016); and (c) in promoting imbibition process/wettability alteration during EOR (Chen et al., 2000) and hydraulic fracking (Alvarez et al., 2014). On these notes, good stability of sodium *surfactin* during adsorption and consequently conferment on methane-water ST reduction, in the range of these dosages, is expected.

However, oil and gas operation are often associated with changes in operating and environmental conditions. Chief among these parameters include temperature and salt concentrations. While temperature changes may affect thermodynamic properties of the system, changes in salt concentration affects electrostatic behaviour of the system and surfactant self-assembly. Therefore, effect of changes in temperature and salt concentration on *surfactin* density were evaluated.

4.2.4.2   Effect temperature on *surfactin* density in aqueous medium

Hydrate formation phenomena involve mass transport operation at low temperature of equilibrium conditions. It therefore become critical to assess and understand *surfactin* behaviour in these temperature ranges. This was done by experimentally measuring the surfactant density up to 1 ^{o}C under atmospheric pressure. Moreover, density of solution is ratio of its mass to the volume it occupies. When a solution is heated, the average kinetic energy of the solution's molecules/atoms increases thereby making them expand. The expansion makes the molecules occupy more volume at elevated temperatures. Consequently, mass to volume ratio decreases, hence density of the solution. Aqueous sodium *surfactin* behaves in this manner when the temperature was increased beyond 5 ^{o}C, across most dosages (except 0.025 %). Figure 4.9 shows this behaviour. The decrease is, however, not completely linear.
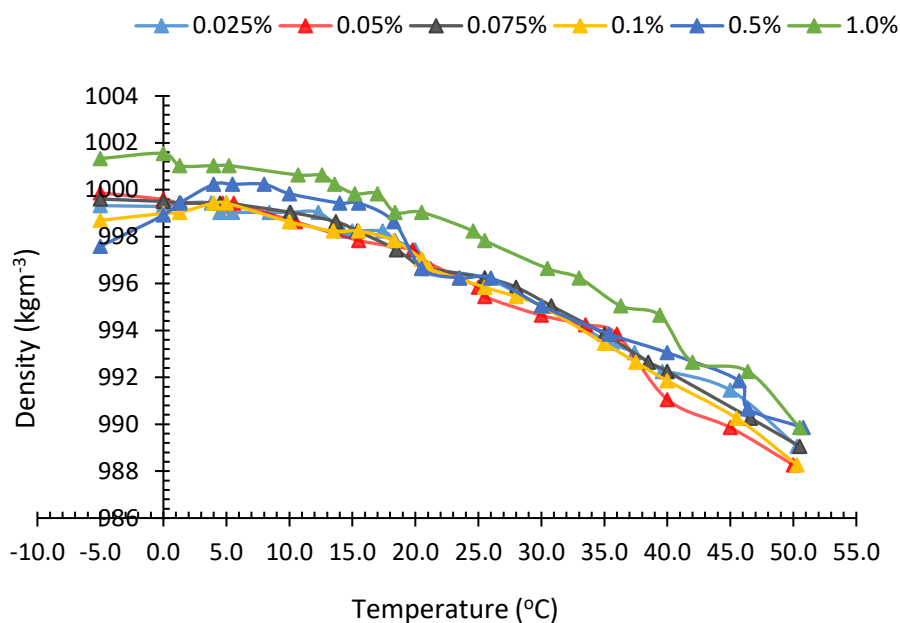
Figure 4.9 Effect of temperature on density of sodium surfactin

Figure 4.9 suggest that temperature has an inverse effect on the density of *surfactin*. This is similar to density behaviour exhibited by SDS and other ionic liquids (Bhattarai et al., 2013; Tao et al., 2013). However, extrapolation of the temperature experimental values to 0 and -5 °C, with average R^2-value of 0.993, indicates that low temperature effect was dosage dependent. Notably, density of 0.1 and 0.5 % *surfactin* increased respectively from 998.695 to 999.433 kg/m^3 and 997.587 to 1000.231 kg/m^3 when temperature increased from -5 to 4 °C. Temperature increase within this range, and these dosages, perhaps induced a coalescence effect on the *surfactin* molecule. As a result, it creates a superficial gel-like behaviour that consequently restrict the volume occupied by the *surfactin* molecule. These resulted in increased density. The behaviour is similar to that of water at temperature between supercooled and 4 °C (Patricia, 2011b). Conversely, dosages 0.025 to 0.075 % maintained a relative decrease in density with increase in temperature from -5 to 4 °C.

Additionally, water has a maximum density of 999.972 kg/m^{-3} at 4 °C. *Surfactin* exhibited relatively lesser density of 999.433 kg/m^{-3} at same temperature and across dosages 0.025 to 0.1 %. This confirm adsorptive and/or dispersive characteristics, and its potential utilization as hydrate-formation inhibitor. Figure 4.9 also indicates different saturation points which are peculiar to individual surfactant dosage. Though density of *surfactin* decreases with increasing temperature, generally, the extent of the temperature effect is dosage dependent.

99

4.2.4.3 Surfactant density behaviour in saline solution

Oil and gas operations are always associated with saline water originating from the formation. Chemical and physical characteristics behaviour of formation fluids vary from one source to another. This depends on the type and composition of the reservoir under study. Utilization of surfactant in oil and gas installations must take into consideration the nature of physical and chemical interaction of the surfactant with formation. Ionic interactions from saline water may induce self-assembly hydrophobic tail or electrostatic repulsion of the hydrophilic head group of surfactants. Consequently, micelle formation becomes affected. Recall that surfactant micellization is an important physical property that affect its performance utilization.

Dissolution of sodium *surfactin* in NaCl saline solution results to general increase in density of surfactant-salt solution (Figure 4.10). The density progressively increased with increasing salt concentration, with an average density of 999.566 kgm^{-3} and 1054.958 kgm^{-3} respectively at 0.05 M and 1.5 M. Obviously, mass of NaCl salt contained in the solution must be responsible for the overall increase in density. Despite this however, effect of salt increase at particular surfactant dosage is clearly insignificant. This is shown by the near overlap of the plot lines.
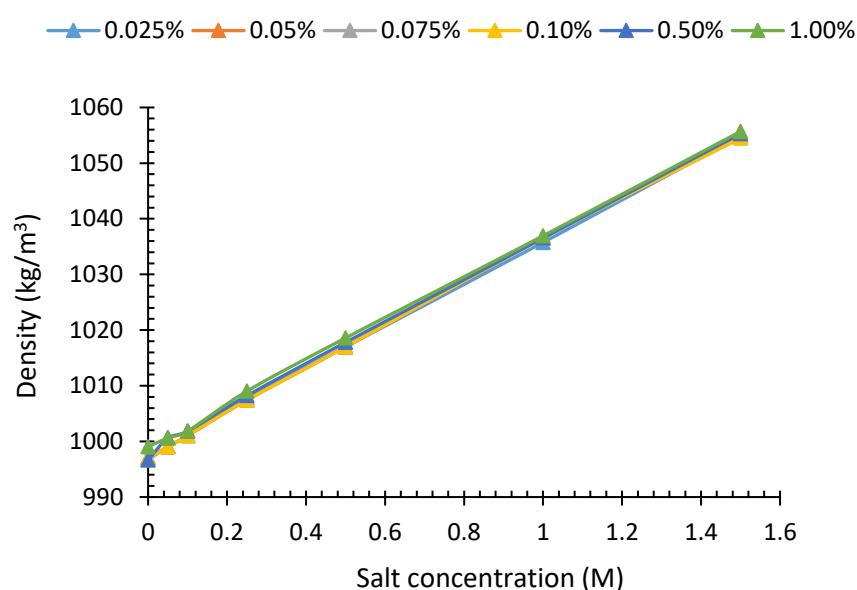
Figure 4.10 Density of sodium *surfactin* in NaCl solution at different NaCl concentration

Notably, beyond 0.5 M salt concentration, plot in Figure 4.10 indicates that micelle formation is, to a large extent, salt-concentration dependent irrespective of the surfactant dosage.

Though Whang *et al.*, (2008); Al-Wahaibi *et al.*, (2014); Saito *et al.*, (2016) reported optimal IFT reduction using aqueous *surfactin* dosage of 0.075–0.1 %, use of *surfactin* in saline solution of 1.0 M concentration and above may pose solubility problem. Scaling in well bore, clogging of formation pores and deposit on walls of pipelines are some of the consequence of partial solubility of surfactants. Use of permeable membrane, such as filter paper, however, may be employed to filter away the precipitate. The filtrate may then be subjected to performance test, such as emulsification index test. Nevertheless, Schaller *et al.*, (2004); Joshi, Bharucha and Desai, (2008); Liu *et al.*, (2016b) reported stability and performance of *surfactin* from *Bacillus subtilis* in NaCl solution in the range of 0 to 0.5 M.

4.2.5 pH characteristics

The pH of a solution is a measure of how much particular chemical constituents is dissolved in it, or how much chemical constituents are available in a given solution samples. This is because at any given pH, a chemical constituent may become more soluble than others. In addition, dissolved minerals may as well influence the performance of surfactants. It distorts the active site available for surfactant adsorption on fluids surface or interface. More so, integrity of separators, heat exchangers, pipelines, cooling towers, etc., is critical in oil and gas operations. Oil and gas equipment designs are perhaps incomplete where corrosion tendencies are neglected. Environmental and personnel concern is of course paramount. This, therefore, becomes a source of worry. Particularly when partial dissolution of either acidic or alkaline minerals/elements occurs by their respective neutralizing agents leaving one or more replaceable hydrogen or hydroxide atoms/ions. Implying that the existences of unbended free hydrogen atom (H^+) or hydroxyl atom (OH^-) can alter the pH of a solution thereby altering its characteristic behaviour and performance.

Furthermore, addition/dissolution of chemically neutral salts alters the pH or the activities of H^+ or OH^-. This however may be dependent on the pH of the solution (solvent) into which the salt is being dissolved. From chemistry perspective, NaCl salt is a neutral compound (Flinnscientific, 2016; Sereshti & Aliakbarzadeh, 2013), whose pH should fall around the centre of the acid–base spectrum (pH 7). Therefore, if dissolved in a solution, it tilts the solution pH towards neutral (Sereshti & Aliakbarzadeh, 2013). This means that when NaCl salt is dissolved in solution with a high pH, it perhaps incrementally lowers the solution pH toward neutral value. Similarly, if dissolved in a solution of low pH, it increases the solution pH towards neutral value.

4.2.5.1 Surfactant pH in aqueous medium

pH of sodium *surfactin* increases with dosage increase at 20.5 °C and atmospheric pressure (Figure 4.11). Distilled water used to prepare aqueous *surfactin* solution had a pH of 5.9. Ideally, pH of water should be about neutral. However, operations under open ambient condition permits materials to interact with components in the surroundings. In this case, therefore, the distilled water might have come in contact with atmospheric CO_2. Dissolution of carbonates in water results in the pH of water becoming more acidic. This resulting effect is what happened to the pH of the distilled water. However, for sodium *surfactin*, there is progression of the pH value from 6.68 at 0.025 % to highest peak value of 7.31 at *surfactin* dosage of 0.5 %. The polar hydrophilic heads of sodium *surfactin* (being anionic) exerts an electrostatic repulsion among them.

The result is an indication that increasing *surfactin* dosages tend to increase the pH towards neutral and/or basic value. This perhaps inferred that sodium *surfactin* is itself either basic or neutral; since it tilts the pH of distil water (5.9) toward neutral value.
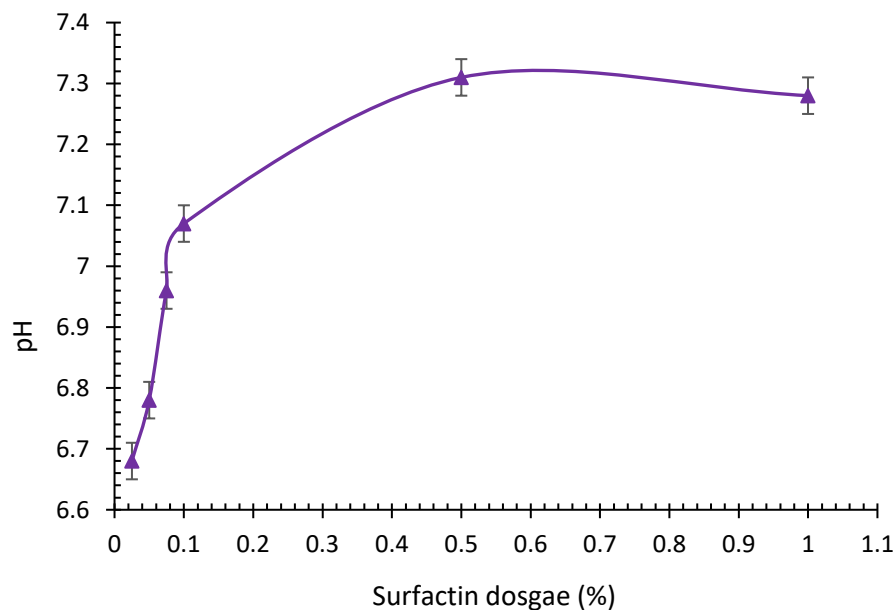
Figure 4.11 pH of various dosages of aqueous sodium surfactin

Anionic surfactant, such as sodium *surfactin*, have high efficiency in reducing IFT during EOR but however exhibit low adsorption on sandstone rocks. Sandstone rocks contain negative charge as anionic surfactants. Obviously, like charges will repel each other. This could be a desirable property though as it will reduce surfactant loss due to adsorption on rock surface. Similarly, increase in pH of surfactant solution reduces the number of hydroxyl group in the surface thereby affecting

hydrogen bond formation (Belhaj et al., 2019). Consequently, hydrated mineral oxides on the surface becomes negatively charged.

Corrosion in oil and gas process lines occurs when contact is established between equipment material (basically metallic) and aqueous environment. First scaling occurs (in the form of rust) at surface which is prelude to corrosion. Over time, continuous operation under same condition will eventually result to corrosion. One of the major parameters that induces rust, in addition to impurities, is the pH of the aqueous phase. However, considering the pH of pure water, sodium *surfactin* can be said to be corrosion safe. This assessment is perhaps uncertain until validated through conductivity testing (presented in Section 4.2.6). In practice, corrosion results from electrolytic ion exchange between anodic and cathodic ions in their attempt to balance their charges.

It is worth noting that pH value of 7.28 is quite very close to 7.3 value reported (confirm) by Kaneka in the certificate of analysis sheet (see Appendix C 1). This therefore validates the accuracy of the measurement method.

Experimental studies conducted for EOR using sodium *surfactin* indicates no report of corrosion threat. Similarly, reports of studies by (Al-Bahry et al., 2013; Al-Wahaibi et al., 2014; Joshi et al., 2016; Liu et al., 2016a) indicated best performance of *surfactin* from strain of *Bacillus,* in terms of interfacial tension (IFT) reduction, in the range of 6–10 pH. At this reported pH, therefore, sodium *surfactin* is inferred to efficiently reduce ST between gas–water, and perhaps be corrosion-safe when used in oil and gas pipelines.

4.2.5.2   Effect of temperature on pH of aqueous sodium *surfactin*

Deliberate attempt at inhibiting hydrate formation in gas system perhaps involves injection of hydrate-inhibiting substances into the gas processing lines. Chemical characteristics of these substances need to be evaluated including its interaction with surrounding phase. This is to ensure safe operating condition and safeguard equipments integrity. More so, hydrate formation phenomena in gas pipelines occurs at a favourable equilibrium condition of temperature and pressure. Therefore, evaluation of how these thermodynamic variables, particularly temperature, will affect pH of the dispersive phase becomes critical.

pH of a solution quantifies, numerically, the concentration of mobile H^+ ion in a solution. Therefore, variables that affect ion mobility, such as temperature, may likely affect pH. More so, increased molecular vibration is linked to temperature rise. Therefore, observable H^+ in solution may increase when temperature rises, leading to decreased hydrogen bond formation tendencies. And

103

consequently, reduces pH. Moreover, pH may be defined in terms of ratio of chemical potential to thermal energy. Increasing thermal energy (temperature) implies a decrease in pH due to increased ionic mobility.

Sodium *surfactin* behaves in contrast to these assertions. Figure 4.12 indicates that at dosages of 0.025 to 0.1 %, the pH progressively increased with temperature increase. Pattern of the increase is not completely linear though.
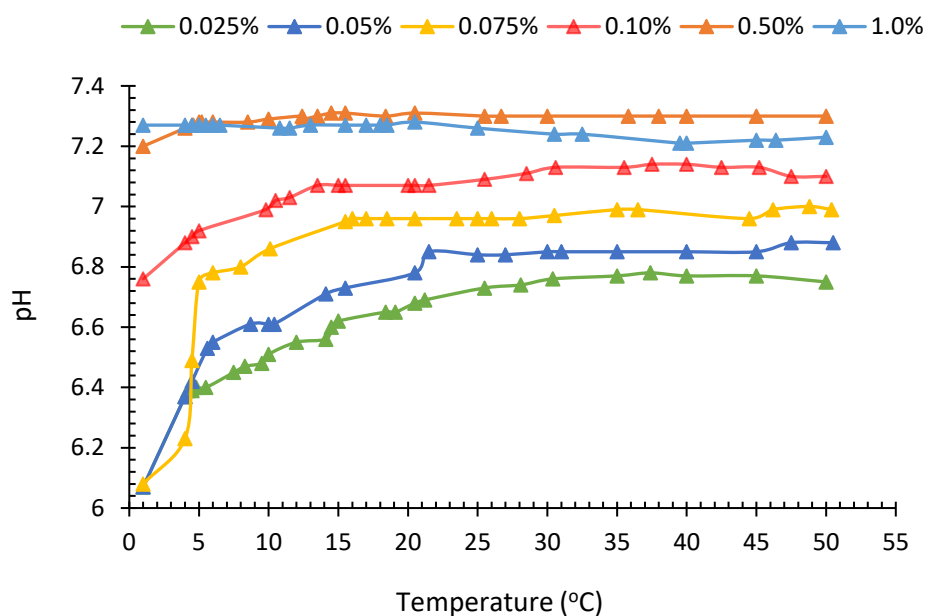
Figure 4.12 Effect of temperature on pH of aqueous sodium *surfactin*

Rise in temperature is likely that it induces micelles formation. Consequently, ionic mobility is restricted by increased hydrogen bonding. Therefore, less H^+ concentration is detected by the probe which ultimately indicates an increase in the solution pH. The pH increase, however, is surfactant dosage dependent. Particularly, effect of temperature rise became less and less significant beyond 0.075 % surfactant dosage.

4.2.5.3 Surfactant pH in saline solution

The addition of NaCl salt, which changed the solution ionic concentration, affected surfactant pH in monotonic pattern. Increase in NaCl concentration resulted in increased ionic concentration of surfactant solution. This impede hydrogen bonding between the surfactant hydrophobic tail. Consequently, more H^+ concentration in the solution led to decrease in pH. The trend continues continued across all surfactant dosage. However, the pH across all dosages reached its minimum at 0.5 M salt concentration with pH of 6.07 and 6.3 respectively at 0.025 and 1.0 % dosages. Similar

104

to NaCl concentration effect on density (see section 4.2.4.3), surfactant alkyl group begin to form an assembly beyond 0.5 M. Therefore, less activity H^+ concentration is detected leading to increased solution pH. Figure 4.13 shows the pH of various dosages of sodium *surfactin* in saline solution.
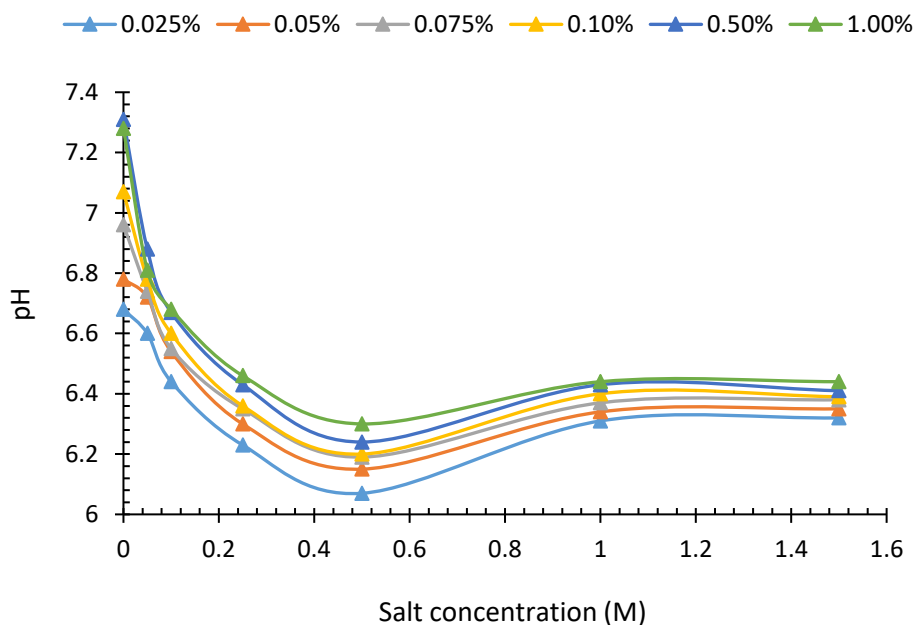
Figure 4.13 pH of various dosages of sodium surfactin in NaCl solution

Despite the salt effect, however, surfactin increases the pH of salt solution with complimentary to rise in surfactant dosage. It therefore indicates that pH is both salinity and dosage dependent. Conclusion of studies by (Sereshti & Aliakbarzadeh, 2013; Shu et al., 2016), indicated that increase in ionic concentration decreases the pH of a solution. This conclusion holds for only certain range of saline concentration. Interestingly, increase in ionic concentration due more NaCl salt induced less significant effect on surfactin pH beyond 1.0 M concentration. Transiting from 1.0 to 1.5 M salt concentration, pH of dosages 0.025 to 0.1 % only increase by value of 0.01. pH of surfactant dosage of 1.0 % remain same 6.44, while that of dosage 0.5 % decreased from 6.43 to 6.41.

Adsorption of surfactant at surfaces/interface occurs through gradual accumulation of unimers at the interface. With increasing surfactant dosage, more monomers adhere the interface and under appropriate condition begins to form micelles until critical saturation is reached (CMC). Figure 4.13 shows that at surfactant dosages of 0.025 and 0.05 % micelles begins to form at 0.05 M salt concentration. It indicates that the low salt concentration induced coalescence of the surfactant hydrophilic head group.

4.2.6 Conductivity characteristics

Electrical conductivity is a degree to which the ability of a material or solution to conduct electric current is described. It depends on the number, and mobility of ions and charged particles present in the solution. In field practice, mass transport of multi-phase components (gas-water) occurs throuhg tortuous pipeline system. Consequently, such agitation could spark ionic activity and consequently increase conductivity of solution mixture in the system. It therefore become critical to evaluate electrical conductivity of the liquid mixture. Similarly, presenec of electrolytes and noneletrolytes can significantly influence formation and characterisitcs of micelles. Besides, hydrophobic interactions and hydrophilic head group repulsion defines surfactant interaction in saline and aqueous media. Therefore, electrical conductivity is a critical tool for evaluating these ionic interaction of surfactants. Critical micelle concentration is a surfactant property that is used to describe surfactant performance. Among the procedures empolyed to determine CMC include plots of surface tension and conductivity measurments against surfactant concentration (Domínguez et al., 1997; Mukerjee & Mysels, 1972; Rosen & Kunjappu, 2012).

For anionic surfactants such as sodium surfactin, the electrical conductivity increases as the surfactant concentration increases. Micelles formation, on the other hand, reduces ionic mobility in the solution and consequently decreases solution conductivity. Figure 4.14 confirms that a near linear relationship exist between surfactant dosage and surfactant conductivity. Simialr condcutivity trend was reported by Kim and Vipulanandan, (2006); Anvari *et al.*, (2015); Zdziennicka, Krawczyk and Jańczuk, (2018). At ambient temperature of 22.5 $^{\circ}$C (and atmospheric pressure), conductivity of sodium surfactin increased from 110.4 to 934.7 µS/cm respectively at 0.025 % and 1.0 %. The findings indicates that addition of sodium surfactin increases the number and mobility of the surfactant ions. However, a notable deviation occurs at 0.05 % surfactin dosage. At this dosage, number of charged carriers perhaps decreased resulting to conductivity decrease to 79.3 µS/cm. This point may indicate the possibility of saturation (micelle formation). More so, this is lower than the 0.075 to 0.1 % inference point for saturation using density and pH measurement. Density and pH were measured at average temperature of 20.25 $^{\circ}$C, while conductivity was measured at 22.5 $^{\circ}$C. During experimental trials, condcutivity was meassured at least five times at this dosage to ensure accuracy.
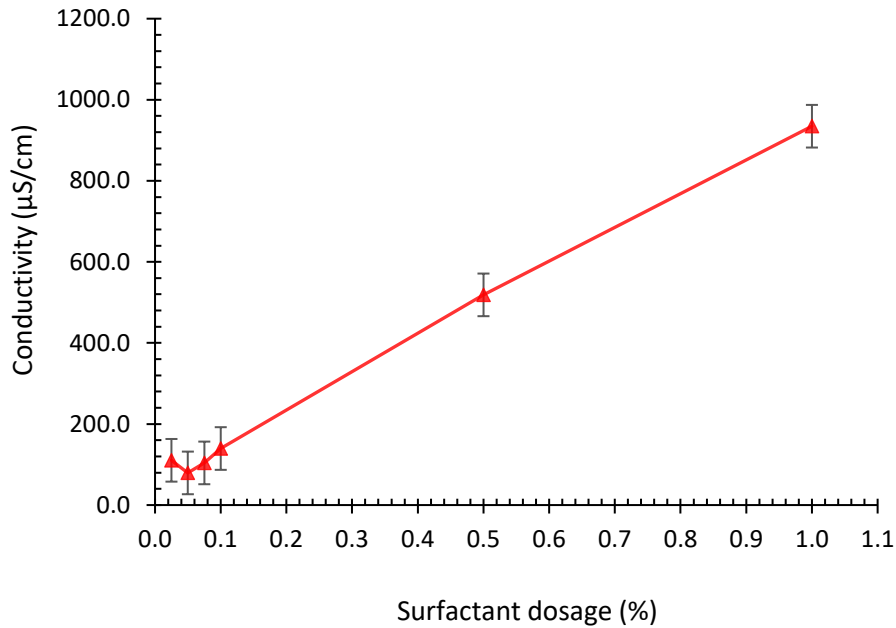
Figure 4.14 Conductivity of aqueous sodium *surfactin*

As explained earlier in section 4.2.5.1, ionic interaction between pipeline and suspending fluid first creates a corrosion site in the form of rust. Consequently, at appropriate equilibrium condition of temperature and pressure, it becomes a nucleation area for hydrate formation. However, conductivity of sodium surfactin is generally low, signifying that it has poor ionizing ability in distilled water. Nonetheless, it much greatre than that of distil water used in the experimental study. Additionally, the low condcutivity value is an indication of surfactin adsorptivity and hence its ability to reduce surface tension (Kronberg et al., 2014b) and being corrosion safe in pipelines.

4.2.6.1   Effect of temperature on conductivity of aqueous surfactant

Temperature is an important parameter controlling many of the physical and chemical processes in the oil and gas industry. Fluctuations in processes variables, including temperature, is very common. Moreover, these instabilities could impact on the behaviour of phase system, which may lead to undesirable response from component of the phase system. However, effect of temperature changes on conductivity of solution could be complex. Increasing temperature could result to: increased ionic collision, due to increase in thermal motion of the ions, and therefore decrease their mobility; increase or decrease in solution viscosity and hydration of ions, and therefore affect ionic mobility. Additionally, Kukade and Bawankar, (2018) indicated that electrical conductivity is dependent mainly on the number and mobility of charge carriers and chemical composition of samples. Against these background, effect of temperature on various dosages of sodium *surfactin* was evaluated.

Temperature in the range of 1-50 $^\circ$C, at an average increase of 2.5 $^\circ$C, was considered in the experiment.

The findings shown in Figure 4.15 indicates that conductivity of sodium *surfactin* exhibits some form parabolic increase with rise in temperature. Similar conductivity behaviour was reported by Tennouga *et al.*, (2015) for SDS and N-dodecylpyridinium chloride in aqueous medium.
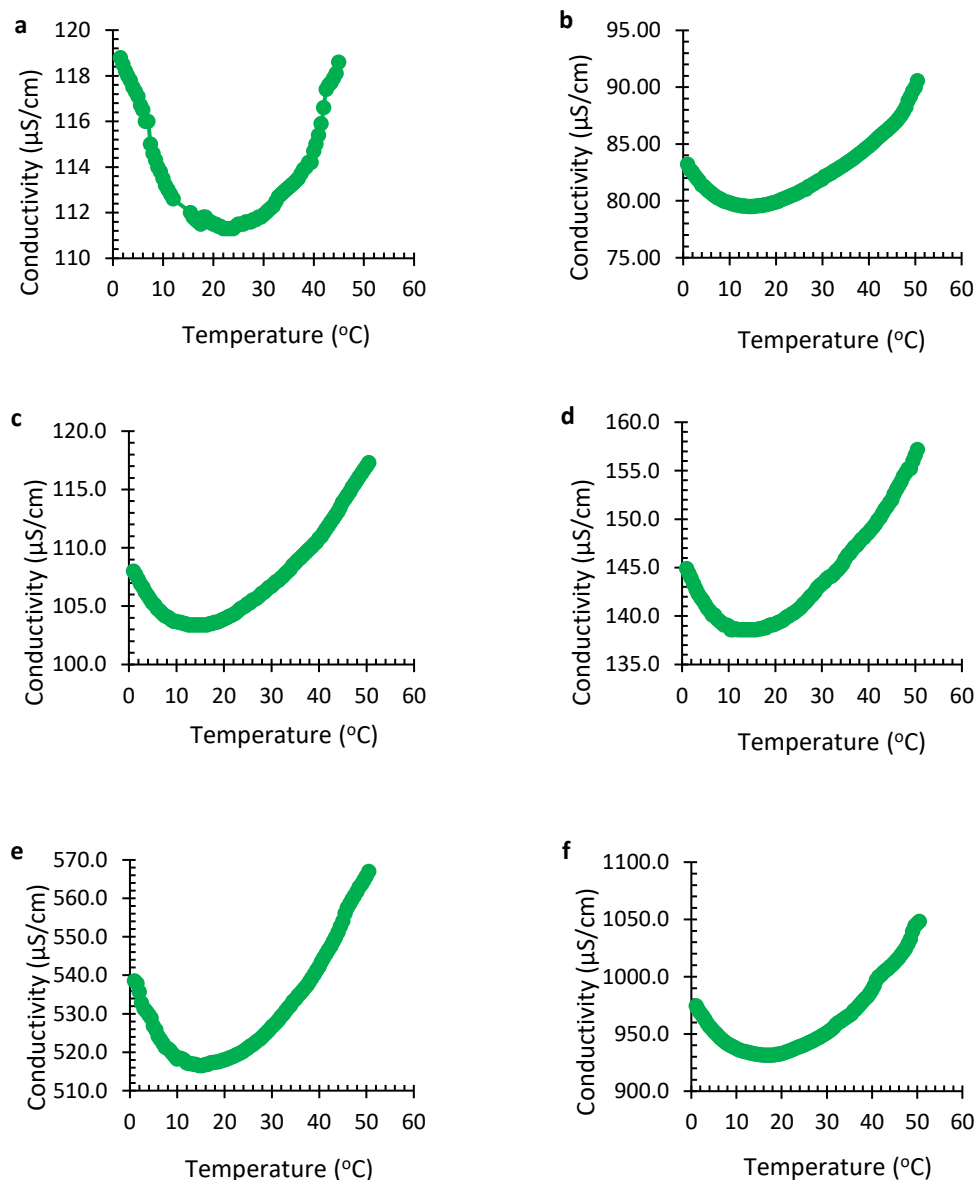
Figure 4.15 Conductivity of sodium surfactin at variable temperatures and (a) 0.025%, (b) 0.05%, (c) 0.075%, (d) 0.1%, (e) 0.5%, and (f) 1.0% dosages

Figure 4.15 further indicates that around low temperature region up to 16 °C (except at dosage 0.025 %), rise in temperature induces hydrophobic interaction of the surfactant tails. Consequently, alkyl chains of the surfactant aggregates and therefore restrict ionic mobility. This resulted to the decrease in detecting ionic charge, hence conductivity. Conversely, further temperature increase (up to 50 °C) resulted in increased ionic mobility electrostatic repulsion of the amino acid hydrophiles.

Effect of temperature can be employed to evaluate thermodynamics of *surfactin* micellization in aqueous medium. Thermodynamic functions including free energy of micelle formation (Gibbs

energy), enthalpy and entropy is employed to evaluate spontaneity of micellization (Zdziennicka et al., 2018).

4.2.6.2   Conductivity of sodium *surfactin* in saline medium

Conductivity of sodium *surfactin* in different concentration of NaCl solution indicates a linear relationship pattern as shown in Figure 4.16. it further suggests that the conductivity is less dependent on surfactant dosage. Clearly, significant increase in the solution conductivity is evidence of the presence of dissociated ions of the NaCl salt. The decreased deflection beyond 0.5 M (for surfactant dosages 0.5 and 1.0 %) may suggest molecular aggregation points, which hinder or reduces the number of mobile ions in the solution.
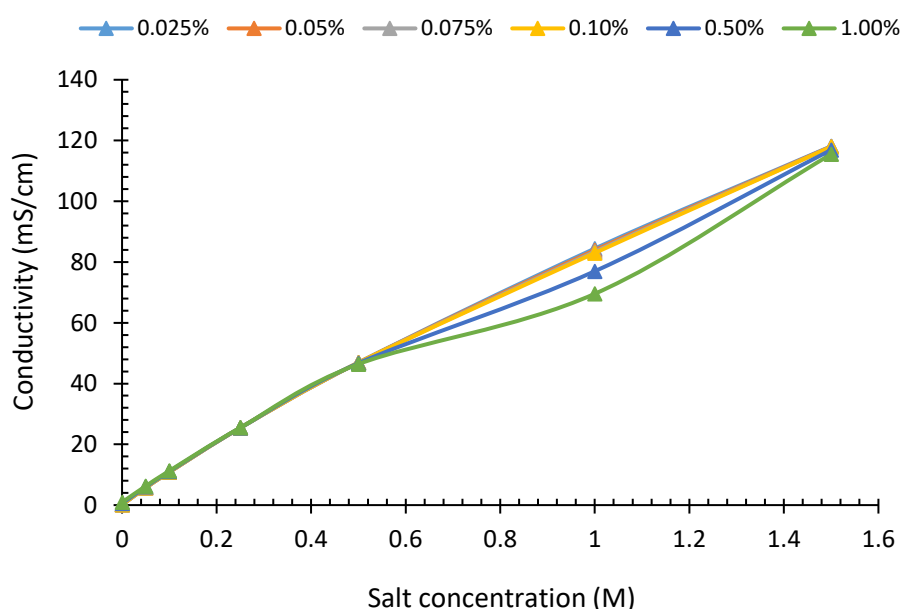
Figure 4.16 Conductivity of various dosages of sodium surfactin in NaCl solution

Surfactant performance depends on its ability to continue to adhere at fluid interface. However, surfactant adsorption is hindered by the accumulation and self-assembly of its unimers. As the unimers continue to assemble, a larger polymeric aggregate is formed which consequently reduces the adsorption capacity of surfactants. A critical concentration of the aggregate (CMC) is reached where no significant positive effect of surfactant is felt, irrespective of dosage added. It is inferring that sodium *surfactin* is likely to reach its CMC at 0.5 M salt concentration and at dosages 0.5 and 1.0 %.

4.2.7 FTIR characterization

The range of spectrum at which molecules (functional group) vibrate is one measure of their unique physical characteristics. In that regard, the infrared (IR) spectroscopy is a useful tool employed as fingerprint to identify or characterise unknown molecules. Successful characterization of biomaterials, using Infrared spectroscopy, is achieved through matching of the range from an unknown material with reference spectra that has already been recorded. IR spectroscopy helps in identifying planar or cyclic nature of biomolecules. Inference of presence of active site and consequently ability of biomolecule (sodium *surfactin*) to adhere on fluid surface/interface becomes possible through functional group identification. Additionally, nature of intermolecular hydrogen bonding in the surfactant aggregates can be inferred using FTIR spectroscopy.

The IR spectra of sodium *surfactin* in Figure 4.17 clearly indicated characteristic of peptides (N−H stretching mode) at 3293 and 1528 cm^{-1} peaks. Furthermore, peaks 2956–2870 cm^{-1} and 1467–1368 cm^{-1} are representative of hydrocarbon C–H group confirming the presence of aliphatic chains (–CH_3; –CH_2–) with symmetric stretching at 2870 cm^{-1} (Coates, 2006); and 1735 cm^{-1} band is a characteristics of C=O (carbonyl group). 1648cm^{-1} band result from the stretching mode of the CO–N bond. 1204 cm^{-1} fingerprint is a representative of aromatic C−H group in-plane bend. The pattern of the IR analysis is a confirmation of; (1) the cyclic nature of sodium *surfactin*, (2) its adsorption ability hence its applicability in surface activity operations, such as ST reduction, and (3) characteristics of lipopeptide biosurfactant previously described by (Bezza & Chirwa, 2015; B. Liu et al., 2016a).
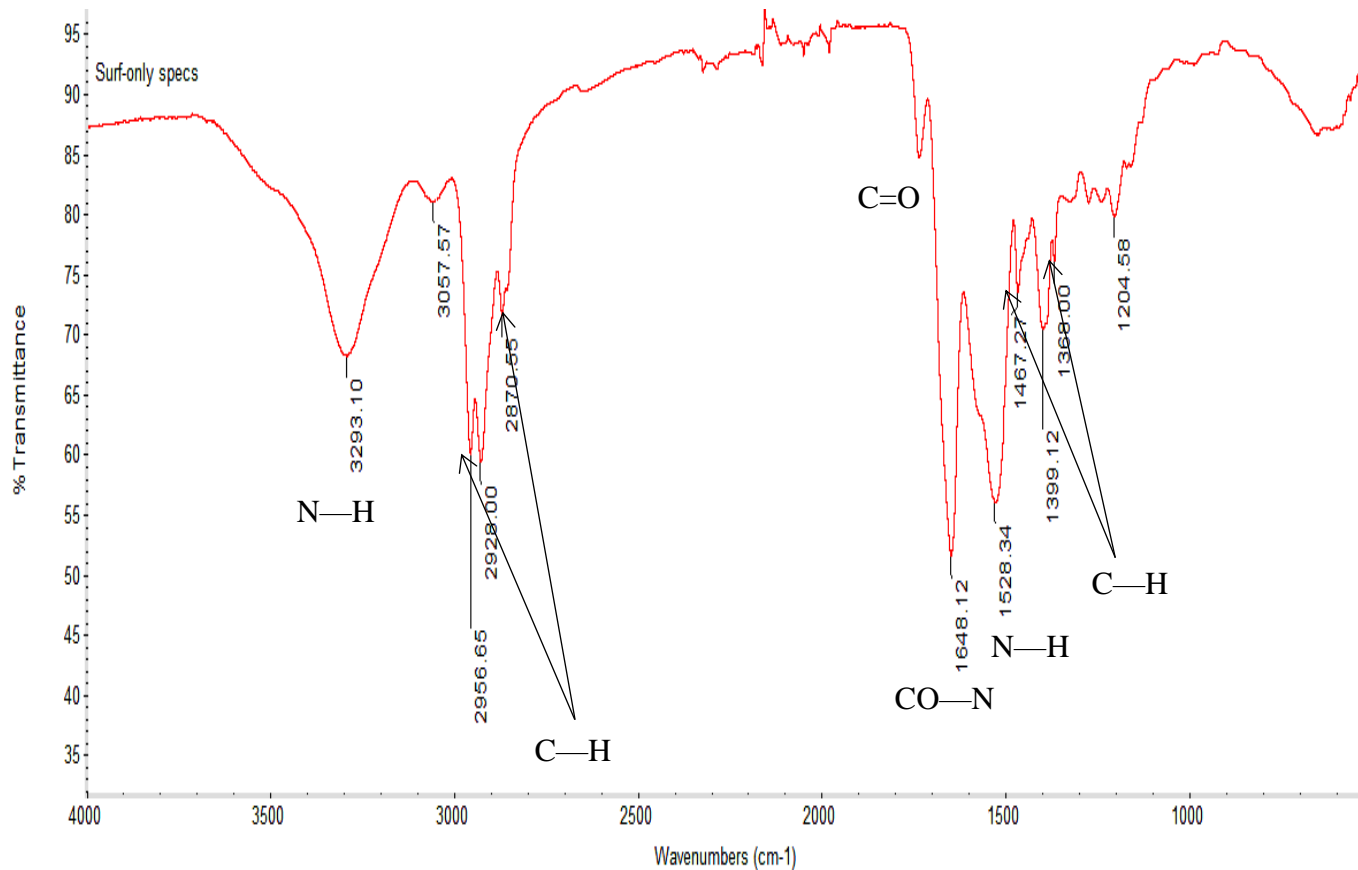
Figure 4.17 Fourier transform infrared spectra (FTIR) spectra of sodium surfactin

Additionally, the result validates the experimental procedure because it is well in agreement with the result of analysis conducted by Kaneka (see Appendix C 3).

4.3   Phase II: Flow Behaviour Characterization

Behavioural changes of working fluids, including surfactant solution, is very common in oil and gas operations. Fluctuations in operating conditions could result to either physical or chemical deformations in the form response to the fluctuation. More so, temperature fluctuations and fluids interaction with saline environment is a common occurrence in oil and gas fields that could affect fluid characteristics. Exhibition of transient or permanent flow behaviour is one form of these effects. During oil and gas field operations, molecular structures of surfactants exhibits some form of transient or permanent flow behaviour, due to exposure to one form of stress or another. Depending on the intensity of the shear, however, the resulting change in flow behaviour is therefore of concern to engineers and scientists. Reason being that it may result to undesirable consequence such as pressure loss in pipes (Sharma et al., 2016), and burn-out of equipment – such as pump (Franck,

2004), during operations, especially at start up. This last case usually happens when solutions are prepared and stored before use.

As a result, rheological characterization of surfactant is a critical factor that improves the result of its performance investigation. Such performances include those relating to surfactant effect on interfacial tension of gas/liquid/sold mixtures during EOR, EGR, and oil/gas transport in pipelines. This is because it defines the extent of response of the surfactant to any form of shear during application, and behaviour at quiescent state. Furthermore, rheological characterization aid: in equipment scaling and material sizing to suit the surfactant operational limits for optimal performance; ensuring mass transport of material thereby enhancing flow assurance; and to inhibit surfactant failure during adsorption at fluid interface. One important phenomenon that defines the transient or permanent structural behaviour of surfactant in solutions is the critical micelle concentration (CMC). In addition to the CMC, other factors such temperature as and ionic concentration of the solution affects rheological behaviour. Tripathy et al, (Tripathy et al., 2018) reported that CMC is a central factor of numerous surface-active characteristics such as solubilisation, lytic action and their interfacing with membranes of biological nature. Similarly, increase in temperature decreases the stability of the hydrogen bond in the micelles, thereby causing dehydration. Consequently, the peptide rings shape becomes planar and the chain length increased (She et al., 2012). This decreases the solvent accessible surface area, and under high temperature, orientation of some hydrocarbon chains became reversed.

Usually, increasing the chain length of the hydrocarbon tail (i.e. increasing hydrophobicity) resulted in decreased CMC values of a surfactant solution and hence increased their surface activity (Mukerjee & Mysels, 1972). When compared to conventional surfactants, cyclic amino acid-based surfactants (such as sodium *surfactin*) possess an advantage of lower CMC values (Morán et al 2004; Pérez et al., 2004; Pinazo et al., 2011) over planar peptides.

Furthermore, Krister *et al.*, (2003) reported the dependence of anionic surfactant (such as sodium dodecyl sulphate) CMC on temperature to be non-monotonic. The authors added that non-ionic surfactant (such as polyoxyethylene) showed a monotonic behaviour, with CMC decreasing with increasing temperature. Therefore, the dependence of surfactant morphology, hence its rheology on temperature is both a function of surfactant chemical structure, dosage and solubilizing medium. Section 4.3.1 present how change in rate of shear impacted on shear stress of different dosages of sodium *surfactin*, at variable temperature.

4.3.1 Viscosity-shear rate effect at different temperature

Steady-state rheology measurement was conducted under atmospheric pressure and variable temperature and data generated is shown in Appendix A 2. Figure 4.18 shows plot of viscosity against shear rate at temperatures of 23, 30, 40 and 50 $^{\circ}$C, designated respectively by a, b, c and d. It indicates that viscosity decreases with increasing rate of shear, depicting pseudoplastic behaviour (Drew, 2006; Jain et al., 2012; Mu et al., 2002) of sodium *surfactin* across all dosages and temperature. Furthermore, three (3) plateau regions, regardless of dosage, were noticed (separated by dashed lines). Low-shear region (region I) that suggest a small shear-induced decrease in viscosity below 85.1 s^{-1} shear rate (Υ). Moreover, within same shear rate boundary, initial viscosity (η) of 1.0% *surfactin* increases from 22.2 to 25.7 mPas (Figure 4.18b), when temperature was increased to 30 $^{\circ}$C. Conversely, viscosity of other dosages decreases within same range of temperature and Υ. The trend became highly dosage dependent at 40 and 50 $^{\circ}$C. Beyond 85.1 s^{-1}, reorientation of *surfactin* molecules became strongly shear-dependent. Υ was sufficiently high to prevent *surfactin* chains from undergoing any form of self-aggregation.
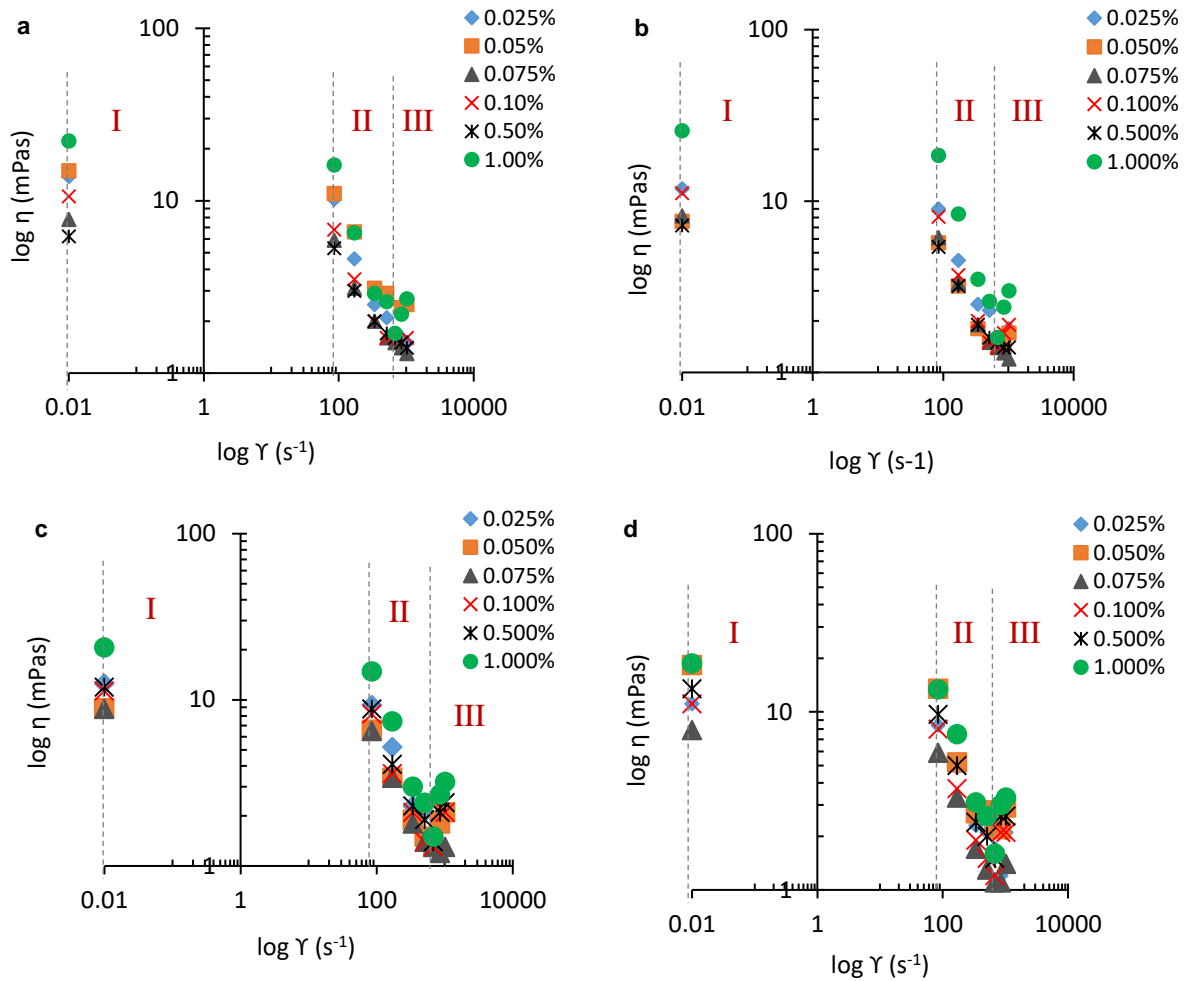
Figure 4.18 Viscosity-shear rate effect of *surfactin* dosages at (a) 23 ºC (b) 30 ºC (c) 40 ºC, and (d) 50 ºC

Consequently, η decreases continuously with increasing ϒ, which suggest a continuous irreversible shear-thinning behaviour (Lutz-Bueno, 2016; Rivero et al., 2012) across all dosages (region II). This form of behaviour is a very useful property for adsorptivity (Schroyen et al., 2017), as drilling fluid additives, and dispersant for flow assurance (Frigaard et al., 2017).

Pseudoplastic behaviour reached a minimum at critical ϒ of 680.9 s^{-1}, and shear-thickening behaviour set in beyond this value (region III). The shear-thickening increase as the temperature increase which is visibly evident in Figure 4.18c and d. Increasing temperature perhaps led to increased micelles concentration and consequently formation of larger aggregates (rod-like micelles). It is worthy to note that dosages 0.075 and 0.1% are least affected by changes in temperature and shear rate. Which may suggest best performance of *surfactin* at this dosage.

115

4.3.2 Dosage effect at zero-shear

To clearly understand effect of dosage on viscosity at different temperatures, plots of *surfactin* dosages used in the study were made against apparent viscosity at zero shear (η_o). Figure 4.19 generally depicts a monotonic response of viscosity to change in *surfactin* dosage. At ambient and 50 °C, the η_o increases with increasing dosages up to critical dosages of 0.075 and 0.1 %. Conversely, temperatures 30 and 40 °C decreases the η_o as the dosage increase. However, irrespective of the temperature change, there seems a convergence at 0.075 and 0.1 % dosage. This indicates that changes in temperature is unable to induce any form of molecular chain mobility of structures (Alves et al., 2010) at critical dosages. It could as well suggest range of the surfactant's critical micelle concentration (CMC).
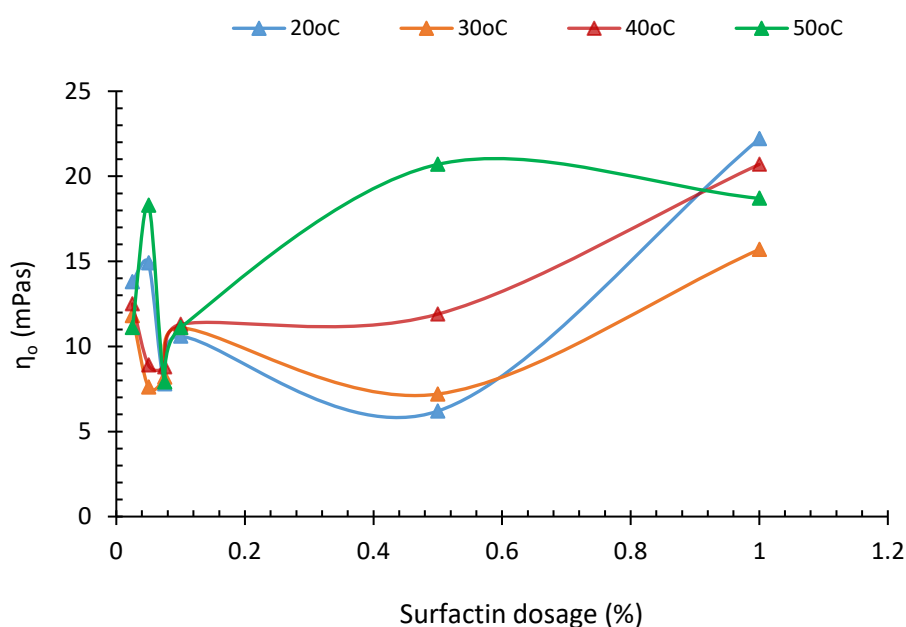
Figure 4.19 Surfactin dosage effect on viscosity at different temperatures

4.3.3 Viscosity-shear rate effect at different salt concentration

Performance of biosurfactant for oil/gas application is dependent on their behaviour in solutions like that of formation water. Of particular significance is the microviscosity, and how it is affected by the micellar phase, in terms of the solubilizing properties of the micellar core (Li et al., 2009). The morphology and molecular architecture of the surfactant may be responsible for this microviscosity effect.

Organic or inorganic salts, cosurfactants and/or strongly binding counterions were reported to have induced sphere-to-wormlike transition in nanostructure of ionic surfactants. This may suggest that

116

exposing sodium *surfactin* to saline environment will impact on micellization hence its interfacial property during adsorption (Schroyen et al., 2017) and rheology.

Change in ionic concentration of dispersion medium may increase or decrease the size and shape of a micelle. Li *et al.*, (2009), hypothesized that there exist two opposing tendencies in the formation of micelles of ionic surfactants: (1) removal of hydrocarbon chains from water favours aggregation; and (2) electrostatic repulsions between the ionic head groups opposes aggregation (Shrestha & Aramaki, 2008). Knoblich *et al.*, (1995), reported *surfactin* micelle to be spherical, ellipsoidal and/or cylindrical with a non-homogeneous size distribution at pH 7, 9.5, and 12. Additionally, Liu *et al.*, (2015) also reported that cylindrical micelles do transformed into spherical and/or ellipsoidal micelles of smaller sizes when exposed to saline solution environment of 100 mM NaCl and 20 mM CaCl₂. These are in line with the findings in this study shown in Figure 4.20, based on data in Appendix A 3.
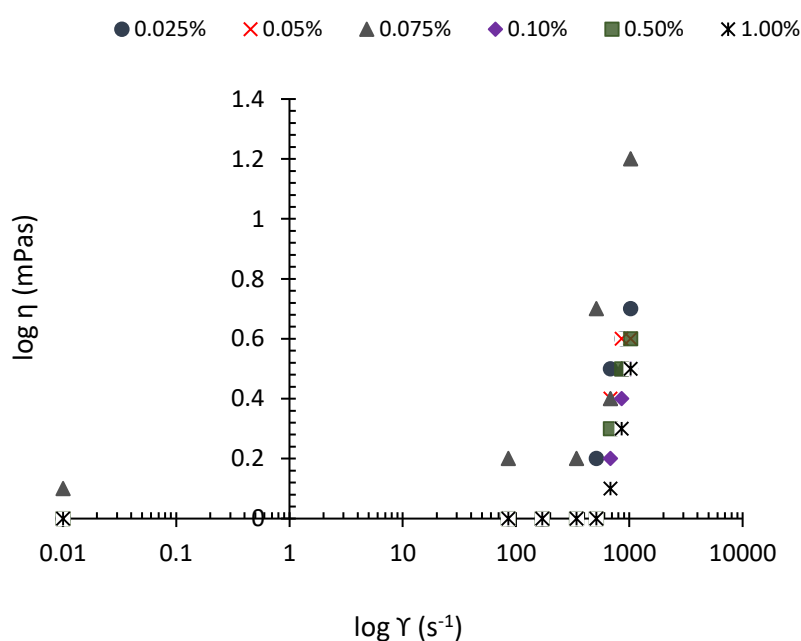
Figure 4.20 Viscosity vs shear rate as a function of surfactin dosage at 0.1 M salt concentrations

0.1 M NaCl salt concentration had a lytic effect on η of *surfactin* molecule. At this concentration, there was increased electrostatic repulsion between surfactant head group which limit micellar growth to small finite particle sizes (Li et al., 2009; Lutz-Bueno, 2016). It consequently led to zero viscosity at shear rate of up to 510 s^{-1} across most dosages. Nevertheless, dosage 0.075 % maintained relatively constant but higher η. Beyond 510 s^{-1} Υ, attractive Van der Waals force between the tails in the micellar became shear induced. Accordingly, that resulted to molecular self-aggregation that caused shear-thickening behaviour.

117

Flow behaviour of *surfactin* at increased salt concentration is like those reported in figure 1. However, increased ionic concentration resulted in increased η at zero-shear and constant temperature. For example, $η_o$ of 1.0 % *surfactin* dosage increased from 22.2 to 25.8 mPas at 0.25 M salt concentration (Figure 4.21a). It further increased to 36.9 mPas at 0.5 M in Figure 4.21b. Increasing salt concentration could have favoured removal of hydrocarbon chains from water. Consequently, it increased electrostatic coalescence between the hydrophilic group, which results in molecular self-aggregation. This effect however became dosage-dependant as the salt concentration increased to 1.0 and 1.5 M (Figure 4.21c and d).
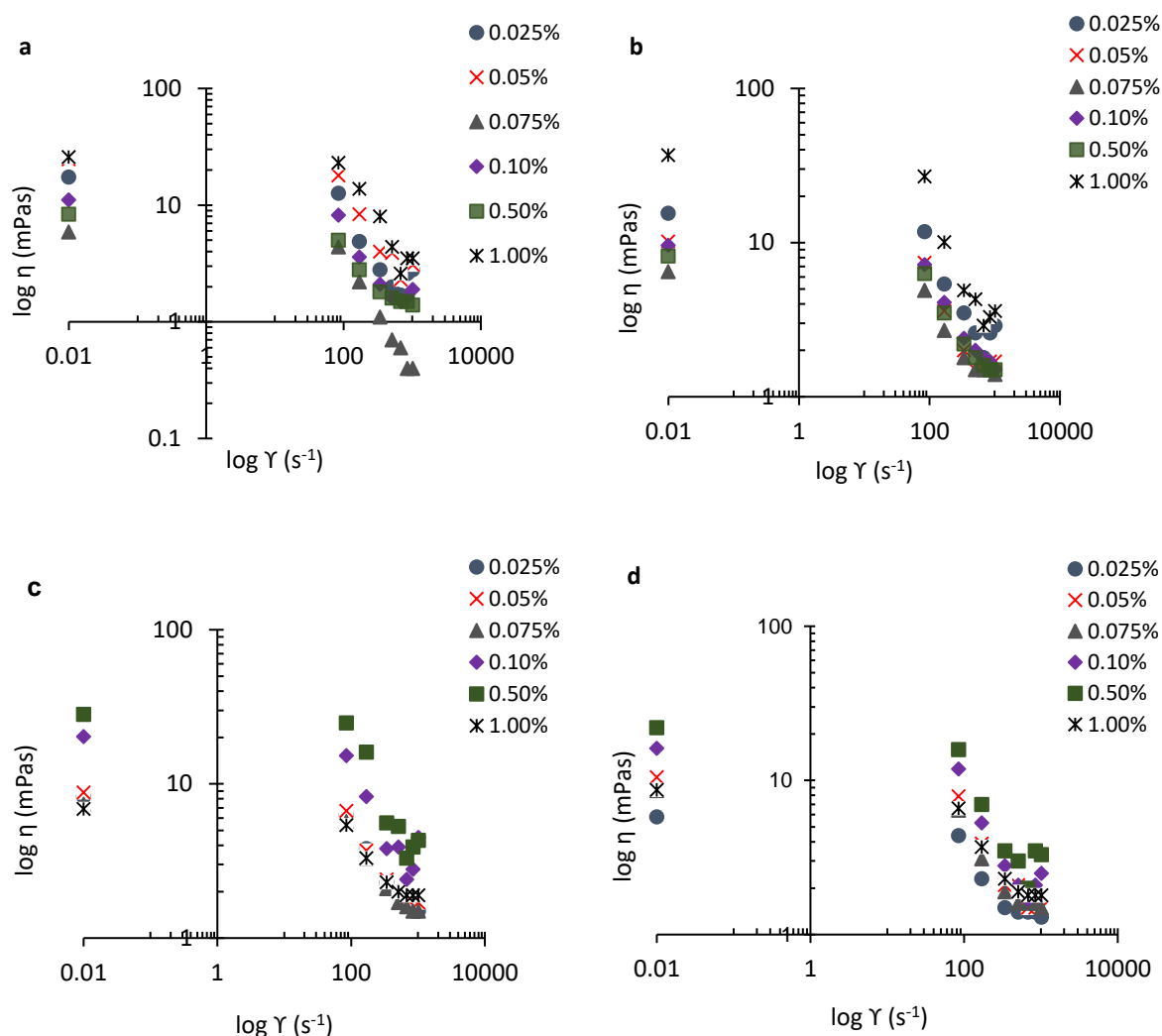
Figure 4.21 Viscosity vs shear rate as a function of surfactin dosage at (a) 0.25M, (b) 0.5M, (c) 1.0M, and (d) 1.5M salt concentrations

Flow behaviour became strongly shear-induced above 850.1 s^{-1}, with *surfactin* exhibiting continuous shear-thinning characteristics. Increase in salinity consequently led to increased electric

118

charge density of the polar shell formed at surface of the micelle (Lutz-Bueno, 2016). This resulted to upsurge of electrostatic repulsions between head groups, which consequentially increased pseudoplastic behaviour of the *surfactin*. Unlike at zero salt concentration, 680.9 s^{-1} critical shear was strongly dosage dependent. Figure 4.21a show that η of 0.075 % dosage continue to decrease with increasing rate of shear to a near zero value.

To stabilize surfactant in ionizing solutions, counterions bind to the micelles and thereby screening the electrostatic repulsion, a process that influence micellization. This phenomenon has been occurring with the surfactant with change in salinity and dosage. It signifies that the ionic concentration increase influenced the molecular mobility of the surfactant. Though the behaviour was generally pseudoplastic, it was shear-induced beyond 850.1 s^{-1} rate.

Additionally, Kronberg, Holmberg and Lindman, (2014a) indicated that shear rates in the range of 10^1-10^3 s^{-1} is typical of situation involving mixing and stirring, and 10^0-10^3 s^{-1} is typical of pipe flow situation. Therefore, it is safe to note suitability and sustainability of sodium *surfactin* utilization in pipe flow related operations.

4.3.4 Effect of temperature on *surfactin* viscosity

Temperature fluctuations is a common occurrence associated with oil and gas operations. It therefore become critical to study response of *surfactin* to these fluctuations at different shear rate. Consequently, effect of temperature on viscosity for different dosages of *surfactin* at different rate of shear was evaluated. Literally, rise in temperature should increase random thermal motion of molecules. As a result, surfactant molecular chains will be free to move, due to increased distance between molecules, leading to viscosity decrease. However, at microscopic level, temperature rise again may increase molecular activity. But could conversely induce a more extended molecular chain which form a more coalescing structure that will increase viscosity.

It is obvious in Figure 4.22 (a and b) that temperature increase resulted in simultaneous breakage and realignment of *surfactin* network at zero-shear. Furthermore, each dosage exhibited peculiar specific apparent viscosity response to changes in temperature.
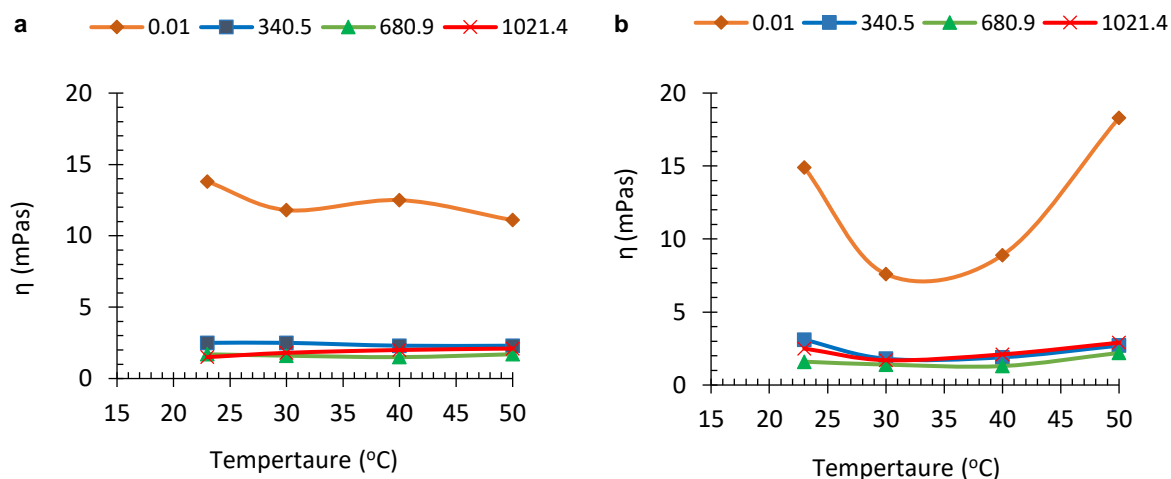
Figure 4.22 Effect of temperature on apparent viscosity of *surfactin* at different shear rate for (a) 0.025%, and (b) 0.05%

Surfactin dosage 0.025 % depicted significant monotonic decrease while 0.05 % depicted a monotonic increase behaviour at 0.01 s^{-1} rate. Additionally, 30 °C caused viscosity decrease effect in both a and b. Of interest (in Figure 4.22b) is the sharp decrease in apparent viscosity (η) from 14.9 to 7.6 mPas when temperature increased from 23 to 30 °C. The increase induced a breakage and realignment of the *surfactin* network. Though it reduced viscosity across the dosage, it could not sustain the network deformation (Kamal, 2016). At higher rate of shear, however, temperature effect became less significantly visible indicating that the molecular rearrangement was shear controlled.

Conversely, temperature increase at zero-shear resulted in molecular aggregation on surfactant dosages 0.075 and 1.0 % (Figure 4.23a and b). The effect, unlike at zero-shear, was less significant at higher rate of shear.
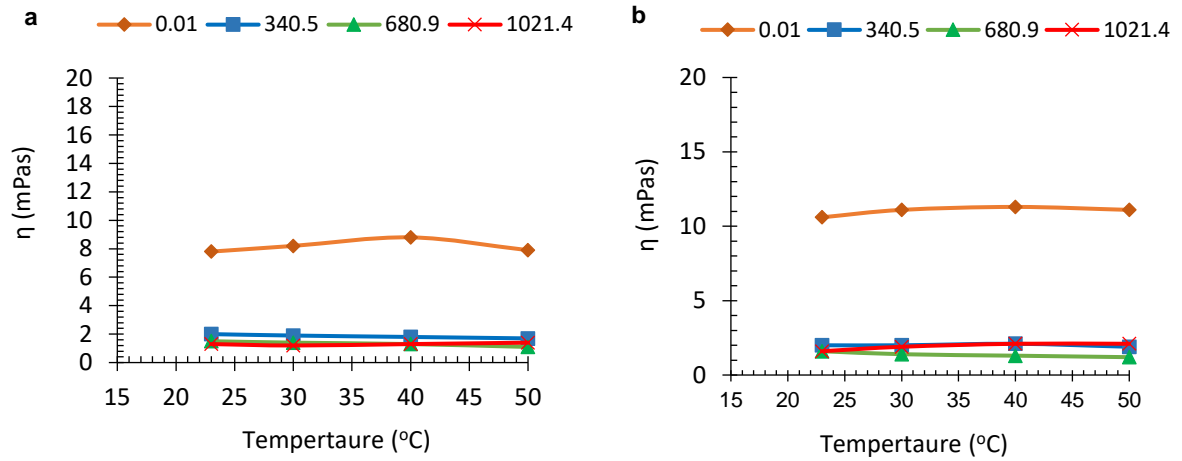
Figure 4.23 Effect of temperature on apparent viscosity of *surfactin* at different shear rate for (a) 0.075%, and (b) 0.1%

Figure 4.24a indicates that increasing temperature results in continuous formation of large aggregates at zero-shear. This is evident by the continuous increase in η. Furthermore, η of 1.0 % dosage increased to a value of 25.7 mPas at 30 °C (Figure 4.24b). But with shear rate increase, η became less sensitive to temperature. At 680 s^{-1}, dosage 1.0 % became highly shear rate induced that the apparent viscosity value was close to unity.

These affirm that apparent viscosity of *surfactin* is more dosage and shear rate dependent than it is on temperature, particularly at high shear rate. Thus, *surfactin* like other biosurfactants, such as extracellular polysaccharides produced from glycerol (Alves et al., 2010), are thermo-rheologically stable.
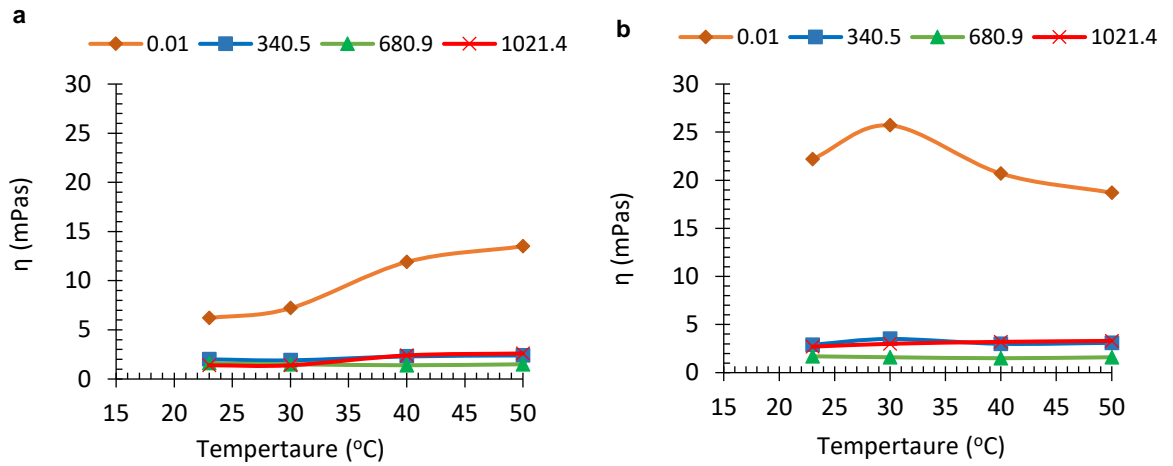
Figure 4.24 Effect of temperature on apparent viscosity of surfactin at different shear rate for (a) 0.5%, and (b) 1.0%

Alternatively, effect of temperature along with flow activation energy can be estimated with application of Arrhenius equation (J. Zhou et al., 2019). Equation (4.3) relates the viscosity at zero shear with system temperature.

$$\mu\,(T) = Ke^{E_\mu/_{RT}} \tag{4.3}$$

Where μ is the zero shear viscosity at temperature, T; K the material constant; R the molecular gas constant; and E_μ the flow activation energy.

Equation (4.4) is obtained by linearizing Equation (4.3).

$$\log\mu = logK - \frac{2.303E_\mu}{R}\left(\frac{1}{T}\right) \tag{4.4}$$

Plot of logμ was made against (1/T) and is described in Appendix A 4. Flow activation energy can be estimated by taking the slope of each plot and using Equation (4.5).

$$slope = -\frac{2.303E_\mu}{R} \tag{4.5}$$

While the present study tends to evaluate rheology only in terms of effect of temperature and salinity on viscosity, the author recommends further evaluation of *surfactin* modulus. Loss during storage and operation should be investigated further in modulus.

4.4 Diffraction Scanning Calorimetry (DSC) Analysis (Thermal analysis)

Analysis of materials using DSC technique is done to evaluate thermal stability of molecules directly in natural state. Transitions undergone by materials, in terms of heat flow as a function temperature increases are presented in thermogram. Basically, the technique takes into consideration the variation in the amount of heat required to rise the sample temperature. Temperature program for DSC analysis is, however, designed in a way that the sample holder temperature increases linearly as a function of time. By so doing, heat change associated with thermal denaturation of biomolecules, including biosurfactant, is measured at constant rate heating. Moreover, material evaluation and characterization are integral part of design process. Furthermore, temperature-dependent processes such as hydrate formation and inhibition require materials stability in the range of operating temperatures. And therefore, evaluating thermal behaviour of *surfactin* will provide information on its stability, expansion, shrinkage, (Nazhat, 2008) and molecular transition as operating condition changes. Ultimately, thermal analysis result aids in identification of processing and end-use performance.

Two (2) samples *surfactin* – a) physically dried powder sample, and b) hydrated sample, were used for the DSC analysis using TA DSC2500 instrument. Figure 4.25 indicates endothermic transition at enthalpy of 131.85 J/g, and peak temperature of 75.68 $^{\circ}$C.
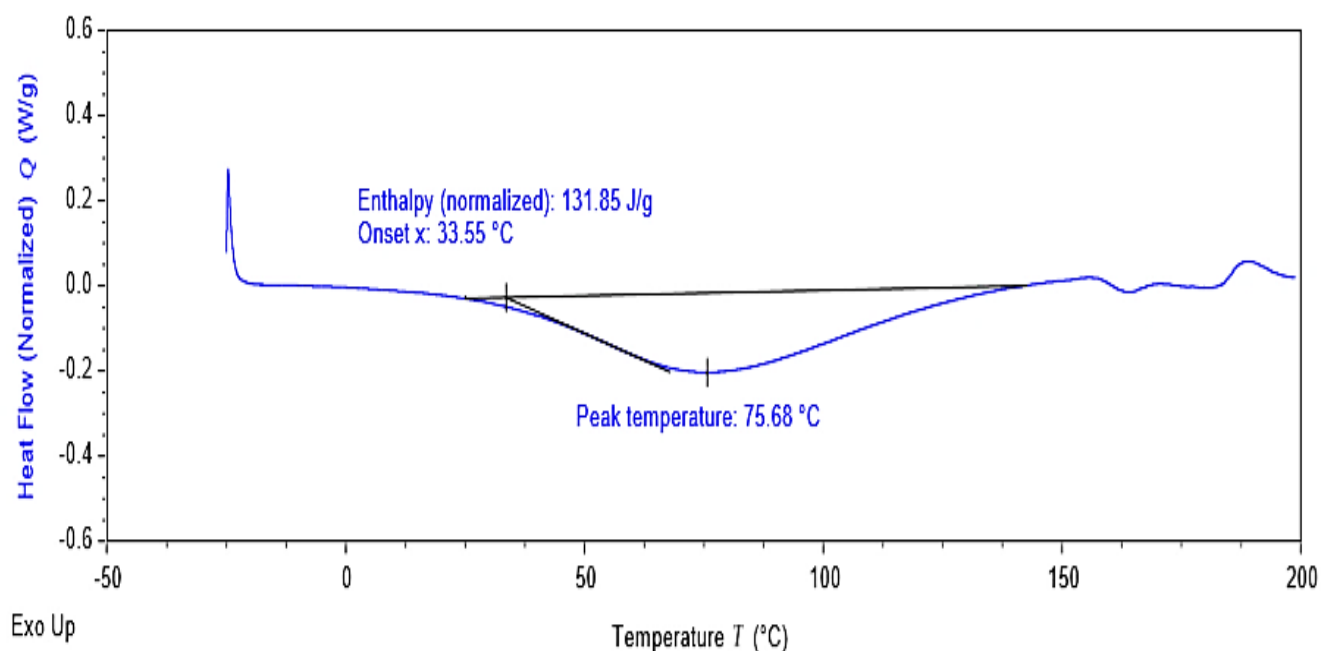
Figure 4.25 DSC thermogram of physically dried (powdered) surfactin

123

The endothermic peak may represent water loss from the sample occurring at 75..68 $^{\circ}$C (Narh et al., 2018; Paul, 2008) or stress relaxation (Paul, 2008) of the powdered sample. Safety data sheet (obtained from Kaneka) indicates that sodium *surfactin* is hygroscopic. Presence of moisture in the sample, as indicated in Figure 4.25, may suggest that the sample has absorbed water from the surrounding during handling. Thermogram around 170 to 200 $^{\circ}$C may represent a melting transition of the anhydrous *surfactin* alkyl chains (Soltero et al., 2001). Such transition at the given temperature suggest thermal stability of the surfactant sample. Moreover, expected operational application of *surfactin* at the end of this study may not surpass temperature of 60 $^{\circ}$C.

4.5   Phase III: CH$_4$-H$_2$O Multiphase System ST

Gas processing industries deals, on regular basis, with systems involving gas-liquid multiphase. More so, most common liquid component of gas-liquid multiphase is either brine or near fresh water. Additionally, nucleation of hydrate is partly an interfacial phenomena (Sun et al., 2004). Interaction of phase components within the system, therefore, depends on the surface area coverage of the gas-water film within the system. As such, gas–water ST becomes one of the most important parameters in the gas processing industries. To a large extent, gas–brine systems could as well affect water-gas contact movement and distribution in both reservoir and transporting pipelines. Consequently, mechanism of gas-water interaction particularly at contact interface becomes critical. In their study, Qin *et al.*, (2016) indicates that a lower ST value suggest a longer hydrate onset time. As such, improving the understanding of how CH$_4$-H$_2$O interaction mechanism works prompted this study, particularly alteration of surface interaction by biosurfactant.

4.5.1   Effect of surfactant on methane-water ST at ambient condition

Therefore, to investigate effect of sodium *surfactin* on tension existing at CH$_4$-H$_2$O interface, ST of the system was measured using rising bubble method. The result of this effect at ambient room pressure and temperature of 20.6 $^{\circ}$C is shown in Figure 4.26.
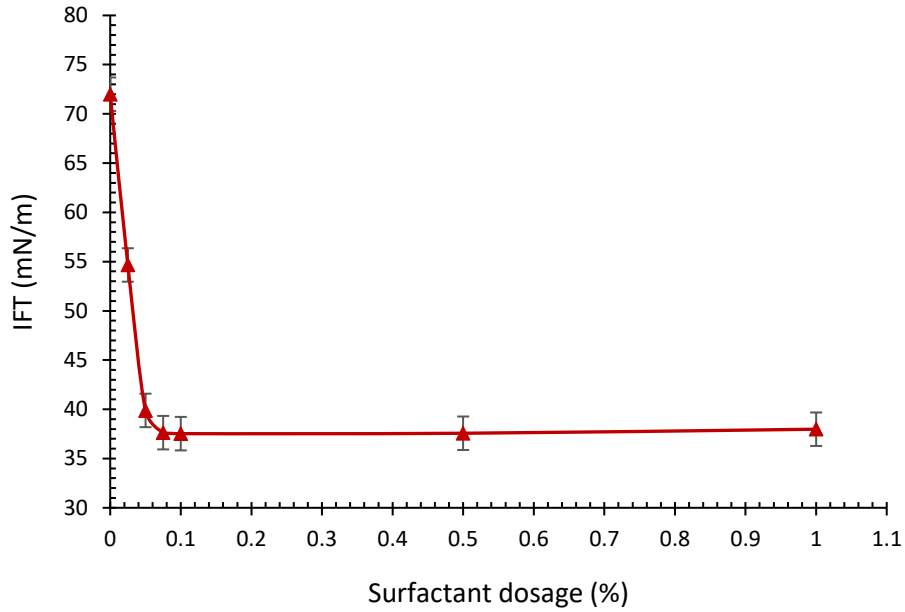
Figure 4.26 Effect of sodium surfactin on CH_4 – H_2O ST

The result showed an outstanding effectiveness of sodium *surfactin* in reducing the ST between CH_4 and distil water, hence inhibiting characteristics. Lower ST implies higher inhibiting characteristics (Qin et al., 2016). The biosurfactant was able to adhere and formed a film at the methane–water interface. This blocks mass transport across the water/hydrocarbon interface. Consequently, the hydrophilic head of sodium *surfactin* formed hydrogen bonds with water via carbonyl oxygen and hence hindered water molecule rearrangement needed to build hydrate cages from liquid water. This however was observed to be dosage dependent. At surfactant dosage as low as 0.025 % the ST dropped to about 54 mN/m. The effect continues, though in a decreasing pattern, with the minimum ST recorded between 0.075 to 1.0 % (37 mN/m). Beyond this dosage, the surfactant effect remains virtually the same. Therefore, it indicates that the surfactant must have reached its CMC at about these dosages. This assertion corresponds to, and validate the earlier findings reported on density. Additionally, ionic surfactants (being electrostatically charged), were reported to better form hydrogen bonds with water (Xiao & Adidharma, 2009). And are thus expected to perform effectively on hydrate inhibition.

Similar results were obtained using SDS (Sun et al., 2004; Watanabe et al., 2005), though at respectively much higher surfactant dosage (500 and 1000ppm) and respective pressure of (about 9 and 3.90 MPa). Similarly, Qin *et al.*, (2016), (2017) indicated lowering of methane-water ST to about 23 mN/m using PVP ramification (PVP-BP). This again occurs at a pressure that induces lowering of ST. Effect of temperature, pressure surfactin dosage interaction is discussed in Section 4.5.2.

The preliminary result may pre-empt the fact that sodium *surfactin* is a potential methane-water hydrate inhibitor, though care must be taken to validate the efficacy of the surfactant by investigating hydrate onset time.

4.5.2 Experimental design result

As noted earlier, hydrate formation phenomenon is critical of prevailing equilibrium thermodynamic conditions. Therefore, any attempt at preventing the occurrence of hydrate in gas processing pipelines must take into consideration pressure-temperature interaction. To study this interaction in the presence of surfactant, the experimental study was designed to effectively capture the interaction using Design-Expert software. The tools in this software was utilized to evaluate the effects of these parameters using optimization strategy based on Response Surface Method (RSM). Result of this design is tabulated in Appendix B 2 (indicates by red colour in ST column).

Result of the investigation, considering the specified conditions, were determined and compared with those corresponding to the predicted outcome suggested by the software. Additionally, cubic model was found to be the "best fit" model for the ST response. The model summary corresponding to the ST fit is shown in Table 4.1.

Table 4.1 Model summary of statistics based on ST fit

Source	Std. Dev.	R^2	Adjusted R^2	Predicted R^2	PRESS	
Linear	5.02	0.4358	0.4012	0.3077	1512.40	
2FI	5.18	0.4359	0.3623	0.0537	2067.32	
Quadratic	2.59	0.8683	0.8407	0.8092	416.75	
Cubic	1.13	0.9807	0.9697	0.9545	99.44	Suggested
Quartic	0.6289	0.9962	0.9906	0.9225	169.42	Aliased

The values in Table 4.1 suggest that least deviation of 1.13 in the experimental ST value, compared to other models. More so, with the experimental (0.9807), adjusted (0.9697) and predicted R^2 (0.9545) value above 0.95%, it is expected that model P-value will be less than 0.5 threshold. The result further indicate that a relationship exists between the independent factors (temperature, surfactant dosage and pressure) and dependent factor (ST). The pressure and temperature interaction with surfactant dosage are graphically shown in the 3D surface plots respectively in Figure 4.28 and Figure 4.27.
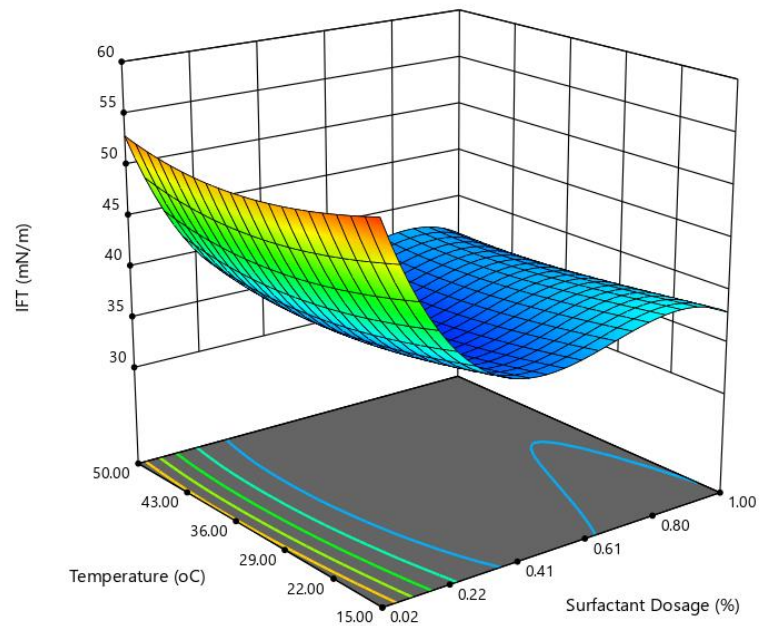
Figure 4.27 Temperature-surfactant dosage effect on ST at 7.58 MPa

Figure 4.27 further indicates that interaction surfactant-temperature interaction at pressure of 7.58 MPa reduced methane-water ST to a minimum of 34.13 mN/m. This shows that: in the presence of surfactant, temperature plays a role in methane-water ST reduction; and sodium *surfactin* has a great potential of being an environmentally friendly hydrate formation inhibitor. Similarly, surfactant-pressure interaction follows the trend depicted in Figure 4.27. Lowest ST value of 34.13 mN/m was obtained due to interactive effect of surfactant and pressure at about temperature of 32 $^{\circ}$C and 0.7 % surfactant dosage. This interaction is shown in Figure 4.28.
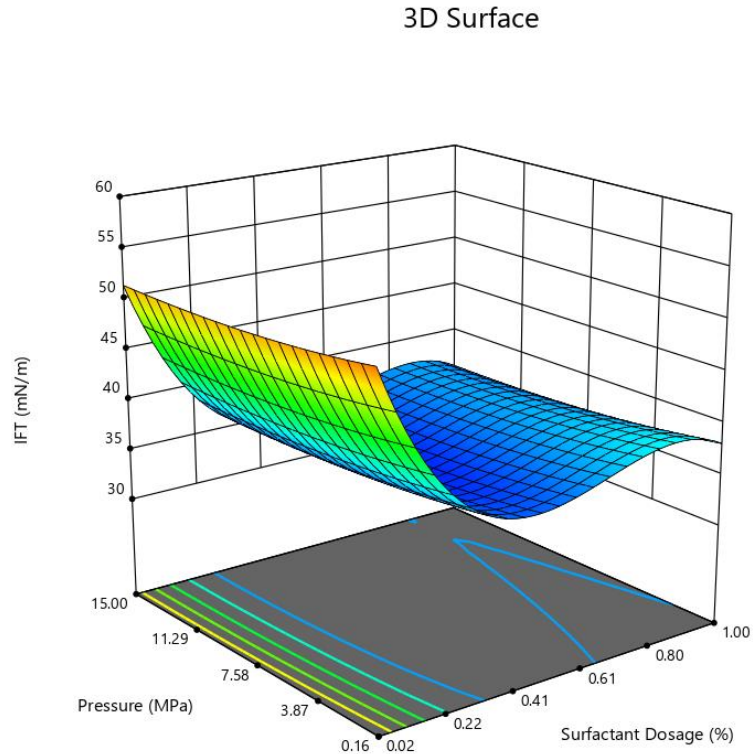
Figure 4.28 Temperature-surfactant dosage effect on ST at 32.50 °C

Additionally, multiple regression analysis of the response data indicates that a cubic polynomial equation that fits the interaction of independent variables was derived. Equation (4.6) shows the coded form of the cubic polynomial equation which can be used to quantify CH_4-H_2O ST within the experimental condition.

$$
\begin{aligned}
ST = \ & 34.88 + 2.92A - 1.10B - 0.8154C - 0.1251AB - 0.0975AC - 0.0033BC \\
& + 9.15A^2 + 1.33B^2 + 0.6520C^2 + 0.0689ABC - 0.0209A^2B \\
& + 0.0171A^2C - 0.7659AB^2 - 0.0124AC^2 + 0.0165B^2C \\
& + 0.0680BC^2 - 10.44A^3 + 0.2864B^3 - 0.0721C^3
\end{aligned}
\tag{4.6}
$$

Where A=Surfactant dosage, B=Temperature and C=Pressure

The outcome of regression after analysis of variance (ANOVA) indicates that the model, having a P-value of 0.0001, is significant (P-value being less than 0.005 threshold). Additionally, "Predicted R²" of 0.9545 can be said to be in reasonable agreement with "Adjusted R²" of 0.9697 (with a difference of less than 0.2). Table of ANOVA is shown in Appendix B 4.

128

4.6 Chapter Summary

After careful implementation of experimental procedure, outcomes of the experimental investigation were presented in this chapter. Foaming and solubility of *surfactin* in aqueous medium was significant which indicates possibility of surface activity; however, it is affected by salinity. Surface activity was further confirmed through emulsification index of 82 %. *Surfactin* showed both emulsifying and demulsifying characteristics. More so, *surfactin* expands when dissolved in distilled water. This was evident by decrease in density of aqueous surfactin, at some points below that water. Two minimum density points were observed which indicates possibility of *surfactin* reaching its CMC. These were further confirmed by pH, rheology and surface tension tests results. Surfactin reduced methane-distilled water surface tension to a minimum of 34.13 mN/m at 32.5 ºC and 7.58 MPa conditions of temperature and pressure respectively. These findings indicate that *surfactin* is indeed a potential hydrate formation inhibitor. Though these findings show positive results to the aim of the research, other research techniques such as kinetic study to explore in real time methane-water nucleation period in the presence of surfactin. Further conclusions and recommendations are presented in Sections 5.1 and 5.2 respectively.

CHAPTER FIVE

5 CONCLUSIONS AND RECOMMENDATIONS

5.1 Conclusions

Having successfully executed the outlined objectives of this study through experimental investigations, conclusions are drawn on the potential utilization of sodium *surfactin* as methane hydrate formation inhibitor. The investigations conducted in the study were categorized into 3 phases. Outcome of these investigations generally suggest that sodium *surfactin* can indeed serve as a 'green' alternative to chemical based surfactants in preventing hydrate formation in pipelines during gas transport. On this note, specific conclusions are drawn based on various phases of the study as follows, viz a viz physicochemical and thermal characterization, rheology investigation and tensioactive capability (surface tension investigation):

- Spontaneous collapse of bubbles after foaming, density behaviour and emulsification index suggest adsorptive capability of *surfactin*. Low density values (less than that of water) are indication of dispersity which enhances mass transport within a medium. Use of surfactants in preventing hydrate formation strongly relies on surfactant's dispersive ability and consequently its transfer to the gas-water surface to form a thin film. No previous study reported density, pH and conductivity characteristics of *surfactin* particularly at variable temperature ranges up to -5 ^{o}C typical for gas hydrate formation. The dispersive ability of sodium *surfactin* is evident in the density value of 996.641 kgm^{-3} and 82 % emulsification index. However, the dispersive efficiency reduced in saline concentration above 0.5 M, a finding that is in conformity with use of *surfactin* for EOR. Additionally, pH and conductivity results indicate that sodium *surfactin* can effectively be used in oil and gas fields without danger of pipeline corrosion.

- Sodium *surfactin* exhibit a pseudoplastic flow behaviour, based on viscosity-shear rate characterization. To the author's knowledge, this is the first report that characterized flow behaviour of *surfactin* and how it is affected by temperature and salinity. Besides, one of desirable characteristics of fluids in oil and gas operations is their ability to flow seamlessly to delivery point. Reduction in viscosity of fluids with shear rate increase ensures continuous flow during operation which suggests pumpability and dispersion characteristics of *surfactin*. On this note, injection of *surfactin* solution at well head for prevention of hydrate

formation and consequently its flow in pipeline will be seamless. Electrostatic effect plays a role in the flow behaviour of *surfactin* at low saline concentration up to 0.1 M and shear rate up to 510 s^{-1}. *Surfactin* flow may likely fail in this range of operational parameters. However, within same salt concentration, flow behaviour can be enhanced by increasing rate of shear beyond 510 s^{-1}. Nevertheless, the biosurfactant is thermo-rheologically stable.

- Methane-water hydrate formation is favoured by the decrease in interface area between the fluids thereby allowing methane to be enveloped by the water molecule. However, formation of sustainable film at methane-water interface ensures that increased surface area continue to exist at the fluids interface. Therefore, an effective surfactant can sustainably form an interfacial film by increasing interfacial surface area. Previous studies using chemical based surfactants indicated that this was achieved by lowering interface surface tension between the water and methane molecule. Methane-water ST was effectively reduced from 72 to 37.53 mN/m at 20.5 °C and atmospheric pressure. Under equilibrium conditions of 7.58 MPa and 32.5 °C respectively of pressure and temperature, *surfactin* optimally reduces methane-water ST to 34 mN/m. This is an indicator that *surfactin* will effectively serve as alternative surfactant in the prevention of methane-water hydrate formation at those operating conditions.

The research study highlights the characteristics behaviour of sodium *surfactin* as potential methane-water hydrae formation inhibitor. The findings are aimed at providing a basic knowledge towards finding alternative environmentally friendly surfactant. Additionally, this information confirms the potential of *surfactin* in the control of gas hydrate formation, and further form a basis for field scale applications.

5.2 Recommendations

This study has achieved, successfully, its set target of aims and objectives. Notwithstanding, more avenues can be created for further studies beyond the scope of the author. These are presented in the form of recommendations as follows:

- Different gas mixtures along with methane should be tested. This is to mimic typical natural gas as obtainable in the industry, although methane takes the highest proportion in the mixture.
- Gas processing operations are not devoid of saline medium particularly when materials are leaving the production well. Consequently, effectiveness of sodium *surfactin* in reducing

methane-water ST can further be extended by investigating its performance in saline medium. This is recommended to be carried out using different salts (monovalent and divalent).

- Further to the rheology investigation conducted in this study, it is recommended that further study on *surfactin* modulus be investigated. This is to ascertain the sustainability and efficiency of *surfactin* when stored over time.

REFERENCES

Abay, H. K., & Svartaas, T. M. (2010). Effect of ultralow concentration of methanol on methane hydrate formation. *Energy and Fuels*, *24*(2), 752–757. https://doi.org/10.1021/ef9009422

Abdel-Mawgoud, A. M., & Stephanopoulos, G. (2018). Simple glycolipids of microbes: chemistry, biological activity and metabolic engineering. *Synthetic and Systems Biotechnology*, *3*(1), 3–19. https://doi.org/10.1016/j.synbio.2017.12.001

Adamson, A. W., & Gast, A. P. (1977). *Physical chemistry of surfaces* (6th ed.). John Wiley and Sons. https://doi.org/10.1149/1.2133374

Adnan, M., Alshammari, E., Ashraf, S. A., Patel, K., Lad, K., & Patel, M. (2018). Physiological and molecular characterization of biosurfactant producing endophytic fungi *xylaria regalis* from the cones of *thuja plicata* as a potent plant growth promoter with its potential application. *BioMed Research International*, *2018*, 1–11. https://doi.org/10.1155/2018/7362148

Akshatha, N., Niki, T., Sripradha, S., Veena, S., & Bhaskara Rao, K. V. (2018). Isolation and characterization of biosurfactant from bacillus amyloliquefaciens vitans6 isolated from oil contaminated soil collected from an automobile workshop in Bangalore, India. *Research Journal of Pharmacy and Technology*, *11*(1), 207–211. https://doi.org/10.5958/0974-360X.2018.00039.2

Al-Bahry, S. N., Al-Wahaibi, Y. M., Elshafie, A. E., Al-Bemani, A. S., Joshi, S. J., Al-Makhmari, H. S., & Al-Sulaimani, H. S. (2013). Biosurfactant production by bacillus subtilis b20 using date molasses and its possible application in enhanced oil recovery. *International Biodeterioration and Biodegradation*, *81*, 141–146. https://doi.org/10.1016/j.ibiod.2012.01.006

Al-Eisa, R. M., Elanany, M. S., Al-Majnouni, K. A., Al-Jabran, A. A., Al-Ajwad, H. A., Abba, I. A., & Al-Malki, A. R. (2015). *Kinetic hydrate inhibitors for natural gas fields: rational design and experimental development*. http://www.saudiaramco.com/content/dam/Publications/Journal-of-Technology/2015_fall/JOT-Fall-2015-Art11.pdf

Al-Sulaimani, H., Al-Wahaibi, Y., Ai-Bahry, S., Elshafie, A., Al-Bemani, A., Joshi, S., & Ayatollahi, S. (2012). Residual-oil recovery through injection of biosurfactant, chemical surfactant, and mixtures of both under reservoir temperatures: induced-wettability and interfacial-tension effects. *SPE Reservoir Evaluation and Engineering*, 210–217. https://doi.org/10.2118/158022-PA

Al-Wahaibi, Y., Al-Hadrami, H., Al-Bahry, S., Elshafie, A., Al-Bemani, A., & Joshi, S. (2016). Injection of Biosurfactant and Chemical surfactant following hot water injection to enhance heavy oil recovery. *Petroleum Science*, *13*(1), 100–109. https://doi.org/10.1007/s12182-015-0067-0

Al-Wahaibi, Y., Joshi, S., Al-Bahry, S., Elshafie, A., Al-Bemani, A., & Shibulal, B. (2014). Biosurfactant production by Bacillus subtilis B30 and its application in enhancing oil recovery. *Colloids and Surfaces B: Biointerfaces*, *114*, 324–333. https://doi.org/10.1016/j.colsurfb.2013.09.022

Ali Khan, A. H., Tanveer, S., Alia, S., Anees, M., Sultan, A., Iqbal, M., & Yousaf, S. (2017). Role of nutrients in bacterial biosurfactant production and effect of biosurfactant production on petroleum hydrocarbon biodegradation. *Ecological Engineering*, *104*, 158–164. https://doi.org/10.1016/j.ecoleng.2017.04.023

Altamash, T., Qureshi, M. F., Aparicio, S., Aminnaji, M., Tohidi, B., & Atilhan, M. (2017). Gas hydrates inhibition via combined biomolecules and synergistic materials at wide process conditions. *Journal of Natural Gas Science and Engineering*, *46*, 873–883. https://doi.org/10.1016/j.jngse.2017.07.034

Alvarez, J. O., Neog, A., Jais, A., & Schechter, D. S. (2014). Impact of surfactants for wettability alteration in stimulation fluids and the potential for surfactant EOR in unconventional liquid reservoirs. *SPE USA Unconventional Resources Conference 2014*, 468–485. https://doi.org/10.2118/169001-MS

Alves, V. D., Freitas, F., Costa, N., Carvalheira, M., Oliveira, R., Gonçalves, M. P., & Reis, M. A. M. (2010). Effect of temperature on the dynamic and steady-shear rheology of a new microbial extracellular polysaccharide produced from glycerol byproduct. *Carbohydrate Polymers*, *79*, 981–988. https://doi.org/10.1016/j.carbpol.2009.10.026

Aman, Z. M., Brown, E. P., Sloan, D. E., Sum, A. K., & Koh, C. A. (2011). Interfacial mechanisms governing cyclopentane clathrate hydrate adhesion/cohesion. *Physical Chemistry Chemical Physics*, *13*, 19796–19806. https://doi.org/10.1039/C1CP21907C

Anderson, B. J., Tester, J. W., Borghi, G. P., & Trout, B. L. (2005). Properties of inhibitors of methane hydrate formation via molecular dynamics simulations. *Journal of the American Chemical Society*, *127*(50), 17852–17862. https://doi.org/10.1021/ja0554965

Anjum, F., Gautam, G., Edgard, G., & Negi, S. (2015). Biosurfactant production through Bacillus sp. MTCC 5877 and its multifarious applications in food industry. *Bioresource Technology*, *213*, 262–269. https://doi.org/10.1016/j.biortech.2016.02.091

Antoniou, E., Fodelianakis, S., Korkakaki, E., & Kalogerakis, N. (2015). Biosurfactant production from marine hydrocarbon-degrading consortia and pure bacterial strains using crude oil as carbon source. *Frontiers in Microbiology*, *6*(APR), 1–14. https://doi.org/10.3389/fmicb.2015.00274

Anvari, S., Hajfarajollah, H., Mokhtarani, B., & Noghabi, K. A. (2015). Physiochemical and thermodynamic characterization of lipopeptide biosurfactant secreted by Bacillus tequilensis HK01. *RSC Advances*, *5*(111), 91836–91845. https://doi.org/10.1039/c5ra17275f

Apaydin, O. G., & Kovscek, A. R. (2001). Surfactant Concentration and End Effects on Foam Flow in Porous Media. *Transport in Porous Media*, *43*(3), 511–536. https://doi.org/10.2118/59286-MS

Arora, A., Cameotra, S. S., Kumar, R., Balomajumder, C., Singh, A. K., Santhakumari, B., Kumar, P., & Laik, S. (2016). Biosurfactant as a promoter of methane hydrate formation: thermodynamic and kinetic studies. *Scientific Reports*, *6*(February), 1–13. https://doi.org/10.1038/srep20893

ASTM. (2017). *Manual of Petroleum Measurement Standards (MPMS)* (No. D1298; 12b). https://compass.astm.org/download/D1298.23779.pdf

Atlas, R. M. (1985). Effects of hydrocarbons on microorganisms and biodegradation in Arctic ecosystems. In F. R. Engelhardt (Ed.), *Petroleum Effect in the Arctic Environment* (pp. 63–99). Elsevier.

Bages-Estopa, S., White, D. A., Winterburn, J. B., Webb, C., & Martin, P. J. (2018). Production and separation of a trehalolipid biosurfactant. *Biochemical Engineering Journal*, *139*, 85–94. https://doi.org/10.1016/J.BEJ.2018.07.006

Banat I. M., Franzetti A, Gandolfi I., Bestetti G., Martinotti M. G., Fracchia L., Smyth T. J., M. R. (2010). Microbial biosurfactants production, applications and future potential. ;:. *Appl Ied Microbiology and Biotechnology*, *87*(2), 427–444. https://doi.org/10.1007/500253-010-2589-0

Baoune, H., Ould El Hadj-Khelil, A., Pucci, G., Sineli, P., Loucif, L., & Polti, M. A. (2018). Petroleum degradation by endophytic Streptomyces spp. isolated from plants grown in contaminated soil of southern Algeria. *Ecotoxicology and Environmental Safety*, *147*(May 2017), 602–609. https://doi.org/10.1016/j.ecoenv.2017.09.013

Barros, F. F. C., De Quadros, C. P., Maróstica, M. R., & Pastore, G. M. (2007). Surfactina: Propriedades químicas, tecnológicas e funcionais para aplicações em alimentos. *Quimica Nova*, *30*(2), 409–414. https://doi.org/10.1590/S0100-40422007000200031

Batista Magalhaes, E. R., Leite Silva, F., Dos Santos Bezerra Sousa, M. A., & Silvino dos Santos, E. (2018). Use of different agroindustrial waste and produced water for biosurfactant production. *Biosciences, Biotechnology Research Asia*, *15*(1), 17–26. https://doi.org/10.13005/bbra/2604

Behera, M. R., Varade, S. R., Ghosh, P., Paul, P., & Negi, A. S. (2014). Foaming in micellar solutions: Effects of surfactant, salt, and oil concentrations. *Industrial and Engineering Chemistry Research*, *53*(48), 18497–18507. https://doi.org/10.1021/ie503591v

Belhaj, A. F., Elraies, K. A., Mahmood, S. M., Zulkifli, N. N., Akbari, S., & Hussien, O. S. E. (2019). The effect of surfactant concentration, salinity, temperature, and pH on surfactant adsorption for chemical enhanced oil recovery: a review. *Journal of Petroleum Exploration and Production Technology*, *0123456789*. https://doi.org/10.1007/s13202-019-0685-y

Ben Ayed, H., Jridi, M., Maalej, H., Nasri, M., & Hmidet, N. (2014). Characterization and stability of biosurfactant produced by Bacillus mojavensis A21 and its application in enhancing solubility of hydrocarbon. *Journal of Chemical Technology and Biotechnology*, *89*(7), 1007–1014. https://doi.org/10.1002/jctb.4192

Berry, J. D., Neeson, M. J., Dagastine, R. R., Chan, D. Y. C., & Tabor, R. F. (2015). Measurement of surface and interfacial tension using pendant drop tensiometry. In *Journal of Colloid and Interface Science* (Vol. 454, pp. 226–237). Academic Press. https://doi.org/10.1016/j.jcis.2015.05.012

Bezerra, K. G. O., Rufino, R. D., Luna, J. M., & Sarubbo, L. A. (2018). Saponins and microbial biosurfactants: Potential raw materials for the formulation of cosmetics. *Biotechnology Progress*, *00*(00), 1–12. https://doi.org/10.1002/btpr.2682

Bezza, F. A., & Chirwa, E. M. N. (2015). Production and applications of lipopeptide biosurfactant for bioremediation and oil recovery by Bacillus subtilis CN2. *Biochemical Engineering Journal*, *101*, 168–178. https://doi.org/10.1016/j.bej.2015.05.007

Bhattarai, A., Chatterjee, S. K., & Niraula, T. P. (2013). Effects of concentration, temperature and solvent composition on density and apparent molar volume of the binary mixtures of cationic-

anionic surfactants in methanol-water mixed solvent media. *SpringerPlus*, *2*(1), 1–9. https://doi.org/10.1186/2193-1801-2-280

Boschee, P. (2012). Gas Hydrate Control Using Monoethylene Glycol in the Gulf of Mexico. *Oil and Gas Facilities*, *1*(3). https://www.spe.org/en/ogf/ogf-article-detail/?art=407

Burch, A. Y., Browne, P. J., Dunlap, C. A., Price, N. P., & Lindow, S. E. (2011). Comparison of biosurfactant detection methods reveals hydrophobic surfactants and contact-regulated production. *Environmental Microbiology*, *13*(10), 2681–2691. https://doi.org/10.1111/j.1462-2920.2011.02534.x

Burch, A. Y., Shimada, B. K., Browne, P. J., & Lindow, S. E. (2010). Novel high-throughput detection method to assess bacterial surfactant production. *Applied and Environmental Microbiology*, *76*(16), 5363–5372. https://doi.org/10.1128/AEM.00592-10

Campos, J. M., Montenegro Stamford, T. L., Sarubbo, L. A., de Luna, J. M., Rufino, R. D., & Banat, I. M. (2013). Microbial biosurfactants as additives for food industries. *Biotechnology Progress*, *29*(5), 1097–1108. https://doi.org/10.1002/btpr.1796

Castellane, T. C. L., Campanharo, J. C., Colnago, L. A., Coutinho, I. D., Lopes, É. M., Lemos, M. V. F., & de Macedo Lemos, E. G. (2017). Characterization of new exopolysaccharide production by Rhizobium tropici during growth on hydrocarbon substrate. *International Journal of Biological Macromolecules*, *96*, 361–369. https://doi.org/10.1016/j.ijbiomac.2016.11.123

Chakrabarti, S. (2012). *Bacterial biosurfactant: characterization, antimicrobial and metal remediation properties* [National Institute of Technology Rourkela]. http://ethesis.nitrkl.ac.in/3113/1/Sneha_thesis-_full.pdf

Chandankere, R., Yao, J., Cai, M., Masakorala, K., Jain, A. K., & Choi, M. M. F. (2014). Properties and characterization of biosurfactant in crude oil biodegradation by bacterium Bacillus methylotrophicus USTBa. *Fuel*, *122*, 140–148. https://doi.org/10.1016/J.FUEL.2014.01.023

Chandran, P. (2010). Biosurfactant production and diesel oil degradation by yeast species trichosporon asahii isolated from petroleum hydrocarbon contaminated soil. *International Journal of Engineering Science and Technology*, *2*(12), 6942–6953.

Chang, C.-H., & Franses, E. I. (1995). Adsorption dynamics of surfactants at the air/water interface: a critical review of mathematical models, data, and mechanisms. *Colloids and Surfaces A:*

Physicochemical and Engineering Aspects, *100*, 1–45. https://doi.org/10.1016/0927-7757(94)03061-4

Chen, C., Sun, N., Li, D., Long, S., Tang, X., Xiao, G., & Wang, L. (2018). Optimization and characterization of biosurfactant production from kitchen waste oil using Pseudomonas aeruginosa. *Environmental Science and Pollution Research*, *25*, 14934–14943. https://doi.org/10.1007/s11356-018-1691-1

Chen, H. L., Lucas, L. R., Nogaret, L. A. D., Yang, H. D., & Kenyon, D. E. (2000). Laboratory monitoring of surfactant imbibition using computerized tomography. *Proceedings of the 2000 SPE International Petroleum Conference and Exhibition in Mexico*, *February*, 271–284. https://doi.org/10.2118/59006-MS

Chen, W. C., Juang, R. S., & Wei, Y. H. (2015). Applications of a lipopeptide biosurfactant, surfactin, produced by microorganisms. *Biochemical Engineering Journal*, *103*, 158–169. https://doi.org/10.1016/j.bej.2015.07.009

Chhabra, R. P. (2010). *Non-Newtonian Fluids: An Introduction* (Lecture Notes). http://www.physics.iitm.ac.in/~compflu/Lect-notes/chhabra.pdf

Chong, H., & Li, Q. (2017). Microbial production of rhamnolipids: Opportunities, challenges and strategies. *Microbial Cell Factories*, *16*(137), 1–12. https://doi.org/10.1186/s12934-017-0753-2

Cirigliano, M. C., & Carman, G. M. (1985). Purification and characterization of liposan, a bioemulsifier from Candida lipolytica. *Applied and Environmental Microbiology*, *50*(4), 846–850.

Coates, J. (2006). Interpretation of Infrared Spectra, A Practical Approach. In R.A. Meyers & M.L. McKelvy (Eds.), *Encyclopedia of Analytical Chemistry* (pp. 1–23). John Wiley and Sons Ltd. https://doi.org/10.1002/9780470027318.a5606

Cooper, D. G., & Paddock, D. A. (1984). Production of a biosurfactant from Torulopsis bombicola. *Applied and Environmental Microbiology*, *47*(1), 173–176. http://aem.asm.org/cgi/content/short/47/1/173

Cruz, J. M., Hughes, C., Quilty, B., Montagnolli, R. N., & Bidoia, E. D. (2018). Agricultural feedstock supplemented with manganese for biosurfactant production by bacillus subtilis. *Waste and Biomass Valorization*, *9*(4), 613–618. https://doi.org/10.1007/s12649-017-0019-6

Crystallography365. (2014). *Fire ice – the structure of methane hydrate I.* https://crystallography365.wordpress.com/2014/01/18/fire-ice-the-structure-of-methane-hydrate-i/

Cunha, C. D., Do Rosário, M., Rosado, A. S., & Leite, S. G. F. (2004). Serratia sp. SVGG16: A promising biosurfactant producer isolated from tropical soil during growth with ethanol-blended gasoline. *Process Biochemistry*, *39*(12), 2277–2282. https://doi.org/10.1016/j.procbio.2003.11.027

Dadrasnia, A., & Ismail, S. (2015). Biosurfactant production by Bacillus salmalaya for lubricating oil solubilization and biodegradation. *International Journal of Environmental Research and Public Health*, *12*(8), 9848–9863. https://doi.org/10.3390/ijerph120809848

Daniel-David, D., Guerton, F., Dicharry, C., Torré, J. P., & Broseta, D. (2015). Hydrate growth at the interface between water and pure or mixed CO2/CH4 gases: Influence of pressure, temperature, gas composition and water-soluble surfactants. *Chemical Engineering Science*, *132*, 118–127. https://doi.org/10.1016/j.ces.2015.04.015

Daraboina, N., Pachitsas, S., & Von Solms, N. (2015). Natural gas hydrate formation and inhibition in gas/crude oil/aqueous systems. *Fuel*, *148*, 186–190. https://doi.org/10.1016/j.fuel.2015.01.103

Dardir, M. M., Mohamed, D. E., Farag, A. B., Ramdan, A. M., & Fayad, M. M. (2017). Preparation and evaluation of cationic bolaform surfactants for water-based drilling fluids. *Egyptian Journal of Petroleum*, *26*(1), 67–77. https://doi.org/10.1016/j.ejpe.2016.01.001

Das, A. J., & Kumar, R. (2018). Utilization of agro-industrial waste for biosurfactant production under submerged fermentation and its application in oil recovery from sand matrix. *Bioresource Technology*, *260*(December 2017), 233–240. https://doi.org/10.1016/j.biortech.2018.03.093

Das, P., Mukherjee, S., & Sen, R. (2008). Genetic regulations of the biosynthesis of microbial surfactants: An overview. *Biotechnology and Genetic Engineering Reviews*, *25*(1), 165–186. https://doi.org/10.5661/bger-25-165

Daverey, A., & Pakshirajan, K. (2010). Sophorolipids from Candida bombicola using mixed hydrophilic substrates: Production, purification and characterization. *Colloids and Surfaces B: Biointerfaces*, *79*(1), 246–253. https://doi.org/10.1016/j.colsurfb.2010.04.002

Davis, D. A., Lynch, H. C., & Varley, J. (1999). The production of Surfactin in batch culture by Bacillus subtilis ATCC 21332 is strongly influenced by the conditions of nitrogen metabolism. *Enzyme and Microbial Technology*, *25*(3–5), 322–329. https://doi.org/10.1016/S0141-

0229(99)00048-4

de Araujo, L. L. G. C., Sodré, L. G. P., Brasil, L. R., Domingos, D. F., de Oliveira, V. M., & da Cruz, G. F. (2019). Microbial enhanced oil recovery using a biosurfactant produced by Bacillus safensis isolated from mangrove microbiota - Part I biosurfactant characterization and oil displacement test. *Journal of Petroleum Science and Engineering*, *180*, 950–957. https://doi.org/10.1016/J.PETROL.2019.06.031

De Franc¸a, Í. W. L., Lima, A. P., Lemos, J. A. M., Lemos, C. G. F., Melo, V. M. M., De Sant'ana, H. B., & Gonc¸alves, L. R. B. (2015). Production of a biosurfactant by Bacillus subtilis ICA56 aiming bioremediation of impacted soils. *Catalysis Today*, *255*, 10–15. https://doi.org/10.1016/j.cattod.2015.01.046

de Oliveira, J. M., Amaral, S. A., & Burkert, C. A. V. (2018). Rheological, textural and emulsifying properties of an exopolysaccharide produced by Mesorhizobium loti grown on a crude glycerol-based medium. *International Journal of Biological Macromolecules*. https://doi.org/10.1016/j.ijbiomac.2018.06.158

Derguine-Mecheri, L., Kebbouche-Gana, S., Khemili-Talbi, S., & Djenane, D. (2017). Screening and biosurfactant/bioemulsifier production from a high-salt-tolerant halophilic Cryptococcus strain YLF isolated from crude oil. *Journal of Petroleum Science and Engineering*, *162*, 712–724. https://doi.org/10.1016/j.petrol.2017.10.088

Desai, J. T., & Banat, I. M. (1997). Microbial production of surfactants and their commercial potential. *Microbiology and Molecular Biology Reviews*, *61*(1), 47–64. https://doi.org/10.1016/S0140-6701(97)84559-6

Diab, A., & Din, D. E. (2013). Application of the biosurfactants produced by Bacillus spp. (SH 20 and SH 26. *African Journal of Environmentakl Science and Technology*, *7*(7), 671–679. https://doi.org/10.5897/AJEST2013.1451

Domínguez, A., Fernández, A., Gonzalez, N., Iglesias, E., & Montenegro, L. (1997). Determination of critical micelle concentration of some surfactants by three techniques. *Journal of Chemical Education*, *74*(10), 1227–1231. https://doi.org/10.1021/ed074p1227

Drelich, J., Fang, C., & White, L. (2006). Measurement of interfacial tension in fluid-fluid systems. In *Encyclopedia of Surface and Colloid Science* (2nd ed.). CRC Press.

Drew, M. (2006). *Surfactant Science and Technology* (3rd ed.). John Wiley and Sons.

Erfani, A., & Varaminian, F. (2017). Experimental investigation on structure H hydrates formation kinetics: Effects of surfactants on interfacial tension. *Journal of Molecular Liquids*, *225*, 636–644. https://doi.org/10.1016/J.MOLLIQ.2016.11.043

Fan, L., Li, H., Niu, Y., & Chen, Q. (2016). Characterization and inducing melanoma cell apoptosis activity of mannosylerythritol lipids-A produced from pseudozyma aphidis. *PLoS ONE*, *11*(2), 1–17. https://doi.org/10.1371/journal.pone.0148198

Felse, P. A., Shah, V., Chan, J., Rao, K. J., & Gross, R. A. (2007). Sophorolipid biosynthesis by Candida bombicola from industrial fatty acid residues. *Enzyme and Microbial Technology*, *40*(2), 316–323. https://doi.org/10.1016/j.enzmictec.2006.04.013

Ferhat, S., Alouaoui, R., Badis, A., & Moulai-Mostefa, N. (2017). Production and characterization of biosurfactant by free and immobilized cells from Ochrobactrum intermedium isolated from the soil of southern Algeria with a view to environmental application. *Biotechnology and Biotechnological Equipment*, *31*(4), 733–742. https://doi.org/10.1080/13102818.2017.1309992

Fernandes, P. L., Rodrigues, E. M., Paiva, F. R., Ayupe, B. A. L., McInerney, M. J., & Tótola, M. R. (2016). Biosurfactant, solvents and polymer production by Bacillus subtilis RI4914 and their application for enhanced oil recovery. *Fuel*, *180*, 551–557. https://doi.org/10.1016/j.fuel.2016.04.080

Finnerty, W. R. (1991). Microbial conversion of hydrocarbons products: commercial perspectives. In A. M. Martin (Ed.), *Bioconversion of Waste Materials to Industrial Products*. Elsevier.

Firouzi, M., & Nguyen, A. V. (2014). Effects of monovalent anions and cations on drainage and lifetime of foam films at different interface approach speeds. *Advanced Powder Technology*, *25*(4), 1212–1219. https://doi.org/10.1016/J.APT.2014.06.004

fisherscientific. (2018). *Sodium chloride, 99.5%, for analysis, ACROS Organics*. https://www.fishersci.co.uk/shop/products/sodium-chloride-99-5-analysis-acros-organics-3/10092740#tab3

Fleming, P. J. S., Tracey, J. P., & Melville, G. J. (2004). Estimating the abundance of feral goats in mountainous terrain: a survival-modified population estimator using the robust design and ancillary data. *Canadian Journal of Physics*, *81*(1–2), 1–44. https://doi.org/10.1139/p03-001

Flinnscientific. (2016). *Acidic, Basic and neutral Salts*. Publication No. 91832. https://www.flinnsci.com/api/library/Download/1f87f104ec4b4492a621f480797fbab1

Fracchia, L., Ceresa, C., & Banat, I. M. (2019). Biosurfactants in Cosmetic, Biomedical and Pharmaceutical Industry. In I. M. Banat & R. Thavasi (Eds.), *Microbial Biosurfactants and their Environmental and Industrial Applications* (1st ed.). CRC Press. https://doi.org/https://doi.org/10.1201/b21950

Franck, A. J. (2004). *Understanding Rheology of Structured Fluids*. TA Instruments. http://www.tainstruments.com/pdf/literature/AAN016_V1_U_StructFluids.pdf.

Franzetti, A., Caredda, P., La Colla, P., Pintus, M., Tamburini, E., Papacchini, M., & Bestetti, G. (2009). Cultural factors affecting biosurfactant production by Gordonia sp. BS29. *International Biodeterioration and Biodegradation*, *63*(7), 943–947. https://doi.org/10.1016/j.ibiod.2009.06.001

Frigaard, I. A., Paso, K. G., & de Souza Mendes, P. R. (2017). Bingham's model in the oil and gas industry. *Rheologica Acta*, *56*(3), 259–282. https://doi.org/10.1007/s00397-017-0999-y

From, C., Hormazabal, V., Hardy, S. P., & Granum, P. E. (2007). Cytotoxicity in Bacillus mojavensis is abolished following loss of surfactin synthesis: Implications for assessment of toxicity and food poisoning potential. *International Journal of Food Microbiology*, *117*(1), 43–49. https://doi.org/10.1016/j.ijfoodmicro.2007.01.013

Gargouri, B., Contreras, M. del M., Ammar, S., Segura-Carretero, A., & Bouaziz, M. (2017). Biosurfactant production by the crude oil degrading Stenotrophomonas sp. B-2: chemical characterization, biological activities and environmental applications. *Environmental Science and Pollution Research*, *24*(4), 3769–3779. https://doi.org/10.1007/s11356-016-8064-4

Gautam, K. K., & Tyagi, V. K. (2006). Microbial surfactants: A Review. *Journal of Oleo Science*, *55*(4), 155–166. https://doi.org/10.5650/jos.55.155

Gbadamosi, A. O., Junin, R., Manan, M. A., Agi, A., & Yusuff, A. S. (2019). An overview of chemical enhanced oil recovery: recent advances and prospects. In *International Nano Letters* (Vol. 9, Issue 3). Springer Berlin Heidelberg. https://doi.org/10.1007/s40089-019-0272-8

Geetha, S. J., Banat, I. M., & Joshi, S. J. (2018a). Biosurfactants: Production and potential applications in microbial enhanced oil recovery (MEOR). *Biocatalysis and Agricultural Biotechnology*, *14*(December 2017), 23–32. https://doi.org/10.1016/j.bcab.2018.01.010

Geetha, S. J., Banat, I. M., & Joshi, S. J. (2018b). Biosurfactants: Production and potential applications in microbial enhanced oil recovery (MEOR). In *Biocatalysis and Agricultural Biotechnology* (Vol. 14, pp. 23–32). Elsevier. https://doi.org/10.1016/j.bcab.2018.01.010

Geissler, M., Heravi, K. M., Henkel, M., & Hausmann, R. (2019). Lipopeptide biosurfactants from bacillus species. *Biobased Surfactants*, 205–240. https://doi.org/10.1016/B978-0-12-812705-6.00006-X

Giavarini, C., & Hester, K. (2011). The structure and formation of gas hydrates. In Springer (Ed.), *Gas Hydrates: Immense Energy Potential and Environmental Challenges* (pp. 23–47).

Gomes, M. B., Gonzales-Limache, E. E., Sousa, S. T. P., Dellagnezze, B. M., Sartoratto, A., Silva, L. C. F., Gieg, L. M., Valoni, E., Souza, R. S., Torres, A. P. R., Sousa, M. P., De Paula, S. O., Silva, C. C., & Oliveira, V. M. (2018). Exploring the potential of halophilic bacteria from oil terminal environments for biosurfactant production and hydrocarbon degradation under high-salinity conditions. *International Biodeterioration and Biodegradation*, *126*, 231–242. https://doi.org/10.1016/j.ibiod.2016.08.014

Gregorich, E. G., Gillespie, A. W., Beare, M. H., Curtin, D., Sanei, H., & Yanni, S. F. (2015). Evaluating biodegradability of soil organic matter by its thermal stability and chemical composition. *Soil Biology and Biochemistry*, *91*, 182–191. https://doi.org/10.1016/j.soilbio.2015.08.032

Gudiña, E. J., Fernandes, E. C., Rodrigues, A. I., Teixeira, J. A., & Rodrigues, L. R. (2015). Biosurfactant production by Bacillus subtilis using corn steep liquor as culture medium. *Frontiers in Microbiology*, *6*(59), 1–7. https://doi.org/10.3389/fmicb.2015.00059

Gudiña, E. J., Rodrigues, A. I., Alves, E., Domingues, M. R., Teixeira, J. A., & Rodrigues, L. R. (2015). Bioconversion of agro-industrial by-products in rhamnolipids toward applications in enhanced oil recovery and bioremediation. *Bioresource Technology*, *177*, 87–93. https://doi.org/10.1016/j.biortech.2014.11.069

Guerra-Santos, L. H., Käppeli, O., & Fiechter, A. (1986). Dependence of Pseudomonas aeruginosa continous culture biosurfactant production on nutritional and environmental factors. *Applied Microbiology and Biotechnology*, *24*(6), 443–448. https://doi.org/10.1007/BF00250320

Gupta, S., Helmig, R., & Wohlmuth, B. (2015). Non-isothermal, multi-phase, multi-component flows through deformable methane hydrate reservoirs. *Computational Geosciences*, *19*(5), 1063–

1088. https://doi.org/10.1007/s10596-015-9520-9

Hadia, N. J., Ottenheim, C., Li, S., Hua, N. Q., Stubbs, L. P., & Lau, H. C. (2019). Experimental investigation of biosurfactant mixtures of surfactin produced by Bacillus Subtilis for EOR application. *Fuel*, *251*, 789–799. https://doi.org/10.1016/J.FUEL.2019.03.111

Hammerschmidt, E. G. (1934). Formation of Gas Hydrates in Natural Gas Transmission Lines. *Industrial and Engineering Chemistry*, *26*(8), 851–855. https://doi.org/10.1021/ie50296a010

Haq, B., Liu, J., Liu, K., & Al Shehri, D. (2019). The role of biodegradable surfactant in microbial enhanced oil recovery. *Journal of Petroleum Science and Engineering*, 106688. https://doi.org/10.1016/J.PETROL.2019.106688

Hayama, H., Fukuzawa, K., Yasuda, K., & Ohmura, R. (2017). Interfacial tension between (methane + ethane + propane) gas mixture and water from 283.2 K to 298.2 K under up to 10 MPa. *The Journal of Chemical Thermodynamics*, *108*, 71–75. https://doi.org/10.1016/j.jct.2017.01.007

Helfrich, M., Ludwig, B., Thoms, C., Gleixner, G., & Flessa, H. (2015). The role of soil fungi and bacteria in plant litter decomposition and macroaggregate formation determined using phospholipid fatty acids. *Applied Soil Ecology*, *96*, 261–264. https://doi.org/10.1016/j.apsoil.2015.08.023

Hema, T., Seghal Kiran, G., Sajayyan, A., Ravendran, A., Gowtham Raj, G., & Selvin, J. (2019). Response surface optimization of a glycolipid biosurfactant produced by a sponge associated marine bacterium Planococcus sp. MMD26. *Biocatalysis and Agricultural Biotechnology*, *18*, 101071. https://doi.org/10.1016/J.BCAB.2019.101071

Heryani, H., & Putra, M. D. (2017). Kinetic study and modeling of biosurfactant production using Bacillus sp. *Electronic Journal of Biotechnology*, *27*, 49–54. https://doi.org/10.1016/j.ejbt.2017.03.005

Hirata, Y., Ryu, M., Oda, Y., Igarashi, K., Nagatsuka, A., Furuta, T., & Sugiura, M. (2009). Novel characteristics of sophorolipids, yeast glycolipid biosurfactants, as biodegradable low-foaming surfactants. *Journal of Bioscience and Bioengineering*, *108*(2), 142–146. https://doi.org/10.1016/j.jbiosc.2009.03.012

Hosseini, H., Apourvari, S. N., & Schaffie, M. (2019). Wettability alteration of carbonate rocks via magnetic fields application. *Journal of Petroleum Science and Engineering*, *172*, 280–287. https://doi.org/10.1016/J.PETROL.2018.08.022

Hou, G., Liang, D., & Li, X. (2018). Experimental study on hydrate anti-agglomeration in the presence of rhamnolipid. *RSC Advances*, *8*(69), 39511–39519. https://doi.org/10.1039/c8ra07215a

Hrůzová, K., Patel, A., Masák, J., Maťátková, O., Rova, U., Christakopoulos, P., & Matsakas, L. (2019). A novel approach for the production of green biosurfactant from Pseudomonas aeruginosa using renewable forest biomass. *Science of The Total Environment*, 135099. https://doi.org/10.1016/J.SCITOTENV.2019.135099

Hussien, S. O., Elraies, K. A., Almansour, A., Husin, H., Belhaj, A., & Ern, L. (2019). Experimental study on the use of surfactant as a fracking fluid additive for improving shale gas productivity. *Journal of Petroleum Science and Engineering*, *183*, 106426. https://doi.org/10.1016/J.PETROL.2019.106426

Ilori, M. O., Amobi, C. J., & Odocha, A. C. (2005). Factors affecting biosurfactant production by oil degrading Aeromonas spp. isolated from a tropical environment. *Chemosphere*, *61*(7), 985–992. https://doi.org/10.1016/j.chemosphere.2005.03.066

Inès, M., & Dhouha, G. (2015). Lipopeptide surfactants: Production, recovery and pore forming capacity. *Peptides*, *71*, 100–112. https://doi.org/10.1016/j.peptides.2015.07.006

Innemanová, P., Filipová, A., Michalíková, K., Wimmerová, L., & Cajthaml, T. (2018). Bioaugmentation of PAH-contaminated soils: A novel procedure for introduction of bacterial degraders into contaminated soil. *Ecological Engineering*, *118*(January), 93–96. https://doi.org/10.1016/j.ecoleng.2018.04.014

Irawan, S., Permatasari, K. A., & Bayuaji, R. (2017). Effect of density and resistivity measurement for foam flooding propagation in static condition. *IOP Conference Series: Materials Science and Engineering*, *267*(1), 1–8. https://doi.org/10.1088/1757-899X/267/1/012031

Jadhav, M., Kalme, S., Tamboli, D., & Govindwar, S. (2011). Rhamnolipid from Pseudomonas desmolyticum NCIM-2112 and its role in the degradation of Brown 3REL. *Journal of Basic Microbiology*, *51*(4), 385–396. https://doi.org/10.1002/jobm.201000364

Jadhav, J. V., Pratap, A. P., & Kale, S. B. (2019). Evaluation of sunflower oil refinery waste as feedstock for production of sophorolipid. *Process Biochemistry*, *78*, 15–24. https://doi.org/10.1016/J.PROCBIO.2019.01.015

Jahanbani Veshareh, M., Ganji Azad, E., Deihimi, T., Niazi, A., & Ayatollahi, S. (2018). Isolation

and screening of Bacillus subtilis MJ01 for MEOR application: biosurfactant characterization, production optimization and wetting effect on carbonate surfaces. *Journal of Petroleum Exploration and Production Technology*, *Nielsen 2010*, 1–13. https://doi.org/10.1007/s13202-018-0457-0

Jain, R. M., Mody, K., Mishra, A., & Jha, B. (2012). Isolation and structural characterization of biosurfactant produced by an alkaliphilic bacterium Cronobacter sakazakii isolated from oil contaminated wastewater. *Carbohydrate Polymers*, *87*(3), 2320–2326. https://doi.org/10.1016/j.carbpol.2011.10.065

Jia, H., Lian, P., Leng, X., Han, Y., Wang, Q., Jia, K., Niu, X., Guo, M., Yan, H., & Lv, K. (2019). Mechanism studies on the application of the mixed cationic/anionic surfactant systems to enhance oil recovery. *Fuel*, *258*, 116156. https://doi.org/10.1016/J.FUEL.2019.116156

Joshi, S., Bharucha, C., & Desai, A. J. (2008). Production of biosurfactant and antifungal compound by fermented food isolate Bacillus subtilis 20B. *Bioresource Technology*, *99*(11), 4603–4608. https://doi.org/10.1016/j.biortech.2007.07.030

Joshi, S. J., Al-Wahaibi, Y. M., Al-Bahry, S. N., Elshafie, A. E., Al-Bemani, A. S., Al-Bahri, A., & Al-Mandhari, M. S. (2016). Production, characterization, and application of bacillus licheniformis W16 biosurfactant in enhancing oil recovery. *Frontiers in Microbiology*, *7*(NOV), 1–14. https://doi.org/10.3389/fmicb.2016.01853

Jovic, S., Guresic, D., Babincev, L., Draskovic, N., & Dekic, V. (2019). Comparative efficacy of machine-learning models in prediction of reducing uncertainties in biosurfactant production. *Bioprocess and Biosystems Engineering*, *42*(10), 1695–1699. https://doi.org/10.1007/s00449-019-02165-y

Joy, S., Khare, S. K., & Sharma, S. (2019). Synergistic extraction using sweep-floc coagulation and acidification of rhamnolipid produced from industrial lignocellulosic hydrolysate in a bioreactor using sequential (fill-and-draw) approach. *Process Biochemistry*. https://doi.org/10.1016/J.PROCBIO.2019.11.014

Kamal, M. S. (2016). A Review of Gemini Surfactants: Potential Application in Enhanced Oil Recovery. In *Journal of Surfactants and Detergents* (Vol. 19, Issue 2, pp. 223–236). https://doi.org/10.1007/s11743-015-1776-5

Kandasamy, R., Rajasekaran, Muneeswari Venkatesan, S. K., & Uddin, M. (2019). New Trends in

the Biomanufacturing of Green Surfactants: Biobased Surfactants and Biosurfactants. In N. K. Rathinam & R. K. Sani (Eds.), *Next Generation Biomanufacturing Technologies* (ACS sympos, pp. 243–260). ACS Publications. https://doi.org/10.1021/bk-2019-1329

Kaneka. (2017). *Biosurfactant made by fermentation technology of KANEKA*. Kaneka Surfactin. http://www.kaneka.co.jp/en/branch/nb_development/surfactin_catalogue_eng.pdf

Kanmani, P., DivyaSri, E., Rajakarvizhi, R., Senthamil, O. S., Sivasankari, V., & Aravind, J. (2017). Optimization of Biosurfactant Production and Crude Oil Emulsification by Bacillus Sp. Isolated from Hydrocarbon Contaminated Soil Sample. In M. Prashanthi, R. Sundaram, A. Jeyaseelan, & T. Kaliannan (Eds.), *Bioremediation and Sustainable Technologies for Cleaner Environment* (Environmen, pp. 305–316). Springer International Publishing. https://doi.org/10.1007/978-3-319-48439-6

Karanth, N. G. K., Deo, P. G., & Veenanadig, N. K. (1999). Microbial production of biosurfactants and their importance. *Current Science*, *77*(1), 116–126.

Karlapudi, A. P., Venkateswarulu, T. C., Tammineedi, J., Kanumuri, L., Ravuru, B. K., Dirisala, V. ramu, & Kodali, V. P. (2018). Role of biosurfactants in bioremediation of oil pollution-a review. *Petroleum*, *4*(3), 241–249. https://doi.org/10.1016/j.petlm.2018.03.007

Katsir, Y., Goldstein, G., & Marmur, A. (2015). Bubble the wave or waive the bubble: Why seawater waves foam and freshwater waves do not? *Colloids and Interface Science Communications*, *6*, 9–12. https://doi.org/10.1016/J.COLCOM.2015.10.002

Kelland, M. A. (2006). History of the development of low dosage hydrate inhibitors. *Energy and Fuels*, *20*(3), 825–847. https://doi.org/10.1021/ef050427x

Khattab, I. S., Bandarkar, F., Khoubnasabjafari, M., & Jouyban, A. (2017). Density, viscosity, surface tension, and molar volume of propylene glycol + water mixtures from 293 to 323 K and correlations by the Jouyban–Acree model. *Arabian Journal of Chemistry*, *10*, S71–S75. https://doi.org/10.1016/j.arabjc.2012.07.012

Kim, H. S., Yoon, B. D., Choung, D. H., Oh, H. M., Katsuragi, T., & Tani, Y. (1999). Characterization of a biosurfactant, mannosylerythritol lipid produced from Candida sp. SY16. *Applied Microbiology and Biotechnology*, *52*(5), 713–721. https://doi.org/10.1007/s002530051583

Kim, H., Veluswamy, H. P., Seo, Y., & Linga, P. (2018). Morphology Study on the Effect of

Thermodynamic Inhibitors during Methane Hydrate Formation in the Presence of NaCl. *Crystal Growth and Design*, *18*(11), 6984–6994. https://doi.org/10.1021/acs.cgd.8b01161

Kim, J., & Vipulanandan, P. (2006). Removal of Lead from Contaminated Water and Clay Soil Using a Biosurfactant. *Journal of Environmental Engineering*, *132*(7), 694–697. https://doi.org/10.1061/(ASCE)0733-9372(2006)132

Kiran, G. S., Hema, T. A., Gandhimathi, R., Selvin, J., Thomas, T. A., Rajeetha Ravji, T., & Natarajaseenivasan, K. (2009). Optimization and production of a biosurfactant from the sponge-associated marine fungus Aspergillus ustus MSF3. *Colloids and Surfaces B: Biointerfaces*, *73*(2), 250–256. https://doi.org/10.1016/j.colsurfb.2009.05.025

Klosowska-Chomiczewsca, I. E., Medrrzycka, K., & Karpenko, E. (2009). *Biosurfactants-Biodegradability, Toxicity , Efficiency in Comparison with Synthetic Surfactants.* https://www.seed.abe.kth.se/polopoly_fs/1.651088!/JPSU17P16.pdf

Knoblich, A., Matsumoto, M., Ishiguro, R., Murata, K., Fujiyoshi, Y., Ishigami, Y., & Osman, M. (1995). Electron cryo-microscopic studies on micellar shape and size of surfactin, an anionic lipopeptide. *Colloids and Surfaces B: Biointerfaces*, *5*(1–2), 43–48. https://doi.org/10.1016/0927-7765(95)01207-Y

Kodera, M., Watanabe, K., Lassiège, M., Alavi, S., & Ohmura, R. (2020). Interfacial tension between decane saturated with methane and water from 283.2 K to 298.2 K under pressures upto 10 MPa. *Journal of Industrial and Engineering Chemistry*, *81*, 360–366. https://doi.org/10.1016/J.JIEC.2019.09.026

Koh, C. A., Westacott, R. E., Zhang, W., Hirachand, K., Creek, J. L., & Soper, A. K. (2002). Mechanisms of gas hydrate formation and inhibition. *Fluid Phase Equilibria*, *194–197*, 143–151. https://doi.org/10.1016/S0378-3812(01)00660-4

Koh, Carolyn A., Sloan, E. D., Sum, A. K., & Wu, D. T. (2011). Fundamentals and Applications of Gas Hydrates. *Annual Review of Chemical and Biomolecular Engineering*, *2*(1), 237–257. https://doi.org/10.1146/annurev-chembioeng-061010-114152

Konishi, M., Fukuoka, T., Morita, T., Imura, T., & Kitamoto, D. (2008). Production of new types of sophorolipids by Candida batistae. *Journal of Oleo Science*, *57*(6), 359–369. https://doi.org/10.5650/jos.57.359

Korathar, S. (2018). *Structure of Phospholipids (With Diagram): Lipid Metabolism*. Biology Discussion. http://www.biologydiscussion.com/plants/lipid-metabolism/structure-of-phospholipids-with-diagram-lipid-metabolism/23196

Krister, H., Bo, J., Bengt, K., & Bjorn, L. (2003). *Surfactants and polymers in aqueous solution* (2nd ed.). John Wiley & Sons ltd.

Kronberg, B., Holmberg, K., & Lindman, B. (2014a). An Introduction to the Rheology of Polymer and Surfactant Solutions. In *Surface Chemistry of Surfactants and Polymers* (pp. 361–376). John Wiley & Sons ltd. https://doi.org/10.1002/9781118695968.ch19

Kronberg, B., Holmberg, K., & Lindman, B. (2014b). Surface and Interfacial Tension. In *Surface Chemistry of Surfactants and Polymers* (1st ed., pp. 231–249). John Wiley & Sons Ltd.

Kruijt, M., Tran, H., & Raaijmakers, J. M. (2009). Functional, genetic and chemical characterization of biosurfactants produced by plant growth-promoting Pseudomonas putida 267. *Journal of Applied Microbiology*, *107*(2), 546–556. https://doi.org/10.1111/j.1365-2672.2009.04244.x

Kubicki, S., Bollinger, A., Katzke, N., Jaeger, K. E., Loeschcke, A., & Thies, S. (2019). Marine biosurfactants: biosynthesis, structural diversity and biotechnological applications. *Marine Drugs*, *17*(7), 1–30. https://doi.org/10.3390/md17070408

Kukade, S. D., & Bawankar, S. V. (2018). Effect of Temperature on Electrical Conductivity of Guaiacol-Guanidine Hydrochloride-Formaldehyde Copolymer Resin. *Journal of Electronic Materials*, *47*(5), 2905–2910. https://doi.org/10.1007/s11664-018-6136-6

Kumaran, V. S. (2010). *Fundamentals of Rheology* (Lecture Notes). http://www.physics.iitm.ac.in/~compflu/Lect-notes/kumaran.pdf

Lee, C. H., Yang, H. E., Bae, Y. C., & Oh, J. S. (2018). Phase equilibria and the surface tension of polypropylene polyol series in water/methanol mixtures: A consideration of structural effects. *Polymer*, *146*, 169–178. https://doi.org/10.1016/j.polymer.2018.05.035

Lee, W., Choi, Y., Kim, Y., Lim, J.-S., & Kang, S.-P. (2019). Rheological investigation of methane hydrate formation with biodegradable emulsifiers as anti-agglomerants. *Journal of Petroleum Science and Engineering*, *183*, 106454. https://doi.org/10.1016/J.PETROL.2019.106454

Li, Y., Zou, A. H., Ye, R. Q., & Mu, B. Z. (2009). Counterion-induced changes to the micellization

of surfactin-C16 aqueous solution. *Journal of Physical Chemistry B*, *113*(46), 15272–15277. https://doi.org/10.1021/jp9062862

Light, T. S., Licht, S., Bevilacqua, A. C., & Morash, K. R. (2005). The Fundamental Conductivity and Resistivity of Water. *Electrochemical and Solid-State Letters*, *8*(1), E16–E19. https://doi.org/10.1149/1.1836121

Lima, T. M. S., Procópio, L. C., Brandão, F. D., Carvalho, A. M. X., Tótola, M. R., & Borges, A. C. (2011). Biodegradability of bacterial surfactants. *Biodegradation*, *22*(3), 585–592. https://doi.org/10.1007/s10532-010-9431-3

Linga, P., Kumar, R., & Englezos, P. (2007). Gas hydrate formation from hydrogen/carbon dioxide and nitrogen/carbon dioxide gas mixtures. *Chemical Engineering Science*, *62*(16), 4268–4276. https://doi.org/10.1016/j.ces.2007.04.033

Liu, B., Liu, J., Ju, M., Li, X., & Yu, Q. (2016a). Purification and characterization of biosurfactant produced by Bacillus licheniformis Y-1 and its application in remediation of petroleum contaminated soil. *Marine Pollution Bulletin*, *107*(1), 46–51. https://doi.org/10.1016/j.marpolbul.2016.04.025

Liu, B., Liu, J., Ju, M., Li, X., & Yu, Q. (2016b). Purification and characterization of biosurfactant produced by Bacillus licheniformis Y-1 and its application in remediation of petroleum contaminated soil. *Marine Pollution Bulletin*, *107*(1), 46–51. https://doi.org/10.1016/j.marpolbul.2016.04.025

Liu, J. F., Mbadinga, S. M., Yang, S. Z., Gu, J. D., & Mu, B. Z. (2015). Chemical structure, property and potential applications of biosurfactants produced by Bacillus subtilis in petroleum recovery and spill mitigation. *International Journal of Molecular Sciences*, *16*(3), 4814–4837. https://doi.org/10.3390/ijms16034814

Liu, Q., Lin, J., Wang, W., Huang, H., & Li, S. (2014). Production of surfactin isoforms by Bacillus subtilis BS-37 and its applicability to enhanced oil recovery under laboratory conditions. *Biochemical Engineering Journal*, *93*, 31–37. https://doi.org/10.1016/j.bej.2014.08.023

Long, X., He, N., He, Y., Jiang, J., & Wu, T. (2017). Biosurfactant surfactin with pH-regulated emulsification activity for efficient oil separation when used as emulsifier. *Bioresource Technology*, *241*, 200–206. https://doi.org/10.1016/j.biortech.2017.05.120

Lutz-Bueno, V. (2016). *Effects of formulation and flow on the structure of micellar aggregates ETH Library* [ETH Zurich]. https://doi.org/10.3929/ethz-a-010782505

Maalej, H., Hmidet, N., Boisset, C., Bayma, E., Heyraud, A., & Nasri, M. (2016). Rheological and emulsifying properties of a gel-like exopolysaccharide produced by Pseudomonas stutzeri AS22. *Food Hydrocolloids*, *52*, 634–647. https://doi.org/10.1016/j.foodhyd.2015.07.010

Machale, J., Majumder, S. K., Ghosh, P., & Sen, T. K. (2019). Development of a novel biosurfactant for enhanced oil recovery and its influence on the rheological properties of polymer. *Fuel*, *257*, 116067. https://doi.org/10.1016/J.FUEL.2019.116067

Madihalli, C., Sudhakar, H., & Doble, M. (2016). Mannosylerythritol Lipid-A as a Pour Point Depressant for Enhancing the Low-Temperature Fluidity of Biodiesel and Hydrocarbon Fuels. *Energy and Fuels*, *30*(5), 4118–4125. https://doi.org/10.1021/acs.energyfuels.6b00315

Mahmood, M., & Al-koofee, D. (2013). Effect of Temperature Changes on Critical Micelle Concentration for Tween Series Surfactant. *Global Journal of Science Frontier Research Chemistry*, *13*(4), 1–7.

Makogon, Y. F., Holditch, S. A., & Makogon, T. Y. (2007). Natural gas-hydrates - A potential energy source for the 21st Century. *Journal of Petroleum Science and Engineering*, *56*(1–3), 14–31. https://doi.org/10.1016/j.petrol.2005.10.009

Marchant, R., & Banat, I. M. (2012a). Biosurfactants: A sustainable replacement for chemical surfactants? In *Biotechnology Letters* (Vol. 34, Issue 9, pp. 1597–1605). https://doi.org/10.1007/s10529-012-0956-x

Marchant, R., & Banat, I. M. (2012b). Microbial biosurfactants: Challenges and opportunities for future exploitation. *Trends in Biotechnology*, *30*(11), 558–565. https://doi.org/10.1016/j.tibtech.2012.07.003

Marti, M. E., Colonna, W. J., Patra, P., Zhang, H., Green, C., Reznik, G., Pynn, M., Jarrell, K., Nyman, J. A., Somasundaran, P., Glatz, C. E., & Lamsal, B. P. (2014). Production and characterization of microbial biosurfactants for potential use in oil-spill remediation. *Enzyme and Microbial Technology*, *55*, 31–39. https://doi.org/10.1016/j.enzmictec.2013.12.001

Matsui, T., Namihira, T., Mitsuta, T., & Saeki, H. (2012). Removal of oil tank bottom sludge by novel biosurfactant, JE1058BS. *Journal of the Japan Petroleum Institute*, *55*(2), 138–141.

https://doi.org/10.1627/jpi.55.138

Matsuyama, T., Tanikawa, T., & Nakagawa, Y. (2011). Serrawettins and other Surfactants Produced by Serratia. In G. Soberón-Chávez (Ed.), *Biosurfactants* (pp. 33–120). Springer Berlin Heidelberg.

Maurya, N. K., & Mandal, A. (2018). Investigation of synergistic effect of nanoparticle and surfactant in macro emulsion based EOR application in oil reservoirs. *Chemical Engineering Research and Design*, *132*, 370–384. https://doi.org/10.1016/j.cherd.2018.01.049

McClements, D. J., & Gumus, C. E. (2016). Natural emulsifiers — Biosurfactants, phospholipids, biopolymers, and colloidal particles: Molecular and physicochemical basis of functional performance. *Advances in Colloid and Interface Science*, *234*, 3–26. https://doi.org/10.1016/j.cis.2016.03.002

Mechri, S., Bouacem, K., Jabeur, F., Mohamed, S., Addou, N. A., Dab, A., Bouraoui, A., Bouanane-Darenfed, A., Bejar, S., Hacène, H., Baciou, L., Lederer, F., & Jaouadi, B. (2019). Purification and biochemical characterization of a novel thermostable and halotolerant subtilisin SAPN, a serine protease from Melghiribacillus thermohalophilus Nari2AT for chitin extraction from crab and shrimp shell by-products. *Extremophiles*, *23*(5), 529–547. https://doi.org/10.1007/s00792-019-01105-8

Meena, K. R., Tandon, T., Sharma, A., & Kanwar, S. S. (2018). Lipopeptide antibiotic production by Bacillus velezensis KLP2016. *Journal of Applied Pharmaceutical Science*, *8*(3), 91–98. https://doi.org/10.7324/JAPS.2018.8313

Meindinyo, R. E. T., Svartaas, T. M., Nordbø, T. N., & Bøe, R. (2015). Gas hydrate growth estimation based on heat transfer. *Energy and Fuels*, *29*(2), 587–594. https://doi.org/10.1021/ef502366u

Mohan, P. K., Nakhla, G., & Yanful, E. K. (2006). Biokinetics of biodegradation of surfactants under aerobic, anoxic and anaerobic conditions. *Water Research*, *40*(3), 533–540. https://doi.org/10.1016/j.watres.2005.11.030

Moldes, A. B., Paradelo, R., Rubinos, D., Devesa-Rey, R., Cruz, J. M., & Barral, M. T. (2011). Ex situ treatment of hydrocarbon-contaminated soil using biosurfactants from lactobacillus pentosus. *Journal of Agricultural and Food Chemistry*, *59*(17), 9443–9447. https://doi.org/10.1021/jf201807r

Moldes, A., Paradelo, R., Vecino, X., Cruz, J. M., Gudiña, E., Rodrigues, L., Teixeira, J. A.,

Domínguez, J. M., & Barral, M. T. (2013). Partial characterization of biosurfactant from lactobacillus pentosus and comparison with sodium dodecyl sulphate for the bioremediation of hydrocarbon contaminated soil. *BioMed Research International*, 1–6. https://doi.org/10.1155/2013/961842

Mondal, S., Goswami, T., Jana, G., Misra, A., & Chattaraj, P. K. (2018). A possible reason behind the initial formation of pentagonal dodecahedron cavities in sI-methane hydrate nucleation: A DFT study. *Chemical Physics Letters*, *691*, 415–420. https://doi.org/10.1016/j.cplett.2017.11.054

Morán, M. C.; Pinazo, A.; Calpés, P.; Angelet, M.; García, M. T.; Vinardell, M. P.; Infante, M. R. (2004). "Green" amino acid-based surfactants. *Green Chem.*, *6*(5), 233–240. https://doi.org/10.1039/B400293H

Morita, T., Fukuoka, T., Imura, T., Hirose, N., & Kitamoto, D. (2012). Isolation and Screening of Glycolipid Biosurfactant Producers from Sugarcane. *Bioscience, Biotechnology, and Biochemistry*, *76*(9), 1788–1791. https://doi.org/10.1271/bbb.120251

Morita, T., Konishi, M., Fukuoka, T., Imura, T., & Kitamoto, D. (2008). Identification of Ustilago cynodontis as a new producer of glycolipid biosurfactants, mannosylerythritol lipids, based on ribosomal DNA sequences. *Journal of Oleo Science*, *57*(10), 549–556. https://doi.org/10.5650/jos.57.549

Mouafi, F. E., Abo Elsoud, M. M., & Moharam, M. E. (2016). Optimization of biosurfactant production by Bacillus brevis using response surface methodology. *Biotechnology Reports*, *9*, 31–37. https://doi.org/10.1016/j.btre.2015.12.003

Mouafo, T. H., Mbawala, A., & Ndjouenkeu, R. (2018). Effect of different carbon sources on biosurfactants' production by three Strains of Lactobacillus spp. *BioMed Research International*, *2018*, 1–15. https://doi.org/10.1155/2018/5034783

Mu, J. H., Li, G. Z., Jia, X. L., Wang, H. X., & Zhang, G. Y. (2002). Rheological properties and microstructures of anionic micellar solutions in the presence of different inorganic salts. *Journal of Physical Chemistry B*, *106*(44), 11685–11693. https://doi.org/10.1021/jp014096a

Mukerjee, P., & Mysels, K. J. (1972). Critical Micelle Concentrations of Aqueous Surfactant Systems. In *National Standard Referance Data System* (NSRDS-NBS). US National Bureau of Standards. https://doi.org/10.1002/jps.2600610254

Mukherjee, S., Das, P., & Sen, R. (2006). Towards commercial production of microbial surfactants. *Trends in Biotechnology*, *24*(11), 509–515. https://doi.org/10.1016/j.tibtech.2006.09.005

Mulligan, C. N. (2005). Environmental applications for biosurfactants. In *Environmental Pollution* (Vol. 133, Issue 2, pp. 183–198). Elsevier. https://doi.org/10.1016/j.envpol.2004.06.009

Muthusamy, K., Gopalakrishnan, S., Ravi, T. K., & Sivachidambaram, P. (2008). Biosurfactants: properties, commercial production and application. *Current Science*, *94*(6), 736–747.

Nam, H. S., Yang, H. J., Oh, B. J., Anderson, A. J., & Kim, Y. C. (2016). Biological control potential of Bacillus amyloliquefaciens KB3 isolated from the feces of Allomyrina dichotoma Larvae. *Plant Pathology Journal*, *32*(3), 273–280. https://doi.org/10.5423/PPJ.NT.12.2015.0274

Narh, C., Frimpong, C., Mensah, A., & Wei, Q. (2018). Rice Bran, an Alternative Nitrogen Source for Acetobacter xylinum Bacterial Cellulose Synthesis. *BioResources*, *13*(2), 4346–4363. https://doi.org/10.15376/biores.13.2.4346-4363

Naughton, P. J., Marchant, R., Naughton, V., & Banat, I. M. (2019). Microbial biosurfactants: current trends and applications in agricultural and biomedical industries. *Journal of Applied Microbiology*, *127*(1), 12–28. https://doi.org/10.1111/jam.14243

Naullage, P. M., Bertolazzo, A. A., & Molinero, V. (2019). How Do Surfactants Control the Agglomeration of Clathrate Hydrates? *ACS Central Science*, *5*(3), 428–439. https://doi.org/10.1021/acscentsci.8b00755

Nazhat, S. N. (2008). Thermal Analysis of Biomaterials. In G. Paul (Ed.), *Principles and Applications of Thermal Analysis* (pp. 256–285). Blackwell Publishing. https://doi.org/10.1002/9780470697702.ch7

Ndlovu, T., Khan, S., & Khan, W. (2016). Distribution and diversity of biosurfactant-producing bacteria in a wastewater treatment plant. *Environmental Science and Pollution Research*, *23*(10), 9993–10004. https://doi.org/10.1007/s11356-016-6249-5

Nguyen, M. T., & Götz, F. (2016). Lipoproteins of Gram-Positive Bacteria: Key Players in the Immune Response and Virulence. *Microbiology and Molecular Biology Reviews*, *80*(3), 891–903. https://doi.org/10.1128/MMBR.00028-16

Nguyen, N. N., Nguyen, A. V., & Dang, L. X. (2017). The inhibition of methane hydrate formation

by water alignment underneath surface adsorption of surfactants. *Fuel*, *197*, 488–496. https://doi.org/10.1016/j.fuel.2017.02.061

Nguyen, P. T., Hampton, M. A., Nguyen, A. V., & Birkett, G. R. (2012). The influence of gas velocity, salt type and concentration on transition concentration for bubble coalescence inhibition and gas holdup. *Chemical Engineering Research and Design*, *90*(1), 33–39. https://doi.org/10.1016/J.CHERD.2011.08.015

Nickzad, A., & Deziel, E. (2016). Adaptive significance of quorum sensing-dependent regulation of rhamnolipids by integration of growth rate in Burkholderia glumae: A trade-off between survival and efficiency. *Frontiers in Microbiology*, *7*(AUG), 1–8. https://doi.org/10.3389/fmicb.2016.01215

Nieminen, T., Rintaluoma, N., Andersson, M., Taimisto, A. M., Ali-Vehmas, T., Seppälä, A., Priha, O., & Salkinoja-Salonen, M. (2007). Toxinogenic Bacillus pumilus and Bacillus licheniformis from mastitic milk. *Veterinary Microbiology*, *124*(3–4), 329–339. https://doi.org/10.1016/j.vetmic.2007.05.015

Niu, Y., Wu, J., Wang, W., & Chen, Q. (2019). Production and characterization of a new glycolipid, mannosylerythritol lipid, from waste cooking oil biotransformation by Pseudozyma aphidis ZJUDM34. *Food Science and Nutrition*, *7*(3), 937–948. https://doi.org/10.1002/fsn3.880

Oliveira, F. J. S., Vazquez, L., de Campos, N. P., & de França, F. P. (2009). Production of rhamnolipids by a Pseudomonas alcaligenes strain. *Process Biochemistry*, *44*(4), 383–389. https://doi.org/10.1016/j.procbio.2008.11.014

Oni, F. E., Geudens, N., Omoboye, O. O., Bertier, L., Hua, H. G. K., Adiobo, A., Sinnaeve, D., Martins, J. C., & Höfte, M. (2019). Fluorescent Pseudomonas and cyclic lipopeptide diversity in the rhizosphere of cocoyam (Xanthosoma sagittifolium). *Environmental Microbiology*, *21*(12), 4887–4887. https://doi.org/10.1111/1462-2920.14520

Palodkar, A. V., & Jana, A. K. (2017). Formulating formation mechanism of natural gas hydrates. *Scientific Reports*, *7*(1), 1–11. https://doi.org/10.1038/s41598-017-06717-8

Paraszkiewicz, K., Bernat, P., Kuśmierska, A., Chojniak, J., & Płaza, G. (2018). Structural identification of lipopeptide biosurfactants produced by Bacillus subtilis strains grown on the media obtained from renewable natural resources. *Journal of Environmental Management*, *209*, 65–70. https://doi.org/10.1016/j.jenvman.2017.12.033

Park, T., Joo, H. W., Kim, G. Y., Kim, S., Yoon, S., & Kwon, T. H. (2017). Biosurfactant as an enhancer of geologic carbon storage: Microbial modification of interfacial tension and contact angle in carbon dioxide/water/quartz systems. *Frontiers in Microbiology*, *8*(JUL), 1–12. https://doi.org/10.3389/fmicb.2017.01285

Patricia, S. (2011a). *Energy and Ocean Currents*. Chemistry 102. http://butane.chem.uiuc.edu/pshapley/genchem1/L21/1.html

Patricia, S. (2011b). *Temperature Effects on Density*. General Chemistry 102. http://butane.chem.uiuc.edu/pshapley/GenChem1/L21/2.html

Paul, G. (2008). A Practical Introduction to Differential Scanning Calorimetry. In G. Paul (Ed.), *Principles and Applications of Thermal Analysis* (pp. 1–263). Blackwell Publishing. https://doi.org/10.1002/9780470697702

Pecci, Y., Rivardo, F., Martinotti, M. G., & Allegrone, G. (2010). LC/ESI-MS/MS characterisation of lipopeptide biosurfactants produced by the Bacillus licheniformis V9T14 strain. *Journal of Mass Spectrometry*, *45*(7), 772–778. https://doi.org/10.1002/jms.1767

Peele, K. A. (2017). *Characterization and Emulsifying Activities of a Quorum Sensing Biosurfactant Produced By a Marine Bacterium* (Issue May). Vignan's Foundation for Science, Technology and Research University.

Pereira, J. F. B., Gudiña, E. J., Costa, R., Vitorino, R., Teixeira, J. A., Coutinho, J. A. P., & Rodrigues, L. R. (2013). Optimization and characterization of biosurfactant production by Bacillus subtilis isolates towards microbial enhanced oil recovery applications. *Fuel*, *111*, 259–268. https://doi.org/10.1016/j.fuel.2013.04.040

Pérez, L., Infante, M. R., Pons, R., Morán, C., Vinardell, P., Mitjans, M., & Pinazo, A. (2004). A synthetic alternative to natural lecithins with antimicrobial properties. *Colloids and Surfaces B: Biointerfaces*, *35*(3–4), 235–242. https://doi.org/10.1016/j.colsurfb.2004.03.014

Perfumo, A., Banat, I. M., & Marchant, R. (2018). Going Green and Cold: Biosurfactants from Low-Temperature Environments to Biotechnology Applications. In *Trends in Biotechnology* (Vol. 36, Issue 3, pp. 277–289). Elsevier Current Trends. https://doi.org/10.1016/j.tibtech.2017.10.016

Pinazo, A., Pons, R., Pérez, L., & Infante, M. R. (2011). Amino acids as raw material for biocompatible surfactants. *Industrial and Engineering Chemistry Research*, *50*(9), 4805–4817.

https://doi.org/10.1021/ie1014348

Prasad, P. S. R., & Kiran, B. S. (2019). Self-preservation and Stability of Methane Hydrates in the Presence of NaCl. *Scientific Reports*, *9*(1), 1–10. https://doi.org/10.1038/s41598-019-42336-1

Purwasena, I. A., Astuti, D. I., Syukron, M., Amaniyah, M., & Sugai, Y. (2019). Stability test of biosurfactant produced by Bacillus licheniformis DS1 using experimental design and its application for MEOR. *Journal of Petroleum Science and Engineering*, *183*. https://doi.org/10.1016/j.petrol.2019.106383

Qin, H.-B., Sun, C.-Y., Sun, Z.-F., Liu, B., & Chen, G.-J. (2016). Relationship between the interfacial tension and inhibition performance of hydrate inhibitors. *Chemical Engineering Science*, *148*, 182–189. https://doi.org/10.1016/J.CES.2016.04.002

Qin, H. B., Zhang, Z. Y., Sun, C. Y., Chen, G. J., Ma, Q. L., & Ning, Z. F. (2017). Interfacial Tension between Methane and Water Containing Kinetic Hydrate Inhibitor PVP Ramification and Its Emulsification Property. *Journal of Chemical and Engineering Data*, *62*(9), 2770–2775. https://doi.org/10.1021/acs.jced.7b00113

Radzuan, M. N., Banat, I. M., & Winterburn, J. (2017). Production and characterization of rhamnolipid using palm oil agricultural refinery waste. *Bioresource Technology*, *225*, 99–105. https://doi.org/10.1016/j.biortech.2016.11.052

Rajnauth, J., Barrufet, M., & Falcone, G. (2012). Hydrate formation: Considering the effects of pressure, temperature, composition and water. *Energy Science and Technology*, *1*(1), 60–67. https://doi.org/10.2118/131663-MS

Ramírez, M. I., Tsaousi, K., Rudden, M., Marchant, R., Alameda, J. E., Román, G. M., & Banat, I. M. (2015). Rhamnolipid and surfactin production from olive oil mill waste as sole carbon source. *Bioresource Technology*, *198*, 231–236. https://doi.org/10.1016/j.biortech.2015.09.012

Rane, A. N., Baikar, V. V., Ravi Kumar, D. V., & Deopurkar, R. L. (2017). Agro-industrial wastes for production of biosurfactant by Bacillus subtilis ANR 88 and its application in synthesis of silver and gold nanoparticles. *Frontiers in Microbiology*, *8*(MAR), 1–12. https://doi.org/10.3389/fmicb.2017.00492

Razafindralambo, H., Paquot, M., Baniel, A., Popineau, Y., Hbid, C., Jacques, P., & Thonart, P. (1996). Foaming properties of surfactin, a lipopeptide biosurfactant from Bacillus subtilis. *JAOCS*,

Journal of the American Oil Chemists' Society, *73*(1), 149–151. https://doi.org/10.1007/BF02523463

Reis, C. B. L. dos, Morandini, L. M. B., Bevilacqua, C. B., Bublitz, F., Ugalde, G., Mazutti, M. A., & Jacques, R. J. S. (2018). First report of the production of a potent biosurfactant with α,β-trehalose by Fusarium fujikuroi under optimized conditions of submerged fermentation. *Brazilian Journal of Microbiology*, *49*, 185–192. https://doi.org/10.1016/J.BJM.2018.04.004

Rikalović, M. G., Vrvić, M. M., & Karadžić, I. M. (2015). Rhamnolipid biosurfactant from Pseudomonas aeruginosa - From discovery to application in contemporary technology. *Journal of the Serbian Chemical Society*, *80*(3), 279–304. https://doi.org/10.2298/JSC140627096R

Rivero, D., Gouveia, L. M., Müller, A. J., & Sáez, A. E. (2012). Shear-thickening behavior of high molecular weight poly(ethylene oxide) solutions. *Rheologica Acta*, *51*(1), 13–20. https://doi.org/10.1007/s00397-011-0569-7

Rocha e Silva, N. M. P., Rufino, R. D., Luna, J. M., Santos, V. A., & Sarubbo, L. A. (2014). Screening of Pseudomonas species for biosurfactant production using low-cost substrates. *Biocatalysis and Agricultural Biotechnology*, *3*, 132–139. https://doi.org/10.1016/j.bcab.2013.09.005

Rogers, R. E., Kothapalli, C., Lee, M. S., & Woolsey, J. R. (2003). Catalysis of gas hydrates by biosurfactants in seawater-saturated sand/clay. *Canadian Journal of Chemical Engineering*, *81*(October), 973–980. https://doi.org/10.1002/cjce.5450810508

Rokni-Zadeh, H., Li, W., Sanchez-Rodriguez, A., Sinnaeve, D., Rozenski, J., Martins, J. C., & Mot, R. De. (2012). Genetic and Functional Characterization of Cyclic Lipopeptide White-Line-Inducing Principle (WLIP) Production by Rice Rhizosphere Isolate Pseudomonas putida RW10S2. *Applied and Environmental Microbiology*, *78*(14), 4826–4834. https://doi.org/10.1128/AEM.00335-12

Ron, E. Z., & Rosenberg, E. (2001). Natural roles of biosurfactants. In *Environmental Microbiology* (Vol. 3, Issue 4, pp. 229–236). https://doi.org/10.1046/j.1462-2920.2001.00190.x

Rosen, M. J., & Kunjappu, J. T. (2012). *Surfactants and Interfacial Phenomenon* (4th ed.). John Wiley and Sons.

Saito, K., Kishimoto, M., Tanaka, R., & Ohmura, R. (2011). Crystal Growth of Clathrate Hydrate at the Interface between Hydrocarbon Gas Mixture and Liquid Water. *Crystal Growth and Design*,

11(1), 295–301. https://doi.org/10.1021/cg101310z

Saito, M., Sugai, Y., Sasaki, K., Okamoto, Y., & Ouyang, C. (2016). Experimental and Numerical Studies on EOR Using a Biosurfactant. *Abu Dhabi International Petroleum and Exhibition Conference*, 1–11. https://doi.org/10.2118/183496-MS

Salaguer, J.-L. (2002). SURFACTANTS Types and Uses. In *Laboratory of Formulation, Interfaces, Rheology and Processes* (No. E300-A; Vol. 2). https://doi.org/10.1016/j.marpolbul.2013.12.019

Salihu, S. M., Abubakar, A. J., Meisam, B., Emmanuel, U. A., Hassan, K. Y., & Aminu, A. Y. (2019). Effect of temperature and salt concentration on rheological behaviour of surfactin. *Society of Petroleum Engineers - SPE Nigeria Annual International Conference and Exhibition 2019, NAIC 2019*. https://doi.org/10.2118/198731-MS

Salihu, S. M., Abubakar, A. J., Meisam, B., & Nasr, G. G. (2018). Physicochemical Characterization of Sodium Surfactin for Oil and Gas Industry Application. *Journal of Engineering Technology*, *6*(2), 342–355.

Sallada, N. D., Harkins, L. E., & Berger, B. W. (2019). Effect of gene copy number and chaperone coexpression on recombinant hydrophobin HFBI biosurfactant production in Pichia pastoris. *Biotechnology and Bioengineering*, *116*(8), 2029–2040. https://doi.org/10.1002/bit.26982

Sandra, H., Katharina, J., & Michael, B. (2005). Genetic Analysis of Biosurfactant Production in Ustilago maydis. *Applied and Environmental Biology*, *71*(6), 3033–3040. https://doi.org/10.1128/AEM.71.6.3033

Santa Anna, L. M., Sebastian, G. V., Pereira, Jr, N., Alves, T. L. M., Menezes, E. P., & Freire, D. M. G. (2001). Production of biosurfactant from a new and promising strain of Pseudomonas aeruginosa PA1. *Applied Biochemistry and Biotechnology*, *91*(1–9), 459–468. https://doi.org/10.1385/ABAB:91-93:1-9:459

Santos, A. P. P., Silva, M. D. S., Costa, E. V. L., Rufino, R. D., Santos, V. A., Ramos, C. S., Sarubbo, L. A., & Porto, A. L. F. (2018). Production and characterization of a biosurfactant produced by Streptomyces sp. DPUA 1559 isolated from lichens of the Amazon region. *Brazilian Journal of Medical and Biological Research*, *51*(2), 1–10. https://doi.org/10.1590/1414-431x20176657

Santos, D. K. F., Rufino, R. D., Luna, J. M., Santos, V. A., & Sarubbo, L. A. (2016). Biosurfactants: Multifunctional biomolecules of the 21st century. *International Journal of Molecular Sciences*,

401(17), 1–31. https://doi.org/10.3390/ijms17030401

Sarubbo, L. A., De Luna, J. M., & De Campos-Takaki, G. M. (2006). Production and stability studies of the bioemulsifier obtained from a new strain of Candida glabrata UCP 1002. *Electronic Journal of Biotechnology*, *9*(4), 1–7. https://doi.org/10.2225/vol9-issue4-fulltext-6

Satpute, S. K., Banat, I. M., Dhakephalkar, P. K., Banpurkar, A. G., & Chopade, B. A. (2010). Biosurfactants, bioemulsifiers and exopolysaccharides from marine microorganisms. *Biotechnology Advances*, *28*(4), 436–450. https://doi.org/10.1016/j.biotechadv.2010.02.006

Saxena, N., Pal, N., Ojha, K., Dey, S., & Mandal, A. (2018). Synthesis, characterization, physical and thermodynamic properties of a novel anionic surfactant derived from: Sapindus laurifolius. *RSC Advances*, *8*(43), 24485–24499. https://doi.org/10.1039/c8ra03888k

Sayed, A. M., Olesen, K. B., Alkahala, A. S., Sølling, T. I., & Alyafei, N. (2019). The effect of organic acids and salinity on the interfacial tension of n-decane/ water systems. *Journal of Petroleum Science and Engineering*, *173*, 1047–1052. https://doi.org/10.1016/J.PETROL.2018.10.097

Schaller, K. D., Fox, S. L., Bruhn, D. F., Noah, K. S., & Bala, G. A. (2004). Characterization of surfactin from Bacillus subtilis for application as an agent for enhanced oil recovery. *Applied Biochemistry and Biotechnology*, *113–116*, 827–836. https://doi.org/10.1385/ABAB:115:1-3:0827

Schroyen, B., Gunes, D. Z., & Vermant, J. (2017). A versatile subphase exchange cell for interfacial shear rheology. *Rheologica Acta*, *56*(1), 1–10. https://doi.org/10.1007/s00397-016-0976-x

Sekhon, K., Khanna, S., & Cameotra, S. (2011). Enhanced biosurfactant production through cloning of three genes and role of esterase in biosurfactant release. *Microbial Cell Factories*, *10*(1), 49. https://doi.org/10.1186/1475-2859-10-49

Sereshti, H., & Aliakbarzadeh, G. (2013). Response surface methodology optimized dispersive liquid–liquid microextraction coupled with UV-Vis spectrophotometry for determination of quinine. *Analytical Methods*, *5*(19), 5253. https://doi.org/10.1039/c3ay40478a

Shabtai, Y., & Gutnick, D. L. (1985). Exocellular esterase and emulsan release from the cell surface of Acinetobacter calcoaceticus. *Journal of Bacteriology*, *161*(3), 1176–1181.

Shah, A., Shahzad, S., Munir, A., Nadagouda, M. N., Khan, G. S., Shams, D. F., Dionysiou, D. D.,

& Rana, U. A. (2016). Micelles as Soil and Water Decontamination Agents. *Chemical Reviews*, *116*(10), 6042–6074. https://doi.org/10.1021/acs.chemrev.6b00132

Shaligram, N. S., & Singhal, R. S. (2010). Surfactin -a review on biosynthesis, fermentation, purification and applications. *Food Technology and Biotechnology*, *48*(2), 119–134. https://doi.org/10.1093/jxb/erf089

Sharma, A. K., Tiwari, A. K., & Dixit, A. R. (2016). Rheological behaviour of nanofluids: A review. *Renewable and Sustainable Energy Reviews*, *53*, 779–791. https://doi.org/10.1016/j.rser.2015.09.033

Sharma, D., Saharan, B. S., & Kapil, S. (2016). Biosurfactants of Probiotic Lactic Acid Bacteria. In *Biosurfactants of Lactic Acid Bacteria* (pp. 17–29). Springer. https://doi.org/10.1007/978-3-319-26215-4_2

Sharma, P., Sangwan, S., & Kaur, H. (2019). Process parameters for biosurfactant production using yeast Meyerozyma guilliermondii YK32. *Environmental Monitoring and Assessment*, *191*(9). https://doi.org/10.1007/s10661-019-7665-z

Sharma, R., Singh, J., & Verma, N. (2018). Production, characterization and environmental applications of biosurfactants from Bacillus amyloliquefaciens and Bacillus subtilis. *Biocatalysis and Agricultural Biotechnology*, *16*, 132–139. https://doi.org/10.1016/j.bcab.2018.07.028

Shavandi, M., Mohebali, G., Haddadi, A., Shakarami, H., & Nuhi, A. (2011). Emulsification potential of a newly isolated biosurfactant-producing bacterium, Rhodococcus sp. strain TA6. *Colloids and Surfaces B: Biointerfaces*, *82*(2), 477–482. https://doi.org/10.1016/j.colsurfb.2010.10.005

She, A. Q., Gang, H. Z., & Mu, B. Z. (2012). Temperature influence on the structure and interfacial properties of surfactin micelle: A molecular dynamics simulation study. *Journal of Physical Chemistry B*, *116*(42), 12735–12743. https://doi.org/10.1021/jp302413c

Shrestha, R. G., & Aramaki, K. (2008). The Study of Salt Induced Viscoelastic Wormlike Micelles in Aqueous Systems of Mixed Anionic / Nonionic Surfactants. *J . Nepal Chem . Soc*, *23*, 65–73. https://doi.org/10.3126/jncs.v23i0.2098

Shu, L., Obagbemi, I. J., Liyanaarachchi, S., Navaratna, D., Parthasarathy, R., Aim, R. Ben, & Jegatheesan, V. (2016). Why does pH increase with CaCl2as draw solution during forward osmosis

filtration. *Process Safety and Environmental Protection*, *104*, 465–471. https://doi.org/10.1016/j.psep.2016.06.007

Silva, R. de C. F. S., Almeida, D. G., Rufino, R. D., Luna, J. M., Santos, V. A., & Sarubbo, L. A. (2014). Applications of biosurfactants in the petroleum industry and the remediation of oil spills. *International Journal of Molecular Sciences*, *15*, 12523–12542. https://doi.org/10.3390/ijms150712523

Silva, S. N. R. L., Farias, C. B. B., Rufino, R. D., Luna, J. M., & Sarubbo, L. A. (2010). Glycerol as substrate for the production of biosurfactant by Pseudomonas aeruginosa UCP0992. *Colloids and Surfaces B: Biointerfaces*, *79*(1), 174–183. https://doi.org/10.1016/j.colsurfb.2010.03.050

Singh, P., Patil, Y., & Rale, V. (2019). Biosurfactant production: emerging trends and promising strategies. *Journal of Applied Microbiology*, *126*(1), 2–13. https://doi.org/10.1111/jam.14057

Singh, R., Glick, B. R., & Rathore, D. (2018). Biosurfactants as a Biological Tool to Increase Micronutrient Availability in Soil: A Review. *Pedosphere*, *28*(2), 170–189. https://doi.org/10.1016/S1002-0160(18)60018-9

Sloan, D. E. (2003). Fundamental principles and applications of natural gas hydrates. *Nature*, *426*, 353–363.

Sloan, D. E., & Koh, C. A. (2008). *Clathrate hydrates of natural gases* (3rd ed.). CRC Press, Taylor and Francis Group.

Sloan, E. D., Subramanian, S., Matthews, P. N., Lederhos, J. P., & Khokhar, A. A. (1998). Quantifying hydrate formation and kinetic inhibition. *Industrial and Engineering Chemistry Research*, *37*(8), 3124–3132. https://doi.org/10.1021/ie970902h

Sohn, Y. hoon, Kim, J., Shin, K., Chang, D., Seo, Y., Aman, Z. M., & May, E. F. (2015). Hydrate plug formation risk with varying watercut and inhibitor concentrations. *Chemical Engineering Science*, *126*, 711–718. https://doi.org/10.1016/j.ces.2015.01.016

Soltero, J. F. A., Puig, J. E., & Ingeniería, D. De. (2001). DSC Analysis of Surfactant-Based Microstructures. In N. Garti (Ed.), *Thermal Behaviour of Dispersed Systems* (pp. 121–180). Marcel Dekker Inc. https://doi.org/10.1201/9780824741464.ch4

Su, C., Xiang, Z., Liu, Y., Zhao, X., Sun, Y., Li, Z., Li, L., Chang, F., Chen, T., Wen, X., Zhou, Y.,

& Zhao, F. (2016). Analysis of the genomic sequences and metabolites of Serratia surfactantfaciens sp. nov. YD25 T that simultaneously produces prodigiosin and serrawettin W2. *BMC Genomics*, *17*(1), 1–19. https://doi.org/10.1186/s12864-016-3171-7

Sun, C. Y., Chen, G. J., & Yang, L. Y. (2004). Interfacial tension of methane + water with surfactant near the hydrate formation conditions. *Journal of Chemical and Engineering Data*, *49*(4), 1023–1025. https://doi.org/10.1021/je049948p

Sung, J. H., Ahn, S. J., Kim, N. Y., Jeong, S. K., Kim, J. K., Chung, J. K., & Lee, H. H. (2010). Purification, molecular cloning, and biochemical characterization of subtilisin JB1 from a newly isolated Bacillus subtilis JB1. *Applied Biochemistry and Biotechnology*, *162*(3), 900–911. https://doi.org/10.1007/s12010-009-8830-6

TA instruments. (2019). *Discover the World's Finest line of Differential Scanning Calorimeters*. https://www.tainstruments.com/wp-content/uploads/Discovery-DSC-Brochure.pdf

Tao, D. J., Cheng, Z., Chen, F. F., Li, Z. M., Hu, N., & Chen, X. S. (2013). Synthesis and thermophysical properties of biocompatible cholinium-based amino acid ionic liquids. *Journal of Chemical and Engineering Data*, *58*(6), 1542–1548. https://doi.org/10.1021/je301103d

Taylor, C. J., Miller, K. T., Koh, C. A., & Sloan, E. D. (2007). Macroscopic investigation of hydrate film growth at the hydrocarbon/water interface. *Chemical Engineering Science*, *62*(23), 6524–6533. https://doi.org/10.1016/j.ces.2007.07.038

Tazdait, D., Salah, R., Mouffok, S., Kabouche, F., Keddou, I., Abdi, N., Grib, H., & Mameri, N. (2018). Preliminary evaluation of a new low-cost substrate (amurca) in production of biosurfactant by Pseudomonas aeruginosa isolated from fuel-contaminated soil. *Journal of Material and Environ*, *9*(3), 964–970. https://doi.org/10.26872/jmes.2018.9.3.107

Teixeira Souza, K. S., Gudiña, E. J., Schwan, R. F., Rodrigues, L. R., Dias, D. R., & Teixeira, J. A. (2018). Improvement of biosurfactant production by Wickerhamomyces anomalus CCMA 0358 and its potential application in bioremediation. *Journal of Hazardous Materials*, *346*, 152–158. https://doi.org/10.1016/j.jhazmat.2017.12.021

Tennouga, L., Mansri, A., Medjahed, K., Chetouani, A., & Warad, I. (2015). The micelle formation of cationic and anionic surfactants in aqueous medium: Determination of CMC and thermodynamic parameters at different temperatures. *Journal of Materials and Environmental Science*, *6*(10), 2711–

2716.

Thavasi, R., Subramanyam Nambaru, V. R. M., Jayalakshmi, S., Balasubramanian, T., & Banat, I. M. (2011). Biosurfactant Production by Pseudomonas aeruginosa from Renewable Resources. *Indian Journal of Microbiology*, *51*(1), 30–36. https://doi.org/10.1007/s12088-011-0076-7

Torres, L., Moctezuma, A., Avendaño, J. R., Muñoz, A., & Gracida, J. (2011). Comparison of bio- and synthetic surfactants for EOR. *Journal of Petroleum Science and Engineering*, *76*(1–2), 6–11. https://doi.org/10.1016/j.petrol.2010.11.022

Tripathy, D. B., Mishra, A., Clark, J., & Farmer, T. (2018). Synthesis, chemistry, physicochemical properties and industrial applications of amino acid surfactants: A review. *Comptes Rendus Chimie*, *21*(2), 112–130. https://doi.org/10.1016/j.crci.2017.11.005

Twigg, M., Tripathi, L., Zompra, K., Salek, K., Irorere, V., Gutierrez, T., Spyroulias, G., Marchant, R., & Banat, I. (2019). Surfactants from the sea: rhamnolipid production by marine bacteria. *Access Microbiology*, *1*(1A), 192. https://doi.org/10.1099/acmi.ac2019.po0066

Urum, K., & Pekdemir, T. (2004). Evaluation of biosurfactants for crude oil contaminated soil washing. *Chemosphere*, *57*(9), 1139–1150. https://doi.org/10.1016/j.chemosphere.2004.07.048

Uzoigwe, C., Burgess, J. G., Ennis, C. J., & Rahman, P. K. S. M. (2015). Bioemulsifiers are not biosurfactants and require different screening approaches. *Frontiers in Microbiology*, *6*(APR), 1–6. https://doi.org/10.3389/fmicb.2015.00245

Varjani, S. J. (2018). Microbial degradation of petroleum hydrocarbons. *Biomedical Research Interantional*, *Vol 2018*(Article ID 5034783), 1–15. https://doi.org/https://doi.org/10.1155/2018/5034783

Varjani, S. J., & Upasani, V. N. (2016). Carbon spectrum utilization by an indigenous strain of Pseudomonas aeruginosa NCIM 5514: Production, characterization and surface active properties of biosurfactant. *Bioresource Technology*, *221*, 510–516. https://doi.org/10.1016/j.biortech.2016.09.080

Varjani, S. J., & Upasani, V. N. (2017). Critical review on biosurfactant analysis, purification and characterization using rhamnolipid as a model biosurfactant. *Bioresource Technology*, *232*, 389–397. https://doi.org/10.1016/j.biortech.2017.02.047

Vecino, X., Rodríguez-López, L., Gudiña, E. J., Cruz, J. M., Moldes, A. B., & Rodrigues, L. R. (2017). Vineyard pruning waste as an alternative carbon source to produce novel biosurfactants by Lactobacillus paracasei. *Journal of Industrial and Engineering Chemistry*, *55*, 40–49. https://doi.org/10.1016/j.jiec.2017.06.014

Veluswamy, H. P., Wong, A. J. H., Babu, P., Kumar, R., Kulprathipanja, S., Rangsunvigit, P., & Linga, P. (2016). Rapid methane hydrate formation to develop a cost effective large scale energy storage system. *Chemical Engineering Journal*, *290*, 161–173. https://doi.org/10.1016/j.cej.2016.01.026

Vera, E. C. S., de Azevedo, P. O. de S., Domínguez, J. M., & Oliveira, R. P. de S. (2018). Optimization of biosurfactant and bacteriocin-like inhibitory substance (BLIS) production by Lactococcus lactis CECT-4434 from agroindustrial waste. *Biochemical Engineering Journal*, *133*, 168–178. https://doi.org/10.1016/J.BEJ.2018.02.011

Veshareh, J. M., & Ayatollahi, S. (2019). Microorganisms' effect on the wettability of carbonate oil-wet surfaces: implications for MEOR, smart water injection and reservoir souring mitigation strategies. *Journal of Petroleum Exploration and Production Technology*, *0123456789*, 1–12. https://doi.org/10.1007/s13202-019-00775-6

Vijayakuma, S., & Saravanan, V. (2015). Biosurfactants-Types, Sources and Applications. *Research Journal of Microbiology*, *10*(5), 181–192. https://doi.org/10.3923/jm.2015.181.192

Wang, Q., Yu, H., Wang, M., Yang, H., & Shen, Z. (2018). Enhanced biosynthesis and characterization of surfactin isoforms with engineered Bacillus subtilis through promoter replacement and Vitreoscilla hemoglobin co-expression. *Process Biochemistry*, *70*(March), 36–44. https://doi.org/10.1016/j.procbio.2018.04.003

Warrier, P., Khan, N. M., Srivastava, V., Maupin, C. mark, & Koh, C. A. (2016). Overview: Nucleation of clathrate hydrates. *The Journal of Chemical Physics*, *145*(21), 211705. https://doi.org/10.1063/1.4968590

Watanabe, K., Niwa, S., & Mori, Y. H. (2005). Surface tensions of aqueous solutions of sodium alkyl sulfates in contact with methane under hydrate-forming conditions. *Journal of Chemical and Engineering Data*, *50*(5), 1672–1676. https://doi.org/10.1021/je050139v

Wei, Y.-H., Wang, L. F., Chang, J. S., & Kung, S. S. (2003). Identification of induced acidification

in iron-enriched cultures of Bacillus subtilis during biosurfactant fermentation. *Journal of Bioscience and Bioengineering*, *96*(2), 174–178. https://doi.org/10.1016/S1389-1723(03)90121-6

Whang, L. M., Liu, P. W. G., Ma, C. C., & Cheng, S. S. (2008). Application of biosurfactants, rhamnolipid, and surfactin, for enhanced biodegradation of diesel-contaminated water and soil. *Journal of Hazardous Materials*, *151*(1), 155–163. https://doi.org/10.1016/j.jhazmat.2007.05.063

White, D. A., Hird, L. C., & Ali, S. T. (2013). Production and characterization of a trehalolipid biosurfactant produced by the novel marine bacterium Rhodococcus sp., strain PML026. *Journal of Applied Microbiology*, *115*(3), 744–755. https://doi.org/10.1111/jam.12287

Wu, Q., Zhi, Y., & Xu, Y. (2019). Systematically engineering the biosynthesis of a green biosurfactant surfactin by Bacillus subtilis 168. *Metabolic Engineering*, *52*, 87–97. https://doi.org/10.1016/J.YMBEN.2018.11.004

Wu, Y., Xu, M., Xue, J., Shi, K., & Gu, M. (2019). Characterization and Enhanced Degradation Potentials of Biosurfactant-Producing Bacteria Isolated from a Marine Environment. *ACS Omega*, *4*(1), 1645–1651. https://doi.org/10.1021/acsomega.8b02653

Xiao, C., & Adidharma, H. (2009). Dual function inhibitors for methane hydrate. *Chemical Engineering Science*, *64*(7), 1522–1527. https://doi.org/10.1016/j.ces.2008.12.031

Yahaya, A. A., Akpan, E. U., Enyi, G. C., Nasr, G. G., & Abbas, J. (2018). Experimental investigation of methane-water and methane-brine IFT measurements using pendant drop (rising bubble) method Journal of Engineering Technology. *Journal of Engineering Technology*, *6*(1), 394–407.

Yanagisawa, S., Nagano, T., Izumida, M., Toshiaki, T., Imura, T., & Kitamoto, D. (2018). *Method of Reducing Critical Micelle Concentration, and Surfactant Composition* (Patent No. US009868097B2). https://patentimages.storage.googleapis.com/92/94/90/efc5062d8eb4c9/US9868097.pdf

Yasuda, K., Mori, Y. H., & Ohmura, R. (2016). Interfacial tension measurements in water-methane system at temperatures from 278.15 K to 298.15 K and pressures up to 10 MPa. *Fluid Phase Equilibria*, *413*, 170–175. https://doi.org/10.1016/j.fluid.2015.10.006

Yeh, M. S., Wei, Y. H., & Chang, J. S. (2005). Enhanced production of surfactin from Bacillus subtilis by addition of solid carriers. *Biotechnology Progress*, *21*(4), 1329–1334.

https://doi.org/10.1021/bp050040c

Youssef, N. H., Duncan, K. E., Nagle, D. P., Savage, K. N., Knapp, R. M., & McInerney, M. J. (2004). Comparison of methods to detect biosurfactant production by diverse microorganisms. *Journal of Microbiological Methods*, *56*(3), 339–347. https://doi.org/10.1016/j.mimet.2003.11.001

Yu, M., Liu, Z., Zeng, G., Zhong, H., Liu, Y., Jiang, Y., Li, M., He, X., & He, Y. (2015). Characteristics of mannosylerythritol lipids and their environmental potential. *Carbohydrate Research*, *407*, 63–72. https://doi.org/10.1016/J.CARRES.2014.12.012

Yunita, P., Irawan, S., & Kania, D. (2016). Optimization of Water-based Drilling Fluid Using Non-ionic and Anionic Surfactant Additives. *Procedia Engineering*, *148*, 1184–1190. https://doi.org/10.1016/j.proeng.2016.06.628

Zdziennicka, A., Krawczyk, J., & Jańczuk, B. (2018). Volumetric properties of rhamnolipid and surfactin at different temperatures. *Journal of Molecular Liquids*, *255*, 562–571. https://doi.org/10.1016/j.molliq.2018.02.015

Zerpa, L. E., Salager, J.-L., Koh, C. A., Sloan, E. D., & Sum, A. K. (2011). Surface Chemistry and Gas Hydrates in Flow Assurance. *Industrial & Engineering Chemistry Research*, *50*(1), 188–197. https://doi.org/10.1021/ie100873k

Zhang, G., Rogers, R. E., French, W. T., & Lao, W. (2007). Investigation of microbial influences on seafloor gas-hydrate formations. *Marine Chemistry*, *103*(3–4), 359–369. https://doi.org/10.1016/j.marchem.2006.10.005

Zhang, J., Xue, Q., Gao, H., Lai, H., & Wang, P. (2016). Production of lipopeptide biosurfactants by Bacillus atrophaeus 5-2a and their potential use in microbial enhanced oil recovery. *Microbial Cell Factories*, *15*(1), 1–11. https://doi.org/10.1186/s12934-016-0574-8

Zhang, Q. Q., Cai, B. X., Xu, W. J., Gang, H. Z., Liu, J. F., Yang, S. Z., & Mu, B. Z. (2015). Novel zwitterionic surfactant derived from castor oil and its performance evaluation for oil recovery. *Colloids and Surfaces A: Physicochemical and Engineering Aspects*, *483*, 87–95. https://doi.org/10.1016/j.colsurfa.2015.05.060

Zhang, Y., Zhu, Y., Zhu, Y., & Li, Y. (2009). The importance of engineering physiological functionality into microbes. *Trends in Biotechnology*, *27*(12), 664–672. https://doi.org/10.1016/j.tibtech.2009.08.006

Zhao, J., & Wen, D. (2017). Pore-scale simulation of wettability and interfacial tension effects on flooding process for enhanced oil recovery. *RSC Advances*, *7*(66), 41391–41398. https://doi.org/10.1039/c7ra07325a

Zhi, Y., Wu, Q., & Xu, Y. (2017a). Production of surfactin from waste distillers' grains by co-culture fermentation of two Bacillus amyloliquefaciens strains. *Bioresource Technology*, *235*, 96–103. https://doi.org/10.1016/J.BIORTECH.2017.03.090

Zhi, Y., Wu, Q., & Xu, Y. (2017b). Production of surfactin from waste distillers' grains by co-culture fermentation of two Bacillus amyloliquefaciens strains. *Bioresource Technology*, *235*, 96–103. https://doi.org/10.1016/j.biortech.2017.03.090

Zhou, D., Hu, F., Lin, J., Wang, W., & Li, S. (2019). Genome and transcriptome analysis of Bacillus velezensis BS-37, an efficient surfactin producer from glycerol, in response to d-/l-leucine. *MicrobiologyOpen*, *8*(8), 1–14. https://doi.org/10.1002/mbo3.794

Zhou, J., Hu, M., & Jing, D. (2019). The synergistic effect between surfactant and nanoparticle on the viscosity of water-based fluids. *Chemical Physics Letters*, *727*, 1–5. https://doi.org/10.1016/J.CPLETT.2019.04.052

Zosim, Z., Gutnick, D., & Rosenberg, E. (1982). Properties of hydrocarbon-in-water emulsions stabilized by Acinetobacter RAG-1 emulsan. *Biotechnology and Bioengineering*, *24*(2), 281–292. https://doi.org/10.1002/bit.260240203

Zouari, O., Lecouturier, D., Rochex, A., Chataigne, G., Dhulster, P., Jacques, P., & Ghribi, D. (2019). Bio-emulsifying and biodegradation activities of syringafactin producing Pseudomonas spp. strains isolated from oil contaminated soils. *Biodegradation*, *30*(4), 259–272. https://doi.org/10.1007/s10532-018-9861-x

APPENDIX A

Rheology measurement and characterization data

Appendix A 1 Calibration standard for rheology analysis

OFITE

Dependable Products From People You Trust

11302 Steeplecrest Dr. Houston, Texas 77065 Phone 832-320-7300 Fax 713.880.9886 www.ofite.com

NIST CERTIFIED CALIBRATION FLUID, 200 cP

OFI PART NO. 132-83

LOT NO. 406404

°C	cP	°C	cP	°C	cP	°C	cP	°C	cP
20	211.3	24	194.4	28	179.2	32	165.6	36	153.4
20.1	210.8	24.1	194.0	28.1	178.9	32.1	165.3	36.1	153.1
20.2	210.4	24.2	193.6	28.2	178.5	32.2	165.0	36.2	152.8
20.3	210.0	24.3	193.2	28.3	178.2	32.3	164.6	36.3	152.5
20.4	209.5	24.4	192.8	28.4	177.8	32.4	164.3	36.4	152.2
20.5	209.1	24.5	192.4	28.5	177.5	32.5	164.0	36.5	151.9
20.6	208.6	24.6	192.0	28.6	177.1	32.6	163.7	36.6	151.6
20.7	208.2	24.7	191.6	28.7	176.7	32.7	163.4	36.7	151.3
20.8	207.8	24.8	191.2	28.8	176.4	32.8	163.1	36.8	151.1
20.9	207.3	24.9	190.9	28.9	176.0	32.9	162.7	36.9	150.8
21	206.9	25	190.5	29	175.7	33	162.4	37	150.5
21.1	206.5	25.1	190.1	29.1	175.3	33.1	162.1	37.1	150.2
21.2	206.0	25.2	189.7	29.2	175.0	33.2	161.8	37.2	149.9
21.3	205.6	25.3	189.3	29.3	174.6	33.3	161.5	37.3	149.6
21.4	205.2	25.4	188.9	29.4	174.3	33.4	161.2	37.4	149.4
21.5	204.7	25.5	188.5	29.5	174.0	33.5	160.9	37.5	149.1
21.6	204.3	25.6	188.1	29.6	173.6	33.6	160.6	37.6	148.8
21.7	203.9	25.7	187.8	29.7	173.3	33.7	160.2	37.7	148.5
21.8	203.5	25.8	187.4	29.8	172.9	33.8	159.9	37.8	148.2
21.9	203.0	25.9	187.0	29.9	172.6	33.9	159.6	37.9	148.0
22	202.6	26	186.6	30	172.2	34	159.3	38	147.7
22.1	202.2	26.1	186.2	30.1	171.9	34.1	159.0	38.1	147.4
22.2	201.8	26.2	185.9	30.2	171.6	34.2	158.7	38.2	147.1
22.3	201.4	26.3	185.5	30.3	171.2	34.3	158.4	38.3	146.9
22.4	200.9	26.4	185.1	30.4	170.9	34.4	158.1	38.4	146.6
22.5	200.5	26.5	184.7	30.5	170.5	34.5	157.8	38.5	146.3
22.6	200.1	26.6	184.4	30.6	170.2	34.6	157.5	38.6	146.1
22.7	199.7	26.7	184.0	30.7	169.9	34.7	157.2	38.7	145.8
22.8	199.3	26.8	183.6	30.8	169.5	34.8	156.9	38.8	145.5
22.9	198.9	26.9	183.3	30.9	169.2	34.9	156.6	38.9	145.2
23	198.5	27	182.9	31	168.9	35	156.3	39	145.0
23.1	198.1	27.1	182.5	31.1	168.5	35.1	156.0	39.1	144.7
23.2	197.6	27.2	182.1	31.2	168.2	35.2	155.7	39.2	144.4
23.3	197.2	27.3	181.8	31.3	167.9	35.3	155.4	39.3	144.2
23.4	196.8	27.4	181.4	31.4	167.6	35.4	155.1	39.4	143.9
23.5	196.4	27.5	181.0	31.5	167.2	35.5	154.8	39.5	143.6
23.6	196.0	27.6	180.7	31.6	166.9	35.6	154.5	39.6	143.4
23.7	195.6	27.7	180.3	31.7	166.6	35.7	154.2	39.7	143.1
23.8	195.2	27.8	180.0	31.8	166.3	35.8	153.9	39.8	142.8
23.9	194.8	27.9	179.6	31.9	165.9	35.9	153.6	39.9	142.6

	A=	B=	C=	D=
For Temp.(T) < 40 °C	-0.00042030	0.08341610	-7.27613870	326.79875780
For Temp.(T) > 40 °C	-0.00013580	0.04433960	-5.51143360	300.63598950

cP= $A(T)^3+B(T)^2+C(T)+D$ (T) IS IN °C

Appendix A 2 Viscosity-shear rate data of *surfactin* at different temperature

	Viscosity	(mPas)	at 20 ℃				Viscosity	(mPas)	at 30 ℃		
Dosage (%)	0.025	0.050	0.075	0.100	0.500	1.000	Dosage (%) 0.025	0.050	0.075	0.100	0.500	1.000
Shear Rate (s⁻¹)							Shear Rate (s⁻¹)					
0.01	13.8	14.9	7.8	10.6	6.2	22.2	0.01	11.8	7.6	8.2	11.1	7.2	25.7
85.1	10.2	11	5.9	6.8	5.3	16.1	85.1	9	5.7	6.1	8.1	5.4	18.5
170.2	4.6	6.6	3.1	3.5	3	6.5	170.2	4.5	3.2	3.3	3.7	3.2	8.4
340.5	2.5	3.1	2	2	2	2.9	340.5	2.5	1.8	1.9	2	1.9	3.5
510.7	2.1	2.9	1.6	1.6	1.7	2.6	510.7	2.3	1.5	1.5	1.5	1.6	2.6
680.9	1.7	1.6	1.5	1.6	1.6	1.7	680.9	1.6	1.4	1.4	1.4	1.5	1.6
851.2	1.6	2.4	1.4	1.5	1.5	2.2	851.2	1.5	1.4	1.3	1.7	1.4	2.4
1021.4	1.5	2.5	1.3	1.6	1.4	2.7	1021.4	1.8	1.7	1.2	1.9	1.4	3

	Viscosity	(mPas)	at 40 ℃				Viscosity	(mPas)	at 50 ℃		
Dosage (%)	0.025	0.050	0.075	0.100	0.500	1.000	Dosage (%) 0.025	0.050	0.075	0.100	0.500	1.000
Shear Rate (s⁻¹)							Shear Rate (s⁻¹)					
0.01	12.5	8.9	8.8	11.3	11.9	20.7	0.01	11.1	18.3	7.9	11.1	13.5	18.7
85.1	9.3	6.6	6.5	8.2	8.8	14.8	85.1	8.4	13.5	5.9	8	9.7	13.4
170.2	5.2	3.4	3.4	3.6	4.1	7.4	170.2	4.9	5.2	3.3	3.7	5	7.5
340.5	2.3	1.9	1.8	2.1	2.3	3	340.5	2.3	2.7	1.7	1.9	2.4	3.1
510.7	2.1	1.5	1.4	1.4	1.9	2.4	510.7	2.1	2.8	1.3	1.5	2	2.6
680.9	1.5	1.3	1.3	1.3	1.4	1.5	680.9	1.7	2.2	1.1	1.2	1.5	1.6
851.2	1.3	1.8	1.2	2.1	2.1	2.7	851.2	1.2	2.2	1.1	2.1	2.6	3
1021.4	2	2.1	1.3	2.1	2.4	3.2	1021.4	2.1	2.9	1.4	2.1	2.6	3.3

Appendix A 3 Viscosity-shear rate data of *surfactin* at different salt concentrations

	Viscosity	(mPas)	at 0.1 M				Viscosity	(mPas)	at 0.25 M		
Dosage (%)	0.025	0.05	0.075	0.1	0.5	1	Dosage (%)	0.025	0.05	0.075	0.1	0.5	1
Shear Rate (s^{-1})							Shear Rate (s^{-1})						
0.01	0	0	0.1	0	0	0	0.01	17.4	24.7	5.9	11.1	8.4	25.8
85.1	0	0	0.2	0	0	0	85.1	12.7	18	4.4	8.2	5	23.1
170.2	0	0	0	0	0	0	170.2	4.9	8.4	2.2	3.6	2.8	13.8
340.5	0	0	0.2	0	0	0	340.5	2.8	4	1.1	2.1	1.8	8
510.7	0.2	0	0.7	0	0	0	510.7	2	3.9	0.7	1.6	1.6	4.4
680.9	0.5	0.4	0.4	0.2	0.3	0.1	680.9	1.7	2.3	0.6	1.5	1.5	2.6
851.2	0.6	0.6	0.5	0.4	0.5	0.3	851.2	2.6	3.5	0.4	1.6	1.5	3.5
1021.4	0.7	0.6	1.2	0.5	0.6	0.5	1021.4	2.8	3.1	0.4	1.9	1.4	3.5

	Viscosity	(mPas)	at 0.5 M				Viscosity	(mPas)	at 1.0 M		
Dosage (%)	0.025	0.05	0.075	0.1	0.5	1	Dosage (%)	0.025	0.05	0.075	0.1	0.5	1
Shear Rate (s^{-1})							Shear Rate (s^{-1})						
0.01	15.5	10.2	6.5	9.6	8.2	36.9	0.01	8.3	8.8	7.4	20.3	28.3	6.9
85.1	11.8	7.4	4.9	7.2	6.3	26.9	85.1	6.3	6.7	5.7	15.3	24.9	5.4
170.2	5.4	3.6	2.7	4.1	3.5	10.1	170.2	3.8	3.7	3.3	8.3	16.1	3.3
340.5	3.5	2	1.8	2.4	2.2	4.9	340.5	2.3	2.4	2.1	3.8	5.6	2.3
510.7	2.6	1.5	1.5	2	1.8	4.3	510.7	2	2	1.7	3.9	5.3	2
680.9	1.8	1.6	1.5	1.8	1.6	2.9	680.9	1.8	1.8	1.6	2.4	3.3	1.9
851.2	2.6	1.7	1.5	1.7	1.5	3.3	851.2	1.6	1.8	1.5	2.8	3.9	1.9
1021.4	2.9	1.7	1.4	1.5	1.5	3.6	1021.4	1.5	1.7	1.5	4.5	4.3	1.9

Dosage (%)	Viscosity	(mPas)	at 1.5 M			
	0.025	0.05	0.075	0.1	0.5	1
Shear Rate (s^{-1})						
0.01	5.8	10.5	8.6	16.2	22	8.7
85.1	4.4	7.9	6.4	11.9	15.9	6.6
170.2	2.3	3.9	3.1	5.3	7	3.7
340.5	1.5	2.1	1.9	2.8	3.5	2.3
510.7	1.4	2.1	1.6	2.1	3	1.9
680.9	1.4	1.5	1.6	1.7	2	1.8
851.2	1.4	1.5	1.6	2.1	3.5	1.8
1021.4	1.3	1.5	1.5	2.5	3.3	1.8

Appendix A 4 Arrhenius temperature effect at variable shear rate and (a) 0.025% (b) 0.05% (c) 0.075% (d) 0.1% (e) 0.05% (f) 1.0% surfactant dosage
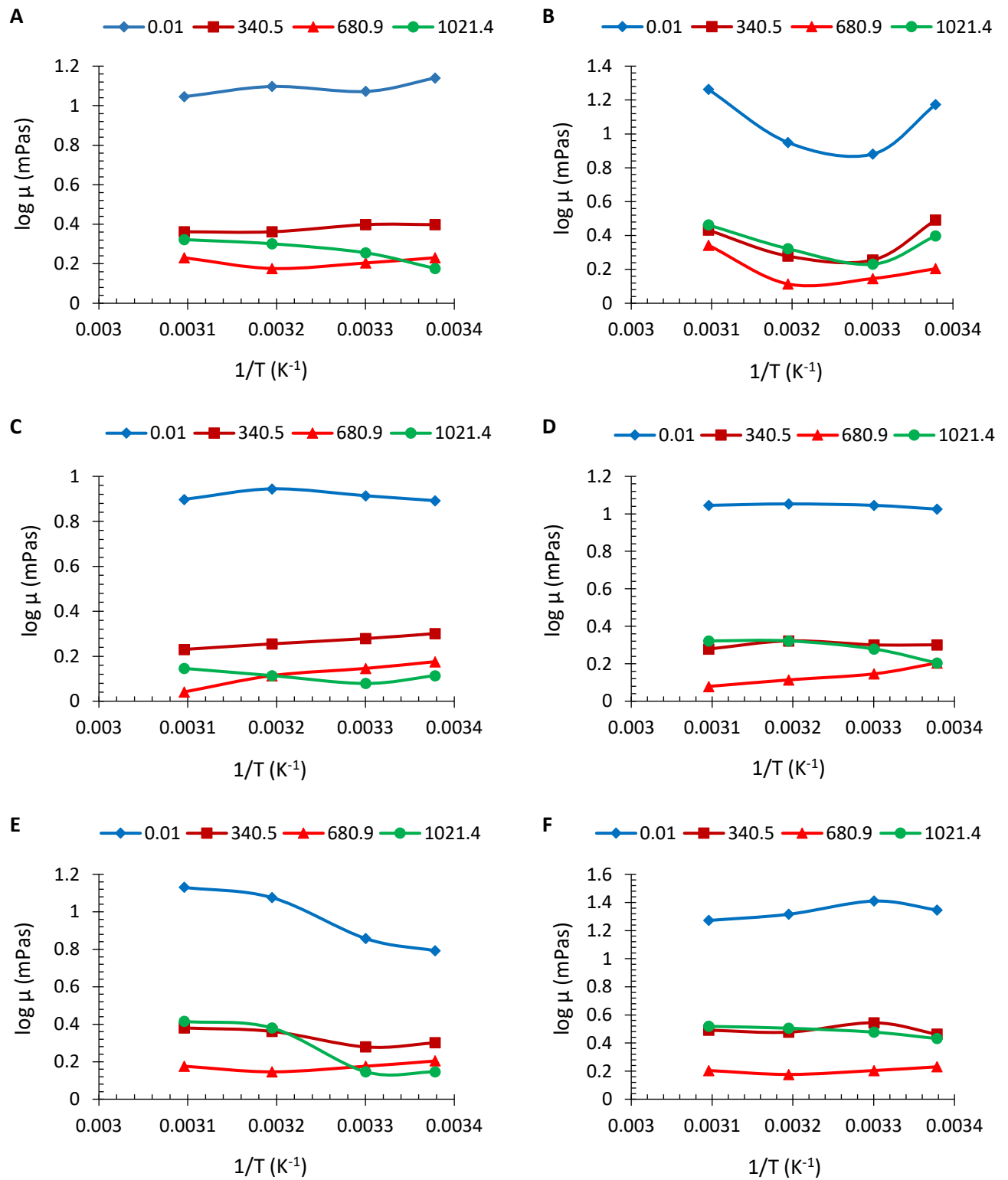
APPENDIX B

Experimental design data

Appendix B 1 Specifying output response on the custom design window in Design-Expert
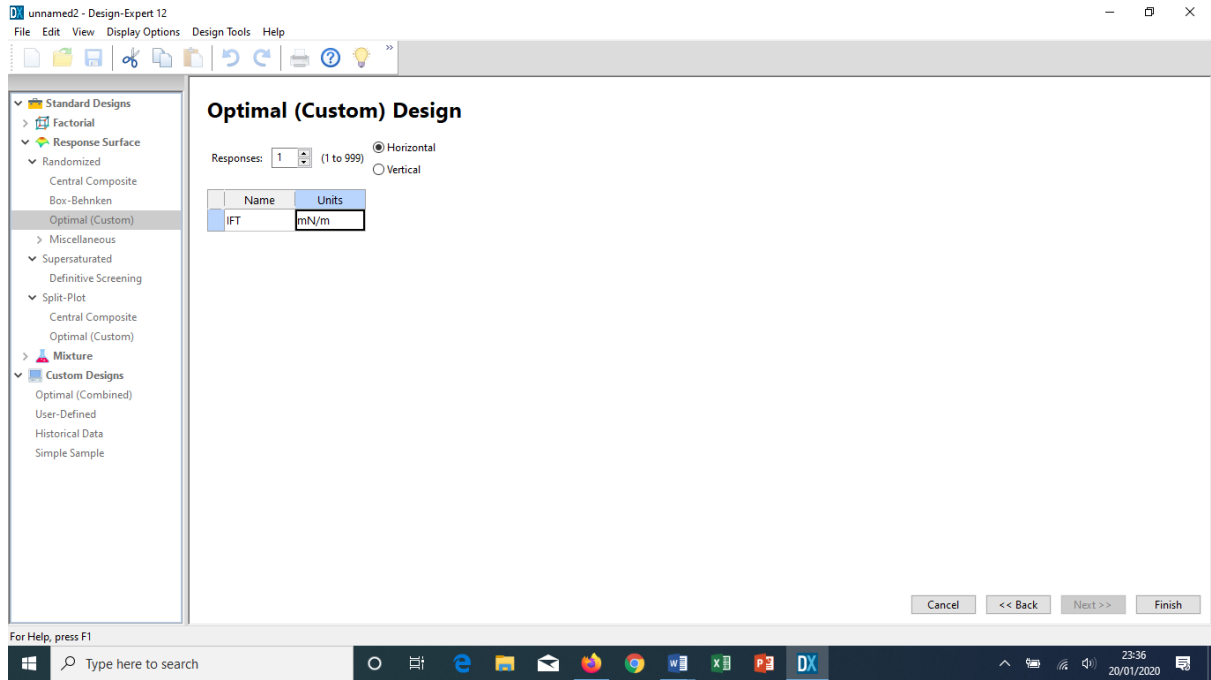
Appendix B 2 ST measurement data at ambient temperature

Surfactant dosage (%)	ST (mN/m)	
0	72	
0.025	54.66	
0.05	39.89	
0.075	37.63	
0.1	37.53	Standard deviation
0.5	37.57	=12.31898
1	37.98	Standard error =
		1.759855

Appendix B 3 Experimental design runs for ST measurement using Design-Expert

	Factor 1	Factor 2	Factor 3	Response 1
Run	A: Surf. Dosage	B: Temperature	C: Pressure	ST
	(%)	(°C)	(MPa)	(mN/m)
1	0.27	23.75	3.87	37.34
2	0.51	15.00	0.16	37.98
3	0.51	50.00	7.58	35.46
4	0.51	15.00	7.58	37.98
5	0.27	41.25	7.58	35.92
6	0.02	32.50	15.00	50.98
7	1.00	50.00	7.58	37.02
8	0.51	50.00	15.00	35.01
9	0.27	41.25	3.87	37
10	0.02	50.00	0.16	54.32
11	1.00	50.00	15.00	35.48
12	0.76	41.25	3.87	36.98
13	1.00	50.00	0.16	37.85
14	1.00	15.00	15.00	37.99
15	0.27	23.75	7.58	37.01
16	1.00	15.00	0.16	39.98
17	0.51	32.50	11.29	35.78
18	0.02	50.00	15.00	52.97
19	0.76	23.75	7.58	37.01
20	0.51	23.75	3.87	37.48
21	0.51	50.00	0.16	36.78
22	1.00	32.50	15.00	36.43
23	0.02	15.00	15.00	54.76
24	0.02	32.50	0.16	53.53
25	0.76	41.25	7.58	36.32
26	0.51	32.50	0.16	37.32
27	0.51	41.25	11.29	36.63
28	0.76	32.50	7.58	37.02
29	0.51	41.25	7.58	34.13

30	0.51	32.50	7.58	36.89
31	0.27	23.75	11.29	36.78
32	0.27	32.50	3.87	37.23
33	0.27	32.50	7.58	36.32
34	1.00	32.50	0.16	37.73
35	0.51	32.50	15.00	36.02
36	0.51	23.75	11.29	36.37
37	0.27	41.25	11.29	35.41
38	0.76	23.75	3.87	37.43
39	0.76	41.25	11.29	35.89
40	0.02	50.00	7.58	53.78
41	0.02	15.00	7.58	54.82
42	0.02	32.50	7.58	51.87
43	0.76	32.50	3.87	37.54
44	0.76	32.50	11.29	36.76
45	0.76	23.75	11.29	36.01
46	0.27	32.50	11.29	36.34
47	0.51	41.25	3.87	34.97
48	0.51	23.75	7.58	36.97
49	0.51	32.50	3.87	37.45
50	0.02	15.00	0.16	55.34
51	1.00	32.50	7.58	36.99
52	1.00	15.00	7.58	38.21
53	0.51	15.00	15.00	35.62

Appendix B 4 Analysis of variance (ANOVA) for cubic model

Source	Sum of Squares	df	Mean Square	F-value	p-value	
Model	2142.62	19	112.770	88.480	< 0.0001	significant
A-Surf. Dosage	21.220	1	21.220	16.650	0.0003	
B-Temperature	2.990	1	2.9900	2.3500	0.1349	
C-Pressure	1.66	1	1.6600	1.3000	0.2624	
AB	0.1995	1	0.1995	0.1565	0.6949	
AC	0.1211	1	0.1211	0.0950	0.7599	
BC	0.0001	1	0.0001	0.0001	0.9917	
A^2	667.74	1	667.74	523.90	< 0.0001	
B^2	14.110	1	14.110	11.0700	0.0022	
C^2	3.390	1	3.3900	2.6600	0.1125	
ABC	0.0386	1	0.0386	0.0303	0.8629	
A^2B	0.0018	1	0.0018	0.0014	0.9704	
A^2C	0.0012	1	0.0012	0.0009	0.9758	
AB^2	2.3800	1	2.38	1.8700	0.1807	
AC^2	0.0006	1	0.0006	0.0005	0.9825	
B^2C	0.0011	1	0.0011	0.0009	0.9767	
BC^2	0.0188	1	0.0188	0.0147	0.9041	
A^3	152.87	1	152.87	119.94	< 0.0001	
B^3	0.1151	1	0.1151	0.0903	0.7657	
C^3	0.0073	1	0.0073	0.0057	0.9402	
Residual	42.060	33	1.27			
Cor Total	2184.68	52				

APPENDIX C

KANEKA validation data

Appendix C 1 Sodium surfactin's certificate of analysis from manufacturer

KANEKA

KANEKA CORPORATION
NEW BUSINESS DEVELOPMENT DEPARTMENT
2-3-18, NAKANOSHIMA, KITA-KU, OSAKA 530-8288, JAPAN
TEL: +81-6-6226-5109 E-mail: Surfactin@kn.kaneka.co.jp

SF-EN-001-02

Date of Issuance : Nov. 27 2017

CERTIFICATE OF ANALYSIS

Product Name : KANEKA Surfactin
INCI Name : Sodium Surfactin
Lot. No. : SF-S08

Tests	Acceptance Criteria	Results
Description	White powder with a slight characteristic odor	Conforms
Identification		
(1) Acid precipitation	Positive	Conforms
(2) Ninhydrin test	Negative	Conforms
(3) Biuret test	Positive	Conforms
(4) IR	Absorption maximum at around 1540, 1650, 1740, 2930, and 2960 cm^{-1}	Conforms
(5)Sodium ion	Positive	Conforms
pH of aqueous solution	6.5-8.0 (1% in distilled water)	7.3
Purity		
(1) Clarity of solution	Practically clear (1%)	Conforms
(2) Heavy metals	Not more than 20 ppm (as Pb)	Conforms
(3) Arsenic	Not more than 2 ppm	Conforms
(4) Water content	Not more than 10%	2.7%
Assay (Nitrogen)	8.0-9.0 % (Kjeldahl method)	9.0%

Certified by

M. Naruse

M. Naruse
Manager
Strategic Planning & Administration Group
New Business Development Department

Appendix C 2 Sodium *surfactin's* safety data sheet from manufacturer

Kaneka KANEKA CORPORATION
2-3-18 NAKANOSHIMA, KITA-KU, OSAKA 530-8288, JAPAN

C_{18}

KANEKA Surfactin - Technical Data Sheet
(Extra Pure Grade)

Chemical Name	Sodium Surfactin
INCI Name	Sodium Surfactin
CAS No.	302933-83-1
Molecular Formula	$C_{55-n}H_{95.5-2n}N_7O_{13}Na_{1.5}$
Molecular Weight	1036 (major species)
Concentration	More than 90%

Handwritten annotations:
leu — Leucine
Asp — Aspartic acid
Val — Valine

Handwritten labels on structure: L-Leu, D-leu, L-Asp, Cyclic peptide (Hydrophilic), L-Val, D-leu, L-Leu, L-Glu, -HC (Hydrophobic), +3/2Na⁺ + 1/2H⁺
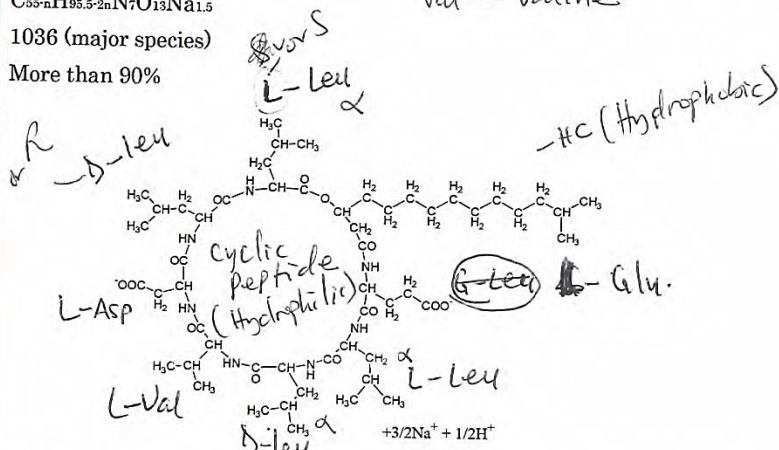
This product is sodium salts of the mixture of surfactin and its variants which have slightly different amino acid arrangements and fatty acid chains. The major species is shown. This product is produced by fermentation.

Chemical Structure

Appearance	White to whitish powder
Odor	Slight characteristic odor
Solubility	Dissolve in water and polar solvents such as MeOH, EtOH, etc.
pH	6.5-8.0 (1% in distilled water)

Powder	Store in an airtight container in cool area. Avoid areas with high temperature and high humidity levels.

179

Appendix C 3 FTIR analysis from Kaneka
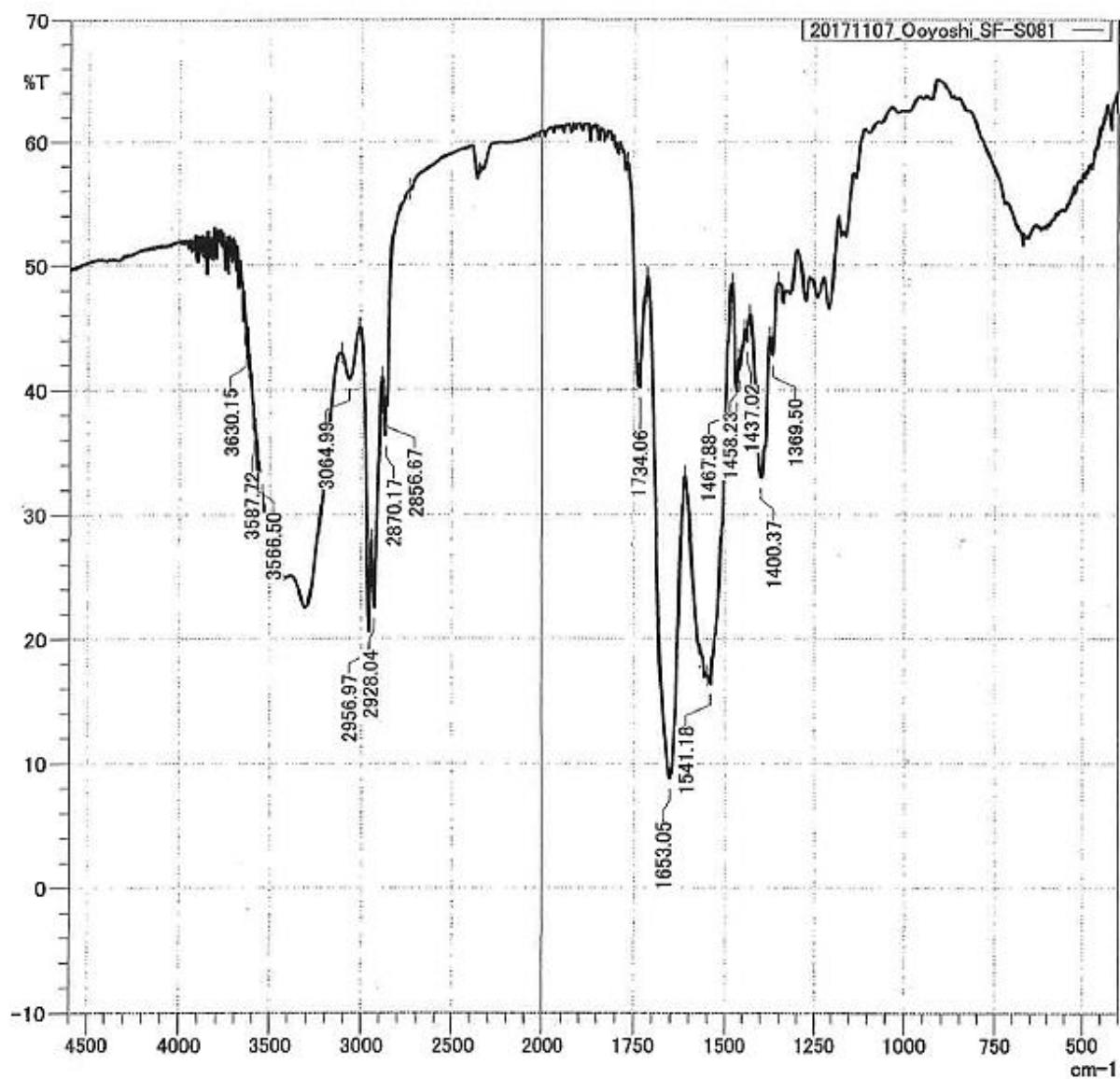
研究員用 - 1-142-2 - 20171107_Ooyoshi_SF-S081.ispd

APPENDIX D

Physicochemical Characterization Data

Appendix D1: Density characteristics of aqueous *surfactin*

0.025 % Surfactant dosage				0.05 % Surfactant dosage				0.075 % Surfactant dosage			
Temperature (°C)	M_{b+l} (g)	M_l (g)	Density (kg/m³)	Temperature (°C)	M_{b+l} (g)	M_l (g)	Density (kg/m³)	Temperature (°C)	M_{b+l} (g)	M_l (g)	Density (kg/m³)
-5.0			99.3210	-5.0			999.8670	-5.0			999.6020
0.0			999.3000	0.0			999.5900	0.0			999.5000
1.4	48.39	25.05	999.4335	1.3	48.39	25.05	999.4335	1.3	48.39	25.05	999.4335
3.8	48.39	25.05	999.4335	4.7	48.39	25.05	999.4335	4.5	48.39	25.05	999.4335
4.5	48.38	25.04	999.0345	5.6	48.39	25.05	999.4335	5.0	48.39	25.05	999.4335
5.5	48.38	25.04	999.0345	10.5	48.37	25.03	998.6355	10.1	48.38	25.04	999.0345
8.4	48.38	25.04	999.0345	15.5	48.35	25.01	997.8376	13.7	48.37	25.03	998.6355
10.0	48.38	25.04	999.0345	19.8	48.34	25.00	997.4386	15.4	48.36	25.02	998.2365
12.3	48.38	25.04	999.0345	20.5	48.33	24.99	997.0396	18.5	48.34	25.00	997.4386
14.2	48.36	25.02	998.2365	23.5	48.31	24.97	996.2417	20.5	48.32	24.98	996.6406
15.0	48.36	25.02	998.2365	25.0	48.30	24.96	995.8427	20.9	48.32	24.98	996.6406
17.4	48.36	25.02	998.2365	25.5	48.29	24.95	995.4437	25.5	48.31	24.97	996.2417
18.4	48.35	25.01	997.8376	30.0	48.27	24.93	994.6457	28.0	48.30	24.96	995.8427

20.0	48.34	25.00	997.4386	33.5	48.26	24.92	994.2468	30.8	48.28	24.94	995.0447
21.2	48.32	24.98	996.6406	36.0	48.25	24.91	993.8478	35.0	48.25	24.91	993.8478
25.5	48.31	24.97	996.2417	40.0	48.18	24.84	991.0550	38.5	48.22	24.88	992.6509
30.0	48.28	24.94	995.0447	45.0	48.15	24.81	989.8580	40.0	48.21	24.87	992.2519
35.6	48.24	24.90	993.4488	50.0	48.11	24.77	988.2621	46.6	48.16	24.82	990.2570
37.4	48.23	24.89	993.0498	55.0	48.07	24.73	986.6662	50.5	48.13	24.79	989.0601
39.6	48.21	24.87	992.2519								
40.0	48.21	24.87	992.2519								
45.0	48.19	24.85	991.4539								
50.3	48.13	24.79	989.0601								

Note: M_{b+l} =Mass of pycnometer + liquid surfactant mixture

M_l = Mass of liquid surfactant mixture

Density of aqueous surfactant @ 20.5 °C

Dosage (%)	Density (kg/m³)	
0.025	997.107	
0.05	997.04	
0.075	996.641	
0.1	997.04	Standard deviation
0.5	996.641	= 0.819864
1	999.034	Standard error
		= 0.136644

0.1 % Surfactant dosage				0.5 % Surfactant dosage				1.0 % Surfactant dosage			
Temperature (°C)	M_{b+l} (g)	M_l (g)	Density (kg/m³)	Temperature (°C)	M_{b+l} (g)	M_l (g)	Density (kg/m³)	Temperature (°C)	M_{b+l} (g)	M_l (g)	Density (kg/m³)
-5.0			998.6950	-5.0			997.5870	-5.0			1001.330
0.0			998.9900	0.0			998.9200	0.0			1001.548
1.3	48.38	25.04	999.0345	1.3	48.39	25.05	999.4335	1.3	48.43	25.09	1001.029
4.0	48.39	25.05	999.4335	4.0	48.41	25.07	1000.231	4.0	48.43	25.09	1001.029
5.0	48.39	25.05	999.4335	5.5	48.41	25.07	1000.231	5.2	48.43	25.09	1001.029
10.0	48.37	25.03	998.6355	8.0	48.41	25.07	1000.231	10.7	48.42	25.08	1000.630
13.5	48.36	25.02	998.2365	10.0	48.4	25.06	999.8324	12.6	48.42	25.08	1000.630
15.5	48.36	25.02	998.2365	14.0	48.39	25.05	999.4335	13.6	48.41	25.07	1000.231
18.3	48.35	25.01	997.8376	15.5	48.39	25.05	999.4335	15.2	48.40	25.06	999.8324
20.5	48.33	24.99	997.0396	18.3	48.37	25.03	998.6355	17.0	48.40	25.06	999.8324
21.1	48.32	24.98	996.6406	20.5	48.32	24.98	996.6406	18.4	48.38	25.04	999.0345
25.5	48.3	24.96	995.8427	23.5	48.31	24.97	996.2417	20.5	48.38	25.04	999.0345
28.0	48.29	24.95	995.4437	26.0	48.31	24.97	996.2417	24.6	48.36	25.02	998.2365
30.0	48.28	24.94	995.0447	30.0	48.28	24.94	995.0447	25.5	48.35	25.01	997.8376
35.0	48.24	24.9	993.4488	35.4	48.25	24.91	993.8478	30.5	48.32	24.98	996.6406
37.5	48.22	24.88	992.6509	40.0	48.23	24.89	993.0498	33.0	48.31	24.97	996.2417
40.0	48.2	24.86	991.8529	45.7	48.2	24.86	991.8529	36.3	48.28	24.94	995.0447
45.5	48.16	24.82	990.2570	46.4	48.17	24.83	990.6560	39.4	48.27	24.93	994.6457
50.3	48.11	24.77	988.2621	50.8	48.15	24.81	989.8580	42.0	48.22	24.88	992.6509
								46.4	48.21	24.87	992.2519
								50.5	48.15	24.81	989.8580

Appendix D 2 pH characteristics of aqueous *surfactin*

0.025 % dosage		0.05 % dosage		0.075 % dosage		0.1 % dosage		0.5 % dosage		1.0 % dosage	
Temp. (°C)	pH	Temp. (°C)	pH	Temp. (°C)	pH	Temp. (°C)	pH	Temp. (°C)	pH	Temp. (°C)	pH
1.0	6.07	1.0	6.07	1.0	6.08	1.0	6.76	1.0	7.20	1.0	7.27
4.0	6.37	4.0	6.37	4.0	6.23	4.0	6.88	4.0	7.26	4.0	7.27
4.2	6.39	4.5	6.42	4.5	6.49	4.5	6.90	4.5	7.27	4.5	7.27
4.5	6.39	5.6	6.53	5.0	6.75	5.0	6.92	4.6	7.27	5.0	7.27
4.8	6.40	6.0	6.55	6.0	6.78	9.8	6.99	5.0	7.28	5.5	7.27
5.5	6.40	8.7	6.61	8.0	6.80	10.5	7.02	5.2	7.28	6.0	7.27
7.5	6.45	10.0	6.61	10.1	6.86	11.5	7.03	6.0	7.28	6.5	7.27
8.3	6.47	10.4	6.61	15.5	6.95	13.5	7.07	8.5	7.28	10.8	7.26
9.5	6.48	14.1	6.71	16.0	6.96	15.0	7.07	10.0	7.29	11.5	7.26
10.0	6.51	15.5	6.73	17.0	6.96	15.5	7.07	12.4	7.30	13.0	7.27
12.0	6.55	20.5	6.78	18.5	6.96	20.0	7.07	12.5	7.29	15.5	7.27
14.1	6.56	21.5	6.85	20.5	6.96	20.5	7.07	13.5	7.30	17.0	7.27
14.5	6.60	25.0	6.84	23.5	6.96	21.5	7.07	14.5	7.31	18.0	7.27
15.0	6.62	27.0	6.84	25.0	6.96	25.5	7.09	15.5	7.31	18.5	7.27
18.4	6.65	30.0	6.85	26.0	6.96	28.5	7.11	18.4	7.30	20.5	7.28
19.1	6.65	31.0	6.85	28.0	6.96	30.6	7.13	20.5	7.31	25.0	7.26

20.5	6.68	35.0	6.85	30.5	6.97	35.5	7.13	25.5	7.30	30.5	7.24
21.2	6.69	40.0	6.85	35.0	6.99	37.5	7.14	26.7	7.30	32.5	7.24
25.5	6.73	45.0	6.85	36.5	6.99	40.0	7.14	30.0	7.30	39.5	7.21
28.1	6.74	47.5	6.88	44.5	6.96	42.5	7.13	35.8	7.30	40.0	7.21
30.4	6.76	50.5	6.88	46.2	6.99	45.2	7.13	38.0	7.30	45.0	7.22
35.0	6.77	52.5	6.85	48.8	7.00	47.5	7.10	40.0	7.30	46.4	7.22
37.4	6.78	55.0	6.85	50.4	6.99	50.0	7.10	45.0	7.30	50.0	7.23
40.0	6.77							50.0	7.30	56.0	7.24
45.0	6.77										
50.0	6.75										

Aqueous surfactant pH data @ 20.5 ºC

Dosage (%)	pH	
0.025	6.68	
0.05	6.78	
0.075	6.96	
0.1	7.07	Standard deviation
0.5	7.31	= 0.25719
1.0	7.28	Standard error
		= 0.03913

Appendix D 3 Conductivity characteristics of aqueous surfactin

0.025 % dosage		0.05 % dosage		0.075 % dosage		0.1 % dosage		0.5 % dosage		1.0 % dosage	
Temp. (°C)	Cond. (mS/cm)	Temp. (°C)	Cond. (mS/cm)	Temp. (°C)	Cond. (mS/cm)	Temp. (°C)	Cond. (mS/cm)	Temp. (°C)	Cond. (mS/cm)	Temp. (°C)	Cond. (mS/cm)
1.0	119.0	1.0	83.22	1.0	108.0	1.0	144.9	1.0	538.5	1.1	974.4
1.5	118.8	1.5	82.75	1.5	107.7	1.5	144.4	1.5	537.9	1.5	971.6
2.0	118.5	2.0	82.55	2.0	107.3	2.0	143.9	2.0	535.7	2.0	968.7
2.5	118.2	2.5	82.25	2.5	106.9	2.5	143.3	2.5	532.8	2.5	965.8
3.0	118.0	3.0	81.98	3.0	106.6	3.0	142.8	3.0	531.3	3.0	962.8
3.5	117.8	3.5	81.75	3.5	106.2	3.5	142.3	3.5	530.6	3.5	959.5
4.0	117.5	4.0	81.38	4.0	105.9	4.0	141.9	4.0	529.7	4.0	956.7
4.5	117.3	4.5	81.27	4.5	105.6	4.5	141.6	4.5	528.9	4.5	954.6
5.0	117.1	5.0	81.08	5.0	105.3	5.0	141.2	5.0	526.8	5.0	952.0
5.5	116.7	5.5	80.89	5.5	105.1	5.5	140.8	5.5	525.8	5.5	950.4
6.0	116.5	6.0	80.71	6.0	104.8	6.0	140.5	6.0	524.1	6.0	948.3
6.5	116.0	6.5	80.56	6.5	104.6	6.5	140.1	6.5	523.3	6.5	946.3
7.0	116.0	7.0	80.41	7.0	104.4	7.0	140.1	7.0	522.3	7.0	944.6
7.5	115.0	7.5	80.27	7.5	104.2	7.5	139.7	7.5	521.3	7.5	943.0
8.0	114.6	8.0	80.19	8.0	104.1	8.0	139.5	8.0	521.0	8.0	941.5
8.5	114.3	8.5	80.05	8.5	104.0	8.5	139.3	8.5	520.5	8.5	940.3
9.0	114.0	9.0	79.97	9.0	103.8	9.0	139.1	9.0	519.7	9.0	939.2
9.5	113.8	9.5	79.89	9.5	103.7	9.5	139.1	9.5	519.0	9.5	938.3
10.0	113.5	10.0	79.83	10.0	103.7	10.0	139.0	10.0	518.2	10.0	937.2
10.5	113.2	10.5	79.76	10.5	103.6	10.5	138.6	10.5	518.5	10.5	936.2
11.0	113.0	11.0	79.69	11.0	103.6	11.0	138.6	11.0	518.3	11.0	935.7
11.5	112.8	11.5	79.65	11.5	103.5	11.5	138.7	11.5	518.0	11.5	934.9
12.0	112.6	12.0	79.61	12.0	103.5	12.0	138.6	12.0	517.2	12.0	934.5
15.5	112.0	12.5	79.57	12.5	103.4	12.5	138.6	12.5	517.1	12.5	933.9
16.0	111.8	13.0	79.55	13.0	103.4	13.0	138.6	13.0	517.0	13.0	933.4
16.5	111.7	13.5	79.53	13.5	103.4	13.5	138.6	13.5	516.9	13.5	933.0
17.0	111.6	14.0	79.52	14.0	103.4	14.0	138.6	14.0	516.8	14.0	932.6
17.5	111.5	14.5	79.52	14.5	103.4	14.5	138.6	14.5	516.6	14.5	932.3
18.0	111.8	15.0	79.52	15.0	103.4	15.0	138.6	15.0	516.5	15.0	932.0
18.5	111.8	15.5	79.53	15.5	103.4	15.5	138.6	15.5	516.6	15.5	931.8
19.0	111.6	16.0	79.55	16.0	103.4	16.0	138.6	16.0	516.8	16.0	931.5
19.5	111.6	16.5	79.58	16.5	103.4	16.5	138.7	16.5	516.8	16.5	931.5
20.0	111.5	17.0	79.60	17.0	103.5	17.0	138.7	17.0	517.2	17.0	931.5
20.5	111.5	17.5	79.64	17.5	103.5	17.5	138.8	17.5	517.3	17.5	931.5

21.0	111.4	18.0	79.67	18.0	103.6	18.0	138.8	18.0	517.4	18.0	931.5
21.5	111.4	18.5	79.72	18.5	103.6	18.5	139.0	18.5	517.5	18.5	931.8
22.0	111.3	19.0	79.79	19.0	103.7	19.0	139.1	19.0	517.6	19.0	932.2
22.5	111.3	19.5	79.83	19.5	103.8	19.5	139.1	19.5	517.9	19.5	932.4
23.0	111.3	20.0	79.89	20.0	103.9	20.0	139.2	20.0	518.0	20.0	932.9
23.5	111.3	20.5	79.95	20.5	104.0	20.5	139.3	20.5	518.2	20.5	933.3
24.0	111.3	21.0	80.06	21.0	104.1	21.0	139.4	21.0	518.5	21.0	934.2
24.5	111.4	21.5	80.15	21.5	104.2	21.5	139.5	21.5	518.7	21.5	934.7
25.0	111.5	22.0	80.23	22.0	104.3	22.0	139.7	22.0	519.0	22.0	935.5
25.5	111.5	22.5	80.31	22.5	104.4	22.5	139.9	22.5	519.3	22.5	936.5
26.0	111.5	23.0	80.40	23.0	104.6	23.0	140.0	23.0	519.6	23.0	937.4
26.5	111.6	23.5	80.50	23.5	104.8	23.5	140.2	23.5	519.9	23.5	938.1
27.0	111.6	24.0	80.58	24.0	104.9	24.0	140.3	24.0	520.2	24.0	938.9
27.5	111.6	24.5	80.67	24.5	105.0	24.5	140.5	24.5	520.7	24.5	939.5
28.0	111.7	25.0	80.77	25.0	105.2	25.0	140.7	25.0	521.1	25.0	940.4
28.5	111.7	25.5	80.88	25.5	105.3	25.5	140.9	25.5	521.6	25.5	941.2
29.0	111.8	26.0	80.99	26.0	105.5	26.0	141.2	26.0	522.0	26.0	942.3
29.5	111.8	26.5	81.02	26.5	105.6	26.5	141.4	26.5	522.5	26.5	943.2
30.0	111.9	27.0	81.24	27.0	105.7	27.0	141.7	27.0	523.0	27.0	944.1
30.5	112.0	27.5	81.35	27.5	105.9	27.5	142.0	27.5	523.4	27.5	945.2
31.0	112.1	28.0	81.48	28.0	106.1	28.0	142.2	28.0	524.0	28.0	946.2
31.5	112.2	28.5	81.59	28.5	106.2	28.5	142.5	28.5	524.6	28.5	947.2
32.0	112.3	29.0	81.73	29.0	106.4	29.0	142.9	29.0	525.2	29.0	948.4
32.5	112.5	29.5	81.82	29.5	106.6	29.5	143.1	29.5	525.8	29.5	949.6
33.0	112.7	30.0	81.94	30.0	106.7	30.0	143.3	30.0	526.6	30.0	951.1
33.5	112.8	30.5	82.14	30.5	106.9	30.5	143.5	30.5	527.1	30.5	952.4
34.0	112.9	31.0	82.24	31.0	107.1	31.0	143.8	31.0	527.8	31.0	953.9
34.5	113.0	31.5	82.36	31.5	107.2	31.5	144.0	31.5	528.5	31.5	955.6
35.0	113.1	32.0	82.47	32.0	107.4	32.0	144.1	32.0	529.3	32.0	958.0
35.5	113.2	32.5	82.62	32.5	107.6	32.5	144.3	32.5	530.0	32.5	959.6
36.0	113.3	33.0	82.73	33.0	107.8	33.0	144.6	33.0	530.8	33.0	960.8
36.5	113.4	33.5	82.86	33.5	108.0	33.5	144.8	33.5	531.6	33.5	962.2
37.0	113.5	34.0	82.99	34.0	108.2	34.0	145.1	34.0	532.2	34.0	963.5
37.5	113.7	34.5	83.12	34.5	108.5	34.5	145.4	34.5	533.2	34.5	965.0
38.0	113.9	35.0	83.25	35.0	108.7	35.0	145.9	35.0	533.8	35.0	966.2
38.5	114.0	35.5	83.39	35.5	108.9	35.5	146.3	35.5	534.6	35.5	967.5
39.0	114.2	36.0	83.53	36.0	109.1	36.0	146.5	36.0	535.2	36.0	970.3
39.5	114.2	36.5	83.67	36.5	109.3	36.5	146.8	36.5	536.0	36.5	971.8

40.0	114.7	37.0	83.82	37.0	109.5	37.0	147.1	37.0	536.7	37.0	973.9
40.5	115.0	37.5	83.98	37.5	109.7	37.5	147.3	37.5	537.5	37.5	976.3
41.0	115.4	38.0	84.14	38.0	109.9	38.0	147.6	38.0	538.4	38.0	978.5
41.5	115.9	38.5	84.29	38.5	110.1	38.5	147.9	38.5	539.3	38.5	980.7
42.0	116.6	39.0	84.47	39.0	110.3	39.0	148.1	39.0	540.3	39.0	982.7
42.5	117.4	39.5	84.64	39.5	110.5	39.5	148.4	39.5	541.3	39.5	985.5
43.0	117.6	40.0	84.79	40.0	110.8	40.0	148.6	40.0	542.3	40.0	988.6
43.5	117.7	40.5	84.97	40.5	111.0	40.5	148.9	40.5	543.5	40.5	992.2
44.0	117.9	41.0	85.15	41.0	111.3	41.0	149.2	41.0	544.5	41.0	997.2
44.5	118.1	41.5	85.34	41.5	111.6	41.5	149.5	41.5	545.6	41.5	999.8
45.0	118.6	42.0	85.57	42.0	111.9	42.0	149.9	42.0	546.6	42.0	1001.2
		42.5	85.73	42.5	112.2	42.5	150.2	42.5	547.6	42.5	1003.6
		43.0	85.89	43.0	112.5	43.0	150.6	43.0	548.8	43.0	1005.3
		43.5	86.06	43.5	112.8	43.5	151.0	43.5	549.9	43.5	1006.7
		44.0	86.25	44.0	113.1	44.0	151.3	44.0	551.2	44.0	1008.5
		44.5	86.42	44.5	113.5	44.5	151.7	44.5	552.7	44.5	1010.3
		45.0	86.61	45.0	113.9	45.0	152.0	45.0	554.1	45.0	1012.2
		45.5	86.80	45.5	114.2	45.5	152.6	45.5	556.1	45.5	1014.5
		46.0	87.02	46.0	114.5	46.0	153.1	46.0	557.6	46.0	1016.3
		46.5	87.28	46.5	114.8	46.5	153.5	46.5	558.7	46.5	1019.2
		47.0	87.54	47.0	115.2	47.0	153.9	47.0	559.8	47.0	1021.7
		47.5	87.85	47.5	115.5	47.5	154.4	47.5	560.7	47.5	1024.5
		48.0	88.23	48.0	115.8	48.0	154.8	48.0	561.8	48.0	1028.7
		48.5	88.84	48.5	116.1	48.5	155.2	48.5	562.9	48.5	1032.9
		49.0	89.18	49.0	116.4	49.0	155.2	49.0	563.8	49.0	1039.6
		49.5	89.63	49.5	116.7	49.5	156.0	49.5	564.8	49.5	1044.5
		50.0	89.98	50.0	117.0	50.0	156.6	50.0	565.8	50.0	1046.3
		50.5	90.58	50.5	117.3	50.5	157.2	50.5	567.0	50.5	1048.4

Conductivity of Aqueous surfactant data @ 20.5 ºC

Dosage (%)	pH	
0.025	110.4	
0.05	79.30	
0.075	104.0	
0.10	139.5	Standard deviation
0.50	518.6	= 315.757
1.00	934.7	Standard error
		= 52.62621

Appendix D 4 Physicochemical characteristics of surfactin in saline medium

	0 M Salinity					
Dosage (%)	**0.025**	**0.05**	**0.075**	**0.1**	**0.5**	**1**
Density (kg/m³)	997.107	997.04	996.641	997.04	996.641	999.034
pH	6.68	6.78	6.96	7.07	7.31	7.28
Conductivity (mS/cm)	0.1115	0.07995	0.104	0.1393	0.5182	0.9333
	0.05 M Salinity					
Dosage (%)	**0.025**	**0.05**	**0.075**	**0.1**	**0.5**	**1**
Density (kg/m³)	999.034	999.034	999.034	999.034	1000.63	1000.63
pH	6.6	6.72	6.74	6.78	6.88	6.81
Conductivity (mS/cm)	5.713	5.726	5.732	5.748	5.971	6.246
	0.1 M Salinity					
Dosage (%)	**0.025**	**0.05**	**0.075**	**0.1**	**0.5**	**1**
Density (kg/m³)	1001.029	1001.029	1001.029	1001.029	1001.827	1001.827
pH	6.44	6.54	6.55	6.6	6.67	6.68
Conductivity (mS/cm)	10.84	10.86	10.88	10.89	11.06	11.27
	0.25 M Salinity					
Dosage (%)	**0.025**	**0.05**	**0.075**	**0.1**	**0.5**	**1**
Density (kg/m³)	1007.812	1007.413	1007.413	1007.413	1008.211	1009.009
pH	6.23	6.3	6.35	6.36	6.43	6.46
Conductivity (mS/cm)	25.44	25.42	25.42	25.43	25.42	25.47
	0.5 M Salinity					
Dosage (%)	**0.025**	**0.05**	**0.075**	**0.1**	**0.5**	**1**
Density (kg/m³)	1016.988	1016.988	1016.988	1016.988	1017.786	1018.584
pH	6.07	6.15	6.19	6.2	6.24	6.3
Conductivity (mS/cm)	46.9	46.9	46.87	46.87	46.7	46.41
	1.0 M Salinity					
Dosage (%)	**0.025**	**0.05**	**0.075**	**0.1**	**0.5**	**1**
Density (kg/m³)	1035.74	1036.538	1036.538	1036.538	1036.538	1036.937
pH	6.31	6.34	6.37	6.4	6.43	6.44
Conductivity (mS/cm)	84.43	83.89	83.39	82.98	76.98	69.55
	1.5 M Salinity					
Dosage (%)	**0.025**	**0.05**	**0.075**	**0.1**	**0.5**	**1**
Density (kg/m³)	1054.891	1054.891	1054.492	1054.492	1055.290	1055.689
pH	6.32	6.35	6.38	6.39	6.41	6.44
Conductivity (mS/cm)	118.1	118.0	117.9	117.9	116.9	115.5

Appendix E

Published papers

Appendix E 1 Published papers

Solubility trapping as a potential secondary mechanism for CO_2 sequestration during enhanced gas recovery by CO_2 injection in conventional natural gas reservoirs: An experimental approach

Muhammad Kabir Abba[*], Abubakar J. Abbas, Ghasem G. Nasr, Athari Al-Otaibi, Martin Burby, Bello Saidu, Salihu M. Suleiman

The University of Salford, Manchester, UK

ARTICLE INFO

ABSTRACT

This study aims to experimentally investigate the potential of solubility trapping mechanism in increasing CO_2 storage during EGR by CO_2 injection and sequestration in conventional natural gas reservoirs. A laboratory core flooding process was carried out to simulate EGR on a sandstone core at 0, 5, 10 wt% NaCl formation water salinity at 1300 psig, 50 °C and 0.3 ml/min injection rate. The results show that CO_2 storage capacity was improved significantly when solubility trapping was considered. Lower connate water salinities (0 and 5 wt%) showed higher CO_2 solubility from IFT measurements. With 10% connate water salinity, the highest accumulation of the CO_2 in the reservoir was realised with about 63% of the total CO_2 injected stored; an indication of improved storage capacity. Therefore, solubility trapping can potentially increase the CO_2 storage capacity of the gas reservoir by serving as a secondary trapping mechanism in addition to the primary structural and stratigraphic trapping and improving CH_4 recovery.

1. Introduction

The incessant utilisation of fossil fuels as sources of energy invariably increases greenhouse gases (GHG) emissions in the atmosphere and eventually lead to the proliferation of global warming. The reduction of these GHG emissions has become paramount, and it is gaining significant attention globally due to its environmental consequences. The main component of the GHGs responsible for nearly 64% of the accrued negative effect on the environment is CO_2 (Ding et al., 2018). Thus, reduction of this anthropogenic CO_2 emission cannot be overemphasised. Carbon Capture technology is a potential approach to reducing the CO_2 emissions from heavy industries (Ding et al., 2018; Li et al., 2013; Pereira et al., 2017) followed by the geological/underground storage and sequestration of the captured CO_2 (Burton et al., 2009; Ganjdanesh and Hosseini, 2017; Mijic et al., 2014; Mutailipu et al., 2018a). In all the underground storage sites, oil and gas reservoirs have the potential or appeal to provide additional throughput in the form of economic incentives (Ding et al., 2018; Kalra and Wu, 2014). These incentives are realised through enhanced recovery techniques – miscible flooding technique in enhanced oil recovery and CO_2 injection in enhanced gas recovery processes. However,

natural gas reservoirs have the upper hand in terms of potential and practicality storage compared to the oil reservoirs due to their existing gas storage capability (Ding et al., 2018). Gas reservoirs have stored natural gas for long periods of time safely without the penchant for surrounding leaks. The extraction of gas from conventional natural gas reservoirs does not require complex processes of altering the reservoir matrix to enhance its production because primary recovery can be in excess of 80% (van der Meer, 2005) depending on the drive mechanism. Oil reservoirs, on the other hand, must be subjected to an array of complex process through artificial stimulation techniques like hydraulic fracturing or matrix acidizing in order to enhance the production which in turn tends to affect the reservoir integrity, and a potential CO_2 leakage and contamination of adjacent freshwater aquifers will ensue overtime as emphasised by (Xiao et al., 2016). CO_2 is a medium for the mobilisation of oil in the reservoir during tertiary recovery and the risk associated with the leaks is the transportation of complex organic compounds present in the crude oil like benzene, toluene, ethylbenzene and xylenes (BTEX) which are highly toxic (Cantrell and Brown, 2014) into adjacent aquifers through fissures and fracture propagation resulting from recovery techniques. This reason, among others as pointed in the works of Kalra et al. (2014), highlights the choice of natural gas

reservoirs as potential sequestration site for anthropogenic CO_2 emissions albeit the current natural gas market compared to oil prices from an economic standpoint. Nonetheless, the drive to exploit the economic viability of EGR through understanding the physics of mixing between the injected CO_2 and the recovered CH_4 and its minimisation should be upheld.

Accordingly, conventional natural gas reservoirs have a storage capacity limitation compared to the most ideal choice i.e. deep saline aquifers (Sminchak et al., 2017) for CO_2 sequestration. Deep saline aquifer utilises a combination of different trapping mechanisms (structural and stratigraphic, solubility, residual, mineral) to store the injected CO_2 and as such increases, significantly, its storage potential. Conversely, the primary trapping mechanism for CO_2 in conventional natural gas reservoirs is structural trapping owing to the geological seals of the reservoir (cap rock) which prevents the natural resource from migrating to the upper strata of the overlying formations and in this case the injected CO_2. However, an additional trapping mechanism that can be explored to further improve the storage capacity of the conventional natural gas reservoir i.e. the solubility trapping mechanism of the CO_2 in the formation water. This can potentially be exploited in tandem with the primary trapping mechanism to increase the storability of the natural gas reservoir. As a secondary CO_2 geological trapping mechanism post injection time (Li et al., 2013), significant volume of CO_2 can be dissolved and stored in the formation water given the high solubility of CO_2 in water. In most cases, solubility trapping mechanism in the purview of CO_2 storage is usually associated, investigated, and adapted in deep saline aquifers alone (Chen et al., 2018; Ding et al., 2018; Jia et al., 2017; Li et al., 2013; Nakajima and Xue, 2017; Oh et al., 2017; Raza et al., 2016; L M Valle et al., 2018; L.M. Valle et al., 2018). Experimental investigation of solubility trapping mechanism in unconventional natural gas reservoirs during EGR is, to the author's knowledge, limited and the practicality of its effectiveness in this regard needs to be evaluated to further present its potential as a viable option for CO_2 sequestration.

Furthermore, CO_2 displaces CH_4 during EGR by advection or diffusion mechanism where displacement is either controlled by interstitial velocity or concentration gradient, unlike EGR by CO_2 injection in unconventional natural gas reservoirs, like coal bed methane and shale gas, whose mechanisms of displacement are desorption of the CH_4 and adsorption of CO_2 where selective adsorption depends on the clay content of the rock (Duan et al., 2016). This displacement mechanism in EGR for this study is quintessential to the assessment of the storability of the injected CO_2 and the recovery of the nascent CH_4 and the interplay between them in the conventional reservoir. The influence of the connate water salinity and its presence in the conventional natural gas reservoir during EGR has already been established in our previous work (Abba et al., 2018). Therefore, this study aims to highlight, experimentally, the feasibility of solubility trapping, in addition to structural trapping, as a secondary trapping mechanism during enhanced gas recovery by CO_2 injection and assess its potential to increase the storage capacity of the reservoirs with respect to natural gas recovery efficiency in conventional sandstone reservoirs.

2. Materials and method

In this study, a core flooding experiment was carried which involved the injection of CO_2 through a core sample saturated with CH_4 and connate water at different salinities. The core sample used was *Grey Berea* sandstone with petrophysical properties and dimensions as shown in Table 1. The salinities of the connate water used were 0, 5, 10 wt% NaCl.

2.1. Materials

High purity Carbon Dioxide and Methane with purities of > 99.999% were used and sourced from BOC UK which is a member

Table 1
Core sample dimensions and petrophysical properties.

Core sample	Length (mm)	Diameter (mm)	Porosimetry Porosity (%)	Gas Permeability (md)
Grey Berea	76.27	25.22	20.3	217

of Linde Group. The core sample was acquired from Kocurek USA. General purpose NaCl salt used in this study was supplied by Fisher Scientific UK.

2.2. Experimental method

A series of experiments were carried out to achieve the aim set out in this study. The core sample was first characterised to evaluate the petrophysical properties of the core sample for concise and dependable measurements of the parameters under investigation. Brines of different test salinities were prepared which were used for the investigation. After these preliminary preparatory tasks were carried out, a core flooding process was conducted on the core sample to evaluate the displacement efficiency of the process in the presence of the test connate water prepared. 5 tests for individual brine concentrations were carried out. The effluent compositions were analysed using gas chromatography at different time intervals using the configured sampling valve. Details of the procedure and set up are presented in our earlier work (Abba et al., 2017). The effluent rates were measured and recorded by the downstream flow meters. These provided the volumes produced by displacement of CH_4 by the injected CO_2 and paved a way to quantify the trapped or stored CO_2 in the core sample after substantial recovery of the desired CH_4. The solubility through interfacial interaction between the different gases in different brine salinities for all the experiments was studied using the rising bubble method of interfacial tension measurement. Details of the experimental set up and procedure is shown in section 2.2.4.

2.2.1. Brine preparation

The connate water of different salts concentration was prepared in a round bottom flask with a magnetic stirrer on a magnetic plate. The stirring was kept at a medium rate as precautionary measure to obtain a homogeneous solution of the brine where all the solute was fully dissolved. Two brines of 5, 10 wt% NaCl concentrations were prepared to simulate the formation water salinities for the investigation.

2.2.2. Core sample saturation

For this study, 10% of characterised core sample was then saturated with the distilled water and prepared brines (5, 10 wt%) to represent the connate water using the vacuum saturation method. Given the nature of the core sample used and the core flooding equipment, 10% saturation was ideal as it provided sufficient surface area for the fluid-rock interaction within the pore matrix. Furthermore, it reduced the risk of damage to the core holder, back pressure regulator and tubing of the core flooding equipment from the acidic effluents formed by the interaction of the supercritical CO_2 and the simulated connate water. Equivalent volume to 10% of the pore volume of the core sample of the tests brines was injected using the set-up in Fig. 1 under vacuum to establish the connate water saturation in the core sample.

2.2.2.1. Apparatus and procedure. Saturation set up shown in Fig. 1. To carry out the saturation process, an equivalent volume of 10% of the core sample's pore volume of brine is measured out and placed in a hydrophobic syringe. The core sample (dried and weighted) was placed in the air tight sleeve in the vacuum chamber. Valve 1 was shut and valve 2 was open and the vacuum pump was run. Valve 2 was then shut off and valve 1 was opened and the brine was injected and valve 1 was shut off. The set up was allowed to sit for 4 h. Slowly, the vacuum
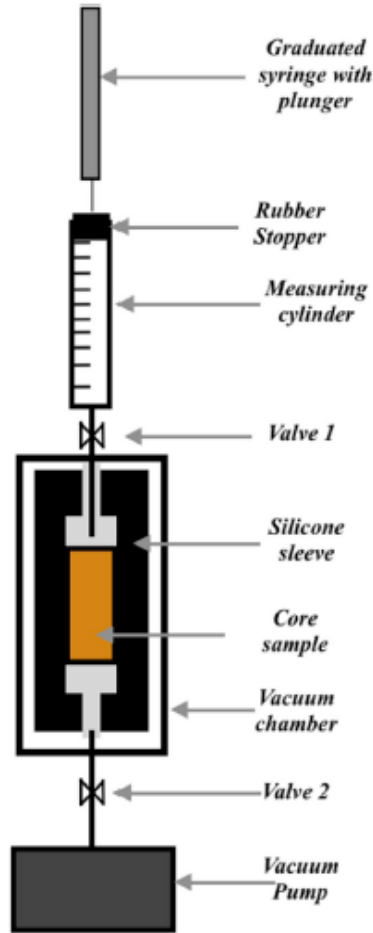
2

191

Fig. 1. Vacuum saturation set up.

considered based on the gas zone density of 0.22 psi/ft, and the injection rate was from our previous work). And as aforementioned, the CO_2 injection was done employing the same procedure, operational conditions and equipment details used in our previous work (Abba et al., 2017). The set-up works based on the principle of Darcy law which defines fluid flow in porous media and its schematics is shown in Fig. 2. An unsteady state flow was adopted to evaluate the mass balance between the injected CO_2 and the effluents realised – which comprised of the displaced CH_4 and the injected CO_2. The concentration profile was measured and recorded at 4–5 min intervals with the corresponding effluent flowrates. And the run came to an end when there were insignificant volumes of CH_4 in the produced effluents.

2.2.4. Interfacial tension measurement (IFT)

Several works have been carried out to measure the interfacial tension in CO_2-brine, CH_4-brine, CO_2-brine-CH_4 systems at different conditions (Amin et al., 2010; Arabloo et al., 2016; Bagalkot et al., 2018; Barati-Harooni et al., 2016; Chow et al., 2016; Dehghan et al., 2015; Duchateau and Broseta, 2012; Kamari et al., 2017; Kashefi et al., 2016; Khaksar Manshad et al., 2016; Mohammad Salehi et al., 2017; Mutailipu et al., 2018a, 2018b; Pereira et al., 2017; Rashid et al., 2017; Stukan et al., 2012; Yasuda et al., 2015) and the relationship between the interfacial tension and solubility highlighted. These investigations have shown that the forces that exist at the interfaces between two phases or fluids interacting are a function of the densities, the temperature and pressures of the fluids system. And there exist mass transfer between the phases in contact which can be well attributed to the solubility of one species of the fluids in another.

2.2.4.1. Apparatus and procedure. Here, the interfacial tension measurement was done to assess the dissolution of the injected CO_2 for the duration of CH_4 displacement for EGR as a result mass transfer between the phases. Each connate water solution with a specific concentration was used to measure the IFT between the connate water and the gases at the core flooding conditions of 1300 psig and 50 °C. The rising bubble technique was used to carry out the measurement using the set up as shown in Figure below. A Corelab high pressure high temperature surface energy experimental set up was used (see Fig. 3). It comprised of the high pressure measurement cell which can withstand pressures of up to 10,000 psig, a Rame-Hart optical system with digital image processing software used for the IFT determination using image analysis of the bubble, a high pressure HiP 62-6-10 manual pump with a pressure rating of 10,000 psig for charging the external phase (brine) and a Temco temperature controller. The IFT is measured using DropImage software which uses a theoretical algorithm to evaluate the parameter based on the bubble profile generated.

Before the measurements, precautionary steps were taken to rid the system of any contaminant and ensure proactive experiments in obtaining reliable results. The accumulators (1&2), the IFT cell (4), the injection needle (10), the delivery tubing was soaked in acetone for 2 h, and this step was repeated for all new samples being investigated. These components were coupled back together and then evacuated using vacuum pump (8). Hot distilled water was then placed inside the accumulators and then injected into IFT cell to flush the whole system. Dry compressed air was then used to dry the entire system in preparation for the IFT measurements.

The external phases (brine/distilled water) were charged into the cell using the manual pump till the desired pressure was attained and also the temperature was set using Corelab temperature controller with an accuracy of ± 0.3 °C as the system pressure was set in order to maintain the temperature at the desired temperature. After the pressures and temperatures have stabilised, the gases (CH_4 or CO_2) were then introduced into the drop phase accumulator. Then the manual pump was used to pressurise the gas in the accumulator to the desire test pressures slightly above the cell pressure. Creating the bubble

pressure was released, by opening the valve 2, and brought the chamber to atmospheric pressure. The now saturated core sample was weighed to verify the saturated volume. The saturated core sample was then prepared by wrapping it in cling film and foil paper. The cling film helps in preventing the foil paper from sticking to the core sample which makes it difficult to remove and clean while the foil paper help to preserve the *vitton* sleeve integrity by reducing the permeation of the supercritical CO_2 from the core sample through the sleeve. This CO_2 permeation can also cause overburden pressure fluctuations, in that the CO_2 passes through the vitton sleeve into the annulus of the core holder set-up housing the hydraulic oil which simulates the overburden pressure on the core sample.

Prior to every experiment, the core sample was cleaned using Soxhlet extraction were a reflux of methanol cycles was used to remove any traces of inorganic compounds (in this case NaCl salts) to restore the original state of the core sample for consistency. Drying in the oven at 100 °C overnight followed. This ensured the removal of any moisture and reagents used in the cleaning process.

2.2.3. Core flooding process

The core flooding process was carried out at 1300 psig and 0.3 mL/min injection rate using the set up shown in Fig. 2 (the pressure was
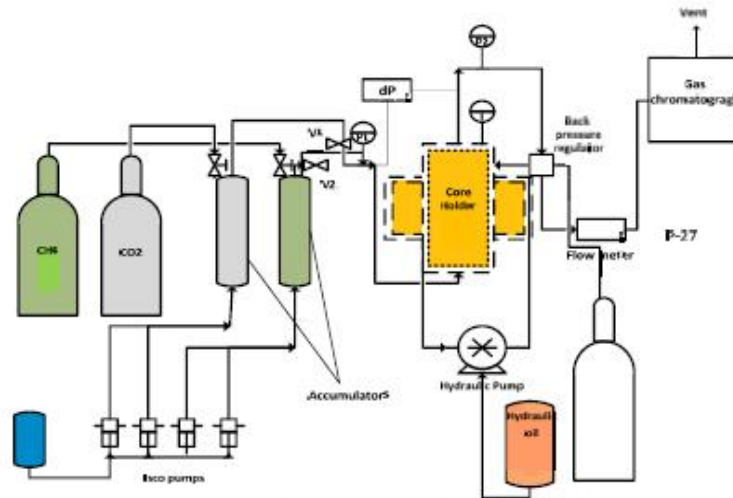
Fig. 2. Schematics of core flooding set up.

inside the test cell was done by gently opening the injection needle valve and monitoring the development of the bubble. The bubble development and collapse were recorded using the DropImage software based on the Young-Laplace equation. Details of which are discussed in Section 3.1.3.

This bubble measurement was repeated for 4 bubbles in each experiment for repeatability and acquired data reliability and the IFT measurement was made repeatedly on each bubble image obtained.

3. Results and discussion

3.1. Core flooding experiment

The recovery efficiency of the experiment was investigated using a laboratory simulated displacement experiment to determine the concentration profiles of the interacting gas species. This entailed injection of the CO_2 into the core sample saturated with CH_4 and connate water.

As already mentioned in Section 2.2, a number of test runs were carried out to assess the repeatability of the experimental methodology and set up and the error analysis for the best three runs prior to the actual runs were selected and shown in the appendix.

3.1.1. Methane recovery

First, the CH_4 produced was evaluated based on the total volume of effluents produced after the core flooding experiment was stopped. These volumes were fractions of the original gas in place in the core sample. The results obtained are presented in Table 2 below.

These results are presented in a graphical form in Fig. 4 which shows the trends observed. As can be seen, the poorest CH_4 recovery in all the runs was realised in the run where 10 wt% of connate water was used. This can be attributed to the poor sweep efficiency of the injected because of the restrictive flow when CO_2 traverses the core sample. This restriction is as a result of the higher salinity (high density) connate water sealing off the narrower pore spaces within the pore matrix due
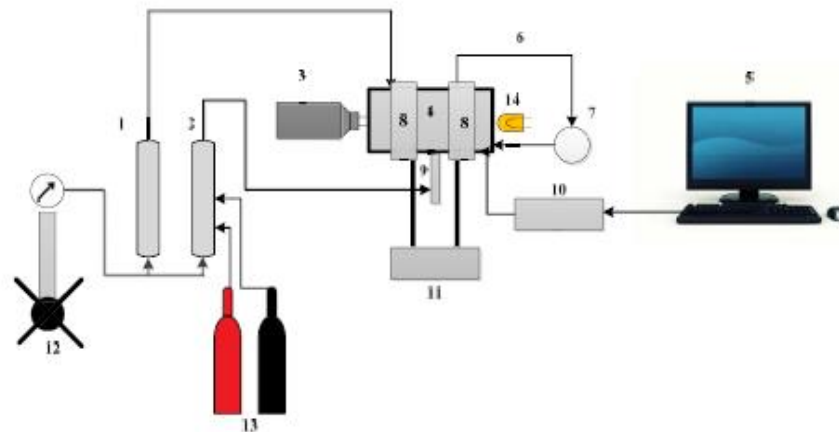
Fig. 3. IFT set up - (1&2) accumulators (3) Rame-Hart digital camera (4) IFT cell (5) Monitor (6) Vent Valve (7) Vacuum Valve (8) Heating element (9) Injection Needle (10) data logger and temperature controller (11) stability controller (12) manual pump (13) gas bottles (CH_4 and CO_2) (14) Light source.

Table 2
CH$_4$ production in pore volumes for all the runs.

Time (min)	PV Produced 10 wt% CH$_4$	Time (min)	PV Produced 5 wt% CH$_4$	Time (min)	PV Produced Distilled CH$_4$	Time (min)	PV Produced Dry CH$_4$
0.17	2.03	0.17	5.13	0.15	7.07	0.16	7.02
5.32	8.31	5.33	21.13	5.49	23.62	5.33	27.82
10.66	9.16	10.67	24.00	10.83	26.27	10.67	29.64
15.99	9.57	15.82	17.12	15.99	10.82	15.83	9.94
21.16	9.90	21.16	7.78	21.32	7.27	21.16	6.86
26.49	3.15	26.49	3.86	26.66	5.10	26.49	5.63
31.66	1.63	31.83	2.70	31.98	3.35	31.82	4.97
37.01	1.16	37.16	1.86	37.16	2.46	37.16	4.53
42.32	0.89	42.33	1.15	42.48	1.91	42.32	4.17
47.66	0.57	47.67	0.58	47.82	1.17	47.82	3.75
53.82	0.31	53.33	0.41	55.98	0.35	54.66	3.31
59.16	0.18	59.49	0.41	61.33	0.11	60	2.99
64.32	0.19	65.16	0.42	66.66	0.08	65.16	2.85

to its density compared to the other runs with lower connate water concentration with lower densities. Because of the forced-homogeneity actualised by the presence of the connate water in the pore matrix, less time was spent by the CO$_2$ as it was injected through the core sample and also early CO$_2$ breakthrough as seen in the concentration profile in Fig. 5.

The original gas in place (OGIP) in the core sample before the commencement of the flooding process was obtained using the same relation in Eq. (1) as employed in our previous work (Abba et al., 2018).

$$G = \frac{v_b \varphi (1 - S_w)}{B_g} \tag{1}$$

Where G is the original gas in place in scm^3, v_b is the bulk volume in cm^3, Sw is initial water saturation fraction, Bg is gas formation volume factor in cm^3/scm^3 for the purpose of this research. This was then used to evaluate the CH$_4$ recovery factor shown in Table 3.

Furthermore, the CH$_4$ recovery was highest when there was no connate water saturation. This is obvious because there was no reduction in the original pore volume for the gas to occupy and hence more volume for nascent CH$_4$. Higher volume of CH$_4$ was realised in the core sample during the dry run and thus higher recovery was observed. This will serve as the benchmark to which other tests are pitted against. So,

analysis will be accentuated in the runs with 10% of their pore volumes saturated with connate water of different salinities (0, 5, 10 wt%). The concentration profile also presented, notably, the variation of the breakthrough times with the salinities. This variation was explained in our previous works where significant pressure drop was seen when CO$_2$ was displacing CH$_4$ at a 10 wt% connate condition (Fig. 6). The same restrictive flow comes into play when explaining the variation in breakthrough times. The higher the salinity of the connate water the more pore throat sealing effect was noticed. Distilled water saturated run did not fully plug the pore throats instead it made them narrower and the flow channels became more tortuous. Similarly, 5 wt% connate water run had lower pressure drop compared to the 10 wt% connate water runs. This means that the pore channels were not significantly reduced thereby allowing more unrestricted flow through the pore matrix.

3.1.2. Carbon dioxide injection and recovery

Using a simple form of gas material balance and mass conservation, the volume of CO$_2$ injected, and CO$_2$ produced can be evaluated to assess the production efficiency of each injection strategy.

$$\sum V_{CO2\,in} = \sum (V_{CO2\,Accumulated} + V_{CO2\,Produced}) \tag{2}$$
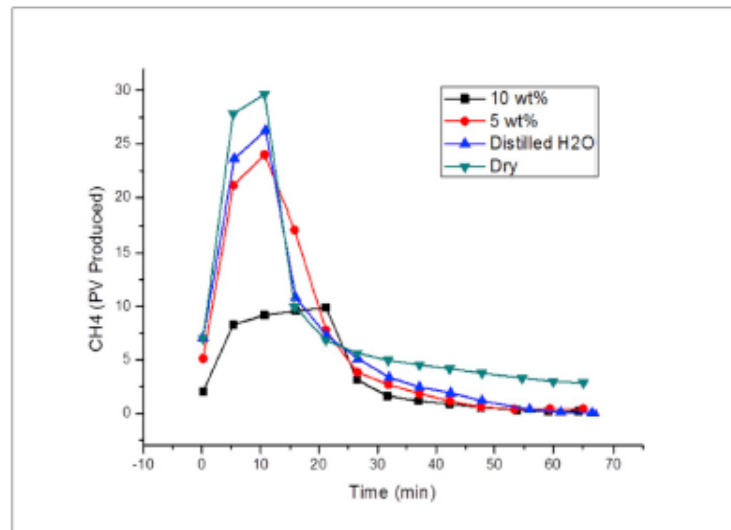

Fig. 4. Graphical representation of CH4 volumes produced from all the experiments.
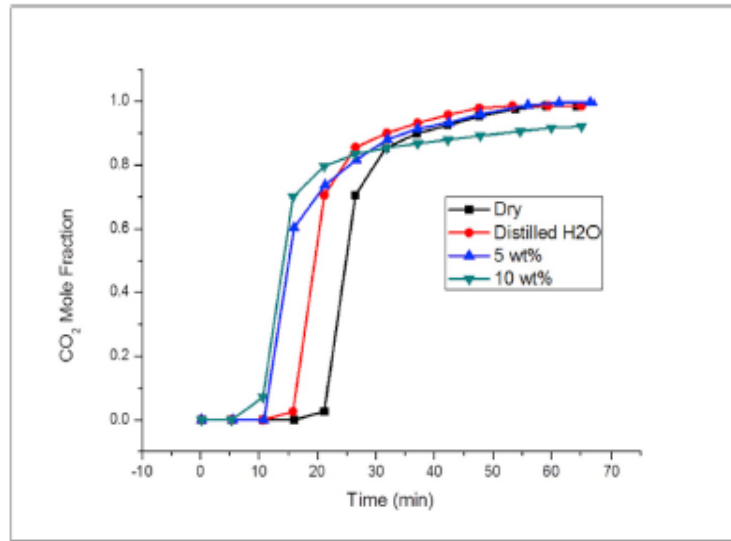
Fig. 5. Concentration profiles of CO_2 produced.

Table 3
CH_4 recovery factor evaluation for each test.

Tests	Swi (%)	CH_4 Produced PV	OGIP PV	Recovery Factor (%)
10 wt%	10	13.62	82.87	16.44
5 wt%	10	53.11	82.87	64.09
Distilled	10	56.17	82.87	67.78
Dry	0	81.55	83.23	97.98

Table 4
CO_2 produced during EGR for all the experimental runs.

Tests	Swi %	PV Injected	PV Produced	PV Accumulated	% CO_2 Stored
10 wt%	10	36.10	13.31	22.79	63.13
5 wt%	10	36.10	29.44	6.66	18.45
Distilled	10	36.10	27.72	8.38	23.21
Dry	0	36.10	33.65	2.45	6.79

Here, CO_2 was injected at a constant flowrate rate and the effluents produced were recorded and analysed. Produced CO_2 results obtained and analysed are shown in Table 4.

From Table 4, it suffices to say that the experimental run with 10 wt % connate water yielded the most significant results in terms of CO_2 storage with 63.13% of the total pore volumes injected stored in the core sample. This is further established and reaffirmed in Fig. 7 where the same run yielded the least CO_2 recovered compared to the other
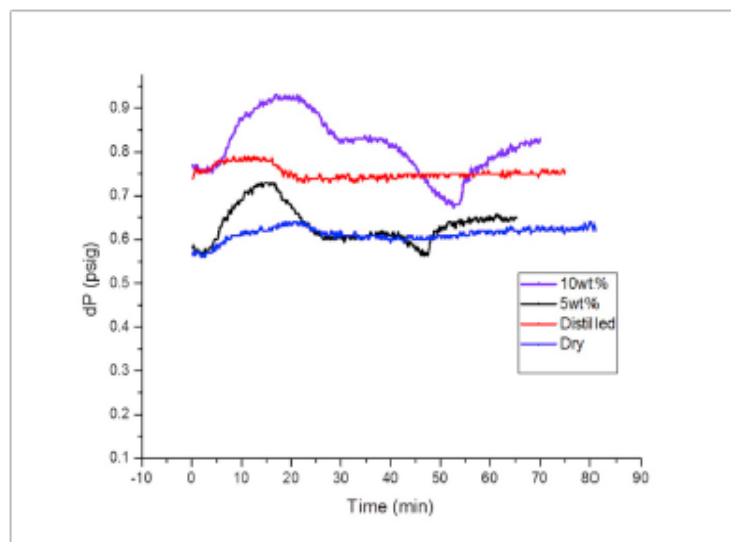
Fig. 6. dP changes during all experimental runs at different connate water salinities at 1300 psig and 50 °C.
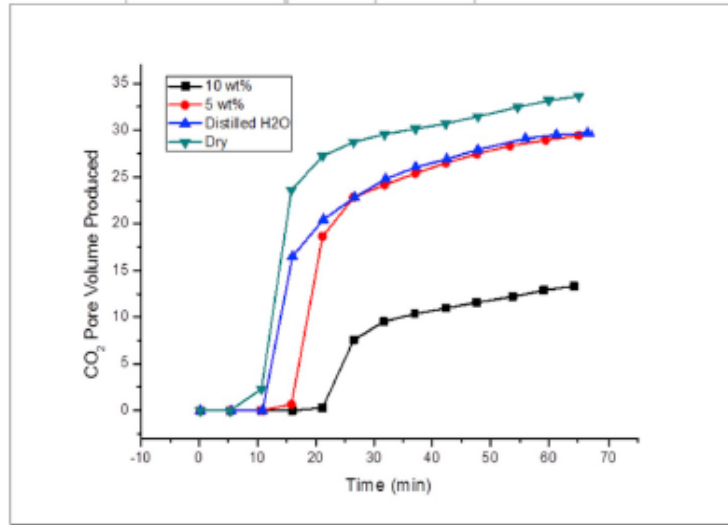
Fig. 7. CO_2 volumes recovered in pore volumes as functions of time.

runs. Also, the restrictive flow during the run as a result of the sealing effect by the connate water aided the storage of the injected CO_2 which was characterised by the large pressure drop observed during the injection. Next, experimental run with the core sample saturated with distilled water provided stored 23.21% of the total pore volumes injected. This was followed closely by the run with 5 wt% connate water and the least efficient storage scenario was the core sample with no connate water with the storage of 6.79% of the total pore volume injected. Given the similar flow behaviour of the injected CO_2 in terms of pressure drops between the distilled water and 5 wt% runs, it was expected that the storage efficiency will be very close.

Consequently, to assess the displacement efficiency in terms of CH_4 recovery and CO_2 sequestration, Tables 2 and 3 were combined to produce Fig. 8.

From the Figure, there seem to be an increase in recovery of CH_4 as the salinity decreases, this can be attributed to the pore matrix of the core sample and the flow physics of the fluid as discussed in section 3.1.1. For CO_2 storage, however, the storage efficiency arguably

decreased as salinity decreased. That cannot be substantiated because the storage efficiency in the distilled water run is fairly higher than that of the 5 wt% run. This could be due to CO_2 solubility in brine and distilled water. Further investigation is thus required to substantiate the claim and expatiate the trend observed.

It is a well-known fact that the CO_2 is highly soluble in water. The mutual solubilities of CO_2 and CH_4 and connate water at different salinities was investigated next using IFT measurement to further drive and explain the narrative already postulated.

3.1.3. IFT measurements

The experimental fluid-fluid IFT measurement was carried out using the rising bubble technique described in Section 2.2.4.1. This technique capitalises on the buoyancy of the gas bubble with respect to the brine used, in that its ability to rise through the denser fluid is exploited. The IFT measurement is evaluated based on the profile of the gas bubble in the brine created in the IFT cell which is deduced using the Young-Laplace equations:
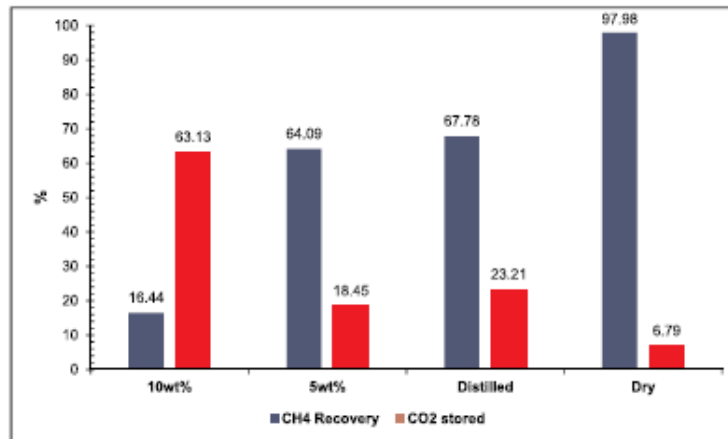

Fig. 8. Efficiency of flooding process terms of CO_2 storage and CH_4 recovery.

7

196

Table 5
IFT measurement of CO_2 at different brine salinities (1300 psig 50°C).

Time (s)	Distilled Water (mN/m)	5 wt% (mN/m)	10 wt% (mN/m)
0.0	55.23	62.30	65.51
1.0	54.89	61.10	64.53
1.9	52.12	59.89	63.63
2.9	48.11	57.19	63.51
4.0	44.22	55.22	63.48
5.0	38.16	53.45	63.41
6.0	33.67	52.32	63.40
6.9	28.32	51.75	63.38
8.0	24.33	50.11	63.07
9.0	22.12	48.29	62.36

$$\gamma = \frac{\Delta\rho g d_e^2}{H} \tag{3}$$

Where

$$\frac{1}{H} = f\left(\frac{d_s}{d_e}\right) \tag{4}$$

$\Delta\rho$ is the density difference between the two fluids, γ is the interfacial tension, g is the acceleration due to gravity, d_e is equatorial diameter of the drop, d_s is the diameter of the bubble at d_e from the apex, H is the bond number which is a function of the ratio of d_s/d_e. The densities of the phases were evaluated using PVTsim at the test conditions of 1300 psig and 50 °C. The IFT was first measured when the external phase (connate water) was not saturated with the drop phase (CO_2) to observe the development and collapse of the bubble generated. The results for all the test fluids are shown in Table 5 where measurements were taken continuously as the bubble shrunk and collapsed.

The shrinking of the bubble signified the rate of mass transfer over the interface between the gas bubbles generated and brine phase in the cell. As seen in Fig. 9, Fig. 10, and Fig. 11, the rate of shrinkage of the gas bubble is more pronounced in the distilled water experiment and the rate decreased as the salinity of the connate water sample increased. The IFT decreased rapidly in the distilled water which explained the shrinkage observed. However, IFT rate decreased at a slower rate when the salinity increased to 5 w% and even slowest at 10 wt% connate water. This is represented graphically in Fig. 12.

After the results of the rate of shrinkage and IFT variation with time in the unsaturated brine were obtained, the next step was to evaluate CO_2 IFT when the brine was saturated with the injected CH_4. The external phase of the experiment (brine) was saturated with the CH_4 by injecting the gas through the injection needle which pressurised the system to the test pressures. IFT measurements were taken at time intervals at the test conditions. Full equilibrium was achieved after about

3 min where the bubble sizes became constant and hence the IFTs. The CH_4 IFT results shown in Fig. 13 are similar to those obtained by (Yahaya et al., 2018) at the equilibrium conditions relevant to this work.

From the results, it follows the same trend as that observed when the measuring the CO_2 IFT in brine, in that the rate of IFT decrease is consequential to the brine salinity, with the lowest IFT measured between the CH_4 and the brine. This reaffirms that the higher the salinity of the brine the lower the gas solubility. The graphical representation of the IFT variation with time is shown in Fig. 13.

Once the equilibrium between CH_4 and the brine was attained, CO_2 was now injected at the same pressure into the CH_4 saturated brine to evaluate the IFT. This was to simulate the rate of CO_2 dissolution in the reservoir during the displacement. It is noted that the connate water in the reservoir was saturated with the CH_4 prior to injection, so this step in IFT determination of the CO_2 in a CH_4 saturated brine gives a representation of the trends observed in Fig. 14.

It is clear that the gases had the highest interfacial tension in the brine with the highest salinity and lowest interfacial tension value in distilled water. This explains why more CO_2 seemed to accumulate during the run with distilled water (Table 4 and Fig. 8) compared to the run with 5 wt%.

The primary trapping mechanisms in the conventional natural gas reservoirs during EGR by CO_2 injection and sequestration are the structural and stratigraphic trapping as seen in Table 4 in the dry run which only about 7% of the injected CO_2 was stored in the core sample. This storage efficiency was considerably increased to about 63% of the injected CO_2 when connate water was introduced into the core sample. This highlights the feasibility that in addition to structural trapping, solubility trapping is realisable during EGR and tends to increase the storage capacity of the conventional natural gas in terms of storage while maintaining substantial recovery of the hydrocarbon resource.

4. Conclusion

In this research, Berea sandstone core sample was used as the conventional porous media to carry out a core flooding process to evaluate the production of CH_4 and CO_2 during EGR scenario in the presence of connate water to realise the effects of its presence. CO_2 storage was highest in the run where the connate water salinity was 10 wt% which is attributed to the restrictive flow of the injected CO_2 to displace the CH_4 and was characterised by low CO_2 and high CH_4 recoveries. Here, structural trapping mechanism was dominant and also solubility trapping to an extent. However, solubility trapping mechanism is most pronounced during the distilled (0 wt%) and 5 wt% salinity runs where both runs had similar CO_2 and CH_4 production, but the distilled water run had the higher CO_2 accumulation. This is due to the higher solubility of the CO_2 in distilled water as seen in their

Fig. 9. Bubble shrinkage of CO_2 bubble in Distilled water L: Onset R: End (10 s interval).
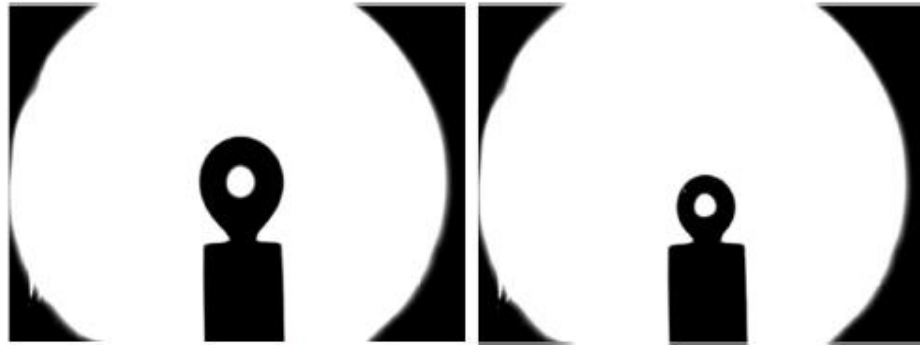
Fig. 10. Bubble shrinkage of CO_2 in 5 wt% brine L: Onset R: End (10 s interval).

Fig. 11. Bubble shrinkage of CO_2 in 10 wt% brine L: Onset R: End (10 s interval).

interfacial tensions – with distilled water having a value of 36.12 mN/m and 48.20 mN/m for 5 wt% brine at the same conditions. CO_2 sequestration during EGR is not just focused on the primary trapping mechanisms of geological sequestration but can also exploit the solubility trapping mechanism in the reservoir connate water to increase the storage capacity. Considering only structural and stratigraphic trapping mechanisms which were simulated using the dry run (no water saturation), only 7% of the injected CO_2 was stored and a substantial
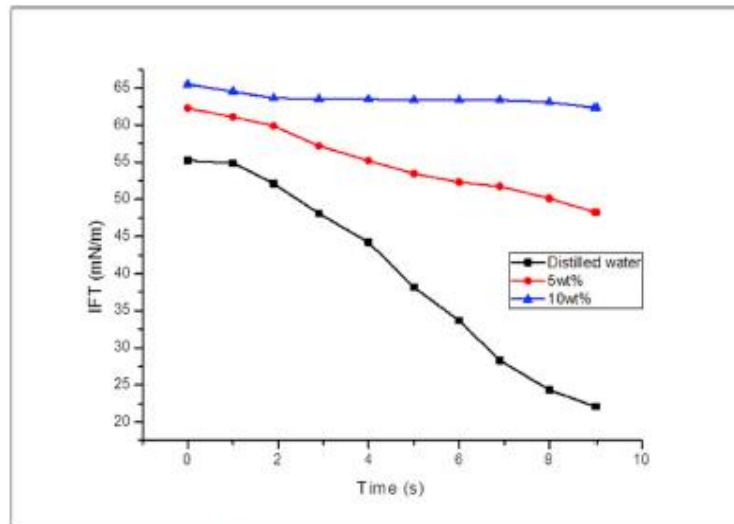
Fig. 12. Graphical representation of CO_2 IFT decrease as a function of time at under-saturated aqueous conditions (1300 psig 50°C).
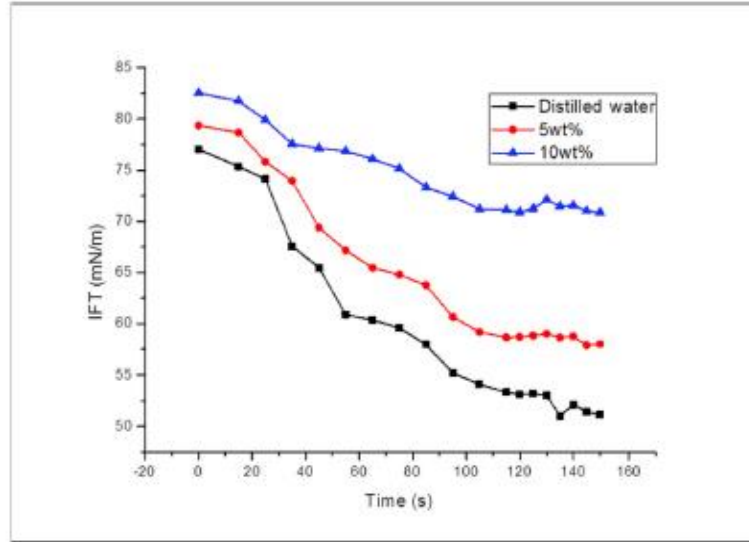
Fig. 13. CH$_4$ IFT as function of time at equilibrium (1300 psig 50°C).
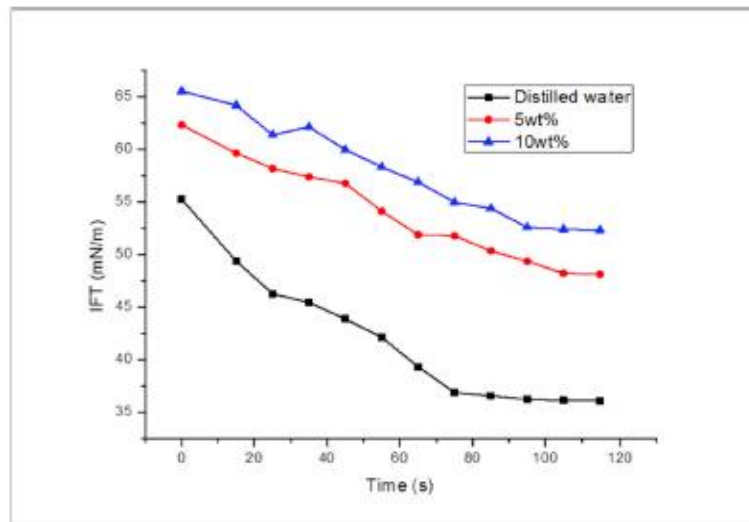
Fig. 14. CO$_2$ IFT as a function of time at saturated conditions.

volume of 63% of the injected CO$_2$ was sequestered when solubility trapping was considered by introducing connate water saturation. This goes on to show there is a potential for additional storage capacity through secondary trapping mechanisms. The salinity of the connate water plays a vital role in promoting the trapping – in this case structural trapping which resulted from the density of the connate water sealing off the narrow pore spaces within the pore matrix as evident in the 10 wt% connate water run. A substantial volume of CH$_4$ was recovered in all the cases which is a win-win scenario for the technique. The recovered CH$_4$ from conventional natural gas reservoir can offset part of the cost of the sequestration process whilst providing good sequestration site CO$_2$ storage. This study shows that structural and stratigraphic trapping mechanisms are not the only exploitable avenue for CO$_2$ storage by showcasing the potential of solubility trapping as a secondary trapping mechanism which increases the storage capacity (the limitation) of natural gas reservoir. Future work will entail investigation of effect of other types of salts on this process and at even higher concentrations and saturations.

Acknowledgements

10

199

Appendix

Error analysis of the core flooding runs

Dry Runs			Distilled water			5 wt% NaCl			10 wt% NaCl		
Time (min)	Average Mol. Frac CO_2 (%)	Standard Deviation CO_2 (%)	Time (min)	Average Mol. Frac CO_2 (%)	Standard Deviation (%)	Time (min)	Average Mol. Frac CO_2 (%)	Standard Deviation (%)	Time (min)	Average Mol. Frac CO_2 (%)	Standard Deviation (%)
0.17	0.0	0.0	0.17	0.0	0.0	0.16	0.0	0.0	0.15	0.0	0.0
5.32	0.0	0.0	5.33	0.0	0.0	5.33	0.0	0.0	5.49	0.0	0.0
10.66	0.0	0.0	10.67	2.3	2.5	10.67	1.7	2.9	10.83	6.3	4.7
15.99	1.0	1.0	15.82	6.5	3.7	15.83	61.8	2.8	15.99	70.7	4.0
21.16	4.9	4.5	21.16	70.8	11.0	21.16	74.6	3.1	21.32	78.6	3.2
26.49	70.2	4.0	26.49	89.2	3.3	26.49	84.2	4.1	26.66	82.8	2.6
31.66	81.1	3.8	31.83	92.0	1.7	31.82	90.4	2.5	31.98	85.1	1.0
37.01	91.0	1.0	37.16	94.7	1.4	37.16	94.1	2.4	37.16	86.6	1.5
42.32	93.5	1.3	42.33	96.6	0.7	42.32	95.8	2.1	42.48	88.0	1.0
47.66	96.1	0.8	47.67	97.6	0.6	47.82	97.0	1.0	47.82	89.5	0.4
53.82	97.5	0.5	53.33	97.9	0.8	54.66	97.0	1.0	55.98	90.3	0.9
59.16	98.5	0.4	59.49	98.2	0.3	60.01	97.3	1.2	61.33	90.6	1.2
64.32	98.5	0.5	65.16	98.2	0.3	65.16	97.5	1.2	66.66	90.8	1.4
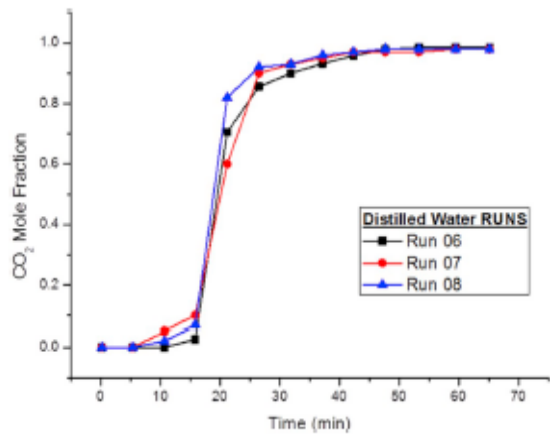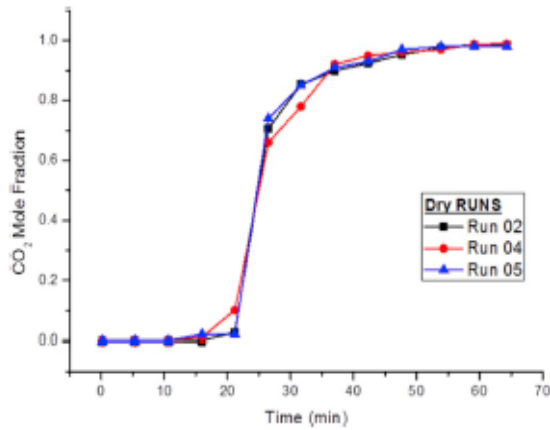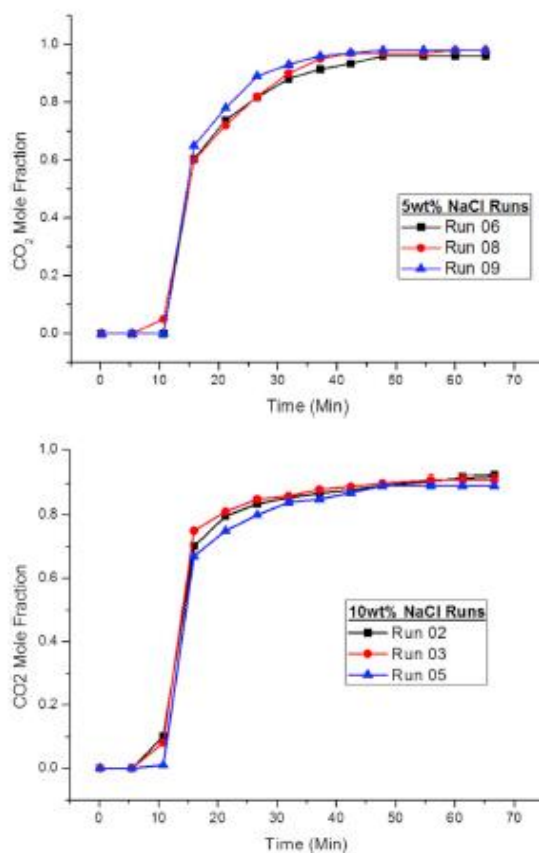
Appendix A. Supplementary data

Supplementary data to this article can be found online at https://doi.org/10.1016/j.jngse.2019.103002.

Nomenclature

CH_4	Methane
CO_2	Carbon dioxide
γ	Interfacial Tension IFT (mN/m)
ρ	Density (g/cm³)
g	Acceleration due to gravity (m/s²)
de	Bubble equatorial diameter (mm)
ds	Bubble diameter from bottom tip of bubble to height de (mm)
H	Bond number
f	Function
PV	Pore volume

References

Abba, M.K., Abbas, A.J., Nasr, G.G., 2017. Enhanced gas recovery by CO2 injection and sequestration: effect of connate water salinity on displacement efficiency. In: SPE Abu Dhabi International Petroleum Exhibition & Conference, . https://doi.org/10.2118/188930-MS.

Abba, M.K., Al-Othaibi, A., Abbas, A.J., Nasr, G.G., Mukhtar, A., 2018. Experimental investigation on the impact of connate water salinity on dispersion coefficient in consolidated rocks cores during Enhanced Gas Recovery by CO2 injection. J. Nat. Gas Sci. Eng. 60, 190–201. https://doi.org/10.1016/j.jngse.2018.10.007.

Amin, R., Sidiq, H., Kennaird, T., Van der Steen, E., 2010. Gas-gas experimental interfacial tension measurement. Fluid Phase Equilib. 295, 230–236. https://doi.org/10.1016/j.fluid.2010.05.020.

Arabloo, M., Ghazanfari, M.H., Rashtchian, D., 2016. Wettability modification, interfacial tension and adsorption characteristics of a new surfactant: implications for enhanced oil recovery. Fuel 185, 199–210. https://doi.org/10.1016/j.fuel.2016.06.088.

Bagalkot, N., Hamouda, A.A., Isdahl, O.M., 2018. Dynamic interfacial tension measurement method using axisymmetric drop shape analysis. MethodsX 5, 676–683. https://doi.org/10.1016/j.mex.2018.06.012.

Barati-Harooni, A., Soleymanzadeh, A., Tatar, A., Najafi-Marghmaleki, A., Samadi, S.J., Yari, A., Roushani, B., Mohammadi, A.H., 2016. Experimental and modeling studies on the effects of temperature, pressure and brine salinity on interfacial tension in live oil-brine systems. J. Mol. Liq. 219, 985–993. https://doi.org/10.1016/j.molliq.2016.

04.013.

Burton, M., Kumar, N., Bryant, S.L., 2009. CO2 injectivity into brine aquifers: why relative permeability matters as much as absolute permeability. Energy Procedia 1, 3091–3098. https://doi.org/10.1016/J.egypro.2009.02.089.

Cantrell, K.J., Brown, C.F., 2014. Source term modeling for evaluating the potential impacts to groundwater of fluids escaping from a depleted oil reservoir used for carbon sequestration. Int. J. Greenh. Gas Control 27, 139–145. https://doi.org/10.1016/J.ijggc.2014.05.009.

Chen, L., Wang, M., Kang, Q., Tao, W., 2018. Pore scale study of multiphase multicomponent reactive transport during CO2dissolution trapping. Adv. Water Resour. 116, 208–218. https://doi.org/10.1016/J.advwatres.2018.02.018.

Chow, Y.T.F., Maitland, G.C., Trusler, J.P.M., 2016. Interfacial tensions of the (CO2 + N2 + H2O) system at temperatures of (298 to 448) K and pressures up to 40 MPa. J. Chem. Thermodyn. 93, 392–403. https://doi.org/10.1016/J.jct.2015.08.006.

Dehghan, A.A., Masihi, M., Ayatollahi, S., 2015. Phase behavior and interfacial tension evaluation of a newly designed surfactant on heavy oil displacement efficiency; effects of salinity, wettability, and capillary pressure. Fluid Phase Equilib. 396, 20–27. https://doi.org/10.1016/J.fluid.2015.03.028.

Ding, S., Xi, Y., Jiang, H., Liu, G., 2018. CO2storage capacity estimation in oil reservoirs by solubility and mineral trapping. Appl. Geochem. 89, 121–128. https://doi.org/10.1016/J.apgeochem.2017.12.002.

Duan, S., Gu, M., Du, X., Xian, X., 2016. Adsorption equilibrium of CO2 and CH4 and their mixture on Sichuan basin shale. Energy Fuels 30, 2248–2256. https://doi.org/10.1021/acs.energyfuels.5b02088.

Duchateau, C., Broseta, D., 2012. A simple method for determining brine-gas interfacial tensions. Adv. Water Resour. 42, 30–36. https://doi.org/10.1016/J.advwatres.2012.03.008.

Ganjdanesh, R., Hosseini, S.A., 2017. Geologic carbon storage capacity estimation using enhanced analytical simulation tool (EASiTool). Energy Procedia 114, 4690–4696. https://doi.org/10.1016/J.egypro.2017.03.1601.

Jia, W., Pan, F., Dai, Z., Xiao, T., McPherson, B., 2017. Probabilistic risk assessment of CO2Trapping mechanisms in a sandstone CO2-EOR field in Northern Texas, USA. Energy Procedia 114, 4321–4329. https://doi.org/10.1016/J.egypro.2017.03.1581.

Kalra, S., Wu, X., 2014. CO2 Injection for Enhanced Gas Recovery. SPE West. North Am. Rocky Mt., pp. 16–18.

Kamari, A., Pournik, M., Rostami, A., Amirlatifi, A., Mohammadi, A.H., 2017. Characterizing the CO2-brine interfacial tension (IFT) using robust modeling approaches: a comparative study. J. Mol. Liq. 246, 32–38. https://doi.org/10.1016/J.molliq.2017.09.010.

Kashefi, K., Pereira, L.M.C., Chapoy, A., Burgass, R., Tohidi, B., 2016. Measurement and modelling of interfacial tension in methane/water and methane/brine systems at reservoir conditions. Fluid Phase Equilib. 409, 301–311. https://doi.org/10.1016/J.fluid.2015.09.050.

Khaksar Manshad, A., Olad, M., Taghipour, S.A., Nowrouzi, I., Mohammadi, A.H., 2016. Effects of water soluble ions on interfacial tension (IFT) between oil and brine in smart and carbonated smart water injection process in oil reservoirs. J. Mol. Liq. 223, 987–993. https://doi.org/10.1016/J.molliq.2016.08.089.

Li, B., Tchelepi, H.A., Benson, S.M., 2013. Influence of capillary-pressure models on CO2 solubility trapping. Adv. Water Resour. 62, 488–498. https://doi.org/10.1016/J.advwatres.2013.08.005.

Mijic, A., LaForce, T.C., Muggeridge, A., 2014. Co2 injectivity in saline aquifers: the

impact of non Darcy flow, phase miscibility and gas compressibility. Water Resour. Res. WR014893, 4163–4185. https://doi.org/10.1002/2013WR014893 (Received).

Mohammad Salehi, M., Omidvar, P., Naeimi, F., 2017. Salinity of injection water and its impact on oil recovery absolute permeability, residual oil saturation, interfacial tension and capillary pressure. Egypt J. Pet. 26, 301–312. https://doi.org/10.1016/J.ejpe.2016.05.003.

Mutailipu, M., Liu, Y., Jiang, L., Zhang, Y., 2018a. Measurement and estimation of CO2–brine interfacial tension and rock wettability under CO2 sub- and super-critical conditions. J. Colloid Interface Sci. https://doi.org/10.1016/J.jcis.2018.09.031.

Mutailipu, M., Liu, Y., Jiang, L., Zhang, Y., 2018b. Measurement and estimation of CO2–brine interfacial tension and rock wettability under CO2 sub- and super-critical conditions. J. Colloid Interface Sci. 534, 605–617. https://doi.org/10.1016/J.jcis.2018.09.031.

Nakajima, T., Xue, Z., 2017. Trapping mechanisms in field scale: results from Nagaoka geologic CO2Storage site. Energy Procedia 114, 5015–5022. https://doi.org/10.1016/J.egypro.2017.03.1650.

Oh, J., Kim, K.Y., Han, W.S., Park, E., 2017. Transport of CO2in heterogeneous porous media: spatio-temporal variation of trapping mechanisms. Int. J. Greenh. Gas Control 57, 52–62. https://doi.org/10.1016/J.ijggc.2016.12.006.

Pereira, L.M.C., Chapoy, A., Burgass, R., Tohidi, B., 2017. Interfacial tension of CO2+ brine systems: experiments and predictive modelling. Adv. Water Resour. 103, 64–75. https://doi.org/10.1016/J.advwatres.2017.02.015.

Rashid, S., Harimi, B., Hamidpour, E., 2017. Prediction of CO2-Brine interfacial tension using a rigorous approach. J. Nat. Gas Sci. Eng. 45, 108–117. https://doi.org/10.1016/J.jngse.2017.05.002.

Raza, A., Rezaee, R., Bing, C.H., Gholami, R., Hamid, M.A., Nagarajan, R., 2016. Carbon dioxide storage in subsurface geologic medium: a review on capillary trapping mechanism. Egypt J. Pet. 25, 367–373. https://doi.org/10.1016/J.ejpe.2015.08.002.

Sminchak, J.R., Babarinde, O., Gupta, N., 2017. Integrated analysis of geomechanical factors for geologic CO2Storage in the midwestern United States. Energy Procedia 114, 3267–3272. https://doi.org/10.1016/J.egypro.2017.03.1458.

Stukan, M., Abdallah, W., East, S.M., 2012. In: Interfacial Tension (IFT) and Surface alteration Interplay. Spe, pp. 11–14. https://doi.org/10.2118/161279-ms.

Valle, L.M., Rodríguez, R., Grima, C., Martínez, C., 2018. Effects of supercritical CO2 injection on sandstone wettability and capillary trapping. Int. J. Greenh. Gas Control 78, 341–348. https://doi.org/10.1016/J.ijggc.2018.09.005.

van der Meer, B., 2005. Carbon dioxide storage in natural gas reservoirs. Oil Gas Sci. Technol. 60, 527–536. https://doi.org/10.2516/ogst:2005035.

Xiao, T., McPherson, B., Pan, F., Esser, R., Jia, W., Bordelon, A., Bacon, D., 2016. Potential chemical impacts of CO 2 leakage on underground source of drinking water assessed by quantitative risk analysis. Int. J. Greenh. Gas Control 50, 305–316. https://doi.org/10.1016/J.ijggc.2016.04.009.

Yahaya, A.A., Akpan, E.U., Enyi, G.C., Nasr, G.G., Abbas, J., 2018. Experimental investigation of methane-water and methane-brine IFT measurements using pendant drop (rising bubble) method Journal of engineering technology. J. Eng. Technol. 6, 394–407.

Yasuda, K., Mori, Y.H., Ohmura, R., 2015. Interfacial tension measurements in water-methane system at temperatures from 278.15 K to 298.15 K and pressures up to 10 MPa. Fluid Phase Equilib. 413, 170–175. https://doi.org/10.1016/J.fluid.2015.10.006.

13

202

SPE-198731-MS

Effect of Temperature and Salt Concentration on Rheological Behaviour of Surfactin

S. M. Salihu, A. J. Abubakar, B. Meisam, U. A. Emmanuel, and K. Y. Hassan, University of Salford, United Kingdom; A. Y. Aminu, Ministry of Petroleum Resources Abuja, Nigeria

Abstract

Behavioural changes of surfactants due to temperature fluctuations, and its interaction with saline environment, is very common during oil and gas operations. Exhibition of transient or permanent flow behaviour is one form of these changes. Therefore, effect of temperature and ionic concentrations (salinity) on flow behaviour of sodium surfactin was experimentally investigated. ORCADA® software-controlled OFITE viscometer (Model 1100) was used to conduct steady-shear study, at 23–50 °C temperature, 0.1–1.5 molar (M) salt concentrations and 0.025–1.0 % surfactin dosages. Sodium surfactin behaves as non-Newtonian fluid, with a pseudoplastic pattern exhibited in aqueous and 0.25-1.5M saline media. Effect of changes in temperature and salinity on apparent viscosity of surfactin was surfactant-dosage dependent. Furthermore, shear-thickening effect set in at a critical shear rate of 680.9 s^{-1}, signifying flow-induced self-aggregation. Surfactant dosages 0.075 and to a lesser extent 0.1% were minimally affected by changes in temperatures, salinity and rate of shear not exceeding 680.9 s^{-1}. The findings suggest pumpability and dispersion characteristics of the biosurfactant.

Introduction

Surfactin, a biological surface-active agent (biosurfactant), produced from *Bacillus subtilis* is increasingly been accepted for many industrial applications including oil and gas (Al-Bahry et al., 2013; Al-Wahaibi et al., 2014; Alves et al., 2010; Bezza & Chirwa, 2015). The acceptance stem from their ease of biodegradability, less toxicity, high detergency, better foaming and wetting properties, and greater stability compared to synthetic surfactants (Bezza & Chirwa, 2015; Chen, Juang, & Wei, 2015; Inès & Dhouha, 2015). Furthermore, successful experimental and numerical study on application of surfactin in oil/gas industry for either soil bioremediation, enhanced oil recovery, and/or heavy oil transport in pipelines have been reported by many authors (Fernandes et al., 2016; Frigaard, Paso, & de Souza Mendes, 2017; Inès & Dhouha, 2015). Success of these applications centres on the ability of the surfactin to remain adhered on oil-water, gas–oil or gas–water interface, thereby hindering inter-particle cohesion hence increasing the surface area along the fluids interface. However, during industrial operations, fluids exhibits some form of transient or permanent flow behaviour due to shear, compression and/or expansion stress. The resulting change in

flow behaviour is of concern to operators. It may result to undesirable consequence such as pressure loss in pipes (Sharma, Tiwari, & Dixit, 2016) due to failure, and burn-out of equipment (such as pump) (Franck, 2004), during operations, especially at start up.

This study will therefore be a tool to enhancing the performance, assessing point of surfactin failure, and investigation on relaxation of surfactin at fluids surfaces/interfaces. It also defines the extent of surfactin response to any form of shear during application, and behaviour at quiescent state.

Available literature indicated that studies regarding response of surfactin to rate of shear in a solution of varying ionic strength, and at varying temperature are limited. However, many factors including temperature, hydrophobic chain length and ionic concentration have been reported to impact micellization. (Al-Bahry et al., 2013) investigated effect of incubation media and time on surfactin viscosity. Authors reported no significant changes in viscosity. (Osman, Høiland, & Holmsen, 1998) studied the effect of pH, temperature and Ca^{+2} on micropolarity and microviscosity of surfactin adopting the use of FTIR and flourometric analysis methods. Further to flow behaviour of biomolecules, (de Oliveira, Amaral, & Burkert, 2018) reported increase in apparent viscosity on addition of $1 molL^{-1}$ NaCl salt. Range of salt concentration used does completely reflect that of produced water from oil and gas operations. Furthermore, (Zdziennicka, Krawczyk, & Jańczuk, 2018) studied the volumetric properties of Rhamnolipid and surfactin at temperatures of 293K, 303K and 313K. Additionally, (Ohadi, Dehghannoudeh, Forootanfar, Shakibaie, & Rajaee, 2018) structural and aggregation behaviour of lipopeptide biosurfactant. The authors, in all these studies, were unable to capture scenarios and conditions typical of applications in oil/gas industries.

In this study, therefore, response of aqueous surfactin to rate of shear at temperature ranges of 23 to 50 °C, and at varying aqueous NaCl salt solution of 0.1–1.5 M concentration was investigated. OFI Testing Equipment (OFITE) viscometer model 1100 was used for the analysis.

Materials and Method

Materials

Sodium Surfactin (Kaneka surfactin) biosurfactant (CAS No.302933-83-1), $C_{55-a}H_{95.5-2a}N_7O_{13}Na1.5$, was purchased, and used as received, from Kaneka Europe Holding Company, Belgium. Aqueous solution of the surfactin was made using distilled water locally made in the Petroleum and Gas Engineering laboratory of University of Salford. Acros Organics brand (207790010/20) analytical grade univalent salt, Sodium chloride (NaCl) with 99.5% purity was purchased from Fisher Scientific, UK.

Method

Sample preparation. Aqueous solution of surfactant was prepared by measuring and directly adding 0.025, 0.05, 0.075, 0.1 0.5 and 1.0 w/v% dosages of surfactant into sample container, and with distilled water subsequently added. The mixture was vigorously agitated and stirred and allowed at least for 5 hours to completely dissolve. Surfactant dosages were adopted based on the works of (Al-Wahaibi et al., 2014; Saito, Sugai, Sasaki, Okamoto, & Ouyang, 2016; Whang, Liu, Ma, & Cheng, 2008).

Saline solutions of 0.1–1.5 M concentration were as well prepared by measuring and dissolving appropriate amount of salt into 2 litres of distilled water. The solution was well stirred using hotplate magnetic stirrer. Each concentration of the saline solution was then used to prepare surfactant solution, using the various dosages stated above.

Measurement of rheology. The rheological experiments were carried out using ORCADA® software–controlled OFITE viscometer (Model 1100), having a shear rate range of 0.01–1000 s^{-1} and 0.001 RPM speed accuracy. Based on its configuration of B1, 42ml of calibration fluid was used to first calibrate the viscometer. Input data (RPM, temperature, etc.) were then specified in the Test Builder, and RP 10B analysis model (combination of Power Law and Bingham Plastic Models) was selected. Temperature in the range of

23 °C (ambience) 30, 40 and 50 °C were inputted with an allowance of ±1 °C. 0–600 RPM were selected for the test, and units of shear stress and viscosity were then specified accordingly. Having keyed in the input data and the test analysis mode selected, 42 ml of each of dosage samples prepared was measured and poured into the sample cup and tightly screwed. "Start Test" button was entered to begin analysis, until all RPM specified were completed. The experimental set-up is shown in Figure 1.
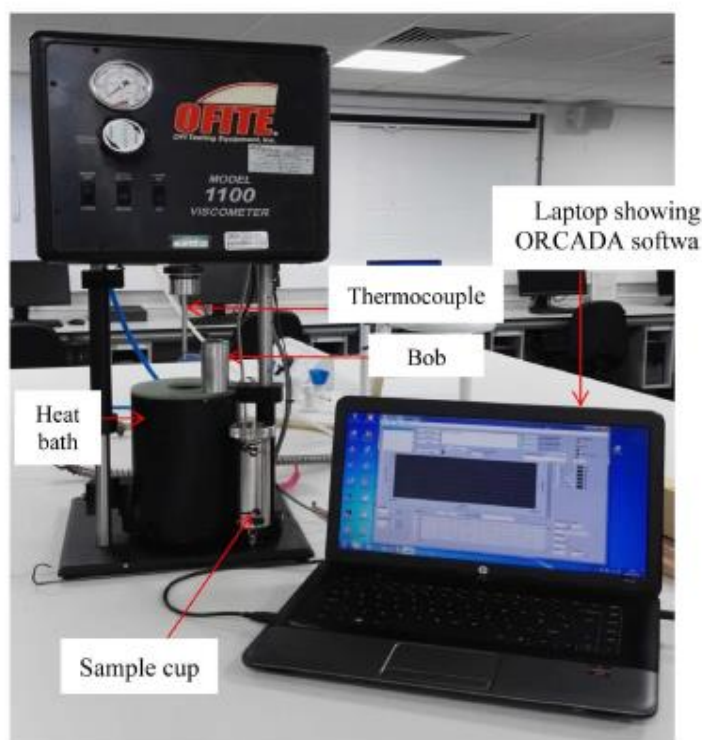

Figure 1—Rheology measurement equipment set-up

This same procedure was repeated for all samples in saline solution, at ambient temperature of 23 °C with an allowance of ±1 °C.

Result and discussion

Steady shear effect at different temperature

Figure 2 shows plot of viscosity against rate of shear at temperatures of 23, 30, 40 and 50 °C, designated respectively by a, b, c and d. It indicates pseudoplastic behaviour (Drew, 2006; Jain, Mody, Mishra, & Jha, 2012; Mu, Li, Jia, Wang, & Zhang, 2002) of sodium surfactin across all dosages and temperature. Furthermore, three (3) plateau regions, regardless of dosage, were noticed. Low-shear region exhibiting characteristics of spherical micelles formation. The region depicts a small shear-induced decrease in viscosity below 85.1 s^{-1} shear rate (Υ). Moreover, within same shear rate boundary, initial viscosity (η) of 1.0% surfactin increases from 22.2-25.7 mPas (Figure 2b), when temperature was increased to 30 °C. Conversely, viscosity of other dosages decreases within same range of temperature and Υ. The trend became highly dosage dependent at 40 and 50 °C. Beyond 85.1 s^{-1}, reorientation of surfactin molecules became

strongly shear-dependent. Υ was sufficiently high to prevent surfactin chains from undergoing any form of self-aggregation.
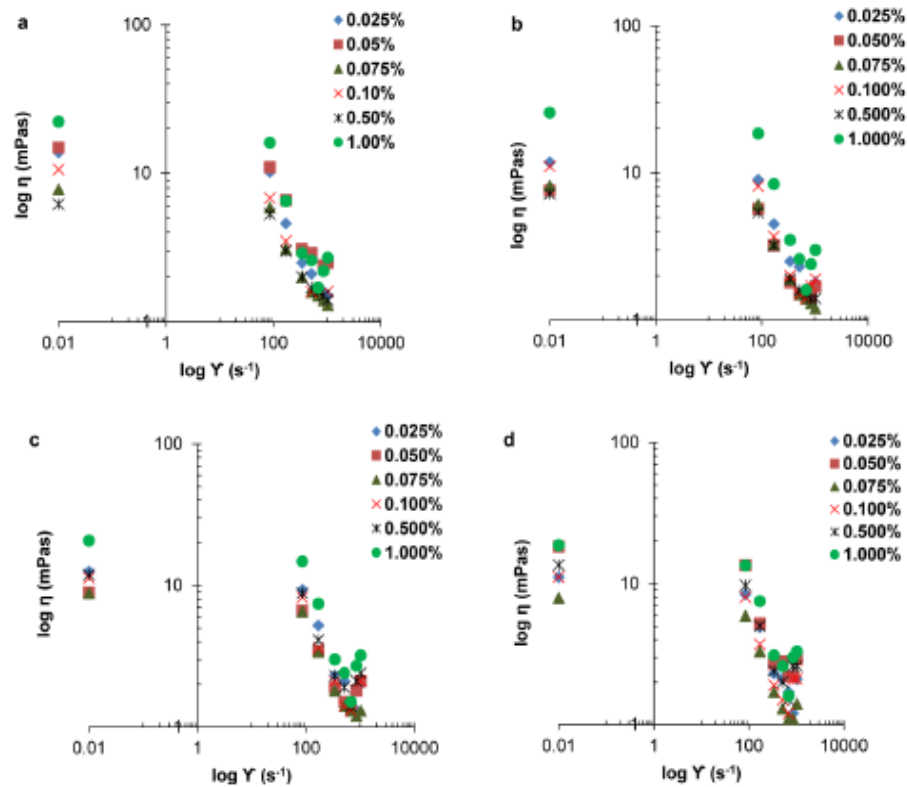

Figure 2—Viscosity vs shear rate of variable surfactin dosages at (a) 23 °C (b) 30 °C (c) 40 °C, and (d) 50 °C

Consequently, viscosity (η) decreases continuously with increasing Υ, depicting a continuous irreversible shear-thinning behaviour (Lutz-Bueno, 2016; Rivero, Gouveia, Müller, & Sáez, 2012) across all dosages. This form of behaviour is a very useful property for adsorptivity (Schroyen, Gunes, & Vermant, 2017), drilling fluid additives, and dispersant for flow assurance (Frigaard et al., 2017).

Pseudoplastic behaviour reached a minimum at critical Υ of 680.9 s^{-1}, and shear-thickening behaviour set in beyond this value. The shear-thickening increase as the temperature increase which is visibly evident in Figure 2c and d. Increasing temperature perhaps led to increased micelles concentration and consequently formation of larger aggregates (rod-like micelles). It is worthy to note that dosages 0.075 and 0.1% are least affected by changes in temperature and shear rate.

Dosage effect at zero-shear

To clearly understand effect of dosage on viscosity at different temperatures, plots of surfactin dosages used in the study were made against apparent viscosity at zero shear (η_o). Figure 3 generally depicts a monotonic response of viscosity to change in surfactin dosage. At ambient and 50 °C, the η_o increases with increasing dosages up to critical dosages of 0.075 and 0.1%. Conversely, temperatures 30 and 40 °C decreases the η_o as the dosage increase. However, irrespective of the temperature change, there seems a convergence at 0.075 and 0.1% dosage. This indicates that, changes in temperature is unable to induce any form of molecular

chain mobility of structures (Alves et al., 2010) at critical dosages. It could as well be an indication of range of the surafctant's critical micelle concentration (CMC).
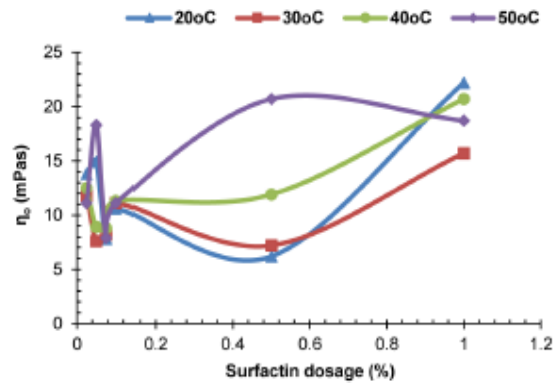

Figure 3—Surfactin dosage effect on viscosity at different temperatures

Temperature effect on apparent viscosity

Temperature fluctuations is a common occurrence associated with oil and gas operations. It therefore become critical to study response of surfactin to these fluctuations at different shear rate. Consequently, effect of temperature on viscosity for different dosages of surfactin at different rate of shear was evaluated. It is obvious in Figure 4 (a and b) that temperature increase resulted in simultaneous breakage and realignment of the surfactin network at zero-shear. Additionally, each dosage exhibited peculiar specific apparent viscosity response to changes in temperature.
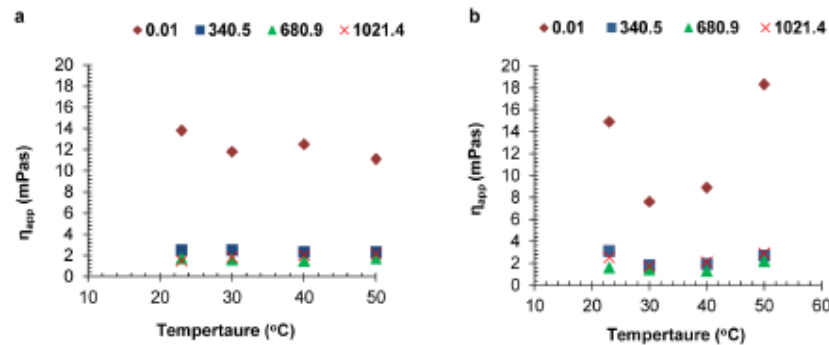

Figure 4—Effect of temperature on apparent viscosity of surfactin at different shear rate for (a) 0.025%, and (b) 0.05%

Surfactin dosage 0.025% depicted significant monotonic decrease while 0.05% depicted a monotonic increase behaviour. Additionally, 30 °C caused viscosity decrease effect in both a and b. Of interest (in figure3b) is the sharp decrease in apparent viscosity (η_{app}) from 14.9 to 7.6 mPas when temperature increased from 23 to 30 °C. The increase induced a breakage and realignment of the surfactin network. Though it reduced viscosity across the dosage, it could not sustain the network deformation (Kamal, 2016). At higher rate of shear, however, temperature effect became less significantly visible indicating that the molecular rearrangement was shear-controlled.

Conversely, temperature increase at zero-shear resulted in molecular aggregation on surfactant dosages 0.075 and 1.0% (Figure 5a and b). The effect, unlike at zero-shear, was less significant at higher rate of shear.
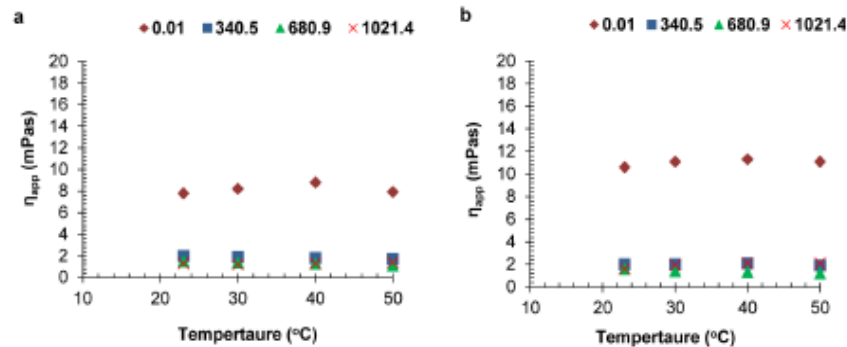
Figure 5—Effect of temperature on apparent viscosity of surfactin at different shear rate for (a) 0.075%, and (b) 0.1%

Figure 6a indicates that increasing temperature results in continuous formation of large aggregates at zero-shear. This is evident by the continuous increase in η_{app}. Furthermore, η_{app} of 1.0% dosage increased to a value of 25.7 mPas at 30 °C (Figure 6b). But with shear rate increase, η_{app} became less sensitive to temperature. At 680 s^{-1}, dosage 1.0% became highly shear rate induced that the apparent viscosity value was close to unity.
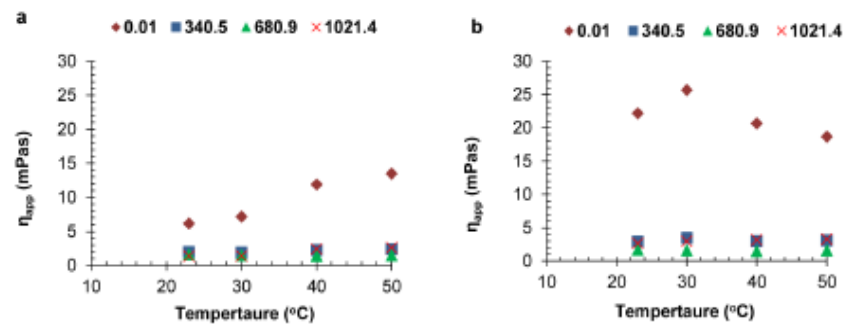

Figure 6—Effect of temperature on apparent viscosity of surfactin at different shear rate for (a) 0.5%, and (b) 1.0%

These affirm that apparent viscosity of surfactin is more dosage and shear rate dependent than it is on temperature, particularly at high shear rate. Thus, surfactin like other biosurfactants, such as extracellular polysaccharides produced from glycerol (Alves et al., 2010), thermo-rheologically stable.

Steady shear effect at different salt concentration
Performance of biosurfactant for oil/gas application is dependent on their behaviour in solutions like that of formation water. Of particular significance is the microviscosity, and how it is affected by the micellar phase, in terms of the solubilizing properties of the micellar core (Li, Zou, Ye, & Mu, 2009). The morphology and molecular architecture of the surfactant may be responsible for this microviscosity effect. Organic or inorganic salts, cosurfactants and/or strongly binding counter ions were reported to have induced sphere-to-wormlike transition in nanostructure of ionic surfactants. This may suggest that exposing sodium surfactin to saline environment will impact on micellization hence its interfacial property during adsorption (Schroyen et al., 2017) and rheology.

Change in ionic concentration of dispersion medium may increase or decrease the size and shape of a micelle. Li (Li et al., 2009), hypothesized that there exist two opposing tendencies in the formation of micelles of ionic surfactants: (1) removal of hydrocarbon chains from water favours aggregation; and (2)

electrostatic repulsions between the ionic head groups opposes aggregation (Shrestha & Aramaki, 2008). Knoblich (Knoblich et al., 1995), reported surfactin micelle to be spherical, ellipsoidal and/or cylindrical with a non-homogeneous size distribution at pH 7, 9.5, and 12. Additionally, Liu (Liu, Mbadinga, Yang, Gu, & Mu, 2015) also reported that cylindrical micelles do transformed into spherical and/or ellipsoidal micelles of smaller sizes when exposed to saline solution environment of 100mM NaCl and 20mM CaCl₂. These are in line with the findings in this study shown in Figure 7.
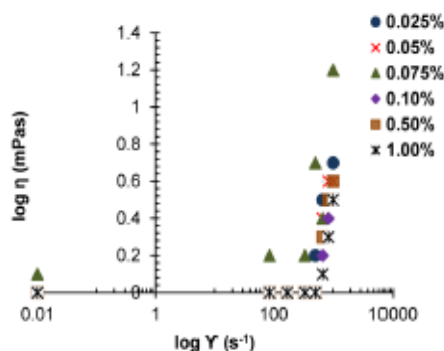

Figure 7—Viscosity vs shear rate as a function of surfactin dosage at 0.1M salt concentrations

0.1M NaCl salt concentration had a lytic effect on η_{app} of surfactin molecule. At this concentration, there was increased electrostatic repulsion between surfactant head group which limit micellar growth to small finite particle sizes (Li et al., 2009; Lutz-Bueno, 2016). It consequently led to zero viscosity at shear rate of up to 510 s⁻¹ across most dosages. Nevertheless, dosage 0.075% maintained relatively constant but higher η_{app}. Beyond 510 s⁻¹ Υ, attractive Van der Waals force between the tails in the micellar became shear induced. Accordingly, that resulted to molecular self-aggregation that caused to shear-thickening behaviour.

Flow behaviour of surfactin at increased salt concentration is like those reported in figure 1. However, increased ionic concentration resulted in increased η_{app} at zero-shear and constant temperature. For example, η_o of 1.0% surfactin dosage increased from 22.2 to 25.8 mPas at 0.25 M salt concentration (Figure 8a). It further increased to 36.9 mPas at 0.5 M in Figure 8b. Increasing salt concentration could have favoured removal of hydrocarbon chains from water. Consequently, it increased electrostatic coalescence between the hydrophilic group, which results in molecular self-aggregation. This effect however became dosage-dependant as the salt concentration increased to 1.0 and 1.5 M (Figure 8c and d).
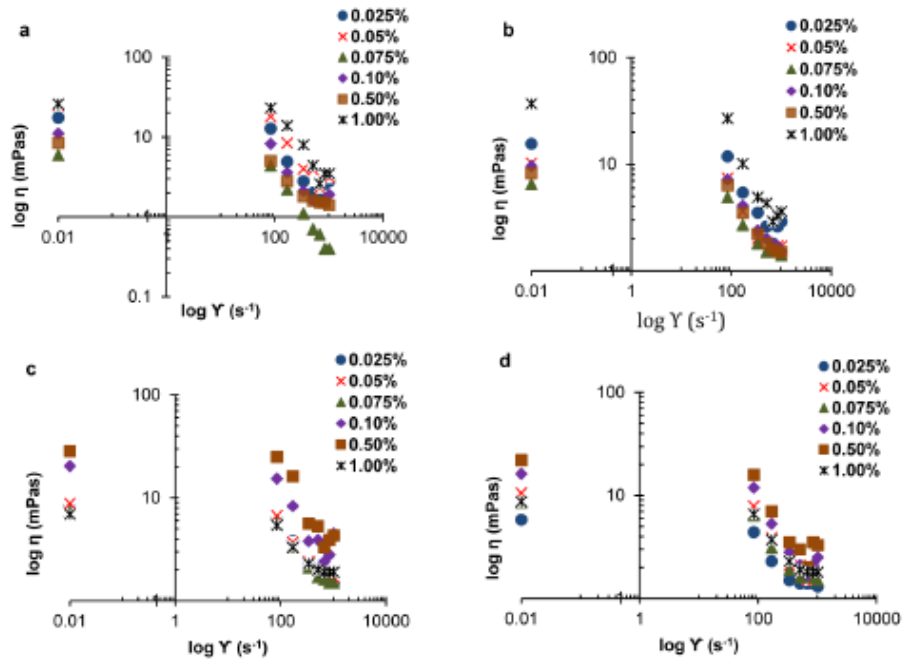
Figure 8—Viscosity vs shear rate as a function of surfactin dosage
at (a) 0.25M, (b) 0.5M, (c) 1.0M, and (d) 1.5M salt concentrations

Flow behaviour became strongly shear-induced above 850.1 s⁻¹, with surfactin exhibiting continuous shear-thinning characteristics. Increase in salinity consequently led to increased electric charge density of the polar shell formed at surface of the micelle (Lutz-Bueno, 2016). This results to upsurge of electrostatic repulsions between head groups, which consequentially increased pseudoplastic behaviour of the surfactin. Unlike at zero salt concentration, 680.9 s⁻¹ critical shear was strongly dosage dependent. Figure 8a shows that η$_{app}$ of 0.075% dosage continue to decrease with increasing rate of shear to a near zero value. To stabilize surfactant in ionizing solutions, counter ions bind to the micelles and thereby screening the electrostatic repulsion, a process that influence micellization. This phenomenon has been occurring with the surfactant with change in salinity and dosage. It signifies that the ionic concentration increase influenced the molecular mobility of the surfactant. Though the behaviour was generally pseudoplastic, it was shear-induced, especially at high shear rate.

Conclusion

Response of sodium surfactin to different rate of shear was evaluated, taking into consideration surfactin dosage, salt concentration and temperature. Based on the findings in this study, sodium surfactin behaves as non-Newtonian fluid, with pseudoplastic flow pattern. Effect of changes in temperature on apparent viscosity of surfactin was largely shear rate dependent. Conversely, change in salt concentration was both dosage and shear rate dependent.

Furthermore, shear-thickening effect set in at a critical shear rate of 680.9s⁻¹, signifying flow-induced self-aggregation. Surfactant dosages 0.075 and to a lesser extent 0.1% were minimally affected by changes in temperatures, salinity and rate of shear not exceeding 680.9s⁻¹. The results suggest pumpability and dispersion characteristics of sodium surfactin, hence its suitability in oil and gas applications.

Acknowledgement

References

Al-Bahry, S. N., Al-Wahaibi, Y. M., Elshafie, A. E., Al-Bemani, A. S., Joshi, S. J., Al-Makhmari, H. S., & Al-Sulaimani, H. S. (2013). Biosurfactant production by Bacillus subtilis B20 using date molasses and its possible application in enhanced oil recovery. *International Biodeterioration and Biodegradation*, **81**, 141–146. https://doi.org/10.1016/j.ibiod.2012.01.006

Al-Wahaibi, Y., Joshi, S., Al-Bahry, S., Elshafie, A., Al-Bemani, A., & Shibulal, B. (2014). Biosurfactant production by Bacillus subtilis B30 and its application in enhancing oil recovery. *Colloids and Surfaces B: Biointerfaces*, **114**, 324–333. https://doi.org/10.1016/j.colsurfb.2013.09.022

Alves, V. D., Freitas, F., Costa, N., Carvalheira, M., Oliveira, R., Gonçalves, M. P., & Reis, M. A. M. (2010). Effect of temperature on the dynamic and steady-shear rheology of a new microbial extracellular polysaccharide produced from glycerol byproduct. *Carbohydrate Polymers*, **79**, 981–988. https://doi.org/10.1016/j.carbpol.2009.10.026

Bezza, F. A., & Chirwa, E. M. N. (2015). Production and applications of lipopeptide biosurfactant for bioremediation and oil recovery by Bacillus subtilis CN2. *Biochemical Engineering Journal*, **101**, 168–178. https://doi.org/10.1016/j.bej.2015.05.007

Chen, W. C., Juang, R. S., & Wei, Y. H. (2015). Applications of a lipopeptide biosurfactant, surfactin, produced by microorganisms. *Biochemical Engineering Journal*, **103**, 158–169. https://doi.org/10.1016/j.bej.2015.07.009

de Oliveira, J. M., Amaral, S. A., & Burkert, C. A. V. (2018). Rheological, textural and emulsifying properties of an exopolysaccharide produced by Mesorhizobium loti grown on a crude glycerol-based medium. *International Journal of Biological Macromolecules*, **120**, 2180–2187. https://doi.org/10.1016/j.ijbiomac.2018.06.158

Drew, M. (2006). *Surfactant Science and Technology* (3rd ed.). New Jersey: John Wiley and Sons.

Fernandes, P. L., Rodrigues, E. M., Paiva, F. R., Ayupe, B. A. L., McInerney, M. J., & Tótola, M. R. (2016). Biosurfactant, solvents and polymer production by Bacillus subtilis RI4914 and their application for enhanced oil recovery. *Fuel*, **180**, 551–557. https://doi.org/10.1016/j.fuel.2016.04.080

Franck, A. J. (2004). Understanding Rheology of Structured Fluids. Retrieved December 10, 2017, from http://www.tainstruments.com/pdf/literature/AAN016_V1_U_StructFluids.pdf.

Frigaard, I. A., Paso, K. G., & de Souza Mendes, P. R. (2017). Bingham's model in the oil and gas industry. *Rheologica Acta*, **56**(3), 259–282. https://doi.org/10.1007/s00397-017-0999-y

Inès, M., & Dhouha, G. (2015). Lipopeptide surfactants: Production, recovery and pore forming capacity. *Peptides*, **71**, 100–112. https://doi.org/10.1016/j.peptides.2015.07.006

Jain, R. M., Mody, K., Mishra, A., & Jha, B. (2012). Isolation and structural characterization of biosurfactant produced by an alkaliphilic bacterium Cronobacter sakazakii isolated from oil contaminated wastewater. *Carbohydrate Polymers*, **87**(3), 2320–2326. https://doi.org/10.1016/j.carbpol.2011.10.065

Kamal, M. S. (2016). A Review of Gemini Surfactants: Potential Application in Enhanced Oil Recovery. *Journal of Surfactants and Detergents*. https://doi.org/10.1007/s11743-015-1776-5

Knoblich, A., Matsumoto, M., Ishiguro, R., Murata, K., Fujiyoshi, Y., Ishigami, Y., & Osman, M. (1995). Electron cryo-microscopic studies on micellar shape and size of surfactin, an anionic lipopeptide. *Colloids and Surfaces B: Biointerfaces*, **5**(1–2), 43–48. https://doi.org/10.1016/0927-7765(95)01207-Y

Li, Y., Zou, A. H., Ye, R. Q., & Mu, B. Z. (2009). Counterion-induced changes to the micellization of surfactin-C16 aqueous solution. *Journal of Physical Chemistry B*, **113**(46), 15272–15277. https://doi.org/10.1021/jp9062862

Liu, J. F., Mbadinga, S. M., Yang, S. Z., Gu, J. D., & Mu, B. Z. (2015). Chemical structure, property and potential applications of biosurfactants produced by Bacillus subtilis in petroleum recovery and spill mitigation. *International Journal of Molecular Sciences*, **16**(3), 4814–4837. https://doi.org/10.3390/ijms16034814

Lutz-Bueno, V. (2016). *Effects of formulation and flow on the structure of micellar aggregates ETH Library*. ETH Zurich. https://doi.org/10.3929/ethz-a-010782505

Mu, J. H., Li, G. Z., Jia, X. L., Wang, H. X., & Zhang, G. Y. (2002). Rheological properties and microstructures of anionic micellar solutions in the presence of different inorganic salts. *Journal of Physical Chemistry B*, **106**(44), 11685–11693. https://doi.org/10.1021/jp014096a

Ohadi, M., Dehghannoudeh, G., Forootanfar, H., Shakibaie, M., & Rajaee, M. (2018). Investigation of the structural, physicochemical properties, and aggregation behavior of lipopeptide biosurfactant produced by Acinetobacter junii B6. *International Journal of Biological Macromolecules*, **112**, 712–719. https://doi.org/10.1016/j.ijbiomac.2018.01.209